

238  
10-3-80  
OK

Doc. 1812

**ornl**

ORNL-5662  
ENDF-299

OAK  
RIDGE  
NATIONAL  
LABORATORY



**An Evaluation of Cross Sections  
for Neutron-Induced Reactions  
in Sodium**

D. C. Larson

**MASTER**

OPERATED BY  
UNION CARBIDE CORPORATION  
FOR THE UNITED STATES  
DEPARTMENT OF ENERGY

ORNL-5662  
ENDF-299  
Dist. Category UC-79d

Contract No. W-7405-eng-26

Engineering Physics Division

AN EVALUATION OF CROSS SECTIONS FOR  
NEUTRON-INDUCED REACTIONS IN SODIUM

D. C. Larson

Date Published: September 1980

DISCLAIMER

This report was prepared as part of the work supported by the United States Government. It is not to be distributed outside the Government and its agencies. It is the property of the United States Government and is loaned to you. It and its contents are not to be distributed outside the Government and its agencies. It is to be returned to the United States Government upon completion of your work. It is not to be used for advertising or promotional purposes, for creating new products, or for resale.

OAK RIDGE NATIONAL LABORATORY  
Oak Ridge, Tennessee 37830  
operated by  
UNION CARBIDE CORPORATION  
for the  
DEPARTMENT OF ENERGY

## CONTENTS

	<u>Page</u>
Abstract . . . . .	v
1. Introduction . . . . .	1
2. Resonance Parameters (File 2, MT=151) . . . . .	2
3. Total Cross Section (File 3, MT=1) . . . . .	4
4. Elastic Scattering Cross Section (File 3, MT=2) . . . . .	5
5. Nonelastic Cross Section (File 3, MT=3) . . . . .	7
6. Total Inelastic Scattering Cross Section (File 3, MT=4) . . . . .	7
7. (n,2n) Cross Section (File 3, MT=16) . . . . .	8
8. Inelastic Scattering Cross Section to Discrete Levels and the Continuum (File 3, MT=51-91) . . . . .	9
9. Neutron Capture Cross Section (File 3, MT=102) . . . . .	14
10. (n,p) Cross Section (File 3, MT=103) . . . . .	15
11. (n, $\alpha$ ) Cross Section (File 3, MT=107) . . . . .	16
12. Elastic Scattering Angular Distributions (File 4, MT=2) . . . . .	17
13. Angular Distributions for Nonelastic Reactions (File 4, MT=16, 51-91, 103 and 107) . . . . .	19
14. Energy Distribution of Neutrons from the (n,2n) Reaction (File 5, MT=16) . . . . .	20
15. Energy Distribution of Neutrons Scattered from the Continuum (File 5, MT=31) . . . . .	21
16. Radioactive Decay (Files 8-9, MT=16, 102, 103 and 107) . . . . .	21
17. Gamma-Ray Multiplicities for Radiative Capture (File 12, MT=102) . . . . .	22
18. Nonelastic Gamma-Ray-Production Cross Sections (File 13, MT=3) . . . . .	23
19. Gamma-Ray Angular Distributions (File 14, MT=3 and 102) . . . . .	26
20. Cross Section Uncertainties (Files 32 and 33) . . . . .	27
21. Model Calculations for $^{23}\text{Na} + n$ . . . . .	28
22. Summary and Conclusions . . . . .	34
Acknowledgements . . . . .	35
References . . . . .	36
Tables . . . . .	42
Figures . . . . .	54

## ABSTRACT

An evaluation of the neutron-induced cross sections of  $^{23}\text{Na}$  has been done for the energy range from  $10^{-5}$  eV to 20 MeV. All significant cross sections are given, including differential cross sections for production of gamma rays. The recommended values are based on experimental data where available and use results of a consistent model code analysis of available data to predict cross sections where there are no experimental data. This report describes the evaluation that was submitted to the Cross Section Evaluation Working Group (CSEWG) for consideration as a part of the Evaluated Nuclear Data File, Version V, and subsequently issued as MAT 1311.

## 1. INTRODUCTION

This evaluation updates the 1971 evaluation of Pitterle, Paik and Perey (PI72), which was adopted for ENDF/B-III. That evaluation covered the energy range from  $10^{-5}$  eV to 15 MeV. The Version III evaluation was carried over for Version IV but extended to 20 MeV. This extension was performed without pretense of analysis simply by scaling the various partial cross sections by the ratio of the total cross section at 20 MeV to the total cross section at 15 MeV. Since 1971, much new experimental data have become available for sodium, and significant advances have been made in nuclear model theory. Utilizing this new information, nearly all of the cross sections were updated for ENDF/B-V.

Although the evaluation is based on available experimental data, extensive model calculations were carried out which simultaneously reproduced the experimental data chosen for use in the evaluation. This provided consistency checks among the various reaction cross sections, and also improved the reliability of the model results, which were used where no data were available.

A summary of the Q-values (G072) and thresholds for the significant neutron reactions with sodium is given in Table A. Since natural sodium is 100%  $^{23}\text{Na}$ , only neutron-induced reactions with  $^{23}\text{Na}$  are listed. There are no experimental data available for the (n,t) or (n, $^3\text{He}$ ) reactions, which have Q values of -10.68 and -16.34 MeV respectively. There are three measurements (FA68, DA69, SA65) at 14 MeV for the (n,d) reaction (Q = -6.57 MeV), to the ground and lowest two excited states ( $^{22}\text{Ne}$  is stable, so the outgoing d must be detected). The combined cross section to the lowest few levels is  $\approx 40 \pm 20$  mb. This reaction was not included in the evaluation due to lack of data and small size of the cross section, but should be looked at again for the next update. Other reactions not included but Q-value allowed are the (n,2p) reaction, (Q = -18.9 MeV), (n,p $\alpha$ ) reaction (Q = -14.5 MeV) and the (n,2 $\alpha$ ) reaction (Q = -12.0 MeV). Model calculations for these reactions which are not included show the cross sections to be negligible, and so are not explicitly given in the evaluation.

Detailed descriptions of each of the reactions included in the evaluation are given on the following pages, along with figures comparing available data with ENDF/B-IV, MAT 1156, hereafter referred to as V4, and ENDF/B-V, MAT 1311, hereafter referred to as V5.

Previous evaluations of sodium include those of Garrison and Drake (GA67) and Pitterle (PI68), in addition to ENDF/B-III (PI72).

## 2. RESONANCE PARAMETERS (File 2, MT=151)

The resolved resonance region in V4 covered the energy range from 600 eV to 150 keV, and included seven resonances. For V5, we have extended the resolved resonance region upper boundary from 150 keV to 500 keV. Eighteen resonances are included in this energy range, and in addition five large resonances above 500 keV are included for the contribution of their tails in the resolved resonance region. Table B gives the parameters of the resonances for V5, and compares the resonance parameters used in V4.

Two resonances deserve further comment. The large resonance at 2.81 keV has been the object of much study in the past (BL66, CL70, GA65, G058, HI60, LY58, M066, RA73, SE50, SH51, ST65a and W048). Questions have arisen concerning its spin, and whether or not spin-dependent radii or negative energy bound states are necessary for a proper description of the cross section in the neighborhood of this resonance. In addition, the  $\Gamma_\gamma$  value for this resonance is difficult to measure experimentally, due mainly to large neutron scattering corrections. The latest study of this resonance was done by Seltzer and Firk (SE74), in which they measured the cross section for this resonance, and demonstrated that an R function analysis (which included effects of far away resonances) of available data for energies below and above this resonance provided a good description of this resonance. Parameters obtained from their analysis ( $\Gamma_n = 376$  eV,  $J = 1$ ) were adopted for V5 (except for  $\Gamma_\gamma$ ), and are noted in Table B. An R-matrix analysis by Rahn *et al.* (RA73) of their data also finds a spin of  $J=1$  for this resonance, but a somewhat larger neutron width of  $\Gamma_n = 400$  eV. However, experimental problems with data for this resonance required a renormalization of this resonance prior to fitting. The capture width of this resonance has also been the subject of many experiments, since it is the source of the thermal capture. The early measurement of Lynn,

Firk and Moxon (LY58) obtained  $\Gamma_{\gamma} = 0.34 \pm 0.01$  eV, and these authors also used a negative energy resonance in their analysis. Hockenbury *et al.* (HO69) measured this resonance and obtained  $\Gamma_{\gamma} = 0.60 \pm 0.06$  eV. However, a later analysis of this measurement by Friesenhahn *et al.* (FR68) found an error in Hockenbury's analysis and obtained  $\Gamma_{\gamma} = 0.47 \pm 0.05$  eV. Friesenhahn also measured the capture cross section for this resonance and obtained  $0.35 \pm 0.04$  eV. Moxon and Pattenden (MO66) reported a value from their measurement of 0.60 eV. Yamamaro *et al.* (YA70) obtained a value of  $0.47 \pm 0.05$  eV, while preliminary results of Macklin *et al.* (MA76) obtained a value of  $0.38 \pm 0.04$  eV. Finally, Wilson *et al.* (WI77) find that  $0.24 \leq \Gamma_{\gamma} \leq 0.40$  eV with 90% certainty, and that the thermal and 2.81-keV capture spectra are essentially the same. The thermal capture cross section value of  $\sigma_{\gamma} = 528 \pm 5$  mb corresponds to a value of  $\Gamma_{\gamma} = 0.353$  eV, if no bound levels are assumed. This assumption is consistent with the observed similarity (WI77) of the thermal and keV capture spectra. Since some of the above measurements are consistent with the  $\Gamma_{\gamma}$  predicted from thermal capture, and there is no experimental evidence for bound levels (WI77), we chose the value of  $\Gamma_{\gamma} = 0.353$  eV for the capture width of the 2.81-keV resonance. This is consistent with a recent recommendation by H. E. Jackson (JA76).

The other important resonance is the s-wave one near 300 keV. The cross section minimum associated with this resonance allows neutrons to "leak through," and is the source of 40% of the integrated tissue dose sensitivity at the CRBR upper axial shield (OB76). New data available for V5 include the thick sample measurements of Brown *et al.* (BR75), and the measurement of Larson *et al.* (LA76). Brown *et al.* measured the transmission of neutrons through sodium using the filtered beam technique. Sodium filters, either 62.2 or 93.3 cm thick were placed in the neutron beam, and a 31.1-cm Na sample was cycled in and out. Their measurement shows that the minimum is much broader than the V4 evaluation. A similar conclusion is drawn from the data of Larson *et al.*, which is in good agreement with the Brown *et al.* data in the minimum. Thus for V5, the evaluation was broadened and lowered to reproduce the results of these measurements. These results are shown in Fig. 1.

The remainder of the resonance parameters listed in Table B (with the exception of the 7.6-keV resonance) were obtained from a multilevel Breit-Wigner analysis of the transmission data of Larson *et al.* (LA76). The code SIOB (deS78) was used for the analysis. The high resolution data covered the energy range from 32 keV to 32 MeV, and had small deadtime and background corrections as well as good statistical accuracy. The neutron widths and spins obtained from this analysis were combined with the capture areas of Musgrove *et al.* (MU77) to obtain the corresponding capture width given in Table B. Uncertainties on the resonance energies are taken from results of the multilevel analysis, while uncertainties on the neutron and capture widths are estimated from fitting uncertainties and quoted uncertainties on the capture areas of Musgrove *et al.* (MU77). The five resonances noted with asterisks were included in the fitting procedure because their low energy tails contributed to the resolved resonance region. The scattering radius is taken as 5.41 f, obtained from the resonance parameter analysis. For the very narrow resonances at 35, 117, 143, 189 and 305 keV, area analysis was used in addition to confirm the neutron and capture widths. For the 7.6-keV resonance, the energy and the capture area was taken from Musgrove *et al.* (MU77).  $\Gamma_\gamma$  was taken from the Hockenbury *et al.* estimate of 0.6 eV, and a g value of 5/8 was assumed to obtain the neutron width. From the parameters in Table B, and the scattering radius of 5.41 f, the calculated cross sections reproduced the data of Larson *et al.* to better than  $\pm 5\%$ , with the exception of some of the narrow resonances. The resonance parameter fit from 50 to 550 keV is shown in Fig. 2.

### 3. TOTAL CROSS SECTION (File 3, MT=1)

From 1.E-5 to 2.E-2 eV, no experimental data are available. Over this energy range, the evaluation is a sum of the scattering cross section and a 1/v capture cross section. The capture cross section is derived from  $\Gamma_\gamma = 0.353$  eV, the capture width of the 2.81-keV resonance. From 2.E-2 eV to 600 eV, the total cross section is based on data of Hodgson *et al.* (H052), Joki *et al.* (J055), Lynn *et al.* (LY58) and Rahn *et al.* (RA73). At 0.0253 eV the cross section is  $3.847 \pm 0.3$  b, and consists of the sum of 0.528 b of capture and 3.319 b of scattering cross sections. The data and evaluation from 1.E-5 to 600 eV are shown in Figs. 3 and 4. From 600 eV to 500 keV

(the resolved resonance region), a background cross section is given to supplement the cross section generated from the resonance parameters. In general, it is less than 10% of the total cross section. Particular attention has been paid to the important region around the 2.81-keV resonance, and to the interference minimum of the 300-keV resonance. From 600 eV to 32 keV, the background cross section was obtained by smoothing the difference between the evaluated data and the cross section obtained from the resonance parameters. From 32 keV to 500 keV, the background cross section was obtained by smoothing the difference between the cross section calculated from the resonance parameters and the data of LA76, with the exception of the 300-keV minimum, where the thick sample data of Brown *et al.* (BR75) was also used. From 500 keV to 20 MeV, the evaluation is based mainly on the data of Larson *et al.* (LA76). The data of Cierjacks *et al.* (CI68, CI69), Foster and Glasgow (F071) and Stoler *et al.* (ST71) were also utilized for comparison purposes. Reference LA76 contains a detailed comparison of V4 with the data used for this evaluation from 32 keV to 20 MeV. A few points are worth noting here. The V4 evaluation was based mainly on Cierjacks data above 290 keV. The present evaluation (V5) is generally in good agreement with V4 above 290 keV; however, V5 is generally from 1-4% larger, except over the 710-keV resonance, where V5 is about 6% larger. However, results from broomstick (thick sample low resolution transmission) measurements at the ORNL Tower Shielding Facility using both Bonner Balls and a NE-213 scintillation spectrometer as detectors indicated the V4 sodium total cross section requires an overall ~6% normalization upward (MA76a). This upward normalization is consistent with results of the V5 evaluation.

Comparison of the data, V4 and V5 evaluations is shown in Figs. 4 through 21 for the energy range from 600 eV to 20 MeV. In addition, the background cross section from 600 eV to 400 keV, which was added to the results from the resolved resonance region, is shown in Figs. 22-24.

#### 4. ELASTIC SCATTERING CROSS SECTION (File 3, MT=2)

In the energy range from  $1.0E-5$  to .02 eV there are no elastic scattering data, and the evaluation results from a downward extrapolation of elastic scattering above .02 eV. From .02 to 600 eV, the elastic

scattering data result from subtraction of the nonelastic (capture) cross section from the total cross section. From 600 eV to 500 keV, this file contains the background cross section which must be added to the elastic scattering cross section generated from the resonance parameters to obtain the total elastic scattering cross section. The first inelastic channel opens at a neutron energy of 459 keV; below this neutron energy the only reaction channels open are elastic scattering and capture. Since the capture cross section is small (<10 mb except over the resonances), the total cross section from 600 eV to 500 keV is approximately equal to the scattering cross section. Between 500 keV and 15 MeV, a number of experimental data sets are available; however, some of them contain only the elastic scattering, while others contain scattering cross sections, i.e., they include inelastic scattering to the 440-keV level. The available data are given in Table C. As noted in the table, some of the scattering cross sections have been converted to elastic only by removing the 440-keV inelastic scattering cross section. This was done by using a measured 440-keV angular distribution at a nearby energy, or relying upon results from a DWBA prediction for the (n,n') cross section angular distribution. The total elastic cross sections are also given in Table C, and were obtained either from the original literature, or by integrating the measured angular distribution. The measurements for which the total elastic is not given are either low energy scattering measurements, for which it is very difficult to remove the inelastic scattering to the 440-keV level due to the large amount of structure in this cross section (e.g., Refs. EL64, LA57 and LA60), or low energy elastic angular distributions (Refs. CH66 and KI76), which will be dealt with in the section on angular distributions. The total elastic scattering evaluations (V4 and V5) along with the data from Table C are shown in Figs. 25 through 31. The structure in this cross section results from subtraction of a relatively "smooth" nonelastic cross section from the structured total cross section, so it may not all be real. Sharp structure in the nonelastic cross section has not been identified experimentally, but is expected to exist.

## 5. NONELASTIC CROSS SECTION (File 3, MT=3)

The nonelastic cross section was formed as the sum of the partial reaction cross sections, in particular the total inelastic,  $(n,2n)$ ,  $(n,\gamma)$ ,  $(n,p)$  and  $(n,\alpha)$  cross sections. There is no experimental data available for the nonelastic cross section. However, up to 4 MeV the nonelastic is essentially equal to the total inelastic, which will be discussed later. Above 6 MeV, V5 is larger than V4, due mostly to a larger total inelastic. Above 15 MeV, the difference between V4 and V5 is due mainly to a more realistic treatment of the  $(n,2n)$  cross section, which will be discussed under the  $(n,2n)$  cross section portion of this report. Comparison of the nonelastic cross sections for V4 and V5 are shown in Fig. 32.

## 6. TOTAL INELASTIC SCATTERING CROSS SECTION (File 3, MT=4)

This cross section is formed by summing the inelastic cross sections for the lowest eighteen levels (or groups of levels), and the continuum cross section. A description of the evaluation for each of the individual levels and the continuum is given in the next section. Data for comparison to the total inelastic is generally not available, since most experiments do not measure scattering from all levels up to the highest kinematically allowed level for a given neutron energy. However, a number of measurements are available for sodium which measured inelastic scattering to most of the allowed levels. The missing cross section can be estimated from model calculations. We have listed the "more complete" measurements in Table D. The data of Donati *et al.* (D077) cover the energy range from 0.52 to 4.23 MeV, but only two representative energies are given in Table D, since the structure in the 440-keV level confuses such comparisons at lower energies. The measurement of Coles (C071) included scattering from all but one of the available levels. The inelastic scattering data of Dickens (DI73) is extracted from his gamma-ray production results by removing the gamma-ray feeding to each level. However, some feeding, and/or decay gamma rays are probably missed for the 7.0-MeV measurement. The measurement of Perey and Kinney (PE70) detected the scattered neutrons, and except for the measurement at 5.44-MeV obtained data for most of the excited levels. The data of Towle and Owens (T067) and Hermsdorf *et al.*

(HE75) did not measure scattering from the 440-keV level, but detected scattered neutrons from most of the remaining levels. Table D also includes the calculated cross sections for the excitation energy regions not covered in the experiment. Details of the model calculations will be covered in a later section. The continuum part of the total inelastic scattering cross section includes neutrons from the  $(n,np)$ ,  $(n,pn)$ ,  $(n,n\alpha)$  and  $(n,\alpha n)$  reactions, but not from the  $(n,2n)$  reaction, which is given separately. Figure 33 shows both V4 and V5 evaluations, compared with the total inelastic scattering data given in Table D.

#### 7. $(n,2n)$ CROSS SECTION (File 3, MT=16)

Evaluation of this cross section is summarized in Ref. LA79, and details are given in Ref. LA80a, so only a brief description will be given here. At the time of the evaluation, eight measurements were available. These are summarized in Table E. Four of these measurements consisted of data at one or two energies between 14 and 15 MeV. The remainder of the measurements covered a wider energy range, from near threshold (12.96 MeV) to >20 MeV. The data of Araminowicz and Dresler (AR73) is much lower than other measurements, and was not used for the evaluation. The data of Paulsen (PA65) is an extension of the measurement by Liskien and Paulsen (LI65), using the same experimental techniques, but was reported later by Paulsen, and not included in Ref. LI65. For purposes of this evaluation, these data will be treated together as one data set.

The difficulty in evaluation of this cross section arises because the three major data sets of Liskien and Paulsen (LI65, PA65), Menlove *et al.* (ME67a) and Picard and Williamson (PI65) each differ from the other by approximately a factor of two. Figure 34 shows the available data for the cross section. At the time each of the three measurements noted above was done, the authors also measured various cross sections for reactions other than  $^{23}\text{Na}(n,2n)$ . In general, cross sections for these other reactions are in good agreement with previous measurements; only the  $(n,2n)$  cross sections for  $^{23}\text{Na}$  appear to have a problem. Part of the experimental difficulty with this reaction is the half-life of the reaction product  $^{22}\text{Na}$ , which is 2.61 years, and thus background corrections become important. Liskien and Paulsen were the only authors who used coincidence

techniques in an attempt to reduce the background. Comprehensive nuclear model calculations (described elsewhere in this report) done as part of the evaluation are in closest agreement with the Liskien and Paulsen measurement, and in view of the discrepant experimental information were used for the V5 evaluation. The V4 evaluation of this reaction deserves a comment. For V4 the evaluation was taken from V3 (which had an upper limit of 15 MeV) and extended to 20 MeV by arbitrarily scaling the 15-MeV cross section by the ratio of  $\sigma_{\text{total}}(20 \text{ MeV})/\sigma_{\text{total}}(15 \text{ MeV})$ . This gives rise to the strange shape for V4.

#### 8. INELASTIC SCATTERING CROSS SECTION TO DISCRETE LEVELS AND THE CONTINUUM (File 3, MT=51-91)

Inelastic scattering cross sections are given for the first twenty levels in  $^{23}\text{Na}$  up to an excitation energy of 6.1 MeV, and for three groups of levels centered at excitation energies of 6.27, 7.11 and 7.79 MeV. Some experimental data exist for all levels up to  $E_x = 5.78 \text{ MeV}$ , mainly from data of Perey and Kinney (PE70) and Dickens (DI73) at the higher excitation energies. Because of experimental resolution problems, some of the excited levels have been grouped together for the evaluation, in particular the (3.85 + 3.92) MeV levels, the (5.74 + 5.76 + 5.78) MeV levels, the (5.94 + 5.97) MeV levels, and the (6.04 + 6.12) MeV levels. Cross sections for all excited levels begin at the threshold energy, and arbitrarily go to zero at neutron energies varying between 10 and 12 MeV, above which there is no experimental data. For neutron energies above these arbitrary cutoffs, the cross sections for the discrete levels are contained in the continuum contribution, which starts at 6.1 MeV and continues to 20 MeV. The only exception is the cross section for the 440-keV level, which is nonzero from threshold to 20 MeV, since there is some available data at the higher neutron energies (in particular at 17.5 MeV).

We now look in detail at cross sections for the individual excited levels. The largest inelastic scattering cross section is for the 440-keV level. A number of data sets are available and are summarized in Table F, most of which are low energy-resolution measurements in which either the scattered neutron or resulting gamma ray are detected. Two high-resolution

measurements are available (PE71, LA78) which show much resonance structure in this cross section up to  $\sim 3$  MeV neutron energy. This structure explains why many of the low-resolution measurements are in apparent disagreement since they have differing energy resolution, and a small error in energy calibration can cause a significant change in cross section, depending on the nearby resonance structure. To understand these differences, data from the various measurements were averaged into energy bins, ranging in size from 100 keV to 500 keV. Various bin sizes were used to insure that enough points from each measurement were in each bin to give a reasonable average cross section for that bin. Such a plot is shown in Fig. 35 for 100-keV bins for selected data sets, as well as the V4 evaluation for the 440-keV level. The general shape of the data sets is similar, with the exception of the measurement by Donati *et al.* (D077), which appears to be shifted  $\sim 125$  keV too high in energy above 1.0 MeV, and the V4 evaluation, which is high between 1.0 and 1.4 MeV. From threshold to 2 MeV, the V4 evaluation was based upon the high resolution measurement of Perey, Kinney and Macklin (PE71), which was normalized to the measurements of Chien and Smith (CH66) and Towle and Gilboy (T062). The other high resolution measurement available is that of Larson and Morgan (LA78), in which they measured the excitation function for the 440-keV gamma ray as part of a  $^{23}\text{Na}(n,\gamma)$  measurement. This measurement, when binned, agrees in shape with the other lower resolution measurements. When the data of Donati *et al.* (D077) above  $\sim 1$  MeV were shifted down in energy by 125 keV (the shifted data are shown in Fig. 35), general agreement in the shape of the averaged cross sections was obtained, with the exception of the data of Perey *et al.* (PE71) from 1-1.4 MeV. However, overall normalization problems were evident, the largest difference being  $\sim 25\%$  around 1.1 MeV. The individual data sets were inspected, and some corrections were applied to account for later more accurate cross section values used for normalization purposes in some of the measurements. However, this did not resolve the normalization problems between the data sets. The final procedure for obtaining the evaluated cross section for the 440-keV level from threshold to 2.4 MeV was as follows: the binned data were weighted by factors determined from 1) quoted uncertainties on the measurements, 2) experimental technique and apparatus used and 3) evaluation judgment.

These weighted cross sections were then averaged, and the high resolution measurement of LA78 was then renormalized to agree with the average of the weighted cross sections, in order to retain the observed structure in the cross section. This resulted in an ~8% downward renormalization of the data of LA78, within the quoted uncertainties of  $\pm 10\%$ . Data sets included for the averaging included those of Smith (SM70, SM77), Fasoli *et al.* (FA69), Freeman and Mortague (FR58), Lind and Day (LI61), Towle and Gilroy (T062), Chien and Smith (CH66), and Larson and Morgan (LA78). It should be noted that the cross section data for the 0.439 gamma ray from Ref. LI61 are entered wrong in the CSISRS data file. The correct values are given by  $\sigma_{\text{correct}} = (\sigma_{\text{CSISRS}} - 0.1) * 10$ . Cross sections for the other gamma rays are correct. The recent measurement of Smith (SM77) received the largest weight. The data of Perey *et al.* (PE71) were not used in the averaging since they were originally normalized to Refs. CH66 and T062. The resulting cross section for V5 is compared with V4 in Fig. 36. The net result is a lowering of the cross section for V5 by 13% over this energy region. This is in agreement with results of Mallen *et al.* (MA74) from a measurement and analysis of fast neutron spectra in a bulk sodium assembly.

From 2.4 to 4.5 MeV the data of Donati *et al.* (D077), Fasoli *et al.* (FA69) and Lind and Day (LI61) were utilized, with the data of Donati *et al.* shifted down in energy by 125 keV to agree in shape with other measurements. Results from the model calculations were also used as a guide, since these measurements were not in particularly good agreement. Figures 37 and 38 show the available data, as well as V4 and V5 evaluations. Above 2.4 MeV the data of LA78 was not used due to gamma-ray feeding to the 440-keV level.

From 4.5 to 20 MeV data of Coles (C071), Crawley and Garvey (CR68), Dickens (DI73), Fasoli *et al.* (FA73) and Perey and Kinney (PE70) formed the basis for the evaluation, again guided by model calculations. Neutron inelastic scattering cross sections were extracted from the gamma-ray data of Dickens by subtracting the feeding of the 440-keV level, using his measured cross sections. They were found to agree within stated uncertainties with the measured neutron inelastic scattering data of Perey and Kinney. Due to the inability to extract this cross section

from the elastic scattering peak at 14 MeV, no data for the 440-keV level were available. To get an estimate of the cross section at higher energies, the 17.5-MeV (p,p') data of Crawley and Garvey (CR68) were used. A DWBA calculation was done for their data, and a deformation parameter  $\beta = 0.1$  was extracted. This deformation parameter was then used in DWBA calculations for (n,n') to estimate the direct interaction component of the cross section. This direct interaction component was then combined with the multi-step Hauser-Feshbach cross section results for the level to get the calculated cross section for inelastic scattering. The calculated cross sections for this level agree within  $\sim 10\%$  with the available data, except below  $\sim 4$  MeV, where the calculated cross sections are 20-25% lower than the data. Figure 38 shows the available data as well as the evaluations for V4 and V5 for the 440-keV level from 4 to 20 MeV.

Evaluation of inelastic scattering from the 2.08-MeV level in  $^{23}\text{Na}$  from threshold to 4.5 MeV is based on data of Donati *et al.* (D077), Fasoli *et al.* (FA69), Freeman and Montague (FR58), Lind and Day (LI61) and Towle and Gilboy (T062). The gamma-ray data of Lind and Day were converted to level cross sections by dividing the cross section for the 1.61-MeV gamma ray by the branching ratio 0.93, as measured in Ref. DI73. The data of Donati *et al.* were again shifted down in energy by 125 keV. Except for the data point of Towle and Gilboy (T062) which is low, and the data of Lind and Day, which is low above 3 MeV, the data are in reasonable agreement. Figure 39 shows a comparison of the corrected data with V4 and V5 of the evaluation. From 4.5 to 10.0 MeV, the evaluation is based on the data of Dickens (DI73), converted to level cross sections as discussed previously, and Perey and Kinney (PE70). These data sets are in good agreement. There is no neutron experimental data available for this level above 8.52 MeV, and the cross section for this level above 10 MeV has been set to zero; the cross section for neutron energies  $>10$  MeV being included in the continuum. Figure 40 compares V4, V5 and the available data from 4.5 to 10.5 MeV.

Evaluation of inelastic scattering from the 2.39-MeV level in  $^{23}\text{Na}$  from threshold to 10 MeV is based on data of Dickens (DI73), Donati *et al.* (D077), Fasoli *et al.* (FA69), Freeman and Montague (FR58), Lind and Day (LI61), Perey and Kinney (PE70) and Towle and Gilboy (T062). The

gamma-ray data of Lind and Day are converted to inelastic scattering cross sections by dividing the cross section for the 2.39-MeV gamma ray by 0.58, the branching ratio observed by Dickens (DI73). However, these corrected data are again low above 3 MeV. The data of Donati *et al.* were again shifted down in energy by 125 keV. The corrected data are compared with V4 and V5 of the evaluation in Fig. 41. The cross section for this level above 10 MeV is contained in the continuum cross section.

Evaluation of the inelastic scattering from the 2.64- and 2.71-MeV levels of  $^{23}\text{Na}$  from threshold to 10 MeV are based on data of Dickens (DI73), Donati *et al.* (D077) and Lind and Day (LI61). The 2.64-MeV level decays 100% to the ground state, so no correction needs to be applied to the data of Ref. LI61; however, these data are again low above 3 MeV. They did not measure the cross section for the 2.71-MeV level. The data of Perey and Kinney are for the combined cross sections for scattering from the (2.64+2.71)-MeV levels, and were split via the model calculations between these levels. The data, V4 and V5 of the evaluations, are shown in Figs. 42 and 43.

Evaluation of the inelastic scattering from the 2.98-MeV level of  $^{23}\text{Na}$  from threshold to 10.5 MeV is based on data of Dickens (DI73), Lind and Day (LI61), Donati *et al.* (D077), and Perey and Kinney (PE70). The Lind and Day data for this level are much larger than the data of Donati *et al.*, or the model calculations, and are discounted. The resulting evaluation, together with the data and V4, are given in Fig. 44. It should be noted that for the data of Donati *et al.* (D077), the data were often larger than other available data sets, in addition to the energy shift. Since it frequently was the only data available, the evaluation was drawn through the lower part of their stated uncertainties.

Evaluation of inelastic scattering from the 3.68-MeV through the 5.78-MeV levels is based on the only available data, which are those of Dickens (DI73) and Perey and Kinney (PE70). These data are consistent, and generally agree within 20-25% with results from the model calculations. The cross sections for these levels are set to zero for neutron energies from 10-12 MeV, depending upon the level. The cross sections for remaining neutron energies up to 20 MeV are included in the continuum cross section. Evaluation of the remaining groups of levels at (5.93+5.97), 6.08, 6.27,

7.11 and 7.79 MeV are taken over from V4, after thinning the number of points. There are no acceptable data for any of these groups of levels, and for the next evaluation, they could be omitted and the cross section be included in the continuum. Figures 45 through 56 show V4, V5 and the available data for inelastic scattering to the remainder of the discrete levels.

The continuum cross section was estimated by subtracting the sum of MT=51-68 (inelastic scattering to all discrete levels) from the calculated total inelastic cross section. The model calculations for the  $(n,n')$  channel were split into the tertiary reactions  $(n,n'\gamma) + (n,np) + (n,n\alpha) + (n,2n)$ . The continuum cross section starts at 6.1 MeV and goes to 20 MeV. Since the  $(n,2n)$  cross section is included explicitly (as discussed earlier) it was subtracted from the inelastic continuum. The inelastic continuum was thus calculated from the recipe: (total inelastic) -  $(n,2n)$  - (sum of scattering to discrete levels) = evaluated continuum. In later evaluations the  $(n,np)$  and  $(n,n\alpha)$  reactions should be separated out and included explicitly, as was done for the  $(n,2n)$  cross section. The resulting value of the continuum cross section at 14.6 MeV provides cross sections in good agreement with the neutron emission spectra of Hermsdorf *et al.* (HE75). A plot of the V4 and V5 inelastic scattering continuum cross section is given in Fig. 57.

## 9. NEUTRON CAPTURE CROSS SECTION (File 3, MT=102)

The thermal capture cross section is given as  $528 \pm 5$  mb, in agreement with data of Ryves and Perkins (RY70) and the 1974 evaluation of Sher (SH74) as given by Zijp in Ref. Z177. The V4 value was 534 mb. The V5 thermal cross section is consistent with the capture width of 0.353 eV (using a multilevel analysis) for the 2.81-keV resonance. From  $1.E-5$  eV to 600 eV, the capture cross section is calculated from the  $\Gamma_\gamma$  using a Breit-Wigner shape. These results are shown in Figs. 58 and 59. This joins on smoothly at 600 eV to the capture cross section calculated from the resonance parameters described in Section 2. These resonance parameters are used to provide the capture cross section from 600 eV to 500 keV. Figure 60 compares V4 and V5 from 1 keV to 1 MeV. From 500 keV to 1 MeV the data of Bame and Cubitt (BA59) were used for the evaluation. From 1

MeV to 20 MeV, the data of Menlove *et al.* (ME67) were used, as well as the data of Csikai *et al.* (CS67a). Figure 61 compares V4 and V5 for the capture evaluation from 0.5 MeV to 20 MeV.

At 1 MeV, the data of Bame and Cubitt and Menlove *et al.* agree to within ~15%, after renormalization to the value of the  $^{235}\text{U}(n,f)$  cross section used for normalization by Menlove *et al.*, and the data of Csikai *et al.* agree well with the data of Menlove in the region of their overlapping measurements between 13 and 15 MeV. Both Menlove *et al.* and Csikai observe a peak in the  $(n,\gamma)$  cross section in the vicinity of 14.5 MeV. This is consistent with semi-direct or collective capture of the neutron through the giant dipole resonance.

#### 10. $(n,p)$ CROSS SECTION (File 3, MT=103)

The available data considered for this reaction are listed in Table G. The data of Bartle (BA75) are in good agreement with data of Bass *et al.* (BA66), but have poorer energy resolution. The measurement of Bass *et al.* overlaps in energy with the measurement of Williamson (WI61) from 5.8 to 9 MeV. In the region from 5.8 to 8 MeV, the results of Bass *et al.* are higher by 20-30% than results of Williamson, while from 8.7 to 9 MeV they agree within quoted uncertainties. Both measurements have good energy resolution and show much structure. There are no data available for this cross section between 10.4 and 14 MeV, where the cross section is large. From 14 to 20 MeV, a number of activation measurements exist, which measure the  $(n,p\gamma)$  component of the  $(n,p)$  reaction, but give no information on the  $(n,pn)$  component. The major data sets are those of Picard and Williamson (PI65) and Williamson (WI61), which are in good agreement.

The evaluation of the  $(n,p)$  cross section for V5 is based on data of Williamson (WI61) from threshold to 5.75 MeV. From 5.75 to 9.0 MeV the data of Bass *et al.* (BA66) and Bartle (BA75) were used, and from 9 to 10.4 MeV the data of Williamson (WI61) were used. The  $(n,pn)$  channel opens at 9 MeV (with a very small cross section below 11 MeV), so above this energy the  $(n,p)$  cross section is given by  $(n,p\gamma) + (n,pn)$ . The activation data measure only the  $(n,p\gamma)$  component, so for energies above 10.4 MeV the  $(n,p)$  cross section is based on results of model calculations which reproduce the experimental data for the  $(n,p\gamma)$  component. Figure 62 shows V4

and V5 of the (n,p) evaluation compared with the available experimental data.

#### 11. (n, $\alpha$ ) CROSS SECTION (File 3, MT=107)

The available data considered for this reaction are listed in Table H. They are basically the same set of measurements as for the (n,p) reaction, with the addition of the measurement by Woelfer and Bormann (W066) from 12.6 to 18.7 MeV, and fewer measurements around 14 MeV. However, the various measurements are not in as good agreement with each other as for the (n,p) cross section. The measurement of Bartle (BA75) is of lower energy resolution but in good average agreement with the measurement of Bass *et al.* (BA66). However, in the region of overlap of data of Bass *et al.* and Williamson (WI61), the data of Williamson are low by  $\sim 10\%$  near 7.5 MeV, and about a factor of 2 from 8.5 to 9 MeV. However, Williamson used neutrons produced by four different reactions to cover the energy range of his measurement. From 4-6.4 MeV the d-d reaction was used, from 6.4-7.9 neutrons from the d- $^{14}\text{N}$  reactions were used, from 8.6-11 MeV neutrons were obtained from the d- $^{14}\text{C}$  reaction, and from 15.8-19 MeV neutrons were obtained from the d-t reaction. This may account for the differences between his data and others over the various energy ranges, in particular the values from 8.6-11 MeV appear to be systematically low. No data are available from 10.5 to 12.5 MeV, which is an important energy region since it appears the cross section may peak there. The (n, $\alpha\text{n}$ ) channel opens at 10.5 MeV, but starts effectively competing with (n, $\alpha\gamma$ ) above  $\sim 14$  MeV. From 12.5 to 20 MeV there are a number of data sets available, mostly with large uncertainties and not in good agreement with each other. All the data are obtained from activation measurements, which measure the (n, $\alpha\gamma$ ) component of the (n, $\alpha$ ) reaction. The data of Picard and Williamson (PI65) had a background problem due to activation of the photomultiplier glass, as well as low flux for the lower energies. The data of Williamson, discussed above, have the lowest cross sections in this region. The measurement of Woelfer and Bormann are the most consistent over this energy region.

Evaluation of the (n, $\alpha$ ) cross section was done as follows: From threshold to  $\sim 9$  MeV the evaluation was based on data of Bass *et al.* and

Bartle, adjusted within uncertainties to agree better with data of Williamson. Above  $\sim 9$  MeV the evaluation was difficult due to the discrepancy among the available data sets, and the poor agreement of the data with model calculations between 9 and 16 MeV. As noted earlier, above 14 MeV the  $(n,\alpha)$  cross section is effectively split into the  $(n,\alpha n) + (n,\alpha\gamma)$  tertiary components, and the activation measurements obtain information only on the  $(n,\alpha\gamma)$  component. Above 16 MeV the calculated  $(n,\alpha\gamma)$  cross section is within uncertainties of the data of Williamson. However, from 12.5 to 16 MeV the calculated  $(n,\alpha\gamma)$  cross section is  $\sim 20\%$  lower than the available data. From 9 MeV to 15 MeV the evaluated cross section rises to match the data of Woelfer and Bormann, then follows their data to  $\sim 15$  MeV, where it approximately matches on to the model calculations for the total  $(n,\alpha)$  cross section to 20 MeV. New activation measurements are badly needed for this cross section between 9 and 16 MeV, and would be very useful out to 20 MeV. The energy region between 9 and 20 MeV should be looked at again for the next evaluation. Figure 63 compares V4 and V5 with the available data.

## 12. ELASTIC SCATTERING ANGULAR DISTRIBUTIONS (File 4, MT=2)

There is no experimental data available below 30 keV. However, the first resonance in sodium is at 2.81 keV, which is an s-wave so the scattering will be isotropic. There is a very narrow p-wave resonance at 7.62 keV, and the next resonance is at 35.4 keV, which is also a p-wave. The available data are given in Table C and discussed in Section 4. For the evaluation, Legendre coefficients  $A_\ell$  in the series

$$\frac{d\sigma}{d\Omega} = \frac{\sigma_{el}}{2\pi} \sum_{\ell=0}^{NL} \left(\frac{2\ell+1}{2}\right) A_\ell P_\ell$$

were used to represent the angular distribution data. These coefficients were either taken from the literature, or a least-squares fit of the angular distribution data was done to obtain the coefficients. In all cases, the minimum number of coefficients to reproduce the data was used.  $\sigma_{el}$  is the total elastic scattering cross section discussed previously. From 30 keV to 200 keV the only data available are those of Langsdorf *et al.* (LA57), and so were used for the evaluation. From 300 to 550 keV data of Chien and Smith (CH66), Elwyn *et al.* (EL64) and Lane and Monahan (LA60)

were available, in addition to the data of Langsdorf, and two data points at 300 and 500 keV by Korzh *et al.* (K065). Inelastic scattering from the 440-keV level is small below 500 keV, so it doesn't matter whether the above measurements separate out the inelastic scattering. The evaluation from 200 keV to 550 keV was based on these four data sets, weighted by the data of Chien and Smith. This data set had the best resolution and was corrected for multiple scattering, while the data of Lane and Monahan were not. This region should be looked at more carefully for the next evaluation as it may be better to use the known resonance parameters to generate the angular distributions from an R-function model.

From 550 keV to 2 MeV, recent high resolution scattering data are available from a measurement by Kinney and Perey (KI76). They measured five point angular distributions in energy steps of 1 keV over this energy range, using ORELA as the neutron source. The data were corrected for multiple scattering effects. Since a maximum of 500 energies is allowed for representation of angular distribution data, the data were thinned using a code from LASL (Y077). The thinning criteria were that from one energy to the next, the maximum overall RMS deviation allowed was 15%, with a maximum angle-to-angle variation of 25%. This reduced the number of angular distributions to 473, while retaining the significant structure in the first three Legendre coefficients. Figures 64-69 show the thinned Legendre coefficients for  $A_1$ ,  $A_2$  and  $A_3$  used for V5 compared with the V4 coefficients from .05 to 2.0 MeV. For V5, the thinned Legendre coefficients from the data of Kinney and Perey were used from 550 keV to 2 MeV. From 2 MeV to 14.1 MeV, the evaluation is based on Legendre fits to data of Refs. C071, EL64, FA69, FA73, KU72, PE70, P072 and T062 corrected for inelastic scattering to the 440-keV level where necessary. As part of the evaluation, optical model fits were obtained for these data sets, and a "best fit" set of parameters was obtained. These parameters were used to generate angular distributions from 15 to 20 MeV. The fitting procedures, as well as the resulting parameters, are discussed in Section 21 of this report. Figures 70-81 show the V5 (and V4, when that energy or one close to it existed in V4) evaluation compared with the measured elastic scattering angular distributions. The Legendre coefficients were taken from File 4/2, while the  $\sigma_{el}$  were taken from File 3/2 for these plots.

13. ANGULAR DISTRIBUTIONS OF NONELASTIC REACTIONS (File 4, MT=16, 51-91, 103, and 107)

For neutrons resulting from the  $(n,2n)$  reaction, isotropy is assumed for both the first and second neutron. No angular distribution data are available for this reaction, since the cross section for the  $(n,2n)$  reaction is very small in the neutron emission measurement at 14.6 by Hermsdorf *et al.* (HE75).

Available angular distribution data for inelastic scattering from the excited levels in  $^{23}\text{Na}$  are summarized in Table I. The  $(n,n')$  angular distribution data of Chien and Smith for the 440-keV level are presented in Ref. CH66 for only three of the twenty-five energies for which the measurements were made. The second group of neutrons from the  $^7\text{Li}(p,n)$  source caused experimental difficulties at some energies and scattering angles. For the three energies shown in their paper, the angular distributions at 1.0 and 1.2 MeV are consistent with an isotropic angular distribution, while the data at 1.4 MeV imply a small  $A_1$  coefficient. The data of Towle and Gilboy (T062) for the 440-keV level at 0.98 MeV are symmetric about  $90^\circ$ , but show a small departure from isotropy. At 1.50 MeV their angular distribution is isotropic, and also at 2.52 MeV after corrections for incomplete separation from the elastic scattering. Their data at 3.97 MeV do not separate the 440-keV level from elastic scattering but angular distributions taken for neutrons scattered from groups of levels at  $(2.08+2.39)$ ,  $(2.64+2.71)$  and at 2.98 MeV are all consistent with isotropy. Fasoli *et al.* (FA69) find isotropic angular distributions for the 440-keV level at neutron energies of 1.51, 2.47 and 4.04 MeV, as well as for levels at  $E_x = 2.08, 2.39, (2.64+2.71)$  and 2.98 MeV, all at a neutron energy of 4.04 MeV. At 6.4 MeV they did not resolve the 440-keV level from the elastic peak, but obtained essentially isotropic angular distributions for groups of levels at  $E_x = (2.08-2.98)$  and  $(3.68-3.92)$ . The measured angular distribution for the level at 4.78 MeV decreases by approximately a factor of 2 from  $80^\circ$  to  $160^\circ$ , while the level at 4.43 MeV has an isotropic angular distribution.

Coles (C071) measured inelastically scattered neutrons at 5.0 MeV from levels at .44, 2.08, 2.39,  $(2.64+2.71)$ , 2.98, 3.68 and  $(3.85+3.92)$  MeV, and found all angular distributions to be isotropic, within uncertainties of the measurement.

Perey and Kinney (PE70) measured inelastically scattered neutrons at incident energies of 5.44, 6.37, 7.60 and 8.52 MeV. In their report they present angular distributions for groups of levels, since angular distributions for some individual levels were only measured at a few angles at some energies. They also give the average cross section, and inspection of the angular distributions shows no significant anisotropy except for scattering from the 440-keV level at 6.37 and 7.60 MeV, and from the 4.43-MeV level at 6.37 MeV.

Fasoli *et al.* (FA73) report scattering at 8.0 MeV from groups of levels at (2.08-2.98), (3.68-3.92) and (4.43-5.53) MeV. These angular distributions are consistent with isotropy, within experimental uncertainties. They did not resolve the 440-keV level from the elastic peak.

The final measurement for inelastic scattering angular distribution data is the neutron emission measurement of Hermsdorf *et al.* (HE75) in which they measured the angular distributions for outgoing neutrons, and later binned into 1-MeV groups. These angular distributions are nearly symmetric about  $90^\circ$  for outgoing neutrons up to 7 MeV, becoming more forward peaked from 7-11 MeV, implying a direct interaction component for the higher energy outgoing neutrons. However, the angular distributions are not isotropic for any of the outgoing neutron energies.

Considering the above experimental information, which is in general agreement with predictions of model calculations, the assumption of isotropic angular distributions for all outgoing neutrons is appropriate at least for incident energies to 8.5 MeV, with few exceptions.

To correctly represent the energy-angular information available from neutron emission measurements such as Hermsdorf *et al.* requires the use of File 6 in the ENDF/B format, which currently is not allowed.

There are at present no angular distribution measurements of outgoing protons or alphas from (n,p) or (n, $\alpha$ ) reactions, so the angular distributions are assumed isotropic.

#### 14. ENERGY DISTRIBUTION OF NEUTRONS FROM THE (n,2n) REACTION (File 5, MT=16)

This part of the evaluation was taken over from ENDF/B-IV without change. The energy distribution is given by an evaporation spectrum

$$\frac{d\sigma(E \rightarrow E')}{dE} = \frac{\sigma(E) E'}{I} e^{-\frac{E'}{\theta}}$$

where I is a normalization constant given by

$$I = \theta^2 \left| 1 - e^{-\frac{(E-U)}{\theta}} \left( 1 + \frac{E-U}{\theta} \right) \right|$$

and U is a constant introduced to define the proper upper limit for the final neutron energy such that  $0 \leq E' \leq E-U$ . For sodium,  $U = 12.414$  MeV, the Q-value for the reaction.  $\theta$  is the nuclear temperature and is tabulated as a function of energy from the relation  $\theta = 0.2 (E-12.95)$  given in Ref. PI68.

The energy distribution for the outgoing neutrons could be better predicted from model calculations, where the competition of the (n,2n) reaction with the (n,n' $\gamma$ ), (n,np) and (n,n $\alpha$ ) reactions significantly modifies the energy distribution, especially for low energy outgoing neutrons. This change should be made for the next evaluation.

#### 15. ENERGY DISTRIBUTION OF NEUTRONS SCATTERED FROM THE CONTINUUM (File 5, MT=91)

This energy distribution is also given as an evaporation shape in V5, as it was in V4. However, the temperatures have been modified for V5. At 14.6 MeV, the temperature was chosen to approximately reproduce the neutron emission spectrum of Hermsdorf *et al.* (HE75). This temperature was then scaled approximately as  $\sqrt{E}$  for other energies. The parameter  $U = 6.1$  MeV, the energy at which the continuum cross section starts. Again, this energy distribution should be taken from model calculations to properly reflect competition from other reaction channels.

#### 16. RADIOACTIVE DECAY (Files 8-9, MT=16, 102, 103 and 107)

The reaction products  $^{22}\text{Na}$ ,  $^{24}\text{Na}$ ,  $^{23}\text{Ne}$  and  $^{20}\text{F}$  resulting from the (n,2n), (n, $\gamma$ ), (n,p) and (n, $\alpha$ ) reactions on  $^{23}\text{Na}$  are all radioactive. Information about how these radioactive products decay is given in File 8 of V5. This information was not included in V4. The half-life of the reaction product is given, along with the significant decay branching ratios leading to the final, stable nuclei. The decay data have been taken from the compilation by Endt and Van der Leun (EN73).

File 9 contains the multiplicities for use in obtaining the neutron cross section associated with the decay. For the above reactions, the multiplicities are all unity.

#### 17. GAMMA-RAY MULTIPLICITIES FOR RADIATIVE CAPTURE (File 12, MT=102)

This file gives the gamma-ray multiplicities used in calculating the gamma-ray spectra from neutron capture. It was taken over directly from V4, since no new data are available for thermal capture, upon which the V4 multiplicities were based. Information on the validity of using the thermal capture spectra at higher neutron energies was obtained from the measurement of Wilson, Jackson and Thomas (WI77), who measured the gamma-ray spectrum resulting from capture in the 2.81-keV resonance. They found the resonance transitions to be very highly correlated with the thermal transitions; linear correlation coefficients were  $>0.96$ . Bergquist *et al.* (BE67) measured the gamma-ray spectra from capture in the 35- and 54-keV resonances, but due to experimental difficulties for sodium, the data are not of much use. There are no measurements for capture spectra at higher energies.

Since the 2.81-keV resonance dominates capture in sodium, and the capture spectrum from this resonance is in good agreement with the thermal capture spectrum, a single gamma-ray spectrum has been used to describe capture over the entire energy range from  $1.E-5$  to  $2.E+7$  eV. With this background, a description of the multiplicities present in the V4 and V5 evaluation is now given.

Three sets of data obtained with GeLi detectors are available. The data of Greenwood *et al.* (GR66) and Nichol *et al.* (NI69) are in very good agreement as to the intensity of the lines. The data of Orphan *et al.* (OR70) are not in good agreement with the previous measurements. Nichol *et al.* do not see seven weak transitions observed by Greenwood *et al.*, the largest one being 1.1 photons/100 captures. The percentage binding energy observed in the spectrum are: Greenwood - 98%, Nichol - 91% and Orphan - 115.8%. Greenwood *et al.* obtain a binding energy of  $6959.3 \pm 0.4$  keV, while Nichol *et al.* obtain  $6960.3 \pm 0.4$  keV. Orphan *et al.* see 22 gamma-ray lines not seen by either Greenwood or Nichol. Fifteen of these lines have intensities greater than 1.0 photon/100 captures.

These 22 lines account for 9.7% of the binding energy, which brings the disagreement down from 115.8% to 106.1%. It is possible that these 22 lines are either in the background or artifacts of the code used to reduce the data. There are 26 gamma-ray lines seen by both other groups, but not seen by Orphan *et al.*, even though some of them have intensities of 10 photons/100 captures.

The evaluation contains multiplicities for 61 gamma rays obtained from the data of Greenwood *et al.* and Nichol *et al.*, generally weighted more heavily by the Greenwood *et al.* data.

#### 18. NONELASTIC GAMMA-RAY-PRODUCTION CROSS SECTIONS (File 13, MT=3)

The non-capture portion of the gamma-ray-production cross sections were extensively revised for V5. For V4, the gamma-ray-production cross sections were derived from the cross sections for neutron inelastic scattering together with the appropriate gamma-ray branching ratios describing how the levels decay. The inelastic scattering cross sections were fairly well known up to 8.5 MeV, but the branching ratios for many of the higher excited levels were poorly known and had to be estimated. Gamma-ray production from the  $(n, p\gamma)$  and  $(n, \alpha\gamma)$  reactions was estimated to be small, and hence was not included. For incident neutron energies from 9 ~ 13 MeV the gamma-production cross sections from the 1967 evaluation by Garrison and Drake (GA67) (represented by smooth continuum cross sections) were combined with the gamma production generated from the inelastic scattering cross sections and branching ratios.

Since the cross sections for inelastic scattering to discrete levels were zero above ~13 MeV, from 13-20 MeV the gamma-production cross sections were only the smooth continuum cross sections of Garrison and Drake. This combination of branching ratios and continuum distributions caused problems for some of the gamma-ray cross section processing codes. In particular, for the case of sodium prior to December 1977, the LAPHNGAS code at ORNL produced libraries containing zero values for the gamma-ray productions for incident neutrons between 8.13 and 9.0 MeV. This problem is discussed more fully in Ref. LA78. When the V4 evaluation was appropriately flux-weighted and compared with a benchmark gamma-ray-production measurement (Ref. MA70), some discrepancies were found. For V5, a number of new gamma-production

cross section measurements for discrete gamma rays were available, as well as a comprehensive  $\text{Na}(n, \gamma)$  measurement from ORELA (LA78) which covered the neutron energy range from 400 keV to 20 MeV, and gamma-ray energies from 350 keV to 10.6 MeV. The ORELA data were compared with other available gamma-production cross sections for  $E_n > 3$  MeV and found to be in good agreement. Since the yield for the 440-keV gamma ray shows strong resonance structure for neutron energies less than  $\sim 3$  MeV, comparisons for  $E_n < 3$  MeV are difficult to interpret and are not done here, due to differing energy spreads of the incident neutron beams, and the possibility of small errors in beam energy. Results of this comparison, along with references for other gamma-ray-production cross sections used for this evaluation, are given in Table J. The column headed  $\Delta E_\gamma$  gives the energy range over which gamma rays were measured by the various authors. The data of LA78 were summed into corresponding gamma-ray bins, and the resulting cross sections are given in the column headed LA78. The results of Donati *et al.* (D077) are larger on the average by  $\sim 18\%$ , while the data of Lachkar *et al.* (LA73) are lower by  $\sim 20\%$ . Otherwise, the data of LA78 agree within experimental uncertainties with the data of other authors. Since the data of LA78 covered the complete neutron energy range for ENDF, and were in good agreement with data of other authors up to  $E_n = 15$  MeV, the data of LA78 were used for the V5 gamma-production file.

The V5 evaluation for the gamma-ray production was done as follows. Since the neutron and gamma-ray cross sections for the 440-keV level are the same up to  $E_n = 2.17$  MeV (where decay of the  $E_x = 2.08$ -MeV level begins to contribute 440-keV gamma rays), File 12/51 is used to pick up the neutron cross sections given in File 3/51 for the 440-keV level up to  $E_n = 1.99$  MeV. This is done so the structure present in the 440-keV gamma ray will be consistent with the neutron scattering for energy balance. For  $E_n > 1.99$  MeV, the cross section for the 440-keV gamma ray is given (along with other gamma rays) in Files 13/3 and 15/3. The data of LA78 were acquired in neutron bins ranging from 300 keV wide at  $E_n = 400$  keV to 3 MeV wide at  $E_n = 14$  MeV, with gamma-ray bins ranging from 15 keV at  $E_\gamma = 350$  keV to 140 keV at  $E_\gamma = 9.4$  MeV. The gamma bins were then rebinned by an algorithm which checks on the cross section in adjacent bins. If it is the same within uncertainties, the bins are combined.

The area under the rebinned curve is required to be the same as under the original. This serves to condense the original 176 gamma-ray bins into fewer bins. The data are then appropriately normalized for separation into gamma-ray-production cross sections for File 13/3, and probability distributions for File 15/3. Since this measurement had a lower limit of 350 keV for gamma rays, we turned to the model calculations to find out what information was not included in the V5 evaluation. Below  $E_n = 15$  MeV calculations predict there is less than 5% of the gamma production cross section below 350 keV. Above  $E_n = 15$  MeV, the 110- and 197-keV gamma rays from the  $(n, n\alpha + n, \alpha n)$  reaction leading to  $^{19}\text{F}$  become important, and at 20 MeV are predicted to be ~15% of the total gamma-production cross section. These gamma rays should be included for the next update of this evaluation. This problem is discussed in Ref. LA80.

There is good agreement in general between V4 and V5 for all gamma rays produced by the  $(n, n'\gamma)$  reaction up to 8 MeV. A comparison between V4 and LA78 (taken over as V5) is shown in Figs. 82 through 96. For gamma rays around 6 MeV in Figs. 90 through 92 the branching ratios for the levels from  $E_x = 5.96$  to 7.79 MeV were not known and had to be estimated for V4. In addition, the cross sections for the groups of levels at  $E_x = 6.27, 7.11$  and 7.79 were not well known and may have been overestimated. The net result was an overestimation of the gamma rays around  $E_\gamma = 6$  MeV for V4. For gamma rays resulting from neutrons above  $E_n = 8$  MeV, significant differences are observed between V4 and V5, with the data used for V5 providing much more structure in the cross section.

In addition to the experimental data, the comprehensive model calculations done for V5 provided more input on the gamma-ray-production cross sections. These results will be discussed in Section 21 on model calculations.

Figures 97 and 98 compare the average gamma-ray cross section as a function of neutron energy for V5 (data of LA78) and V4, with and without the processing code cutoff discussed previously. Figures 99 and 100 provide similar comparisons for the average gamma-ray energy.

## 19. GAMMA-RAY ANGULAR DISTRIBUTIONS (File 14, MT=3 and 102)

For V4 and V5, all gamma rays are assumed to have isotropic angular distributions. This assumption for the most part is in agreement with available data. Gamma-ray angular distributions have been measured by Smith (SM77) for the 440-keV gamma ray at seven energies between 0.64 and 2.04 MeV, and are consistent with the assumption of isotropy. An earlier measurement by Smith (SM70) at neutron energies from 0.75-1.55 MeV also resulted in isotropic angular distributions for the 440-keV gamma ray. Buchanan *et al.* (BU71) measured the angular distribution for the 440-keV gamma ray at 1.0 MeV, and found it to be isotropic. Donati *et al.* measured angular distributions for the 440-keV gamma ray at 10 energies from 0.73 to 3.82 MeV, and the angular distribution for the 1638-keV gamma ray at four energies from 2.67 to 3.87 MeV. The 440-keV angular distributions are approximately isotropic at the lower energies but show increasing anisotropy with increasing energy, being  $\sim 20\%$  at the higher energies. The angular distributions for the 1638-keV gamma ray are consistent with isotropy. Towle and Gilboy measured the angular distribution of the 440-keV gamma ray at 1.5 MeV and observed  $\sim 14\%$  anisotropy. They also measured the anisotropy at 1.3 and 1.7 MeV, and found it to be consistent with zero. Finally, at higher energies, Abbondanno *et al.* (AB73) have measured the angular distributions for the 0.44, 0.64, 1.27 and 1.63 MeV gamma rays at 14.2 MeV. Within quoted uncertainties, all angular distributions are consistent with isotropy - however, the angular distribution for the 1.27-MeV gamma ray has large uncertainties and the fitted  $A_4$  coefficient is also large. The final experimental information comes from the measurement at 14.1 MeV by Martin and Stewart (MA65) of the angular distribution of the 440-keV gamma ray, which they also find isotropic. Thus in summary, most of the experimental information is consistent with the assumption of isotropy for the gamma-ray angular distributions, with the largest exceptions being  $\sim 20\%$  for the 440-keV gamma rays at a few lower neutron energies.

## 20. CROSS SECTION UNCERTAINTIES (Files 32 and 33)

This set of uncertainty files constitutes an initial attempt at quantifying estimated uncertainties and correlations for the major cross sections of sodium. They are based on the author's knowledge of the data, gained from evaluating cross sections for this material for ENDF/B-V, quoted uncertainties for the data, and the experimental technique used for the measurement.

In general, the files were generated by looking at all of the available data, utilizing any renormalizations or changes made during the evaluation. Based on the spread of the data, lines were drawn at approximately the 90% confidence limits, and the  $\pm 1\sigma$  uncertainties were then extracted from the plots. For cross sections where data were sparse, uncertainty estimates were made based on experience with other similar cross sections, other work done by the authors, and in some cases, calculated cross sections. Correlation ranges were determined from energy ranges covered by the different measurements, and by energy regions where different experimental methods were used.

For sodium, uncertainty files are provided for the resonance parameters given in File 2, and for all reactions in File 3. The uncertainties in the resonance parameters have been estimated from the process of fitting transmission data to obtain the neutron resonance parameters, and uncertainties in the capture areas. Correlations between the neutron and capture resonance parameters are taken to be zero. These uncertainties are useful mainly for self-shielding problems.

Uncertainties files corresponding to File 3 data cover the energy range of the File 3 data. LB=1 types of correlations are used, i.e., fractional components correlated only within each energy interval. Two or three sets of LB=1 sections are typically used to represent short-range and long-range correlations. Sections for the elastic, nonelastic and total inelastic cross sections are derived files (NC-type subsections). All other files are given explicitly as NI-type subsections. Uncertainties for the neutron total cross section, (n,2n) and the continuum inelastic are about the same quality over the whole energy range. File 33/5; (inelastic scattering to the 440-keV level) is better up to 4 MeV than

from 4 MeV to 20 MeV. Files 33/52-68 for inelastic scattering to the remaining levels are of higher reliability for the first few MeV above threshold than for the higher energies. File 33/102 is best up to about 1 MeV, while files 33/103 and 33/107 are more reliable from threshold to about 8 or 9 MeV. These comments on reliability reflect the assumption that uncertainty files are easier to estimate in energy regions where data exist than regions where there is little or no data.

## 21. MODEL CALCULATIONS FOR $^{23}\text{Na} + n$

Nuclear model calculations play an important role in modern evaluations for the interpolation and extrapolation of cross sections to energy regions where no data exist, and for predictions of reaction cross sections for which there is little or no experimental data. However, in order to insure internal consistency, the model calculations should simultaneously reproduce as much of the experimental information as possible for as many reaction channels as reliable data is available. We will now look in detail at the four areas in which model calculations were used in this evaluation — namely 1) fitting the neutron total cross section data with a multilevel Breit-Wigner model to obtain resonance parameters, 2) fitting available elastic scattering angular distribution and total cross section data to obtain neutron optical model parameters, 3) using an advanced multistep Hauser-Feshbach code to reproduce cross section data for the various reaction channels above  $E_n \sim 500$  keV and 4) use of a Distorted Wave Born Approximation (DWBA) code to supplement the multistep Hauser-Feshbach results to account for inelastic scattering to collective levels in  $^{23}\text{Na}$ .

### A. Resonance Parameter Fitting

The multilevel Breit-Wigner code SIOB (deS78) was used to fit the high resolution transmission data of LA76 from 32 keV to 500 keV. In addition, estimated values of resonance parameters at 2.81, 538, 598, 697, 727 and 780 keV were included in the fitting procedure but not searched on. They are the major resonances outside of the energy region which was fit, and were included for the effects of the resonance tails. The parameters searched on were the scattering radius, the resonance energies and the neutron widths  $\Gamma_n$ . The  $\Gamma_\gamma$  values were estimated by combining results of

an initial fit with the capture areas of Musgrove *et al.* (MU77). These values of  $\Gamma_Y$  were then fixed since for all resonances which were able to be fit,  $\Gamma_Y \ll \Gamma_n$ .

Various combinations of  $J$  and  $l$  angular momentum values were tried until the best fit was obtained, and this fit, together with the transmission data, is shown in Fig. 2. The resulting resonance parameters are given in Table B. It should be noted that the data can be fit better by allowing different radii for different  $l$ -wave resonances, but this option is not currently allowed by ENDF/B formats.

#### B. Optical Model Analysis of Elastic Scattering Angular Distributions

The optical model code GENOA (PE67) was used to fit nine selected sets of elastic scattering angular distribution data, in addition to the total cross section. The angular distribution data sets selected for fitting were the data of Towle and Gilboy (T062) at 3.97 MeV, Coles (C071) at 5.0 MeV, Perey and Kinney (PE70) at 5.44, 6.37, 7.60 and 8.52 MeV and the data of Fasoli *et al.* (FA73) at 8.0, 9.7 and 14.1 MeV, and the total cross section data of Larson *et al.* (LA76). Compound elastic scattering angular distributions were calculated for each of the above incident neutron energies, and used as input to GENOA. The magnitude of the compound elastic contribution was searched on, along with the optical model parameters, to obtain a minimum chi-square. The energy dependent magnitude of the compound elastic contribution was represented by the empirical relation

$$\sigma_{CE}(E) = \alpha e^{-.465E}$$

Initially, searches were done on each individual data set, fixing  $\sigma_T$  and varying  $\alpha$ , and optical model parameters in groups of  $(V,W)$ ,  $(r_r, r_I)$ ,  $(a_r, a_I)$  and finally  $(V,W,V_{s.o.})$ . The best fit parameters from each data set were then averaged and global searches were initiated on all data sets simultaneously, adjusting the parameters in the above sequence. The searching technique followed is fully described in Ref. FU76. The real strength  $V$  was found to be best represented by a constant rather than the usual energy dependent term. The final best fit set of optical model parameters obtained from this work is given in Table K, and the resulting total cross sections are compared with the data of Ref. LA76 in Fig. 101.

The global optical model fits and the experimental angular distributions are shown in Figs. 102 through 110. This set of neutron optical model parameters was then used for the rest of the model calculations to generate required neutron transmission coefficients.

### C. Calculation of Partial Cross Sections with the Multistep Hauser-Feshbach Code TNG

The model code TNG (FU79), developed by C. Y. Fu at ORNL, was used exclusively for this analysis. During the time of the calculations for V5, this model code was undergoing extensive revision to incorporate new theoretical advances and improve its efficiency. Due to this upgrade, it was not possible in the available time to do all the necessary calculations in a final form for use in the evaluation. In particular, as noted earlier, the energy distributions for outgoing neutrons from the  $(n,2n)$  reaction and the inelastic continuum would be better represented by tabulated distributions from the model calculations than by evaporation spectra as given in V5. However, full calculations done during the Phase I Review of V5 generally confirmed the preliminary results used in V5, and changes will be given in future updates of this evaluation.

As noted earlier, the neutron optical model parameters were obtained by fitting elastic scattering data. The proton optical model parameters were taken from the work of Hellstrom, Dallimore and Davidson (HE69). These parameters reproduce the cross section for  $(n,p_0)$  and  $(n,p_1)$  as measured by Bass *et al.* (BA66). The alpha optical model parameters were taken from the work of Lucas, Casper and Johnson (LU66), with the real and imaginary strengths adjusted to reproduce the low energy part of the  $(n,\alpha)$  cross section. The final proton and optical model parameters are also given in Table K. Level density parameters for  $^{23}\text{Na}$  and  $^{22}\text{Na}$  were taken initially from Gilbert and Cameron, and then empirically adjusted to reproduce the observed level densities of the residual nuclei as reported in EN73 and M076. For the residual nuclei  $^{23}\text{Ne}$ ,  $^{20}\text{F}$ ,  $^{22}\text{Ne}$  and  $^{19}\text{F}$  there are no level density parameters listed by Gilbert and Cameron, and the initial parameters were estimated by extrapolation of parameters for similar nuclei, and then adjusted to match the number of observed levels, based on experimental level information in EN73. These level densities

were then used for initial calculations, and further adjusted to reproduce available cross section data for higher excitation energies where the level densities take over from the discrete levels. Table L lists final level density parameters as well as the incident neutron energy at which the continuum starts for the various reactions, and we note that level densities for  $^{19}\text{F}$ ,  $^{22}\text{Ne}$  and  $^{22}\text{Na}$  are only important for  $E_n \gtrsim 15$  MeV.

Spins and parities of levels in  $^{23}\text{Na}$  were taken mainly from the compilation of Endt and Van der Leun (EN73). Spins of some of the higher lying levels were estimated based on systematics. Results of Thornton *et al.* (TH78), available after the evaluation was complete, confirmed the values of the estimated spins and parities. Spins and parities for levels in  $^{23}\text{Ne}$  were taken from EN73 and supplemented by experimental and theoretical data from Christiansson *et al.* (CH74). Spins and parities for  $^{20}\text{F}$  were taken from Ajzenberg-Selove (SE72), Pronko (PR73), Fortune and Betts (F074) and Fortune and Garrett (F076). No consistent  $J^\pi$  information was available for the levels at 3.175, 3.769 and 3.974 MeV. For  $^{22}\text{Ne}$ , spins and parities were taken from EN73. In the latest evaluation of Endt and Van der Leun (EN78), the  $J^\pi$  value of the 5.914-MeV level was changed to  $3^-$ . For  $^{19}\text{F}$ , spins and parities were taken from SE72. For  $^{22}\text{Na}$ , spins and parities were taken from EN73, with estimates of  $J^\pi$  for levels at 4.294, 4.583 and 4.622 MeV. The excitation energies, spins and parities adopted for the calculations are given in Table M.

Branching ratios for gamma-ray transitions in the final nuclei were needed for the gamma-ray production calculations. For  $^{23}\text{Na}$ , the branching ratios were obtained from EN73, with the branching ratios from the 6.117-MeV level being estimated. The branching ratios for the 5.967-MeV level were taken from DI73. For  $^{23}\text{Ne}$ , the work of CH74 provided the ratios, while for  $^{20}\text{F}$  the branching ratios were taken from SE72 and PR73, the results being averaged for most levels. The  $^{22}\text{Ne}$  results were taken from EN73, and the  $^{19}\text{F}$  branching ratios were obtained from SE72. The branching ratios for  $^{22}\text{Na}$  were also taken from EN73. The branching ratios used in the calculations are listed in Table N.

The optical model parameters, discrete level information and level densities were used as input to the multistep Hauser-Feshbach code TNG. An earlier version of this code was used for the calculations discussed in

this paper, prior to the fully consistent treatment of the compound and precompound reactions. At the time of the model calculations (late 1977) the code treated the competition among the binary reaction channels in the usual Hauser-Feshbach formalism, and also treated competition between the various tertiary reaction channels, with angular momentum conservation being taken into account in all final channels. An approximate angular momentum conservation scheme was utilized for the precompound part of the calculation, and is described in Ref. FU77. The  $(n,n')$ ,  $(n,p)$  and  $(n,\alpha)$  channels were included in the binary step of the calculations, and above  $\sim 9$  MeV, the  $(n,n')$  channel was split into the  $(n,2n) + (n,np) + (n,n\alpha)$  tertiary channels as the Q-values allowed these channels to open. In the calculations for the V5 evaluation, the  $(n,p)$  and  $(n,\alpha)$  channels were not allowed to split into their tertiary components, namely  $(n,p\gamma+n,pn)$  and  $(n,\alpha\gamma+n,\alpha n)$ . However, during the Phase I reviews of the evaluations, the calculations were redone, with full competition allowed among all competing channels, and results for the  $(n,p\gamma)$  and  $(n,\alpha\gamma)$  channels were found to be in good agreement with available activation data for these channels. An improved numerical treatment of inelastic scattering to the continuum resulted in a small increase in the  $(n,2n)$  cross section such that it is in very good agreement with the experimental results of Liskien and Paulsen (LI65) and Paulsen (PA65).

Experimental data reproduced by these calculations include inelastic scattering to levels up to 5.8 MeV excitation energy in  $^{23}\text{Na}$  (Table F),  $^{23}\text{Na}(n,p)$  and  $(n,\alpha)$  activation measurements (Tables G and H), a neutron production measurement by Hermsdorf *et al.* (HE75), and a gamma-ray-production measurement (LA78), calculated from 1 to 20 MeV. Results of the inelastic scattering cross sections are compared with the available data and V5 evaluation in Figs. 35 through 56. Calculated results for the  $(n,p)$  and  $(n,\alpha)$  cross sections are shown in Figs. 111 and 112. Note that only the  $(n,p\gamma)$  and  $(n,\alpha\gamma)$  components of the  $(n,p)$  and  $(n,\alpha)$  reactions are obtained via the activation measurements. These calculated results, obtained after completion of V5, are in good agreement with preliminary results used in V5. These figures illustrate the importance of including competition between the tertiary channels in order to properly interpret the measured data. The calculated neutron emission spectrum (in 0.5-MeV bins) is compared with

the data of Hermsdorf *et al.* (HE75) in Fig. 113. The separate components of the total emission spectra are also shown, and we see the importance of properly treating the competition among the various reactions. In particular, the energy spectra for the (n,2n) and (n,n' $\gamma$ ) spectra are not well represented by the evaporation shapes actually used in the V5 evaluation. The calculated gamma-ray-production results are described in more detail in Ref. LA80, and are compared with the measured spectra in Figs. 114 through 130.

#### D. Distorted Wave Born Approximation Calculations for Inelastic Scattering

The final application of model codes was the use of the Distorted Wave Born Approximation (DWBA) code DMUCK (KU72a) to predict the direct interaction component of inelastic scattering to the 440-keV level in  $^{23}\text{Na}$ . Neutron optical model parameters given in Table K were used, and a collective model form factor provided an adequate fit to the 17.5-MeV (p,p') measurement of CR68. A deformation parameter  $\beta = 0.1$  was extracted by normalization of the calculations to the data, and used to predict the direct interaction cross section for the 440-keV level for incident neutron energies from 2-20 MeV. This cross section was then used as input to TNG, whose results for the nonelastic cross section were internally renormalized to account for the externally added direct interaction cross section. This significantly improved the model prediction for inelastic scattering to the 440-keV level.

Results of the model calculations were used for guidance in evaluating the inelastic scattering cross sections for V5, the evaluation being based on data where available. The (n,p) and (n, $\alpha$ ) cross sections are guided by the calculations above 11 MeV, where the measured data only reflect single components of the total reactions. The calculations were used for the (n,2n) cross section, in view of the discrepant experimental information. This aspect of the evaluation is treated in more detail in Ref. LA80a. Finally, the gamma-ray-production cross sections were taken from the measurement of LA78, which were in good agreement (up to 14 MeV) with results of the model calculations. Discrepancies below  $\sim E_n = 3.0$  MeV and above 15.5 MeV are discussed in Ref. LA80. In future evaluations, the calculated energy distributions for the (n,2n) and (n,n') reactions should be used, since

they provide a better representation of the available data than the simple evaporation model.

## 22. SUMMARY AND CONCLUSIONS

In the first evaluation of sodium for ENDF/B since 1971, significant changes have been made. The total cross section has been completely revised, including new resonance parameters for the important 2.81-keV resonance. The capture width of the 2.81-keV resonance has been lowered from 0.47 eV to 0.353 eV, based on new information, so as to give the correct thermal capture of 528 mb, and the neutron width  $\Gamma_n$  was lowered from 410 to 376 eV. The resolved resonance region has been extended from 160 keV to 500 keV, based on a multilevel analysis of new experimental results. The minimum of the 300-keV resonance, important for shielding problems, has been carefully defined. The capture cross section has also been changed significantly up to 500 keV. Inelastic scattering from the 440-keV level has been lowered by 5-15% from threshold up to  $E_n = 2.4$  MeV, and modified from 2.4 to 20 MeV. Changes have also been made, based on new experimental data and model calculations, for inelastic scattering from levels up to  $E_x = 5.8$  MeV. The (n,2n) cross section has been increased by a factor of  $\sim 2$  at 16 MeV and  $\sim 4$  at 20 MeV (to 200 mb) based on results of extensive model calculations. The elastic scattering angular distribution file has been extensively modified from 500 keV to 2 MeV to reflect recently measured structure in this cross section. Gamma-ray-production has been significantly modified for incident neutron energies above 8 MeV. Information about radioactive decay of product nuclei has been included. Uncertainty files for all cross sections except the angular and energy distributions and gamma-ray production have been included for the first time.

Further measurements would be useful for both  $\Gamma_n$  and  $\Gamma_\gamma$  of the 2.81-keV resonance. Inelastic scattering data for the 440-keV level to better determine its magnitude from threshold to 20 MeV are needed. Inelastic scattering data for all levels above  $E_n = 8$  MeV are also needed. New data to help resolve the present (n,2n) cross section discrepancy would be most helpful for future evaluations, and new (n,p $\gamma$ ) and (n, $\alpha\gamma$ ) activation data from 8-20 MeV are needed, especially from  $\sim 10$ -14 MeV. Finally, more detailed

discussions of experimental uncertainties and correlations in measurements are desperately needed to provide a basis for deriving more meaningful uncertainty files in future evaluations.

Future evaluation work on sodium should include an estimate of the  $(n,d)$ ,  $(n,t)$  and  $(n,^3\text{He})$  cross sections, a unified resonance parameter analysis including data from  $\sim 60$  eV to 500 keV for both neutron and capture data simultaneously, and a better treatment of inelastic scattering, giving cross section values for all discrete levels out to 20 MeV. The "pseudo levels" for  $E_x \gtrsim 5.8$  MeV should not be used, but included in the inelastic continuum cross section. The energy distribution of neutrons from the continuum should be taken from self-consistent nuclear model calculations, reflecting competition from other channels. The tertiary reactions  $(n,np)$ ,  $(n,n\alpha)$ ,  $(n,pn)$  and  $(n,\alpha n)$  should be explicitly given rather than included in the inelastic continuum as presently done. Also, the energy distribution of neutrons from the  $(n,2n)$  reaction should be represented as a probability distribution taken from the model calculations, rather than the simple evaporation form. The  $(n,\alpha)$  reaction needs to be looked at more carefully for  $E_n > 10$  MeV if no new data become available. Finally, more attention should be paid to cross section uncertainties and the correlations among the data sets should be represented more accurately.

#### ACKNOWLEDGEMENTS

The author wishes to thank D. M. Hetrick for making all the figures in this report, C. Y. Fu for helpful discussions concerning the use of TNG, and Jan Lundy for typing and assembling the report.

## REFERENCES

- A673 U. Abbondanno, R. Giacomich, M. Lagonegro and G. Pauli, *J. Nucl. Energy* 27, 227 (1973).
- AD49 R. K. Adair, H. H. Barschall, C. K. Bockelman and O. Sala, *Phys. Rev.* 75, 1124 (1949).
- AL61 D. L. Allan, *Nucl. Phys.* 24, 274 (1961).
- AR73 J. Araminowicz and J. Dresler, "Investigation of the (n,2n) Reactions at 14.6 MeV for 42 Nuclides," Report INR-1464, p. 14 (1973).
- BA59 S. J. Bame, Jr. and R. L. Cubitt, *Phys. Rev.* 113, 256 (1959).
- BA66 R. Bass, P. Haug, K. Krüger and B. Staginnus, "Fast Neutron Excitation Functions by Activation Techniques," and R. Bass, Fatma Saleh and B. Staginnus, "Fast Neutron Cross Sections of  $^{23}\text{Na}$  by Spectroscopy of Prompt Charged Particles in NaJ and Coincident Gamma Rays," EANDC(U)66, p. 64 (1965).
- BA69 R. C. Barrali, J. A. Holmes and M. Silbergeld, "High Energy Neutron Cross Section Validation and Neutron Flux Spectrum Using the HENRE Source," Report AFWL-TR-68, p. 134 (1969).
- BA75 C. M. Bartle, *Nucl. Instrum. Methods* 124, 547 (1975).
- BE67 I. Bergquist, J. A. Biggerstaff, J. H. Gibbons and W. M. Good, *Phys. Rev.* 158, 1049 (1967).
- BI62 F. G. Bizzeti, A. M. Bizzeti-Sona and M. Bocciolini, *Nucl. Phys.* 36, 38 (1962).
- BL66 R. C. Block, *Phys. Rev.* 109, 1217 (1958).
- BR75 P. H. Brown, B. L. Quan, J. J. Weiss and R. C. Block, *Trans. Am. Nucl. Soc.* 21, 505 (1975).
- BU71 P. S. Buchanan, D. J. Nellis and W. E. Tucker, "A Compilation of Cross Sections and Angular Distributions of Gamma Rays Produced by Neutron Bombardment of Various Nuclei," Report ORO-2791-32 (1971).
- CH66 J. F. Chien and A. B. Smith, *Nucl. Sci. Eng.* 26, 500 (1966).
- CH74 J. E. Christiansson, J. Dubois, H. Odelius and H. Roth, *Physica Scripta* 10, 65 (1974).
- CI68 S. Cierjacks, P. Forti, D. Kopsch, L. Kropp, J. Neve and H. Unsel, "High Resolution Total Neutron Cross Sections Between 0.5 to 30 MeV," Karlsruhe Report KFK-1000 (June 1968).
- CI69 S. Cierjacks, P. Forti, D. Kopsch, L. Kropp and J. Nebe, *Phys. Lett.* 29B, 417 (1969).
- CL70 E. Clayton, *Aust. J. Phys.* 23, 823 (1970).
- C071 R. E. Coles, "Elastic and Inelastic Scattering of 5.0 MeV Neutrons by Sodium," Report AWRE/O-3/71 (1971).
- CR68 G. M. Crawley and G. T. Garvey, *Phys. Rev.* 167, 1070 (1968).
- CS67 J. Csikai and S. Nagy, *Nucl. Phys.* A91, 222 (1967).

- CS67a J. Csikai, G. Petö, M. Buczkó, Z. Miligy and N. A. Eissa, Nucl. Phys. A95, 229 (1967).
- DA69 W. Dabrowska, B. Sikorska, J. Toke and E. Wesolowski, "(n,d) Reactions on  $^{23}\text{Na}$ ,  $^{35}\text{Cl}$ ,  $^{39}\text{K}$ ,  $^{41}\text{K}$ ,  $^{89}\text{Y}$  and  $^{141}\text{Pr}$  at 14.1 MeV," Report INDC(P01)-2/G (1969).
- deS78 G. de Saussure, D. K. Olsen and R. B. Perez, "SIOB: A Fortran Code for Least-Squares Shape Fitting Several Neutron Transmission Measurements Using the Breit-Wigner Multilevel Formula," Report ORNL/TM-6286 (May 1978).
- DI73 J. K. Dickens, Nucl. Sci. Eng. 50, 98 (1973).
- D077 D. R. Donati, S. C. Mathur, E. Sheldon, B. K. Barnes, L. E. Beghian, P. Harihar, G. H. R. Kegel and W. A. Schier, Phys. Rev. C16, 939 (1977).
- EL64 A. J. Elwyn, J. E. Monahan, R. O. Lane and A. Langsdorf, Jr., Nucl. Phys. 59, 113 (1964).
- EN67 F. C. Engesser and W. E. Thompson, J. Nucl. Energy 21, 487 (1967).
- EN73 P. M. Endt and C. Van der Leun, Nucl. Phys. A214, 1 (1973).
- EN78 P. M. Endt and C. Van der Leun, Nucl. Phys. A310, 1 (1978).
- FA68 M. Fazio, P. Guazzoni, S. Micheletti, M. Pignanelli and L. Zetta, Nucl. Phys. A111, 255 (1968).
- FA69 U. Fasoli, D. Toniolo, G. Zago and V. Benzi, Nucl. Phys. A125, 227 (1969).
- FA73 U. Fasoli, D. Toniolo, G. Zago, V. Benzi, P. L. Ottaviani and L. Zuffi, "Elastic and Inelastic Scattering of Neutrons by Na at 8.0, 9.7 and 14.1 MeV," Report CEC(73)7 (1973).
- FL67 F. Flesch and P. Hille, Oesterr. Akad. Wiss. 176, 45 (1967).
- F071 D. G. Foster, Jr. and D. W. Glasgow, Phys. Rev. C3, 576 (1971).
- F074 H. T. Fortune and R. R. Betts, Phys. Rev. C10, 1292 (1974).
- F076 H. T. Fortune and J. D. Garrett, Phys. Rev. C14, 1595 (1976).
- FR58 J. M. Freeman and J. H. Montague, Nucl. Phys. 9, 181 (1958).
- FR68 S. J. Friesenhahn, W. M. Lopez, F. H. Fröhner, A. D. Carlson and S. G. Costello, "Radiation Width of the 2.85-keV Resonance in  $^{23}\text{Na}$ ," Conf. on Neutron Cross Sections for Technology, Washington, p. 695 (1968).
- FU76 C. Y. Fu, Atomic Data and Nuclear Data Tables 17, 127 (1976).
- FU77 C. Y. Fu, "Multi-Step Hauser-Feshbach Codes with Precompound Effects: A Brief Review of Current and Required Developments and Applications up to 40 MeV," Proc. Symposium on Neutron Cross Sections from 10 to 40 MeV, Brookhaven National Laboratory, Report BNL-NCS-50681 (1977).
- FU79 C. Y. Fu, "A Consistent Nuclear Model for Compound and Precompound Reactions with Conservation of Angular Momentum," Report ORNL/TM-7042 (May 1980).

- GA65 J. B. Garg, J. Rainwater, S. Wynchank and W. W. Havens, Jr., EANDC Conference on Study of Nuclear Structure with Neutrons, Antwerp (1965).
- GA67 J. D. Garrison and M. K. Drake, "Neutron and Gamma-Ray-Production Cross Sections for Sodium, Magnesium, Chlorine, Potassium and Calcium," Report NDL-TR-89-II (1967).
- G058 W. M. Good, J. H. Neiler and J. H. Gibbons, Phys. Rev. 109, 926 (1958).
- G072 N. B. Gove and A. H. Wapstra, Nucl. Data Tables 11, 127 (1972).
- GR66 R. C. Greenwood, Phys. Lett. 23, 482 (1966).
- HE69 J. Hellstrom, P. J. Dallimore and W. F. Davidson, Nucl. Phys. A132, 581 (1969).
- HE75 D. Hermsdorf, A. Meister, S. Sassonoff, D. Seeliger, K. Seidel and F. Shahin, "Differential Neutron Emission Cross Sections  $\sigma(E_0, E, \theta)$  for 14.6 MeV Incident Energy for Elements Be, C, Na, Mg, Al, Si, P, S, Ca, Ti, V, Cr, Mn, Fe, Co, Ni, Cu, Zn, Ga, Se, Br, Zr, Nb, Cd, In, Sn, Sb, I, Ta, W, Au, Hg, Pb and Bi," Report ZFK-277, INDC(GDR)-2/L (1975).
- HI52 C. T. Hibdon, A. Langsdorf, Jr. and R. E. Holland, Phys. Rev. 85, 595 (1952).
- HI60 C. T. Hibdon, Phys. Rev. 118, 514 (1960).
- H052 E. R. Hodgson, J. F. Gallagher and E. M. Bowey, Proc. Phys. Soc. A 65, 992 (1952).
- H069 R. W. Hockenbury, Z. M. Bartolome, J. R. Tatarczuk, W. R. Moyer and R. C. Block, Phys. Rev. 178, 1746 (1969).
- JA73 J. Janczyszyn and L. Gorski, J. Radioanalytical Chem. 14, 201 (1973).
- JA76 H. E. Jackson, "Review of Standard Reference Data and Important Cross Section Discrepancies," Report NEANDC-105/L (November 1976).
- J055 E. G. Joki, L. G. Miller and J. E. Evans, Phys. Rev. 99, 610 (1955).
- KA65 L. Ya. Kasakova, V. E. Kolesov, V. I. Popov, O. A. Salnikov, V. M. Sluhevskaja and V. I. Trikova, "Elastic Scattering of Neutrons with Initial Energy 2 MeV," Antwerp Conference (1965).
- KH65 C. S. Khurana and I. M. Govil, Nucl. Phys. 69, 153 (1965).
- KI76 W. E. Kinney and F. G. Perey, "High Resolution Elastic Scattering Angular Distributions from 550 keV to 2 MeV," private communication from W. E. Kinney (deceased); technique discussed in Nucl. Sci. Eng. 63, 418 (1977).
- K065 I. A. Korzh, N. S. Kopitin, M. V. Pasechnik, N. M. Pravdivii, N. T. Sklyar and I. A. Totskii, J. Nucl. Energy 19, 141 (1965).
- KU72 P. Kuijper, J. C. Veeffkind and C. C. Jonker, Nucl. Phys. A181, 545 (1972).
- KU72a P. D. Kunz, "Distorted Wave Code DWUCK72," Univ. of Colorado, unpublished (1972).
- LA57 A. Langsdorf, Jr., R. O. Lane and J. E. Monahan, Phys. Rev. 107, 1077 (1957)

- LA60 R. O. Lane and J. E. Monahan, Phys. Rev. 118, 533 (1960).
- LA73 J. Lachkar, Y. Patin and J. Sigaud, "Sections Efficaces de Production des Rayonnements  $\gamma$  Emis par les Reactions  $^{23}\text{Na}(n,n'\gamma)$ ,  $^{58}\text{Ni}(n,n'\gamma)$   $^{60}\text{Ni}(n,n'\gamma)$ ," Nat'l. Soviet Conf. on Neutron Physics, Kiev (1973).
- LA76 D. C. Larson, J. A. Harvey and N. W. Hill, "Measurement of the Neutron Total Cross Section of Sodium from 32 keV to 37 MeV," Report ORNL-TM-5614 (October 1976).
- LA78 D. C. Larson and G. L. Morgan, "The  $\text{Na}(n,x\gamma)$  Reaction Cross Section for Incident Neutron Energies between 0.2 and 20.0 MeV," Report ORNL/TM-6281 (May 1978).
- LA79 D. C. Larson, "Evaluation of  $^{23}\text{Na}$  for ENDF/B-V," Paper AB6, Proc. Int. Conf. on Nuclear Cross Sections for Technology, Bull. Am. Phys. Soc. 24, 863 (1979).
- LA80 D. C. Larson and G. L. Morgan, "Measurement and Analysis of the  $^{23}\text{Na}(n,x\gamma)$  Reaction Cross Section for  $0.2 \leq E_n \leq 20$  MeV," Nucl. Sci. Eng. 75, 151 (1980).
- LA80a D. C. Larson, "Evaluation of the  $^{23}\text{Na}(n,2n)$  Reaction for ENDF/B-V," submitted to Nucl. Sci. Eng.
- LI61 D. A. Lind and R. B. Day, Ann. Phys. 12, 485 (1961).
- LI65 H. Liskien and A. Paulsen, Nucl. Phys. 63, 393 (1965).
- I.U66 B. T. Lucas, S. W. Cospser and O. E. Johnson, Phys. Rev. 144, 972 (1966).
- LY58 J. E. Lynn, F. W. K. Firk and M. C. Moxon, Nucl. Phys. 5, 603 (1958).
- MA65 P. W. Martin and D. L. Stewart, J. Nucl. Energy A/B 19, 447 (1965).
- MA70 R. E. Maerker and F. J. Muckenthaler, Nucl. Sci. Eng. 42, 335 (1970).
- MA72 G. N. Maslov, F. Nasyrov and N. F. Pashkin, "The Experimental Cross Sections of the Nuclear Reactions for 14 MeV Neutrons," Obninsk Report YK-9, p. 50 (1972).
- MA74 A. N. Malen, N. N. Kaushal, B. K. Malaviya and E. R. Gaerttner, "Assessments of Cross-Section Data Files for Sodium," Trans. Am. Nucl. Soc. 18, 311 (1974).
- MA76 R. L. Macklin, "Value of 2.81 keV  $\Gamma_\gamma$ ," private communication, ORNL, (1976).
- MA76a R. E. Maerker, C. E. Clifford and F. J. Muckenthaler, "Neutron Total Cross Section Checks for Iron, Chromium, Nickel, Stainless Steel, Sodium and Carbon," Report ORNL-5013 (April 1976).
- ME59 E. Merzbacher, P. W. Crutchfield, Jr. and H. W. Newson, Ann. Phys. 8, 194 (1959).
- ME67 H. O. Menlove, K. L. Coop, H. A. Grench and R. Sher, Phys. Rev. 163, 1308 (1967).
- ME67a H. O. Menlove, K. L. Coop, H. A. Grench and R. Sher, Phys. Rev. 163, 1299 (1967).
- MI66 B. Mitra and A. M. Ghose, Nucl. Phys. 83, 157 (1966).

- MO66 M. C. Moxon and N. J. Pattenden, "Low-Energy Neutron Cross-Sections of Sodium," First IAEA Conf. on Nucl. Data for Reactors, Paris, Vol. 1, 129 (1966).
- MO76 C. E. Moss, Nucl. Phys. A269, 429 (1976).
- MU77 A. R. deL. Musgrove, B. J. Allen and R. L. Macklin, "The Radiative Capture Cross Section of Sodium above 3 keV," Proc. Int. Conf. on Neutron Physics and Nucl. Data for Reactors, Harwell, United Kingdom, p. 426 (September 1978).
- NI69 L. W. Nichol, A. H. Colenbrander and T. J. Kennett, Can. J. Phys. 47, 953 (1969).
- OB76 E. M. Oblow, "Survey of Shielding Sensitivity Analysis Development and Applications Program at ORNL," Report ORNL/TM-5176 (January 1976).
- OR70 V. J. Orphan, N. C. Rasmussen, T. L. Harper, J. Cunningham and S. A. Ali, "Line and Continuum Gamma-Ray Yields from Thermal-Neutron Capture in 75 Elements," Gulf General Atomic Report GA-10248 (July 1970).
- PA65 A. Paulsen, private communication to CCDN (1965).
- PA67 A. Pasquarelli, Nucl. Phys. A93, 218 (1967).
- PE67 F. G. Perey, computer code GENOA, ORNL, unpublished (1967).
- PE70 F. G. Perey and W. E. Kinney, "Neutron Elastic and Inelastic Scattering Cross Sections for Na in the Range of 5.4 to 8.5 MeV," Report ORNL-4518 (1970).
- PE71 F. G. Perey, W. E. Kinney and R. L. Macklin, "High Resolution Inelastic Cross Section Measurements for Na, Si and Fe," Third Conf. on Neutron Cross-Sections and Technology, Knoxville, Tenn., p. 191 (1971).
- PI65 J. Picard and C. Williamson, Nucl. Phys. 63, 673 (1965).
- PI68 T. A. Pitterle, "Evaluated Neutron Cross Sections of Sodium-23 for the ENDF/B File," Atomic Power Development Associates, Inc., Report APDA-217 (ENDF-121) (June 1968).
- PI72 T. A. Pitterle and N. C. Paik, "Evaluation of Sodium-23 Neutron Data for the ENDF/B Version III File," Westinghouse Advanced Reactors Division Quarterly Progress Report WARD-3045T4B-2, Appendix A (June 1972).
- P072 V. I. Popov and V. I. Trykova, "Elastic and Inelastic Scattering of Neutrons with Initial Energy 4.37 MeV," Conf. on Neutron Physics, Kiev (1971).
- PR55 R. J. Prestwood, Phys. Rev. 98, 47 (1955).
- PR66 R. Prasad and D. C. Sarkar, Nucl. Phys. 85, 476 (1966).
- PR73 J. G. Pronko, Phys. Rev. C7, 127 (1973).
- RA73 F. Rahn, H. S. Camarda, G. Hacken, W. W. Havens, Jr., H. I. Liou, J. Rainwater, U. N. Singh, M. Slagowitz and S. Wynchank, Phys. Rev. C8, 1827 (1973).
- RY70 T. B. Ryves and D. R. Perkins, J. Nucl Energy 24, 419 (1970).
- SA65 B. Saeki, Nucl. Phys. 73, 631 (1965).

- SE50 W. Selove, Phys. Rev. 80, 290 (1950).
- SE72 F. Ajzenberg-Selove, Nucl. Phys. A190, 1 (1972).
- SE74 J. Seltzer and F. W. K. Firk, Nucl. Sci. Eng. 53, 415 (1974).
- SH51 C. G. Shull and E. O. Wollan, Phys. Rev. 81, 527 (1951).
- SH74 R. Sher, "2200 m/s Neutron Activation Cross Sections," Contribution to *Handbook on Nuclear Activation Cross Sections*, Technical Reports Series 156, IAEA, Vienna (1974).
- SM70 D. L. Smith, "Fast Neutron Inelastic Gamma-Ray Studies of Arsenic and Sodium," Report ANL-7710, p. 15 (1971).
- SM77 D. L. Smith, "Measurement of Cross Sections for the  $^{23}\text{Na}(n,n'\gamma)^{23}\text{Na}$  Reaction near Threshold," Nucl. Sci. Eng. 64, 897 (1977).
- ST65 J. E. Strain and W. J. Ross, "14-MeV Neutron Reactions," Report ORNL-3672 (1965).
- ST65a T. W. Stephenson, "The Neutron Cross Section of Sodium Below 40 keV," Brookhaven National Laboratory Report BNL-651 (1965).
- ST71 P. Stoler, P. F. Yergin, J. C. Clement, C. G. Goulding and R. Fairchild, "The MeV Total Neutron Cross Section Program at RPI," Third Conf. on Neutron Cross Sections and Technology, Knoxville, Tenn., p. 311 (1971).
- TH78 S. T. Thornton, D. E. Gustafson, K. R. Cordell, L. C. Dennis and T. C. Schweizer, Phys. Rev. C17, 576 (1978).
- T055 A. L. Toller, H. W. Newson and E. Merzbacher, Phys. Rev. 99, 1625 (1955).
- T062 J. H. Towle and W. B. Gilboy, Nucl. Phys. 32, 610 (1962).
- T067 J. H. Towle and R. O. Owens, Nucl. Phys. A100, 257 (1967).
- WI61 C. F. Williamson, Phys. Rev. 122, 1877 (1961).
- WI77 W. M. Wilson, H. E. Jackson and G. E. Thomas, Nucl. Sci. Eng. 63, 55 (1977).
- W048 E. O. Wollan and C. G. Shull, Phys. Rev. 73, 830 (1948).
- W066 G. Woelfer and M. Bormann, Z. Physik 194, 75 (1966).
- YA70 N. Yamamuro, R. W. Hockenbury, R. C. Block and R. H. Wolfe, Nucl. Sci. Eng. 41, 445 (1970).
- Y077 P. G. Young, private communication from P. G. Young, LASL (1977).
- ZI77 W. L. Zijp, "Reactor Core Dosimetry Standards," Proc. Symposium on Neutron Standards and Applications, NBS Report 493 (1977).

## LIST OF TABLES

	<u>Page</u>
A Q Values and Thresholds . . . . .	43
B Resonance Parameters . . . . .	44
C Total Elastic Scattering Cross Sections . . . . .	45
D Total Inelastic Scattering Cross Sections . . . . .	46
E (n,2n) Cross Section Data . . . . .	46
F (n,n') Cross Section References . . . . .	47
G (n,p) Cross Section Data . . . . .	48
H (n, $\alpha$ ) Cross Section Data . . . . .	48
I (n,n') Angular Distribution Data . . . . .	49
J Gamma-Production Cross Section Comparisons . . . . .	50
K Optical Model Parameters . . . . .	51
L Level Density Parameters . . . . .	51
M Excitation Energies and $J^\pi$ Values Adopted for V5 . . . . .	52
N Branching Ratios Adopted for V5 . . . . .	53

Table A. Q-Values and Thresholds for  
Neutron-Induced Reactions on  $^{23}\text{Na}$   
Included in this Evaluation.

Reaction	Q-Value (MeV)	Neutron Threshold (MeV)
$^{23}\text{Na}(n,\gamma)^{24}\text{Na}$	6.959	—
$^{23}\text{Na}(n,n)^{23}\text{Na}$	0.0	—
$^{23}\text{Na}(n,n')^{23}\text{Na}^*$	-0.440	.459
$^{23}\text{Na}(n,p)^{23}\text{Ne}$	-3.597	3.755
$^{23}\text{Na}(n,\alpha)^{20}\text{F}$	-3.866	4.036
$^{23}\text{Na}(n,np)^{22}\text{Ne}$	-8.793	9.179
$^{23}\text{Na}(n,\alpha\alpha)^{19}\text{F}$	-10.468	10.927
$^{23}\text{Na}(n,2n)^{22}\text{Na}$	-12.414	12.950

Table B.  $n + {}^{23}\text{Na}$  Resonance Parameters given  
in ENDF/B-IV and ENDF/B-V.

$E_R$ (keV)	$\Gamma_n$ (eV)	$\Gamma_\gamma$ (eV)	J	$\ell$
2.81±.04 (2.85)	376±15 (410)	0.353±0.05 (0.47)	1 (1)	0 (0)
7.617±.010 (7.53)	0.0058±0.003 (0.012)	0.6±0.30 (1.5)	2 (1)	1 (1)
35.39±.12 (35.4)	1.6±0.8 (0.86)	1.9±0.3 (0.76)	1 (3)	1 (1)
53.22±.04 (53.0)	1112±16 (1200)	0.785±0.270 (1.48)	2 (2)	1 (1)
117.43±.02 (114.7)	26.8±3.2 (11.0)	4.23±1.38 (2.72)	1 (2)	1 (0)
143.13±.08 (139.1)	16.5±9.9 (3.33)	7.10±3.0 (1.5)	0 (2)	1 (1)
190.06±.15	18.2±9.0	9.30±4.69	0	2
201.15±.09	4925±76	2.94±0.36	1	1
214.30±.41	14280±241	4.64±0.96	0	1
236.71±.03	65.2±7.0	1.59±0.42	2	2
239.05±.07	5349±53	1.20±0.12	2	1
242.97±.03	328±18	1.50±0.78	1	0
298.32±.04	2038±26	1.02±0.09	2	0
299.41±.05	130±15	2.56±0.77	1	1
305.20±.20	68.3±34.6	9.70±4.90	0	2
392.32±.36	22760±247	9.87±1.55	1	1
430.90±.44	4000±375	5.29±1.58	0	2
448.82±.18	7026±167	3.52±0.65	2	2
538.57*	62770	10.14	1	0
598.0*	25800	—	1	1
697.0*	60000	—	4	2
727.0*	45000	—	3	1
780.0*	44000	—	4	2

Parameters in parentheses are from V4. In addition, V4 has a resonance at 129.5 keV not included for V5. The asterisks designate resonances outside the resolved resonance region, but included in V5 for long-range effects. Resonance energies are in the lab system.

Table C. Neutron Scattering Measurements on Sodium.

Author	$E_{\min} - E_{\max}$ (MeV)	Measurement Type*	Ref.	$\sigma_{el}$ (b)
Chien & Smith	0.3-1.5	E	CH66	
Coles <i>et al.</i>	5.0±0.03	E	C071	0.88±0.04
Elwyn <i>et al.</i>	0.2-2.2	S	EL64	
Fasoli <i>et al.</i>	1.51±0.06	E	FA69	2.02±0.20
	2.47±0.04	E		2.79±0.28
	4.04±0.03	E		1.29±0.13
	6.40±0.08	S(E)		0.74±0.10
Fasoli <i>et al.</i>	8.0 ±0.15	S(E)	FA73	0.71±0.11
	9.7 ±0.30	S(E)		0.70±0.11
	14.1 ±0.05	S(E)		0.95±0.24
Kasakova <i>et al.</i>	2.0 ±0.10	E	KA65	2.6±0.30
Kuijper <i>et al.</i>	14.76±0.05	S(E)	KU72	0.95±0.08
Korzh <i>et al.</i>	0.3,0.5,0.8	S	K065	
Langsdorf <i>et al.</i>	0.03-1.37	S	LA57	
Lane & Monahan	0.2 - 0.8	S	LA60	
Perey & Kinney	5.44±0.17	E	PE70	0.97±0.07
	6.37±0.13	E		0.85±0.06
	7.60±0.10	E		0.72±0.05
	8.52±0.08	E		0.61±0.04
Popov & Trykova	4.37±0.18	E	P072	1.42±0.30
Towle & Gilboy	0.98±0.10	E	T062	3.52±0.11
	1.50±0.08	E		2.10±0.06
	2.52±0.06	E		2.44±0.08
	3.97±0.06	E		1.17±0.08
Kinney & Perey	0.5 - 2.0	E	KI76	

\* E - elastic scattering only

S - elastic and inelastic scattering to 440-keV level

(E) - estimate of inelastic scattering to 440-keV level has been subtracted

Table D. Total Inelastic Scattering Cross Sections.

Author	$E_n$	$\Delta E_x$	$\sigma$	$\sigma^{TNG}$	Total	Ref.
Donati <i>et al.</i>	3.02±0.07	0.44-2.64	811±92	21±2	832±94	D077
Donati <i>et al.</i>	4.03±0.04	0.44-2.98	867±119	21±2	888±121	D077
Dickens	4.85±0.20	0.44-4.78	814±92	—	814±92	DI73
Coles	5.00±0.03	0.44-3.92	805±69	16±2	821±71	D071
Dickens	5.40±0.15	0.44-4.78	893±98	—	893±98	DI73
Perey & Kinney	5.44±0.17	0.44-2.08	409±38	536±54	945±92	PE70
Dickens	5.90±0.15	0.44-5.74	910±106	—	910±106	DI73
Perey & Kinney	6.37±0.13	0.44-4.78	846±80	89±9	935±89	PE70
Dickens	6.45±0.15	0.44-5.97	975±129	15±2	990±131	DI73
Towle & Owens	7.00±0.15	2.08-6.06	786±24	206±21	992±45	T067
Dickens	7.00±0.15	0.44-6.12	895±120	41±5	936±120	DI73
Perey & Kinney	7.60±0.10	0.44-5.78	670±71	214±22	884±93	PE70
Perey & Kinney	8.52±0.08	0.44-5.78	534±52	375±38	909±90	PE70
Hermsdorf <i>et al.</i>	14.6±0.2	2.0-11.0	564±70	219±22	783±92	HE75

$\Delta E_x$  is the excitation energy range covered in the measurement, and  $\sigma$  is the cross section measured for this energy range.  $\sigma^{TNG}$  is the cross section calculated for the remaining levels not included in the measurement, and Total is the sum of  $\sigma + \sigma^{TNG}$  and gives the predicted total inelastic scattering cross section for the incident energy  $E_n$ .

Table E. (n,2n) Data References.

Author	Year	Number of Points	Energy Range of Measurement (MeV)	Reference
J. Araminowicz J. Dresler	1973	1	14.6	AR73
Barrar <i>et al.</i>	1969	1	14.6	BA69
Liskien and Paulsen	1965	16	12.6 - 16.6	LI65
Maslove <i>et al.</i>	1972	2	14.2, 14.6	MA72
Menlove <i>et al.</i>	1967	7	13.5 - 19.4	ME67
Paulsen	1965	7	17.3 - 19.6	PA65
Picard and Williamson	1965	6	14.9 - 21.0	PI65
Prestwood	1955	1	14.1	PR55

Table F. Inelastic Scattering Measurements.

Author	Ref.	Particle Detected	$E_n$ (MeV)	$\Delta E_x^*$ (MeV)	Angle	Comments
Smith	SM77	gamma	0.50±0.08-2.04±0.06	0.440	55°	440-keV gamma ray angular distribution at 7 energies
Perey <i>et al.</i>	PE71	gamma	0.5-2.2	0.440	4π	high resolution
Colas	C071	n	5.0±0.025	0.44-3.92	30°-135°	(n,n') to 7 levels
Fasoli	FA69	n	1.51±0.06 2.47±0.04 4.04±0.03 6.40±0.08	0.44 0.44 0.44-2.98 2.08-4.43	20°-150° 20°-150° 20°-150° 20°-150°	(n,n') to 6 levels (n,r') to 4 groups of levels
Towle & Owens	T067	n	7.0±0.15	2.08-6.06	90°	4πσ(90°) for E' > .440 MeV
Chien & Smith	CH66	n	0.825±0.02-1.5±0.02	0.44	20°-145°	
Towle & Gilboy	T062	gamma	0.5±0.1-2.0±0.08	0.44	125°	4πσ(125°) excitation function
		n	0.98±0.1	0.44	30°-140°	
		n	1.50±0.08	0.44	30°-140°	
		n	2.52±0.065	0.44	30°-140°	
		n	3.97±0.60	2.08-2.98	30°-140°	(n,n') to 3 groups of levels
Freeman & Montague	FR58	gamma	0.49±0.05-3.7±0.05	0.44-2.39	90°	4πσ(90°) ring geometry
Fasoli <i>et al.</i>	FA73	n	8.0±0.15	2.08-5.53	20°-150°	(n,n') to 3 groups of levels
Perey & Kinney	PE70	n	5.44±0.17 6.37±0.13 7.60±0.10 8.52±0.08	0.44-2.08 0.44-4.78 0.44-5.78 0.44-5.78	50°-115° 30°-140° 30°-140° 30°-140°	nearly all levels resolved ↓
Donati <i>et al.</i>	D077	gamma	0.52± - 4.23±	0.44-2.98	25°-135°	(n,n') cross sections extracted from gamma production data, gamma ray angular distribution
Dickens	D173	gamma	5.40±0.15 5.90±0.15 6.45±0.15 7.00±0.15	0.44-4.78 0.44-5.74 0.44-5.97 0.44-6.12	125°	(n,n') cross sections extracted from gamma production data from 4πσ(125°)
Smith	SM70	gamma	0.75 -1.55	0.44	50°-110°	
Lind & Day	LI61	gamma	0.44- 3.32	0.44-2.98	94°	4πσ(94°), (n,n') cross section data extracted from gamma production data
Larson & Morgan	LA78	gamma	0.4-2.0	0.44	125°	4πσ(125°) high resolution
Crawley & Garvey	CR68	proton	$E_p=17.5$	0.44	20°-140°	(p,p') result

\*  $\Delta E_x$  is the region of excitation energy covered in the measurement.

Table G. (n,p) Cross Section Measurements Used for ENDF/B-V.

Author	$\Delta E_{inc}^*$ (MeV)	# Points	Reference
Williamson	4.00-19.0	103	WI61
Bartle	5.51-8.56	34	BA75
Bass <i>et al.</i>	5.80-8.98	128	BA66
Picard & Williamson	14.18-21.0	12	PI65
Allan	14.0	1	AL61
Csikai & Nagy	14.7	1	CS57
Flesch & Hille	14.7	1	FL67
Pasquarelli	14.7	1	PA67
Khurana & Gov	14.8	1	KH55
Mitra & Ghose	14.8	1	MI66
Prasad & Sarkar	14.8	1	PR66

Table H. (n, $\alpha$ ) Cross Section Measurements Used for ENDF/B-V.

Author	$\Delta E_{inc}^*$ (MeV)	# Points	Reference
Williamson	6.30-19.0	39	WI61
Bartle	6.77-8.56	7	BA75
Bass <i>et al.</i>	6.80-8.98	88	BA66
Woelfer & Bormann	12.6-18.7	7	WO66
Picard & Williamson	14.18-21.0	12	PI65
Janczyszyn & Gorski	14.0	1	JA73
Bizzeti	14.05	1	BI62
Flesch & Hille	14.7	1	FL67
Strain & Ross	14.7	1	ST65

\* $\Delta E_{inc}$  is the range of incident energies covered in the measurement.

Table I. Inelastic Angular Distribution Measurements (n detected).

Author	Ref.	$\Delta E_{inc}^*$	$\Delta\theta$	$\Delta E_x^*$	Comments
Chien & Smith	CH66	0.825-1.5	20°-145°	.44	~ isotropic except 1.4
Towle & Gilboy	T062	.98±.1	30°-160°	.44	isotropic
		1.50±.08		.44	
		2.52±.06		.44	isotropic
		3.97±.60		2.08+2.39 2.64+2.71 2.98	all 3 groups isotropic
Fasoli <i>et al.</i>	FA69	1.51±.06	20°-150°	.44	{ all } dist. ~ isotropic
		2.47±.04		.44	
		4.04±.03		.44-2.98	
		6.40±.08			
Coles	C071	5.0±.025	30°-135°	.44-3.92	all isotropic
Perey & Kinney	PE70	5.44	50°-115°	.44-2.08	See text
		6.37	30°-140°	.44-4.78	
		7.60	30°-140°	.44-5.78	
		8.52	30°-140°	.44-5.78	
Fasoli <i>et al.</i>	FA73	8.0±.15	20°-150°	2.08-5.53	~ isotropic
Hermesdorf <i>et al.</i>	HE75	14.6±0.2	40°-150°	2.0-11.0	See text

\*  $\Delta E_{inc}$  is the range of incident energies covered in the measurement, and  $\Delta E_x$  is the region of excitation energy covered.

Table J. Comparison of Gamma-Ray-Production Results from Ref. LA78 with Results of Others.

Author	Ref.	$E_n$ (MeV)	$\Delta E_Y$ (MeV)	$\sigma$ (b)	Ref. LA78 (b)
Lind & Day	LI61	3.12	0.4-3.0	$0.76 \pm 0.06$	$0.85 \pm 0.09$
Donati <i>et al.</i>	DO77	4.25	0.4-3.0	$1.31 \pm 0.07$	$1.11 \pm 0.12$
Buchanan <i>et al.</i>	BU71	4.0	0.439	$0.70 \pm 0.09$	$0.64 \pm 0.06$
		4.0	0.4-3.3	$1.07 \pm 0.13$	$1.09 \pm 0.11$
		4.1	0.439	$0.63 \pm 0.13$	$0.63 \pm 0.06$
		5.0	0.4-4.0	$1.11 \pm 0.14$	$1.20 \pm 0.12$
Dickens	DI73	4.85	0.4-4.5	$1.20 \pm 0.14$	$1.15 \pm 0.12$
		5.40	0.4-4.5	$1.43 \pm 0.16$	$1.33 \pm 0.13$
		5.90	0.4-5.3	$1.48 \pm 0.17$	$1.40 \pm 0.15$
		6.45	0.4-5.9	$1.68 \pm 0.22$	$1.50 \pm 0.16$
		7.00	0.4-7.0	$1.52 \pm 0.20$	$1.58 \pm 0.16$
Lachkar <i>et al.</i>	LA73	6.3	0.4-3.0	$1.05 \pm 0.12$	$1.26 \pm 0.12$
		7.3	0.4-2.3	$0.87 \pm 0.09$	$1.11 \pm 0.11$
		8.3	0.4-4.0	$1.13 \pm 0.14$	$1.39 \pm 0.15$
		8.2	0.4-4.0	$1.13 \pm 0.15$	$1.39 \pm 0.15$
Martin & Stewart	MA65	14.1	0.439	$0.46 \pm 0.06$	$0.46 \pm 0.10$
Abbondanno <i>et al.</i>	AB73	14.1	0.439	$0.44 \pm 0.04$	$0.46 \pm 0.10$
			0.4-1.7	$0.87 \pm 0.05$	$0.89 \pm 0.10$
Engesser & Thompson	EN67	14.7	0.4-2.5	$1.10 \pm 0.15$	$1.14 \pm 0.15$
Buchanan <i>et al.</i>	BU71	14.8	0.5-6.5	$0.93 \pm 0.18$	$1.04 \pm 0.18$

Table K. Optical Model Parameters

	V (MeV)	$r_o$ (fm)	a (fm)	$W_D$ (MeV)	$r_I$ (fm)	$a_I$ (fm)
n + $^{23}\text{Na}$	42.84	1.292	0.629	10.25	1.198	0.486
n + $^{22}\text{Na}$						
n + $^{22}\text{Ne}$						
p + $^{23}\text{Ne}$	46.8	1.25	0.65	10.0	1.25	0.47
p + $^{22}\text{Ne}$						
$\alpha$ + $^{20}\text{F}$	84.4	1.55	0.58	13.2	1.55	0.58
$\alpha$ + $^{19}\text{F}$						
n + $^{19}\text{F}$	41.0	1.263	0.695	6.3	1.30	0.48

Table L. Level Density Parameters\* for Residual Nuclei

	$E_c$ (MeV)	$E_f$ (MeV)	$E_o$ (MeV)	T (MeV)	a (MeV $^{-1}$ )	c (MeV $^{-1}$ )	$\Delta$ (MeV)	$E_n^c$ (MeV)
$^{23}\text{Na}$	6.1	10.67	0.22	2.04	3.68	2.64	2.67	7.8
$^{23}\text{Ne}$	3.9	3.00	0.0	2.00	3.70	2.65	2.50	7.8
$^{20}\text{F}$	4.1	4.00	-0.30	1.59	3.68	2.50	0.0	8.4
$^{22}\text{Na}$	4.8	7.50	-2.00	2.23	3.13	2.25	0.0	17.9
$^{21}\text{Ne}$	6.0	14.6	0.50	2.07	4.08	2.93	4.75	15.4
$^{19}\text{F}$	5.4	10.4	0.70	1.73	2.41	1.47	-5.05	16.6

\*Level density formulas and symbol definitions are as given in Ref. FU76.  $E_n^c$  is the incident neutron energy at which the level density takes over from the discrete levels.

Table M. Adopted Excitation Energies, Spins and Parities.

$^{23}\text{Na}$		$^{23}\text{Ne}$		$^{20}\text{F}$		$^{22}\text{Na}$		$^{19}\text{F}$		$^{22}\text{Ne}$	
0.0	$3/2^+$	0.0	$5/2^+$	0.0	$2^+$	0.0	$3^+$	0.0	$1/2^+$	0.0	$0^+$
0.440	$5/2^+$	1.016	$1/2^+$	0.655	$3^+$	0.583	$1^+$	0.110	$1/2^-$	1.275	$2^+$
2.076	$7/2^+$	1.703	$7/2^+$	0.822	$4^+$	0.657	$0^+$	0.197	$5/2^+$	3.356	$4^+$
2.391	$1/2^+$	1.822	$3/2^+$	0.980	$1^-$	0.891	$4^+$	1.346	$5/2^-$	4.457	$2^+$
2.640	$1/2^-$	2.314	$5/2^+$	1.057	$1^+$	1.528	$5^+$	1.458	$3/2^-$	5.144	$2^-$
2.704	$9/2^+$	2.520	$9/2^+$	1.311	$2^-$	1.937	$1^+$	1.554	$3/2^+$	5.335	$1^+$
2.982	$3/2^+$	3.221	$3/2^-$	1.824	$5^+$	1.952	$2^+$	2.780	$9/2^+$	5.360	$2^+$
3.678	$3/2^-$	3.433	$3/2^+$	1.843	$2^-$	1.983	$3^+$	3.907	$3/2^+$	5.521	$4^+$
3.848	$5/2^-$	3.458	$1/2^+$	1.969	$3^-$	2.212	$1^-$	3.998	$7/2^-$	5.637	$3^+$
3.915	$5/2^+$	3.831	$7/2^-$	2.044	$2^+$	2.572	$2^-$	4.032	$9/2^-$	5.914	$2^+$
4.432	$1/2^+$	3.838	$1/2^-$	2.198	$3^+$	2.969	$3^+$	4.378	$7/2^+$		
4.776	$7/2^+$	3.843	$11/2^+$	2.867	$3^-$	3.060	$2^+$	4.555	$5/2^+$		
5.380	$5/2^+$			2.971	$3^+$	3.521	$3^-$	4.558	$3/2^-$		
5.536	$1/2^+$			3.175	$(2^+)$	3.708	$6^+$	4.648	$13/2^+$		
5.741	$3/2^+$			3.498	$1^+$	3.944	$1^+$	4.683	$5/2^-$		
5.766	$1/2^+$			3.533	$0^+$	4.071	$4^+$	5.106	$5/2^-$		
5.781	$1/2^+$			3.595	$3^+$	4.294	$(2^+)$	5.340	$1/2^+$		
5.931	$3/2^+$			3.687	$4^+$	4.319	$1^+$				
5.967	$3/2^-$			3.769	$(4^-)$	4.360	$2^+$				
6.043	$7/2^-$			3.974	$(2^+)$	4.466	$4^-$				
6.117	$11/2^+$			4.090	$1^+$	4.522	$7^+$				
						4.583	$(3^+)$				
						4.622	$(1^-)$				
						4.708	$5^+$				
						4.770	$3^+$				

Note:  $J^\pi$  values in parentheses are estimated, since data are non-existent or conflicting.

Table N. Branching Ratios Adopted for V5.

<b>23NA</b>																				
2	1	1	1	1	1	1	1	1	1	1	1	1	1	1	1	1	1	1	1	1
7	1	1	1	1	1	1	1	1	1	1	1	1	1	1	1	1	1	1	1	1
9	1	1	1	1	1	1	1	1	1	1	1	1	1	1	1	1	1	1	1	1
11	4	1	1	1	1	1	1	1	1	1	1	1	1	1	1	1	1	1	1	1
14	6	4	1	1	1	1	1	1	1	1	1	1	1	1	1	1	1	1	1	1
18	2	2	1	1	1	1	1	1	1	1	1	1	1	1	1	1	1	1	1	1
20	9	2	1	1	1	1	1	1	1	1	1	1	1	1	1	1	1	1	1	1
<b>23NE</b>																				
2	1	1	1	1	1	1	1	1	1	1	1	1	1	1	1	1	1	1	1	1
6	3	1	1	1	1	1	1	1	1	1	1	1	1	1	1	1	1	1	1	1
9	2	1	1	1	1	1	1	1	1	1	1	1	1	1	1	1	1	1	1	1
<b>20F</b>																				
2	1	1	1	1	1	1	1	1	1	1	1	1	1	1	1	1	1	1	1	1
7	1	1	1	1	1	1	1	1	1	1	1	1	1	1	1	1	1	1	1	1
10	2	1	1	1	1	1	1	1	1	1	1	1	1	1	1	1	1	1	1	1
14	4	1	1	1	1	1	1	1	1	1	1	1	1	1	1	1	1	1	1	1
17	10	1	1	1	1	1	1	1	1	1	1	1	1	1	1	1	1	1	1	1
21	1	1	1	1	1	1	1	1	1	1	1	1	1	1	1	1	1	1	1	1
<b>22NA</b>																				
2	1	1	1	1	1	1	1	1	1	1	1	1	1	1	1	1	1	1	1	1
9	1	1	1	1	1	1	1	1	1	1	1	1	1	1	1	1	1	1	1	1
13	1	1	1	1	1	1	1	1	1	1	1	1	1	1	1	1	1	1	1	1
15	7	1	1	1	1	1	1	1	1	1	1	1	1	1	1	1	1	1	1	1
19	7	1	1	1	1	1	1	1	1	1	1	1	1	1	1	1	1	1	1	1
24	8	1	1	1	1	1	1	1	1	1	1	1	1	1	1	1	1	1	1	1
<b>22NE</b>																				
2	1	1	1	1	1	1	1	1	1	1	1	1	1	1	1	1	1	1	1	1
7	1	1	1	1	1	1	1	1	1	1	1	1	1	1	1	1	1	1	1	1
10	4	1	1	1	1	1	1	1	1	1	1	1	1	1	1	1	1	1	1	1
<b>19F</b>																				
2	1	1	1	1	1	1	1	1	1	1	1	1	1	1	1	1	1	1	1	1
6	2	1	1	1	1	1	1	1	1	1	1	1	1	1	1	1	1	1	1	1
10	4	1	1	1	1	1	1	1	1	1	1	1	1	1	1	1	1	1	1	1
13	2	1	1	1	1	1	1	1	1	1	1	1	1	1	1	1	1	1	1	1
16	3	1	1	1	1	1	1	1	1	1	1	1	1	1	1	1	1	1	1	1

The notation above is: initial level, final level, branching ratio, where the level numbers correspond to levels in Table M.

## LIST OF FIGURES

		<u>Page(s)</u>
Figs. 1-24	Total Cross Sections . . . . .	55-68
Figs. 25-31	Total Elastic Cross Sections . . . . .	69-75
Fig. 32	Nonelastic Cross Section . . . . .	76
Fig. 33	Total Inelastic Cross Section . . . . .	77
Fig. 34	(n,2n) Cross Section . . . . .	78
Figs. 35-57	(n,n') Level Cross Sections . . . . .	79-100
Figs. 58-61	Capture Cross Sections . . . . .	101-104
Fig. 62	(n,p) Cross Section . . . . .	105
Fig. 63	(n, $\alpha$ ) Cross Section . . . . .	106
Figs. 64-81	Elastic Scattering Angular Distributions . . .	107-123
Figs. 82-100	Gamma-Ray-Production Cross Sections . . . . .	124-142
Figs. 101-130	Model Calculation Results Compared with Data .	143-172

# Cross Section (b)

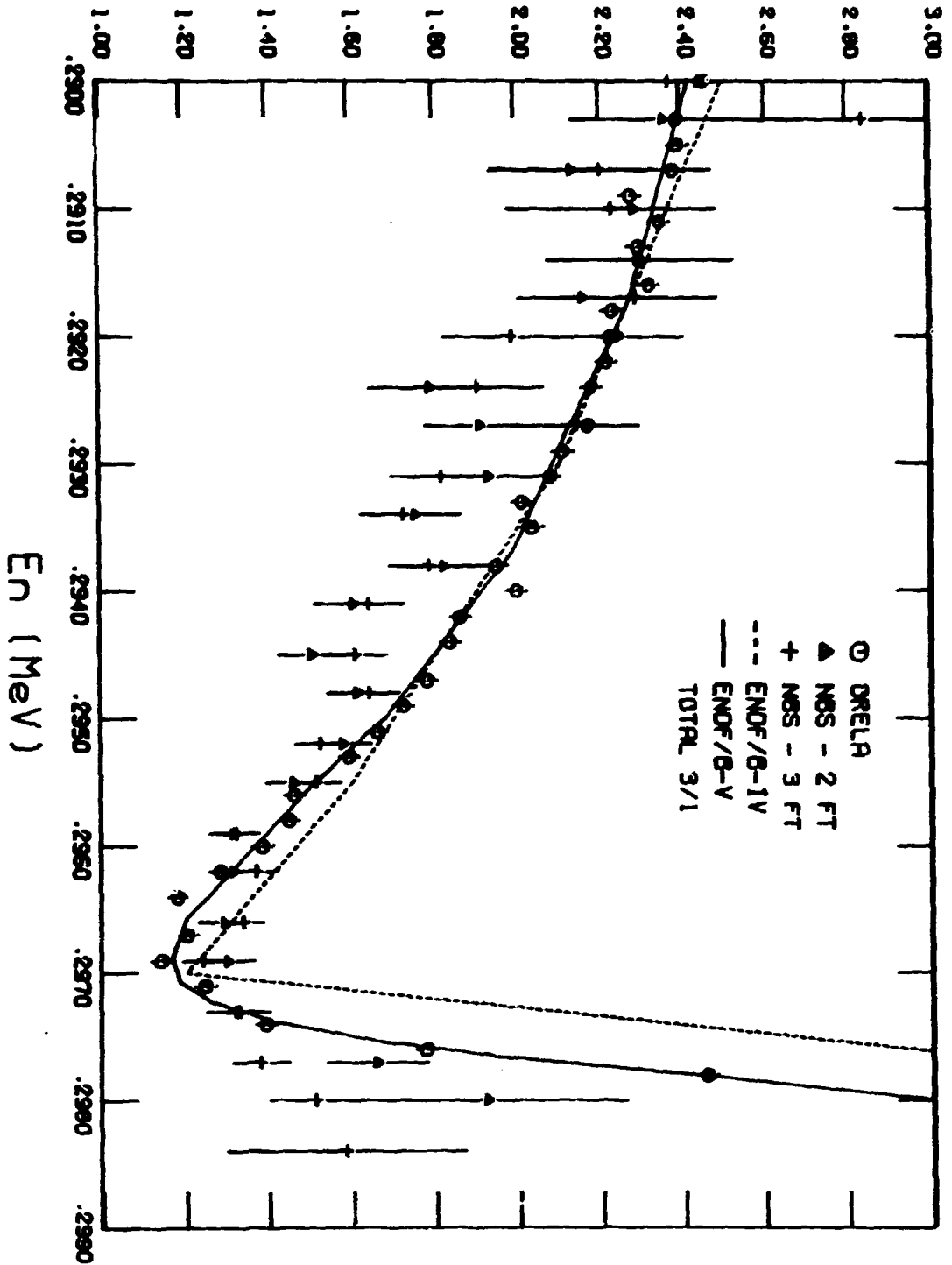


Fig. 1. Comparison of V4 and V5 with data of LA76 and BR75 near the 300-kev minimum.

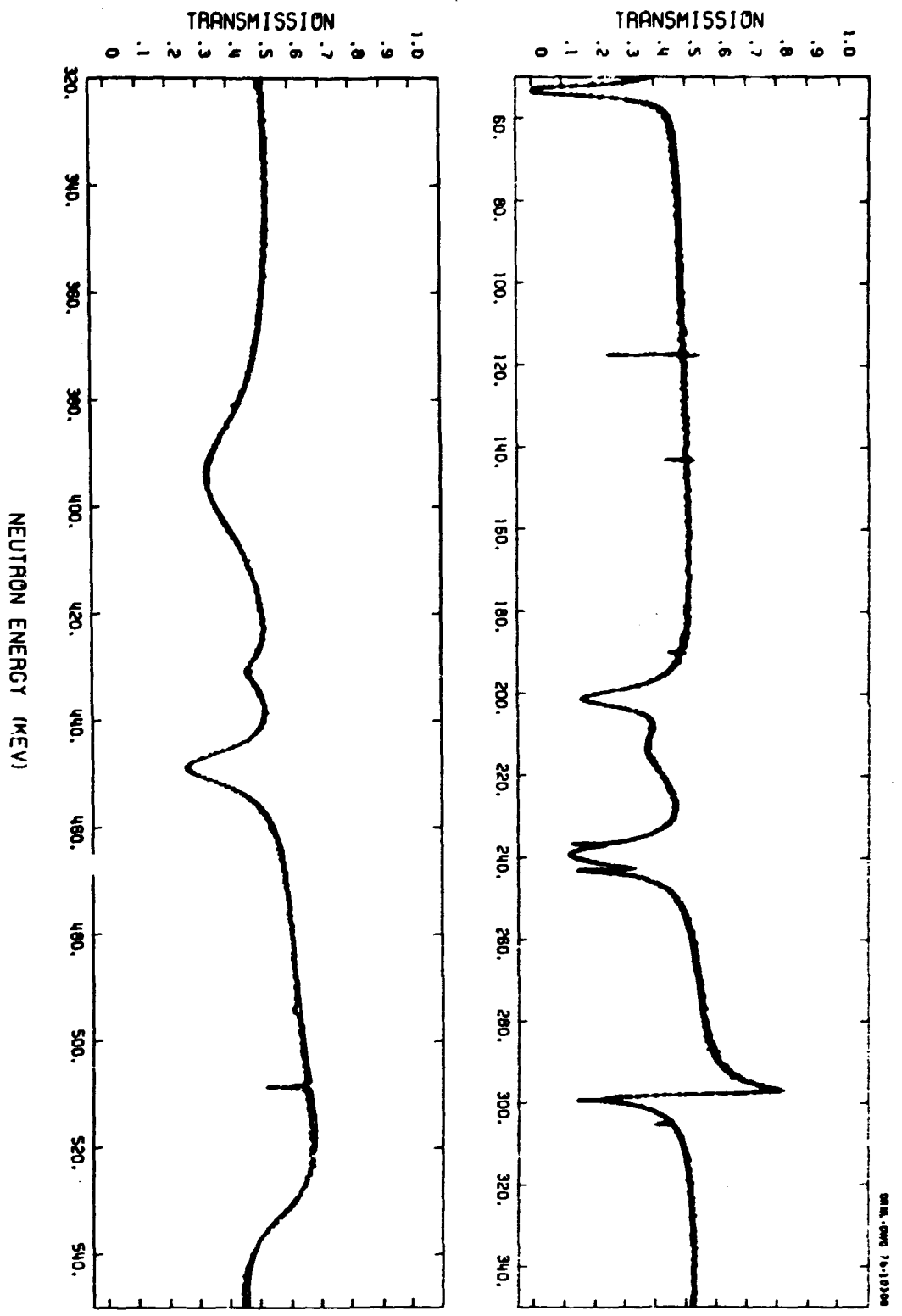


Fig. 2. Comparison of resonance parameter fit with data of LA76.

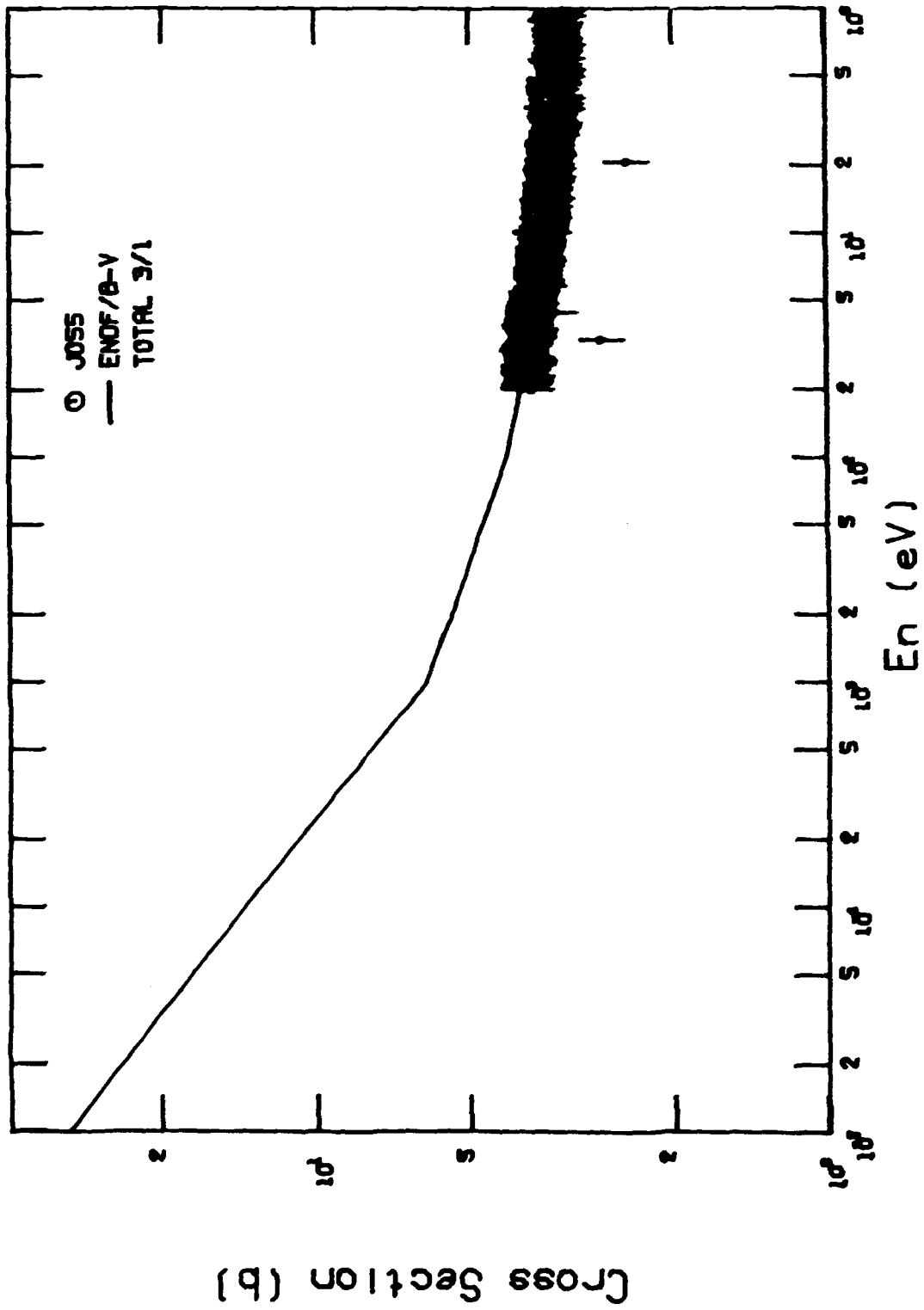


Fig. 3. Comparison of V5 total cross section with data of ref. J055.

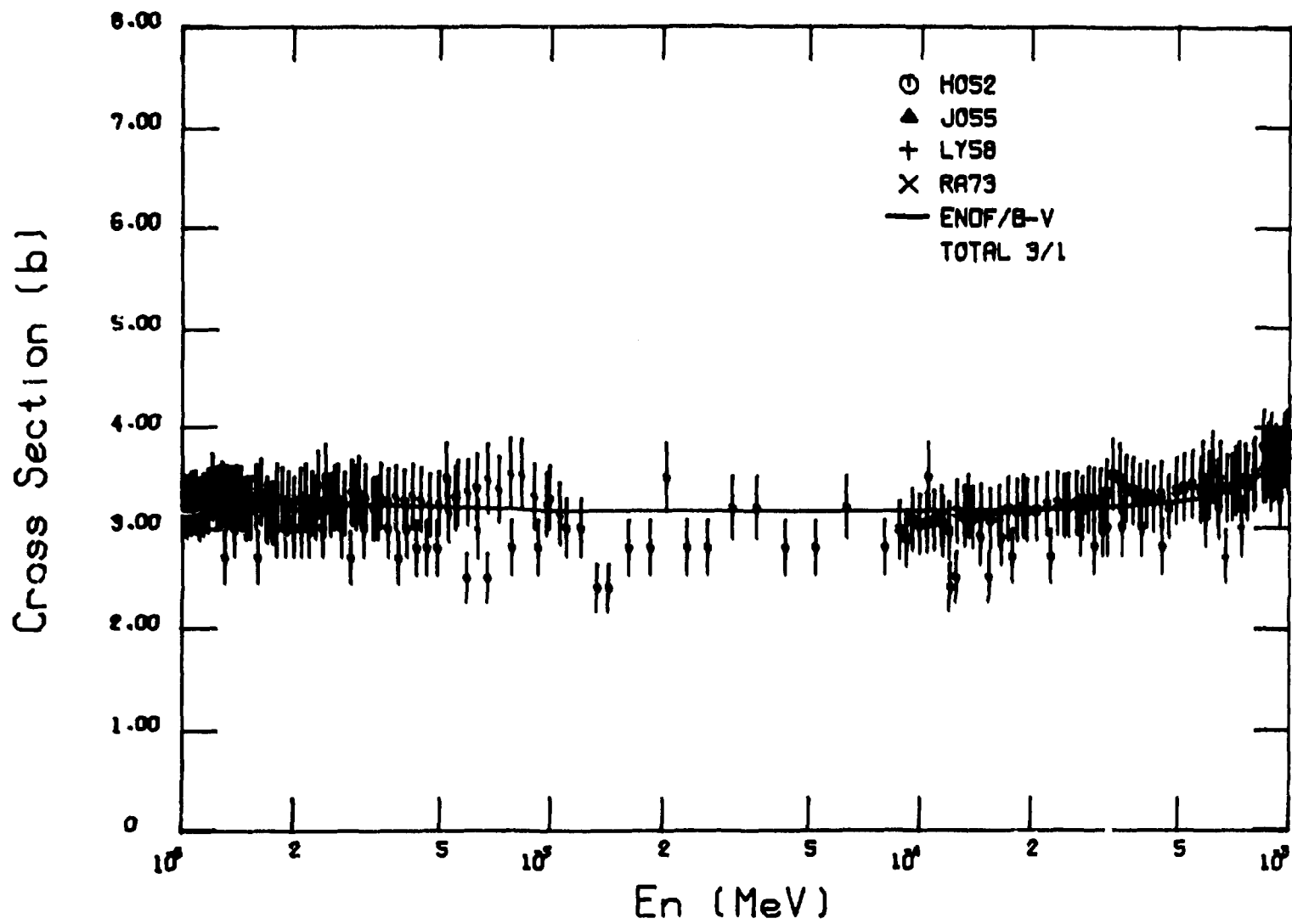


Fig. 4. Comparison of V5 total cross section with available data.

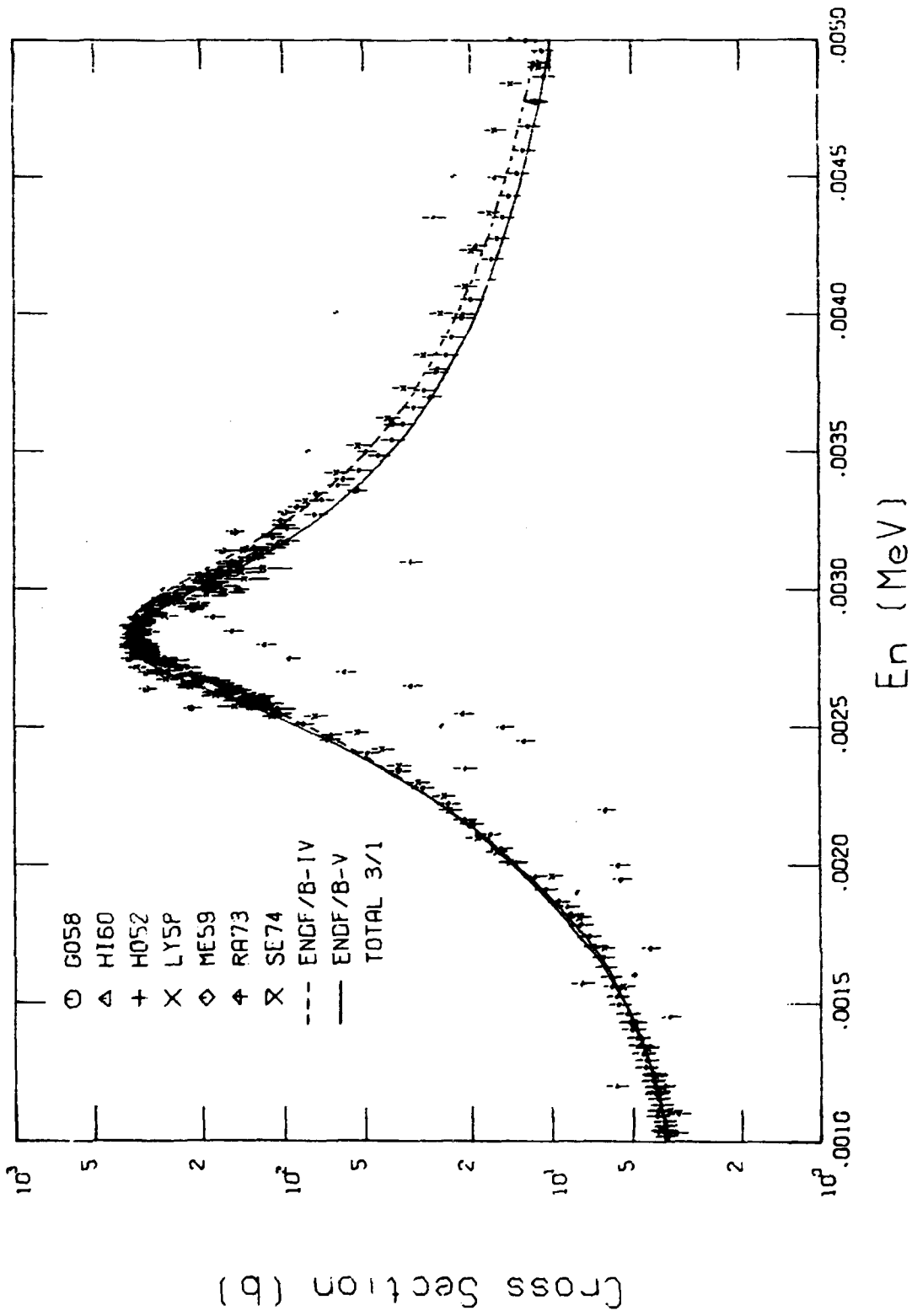


Fig. 5. Comparison of V4 and V5 total cross section with available data.

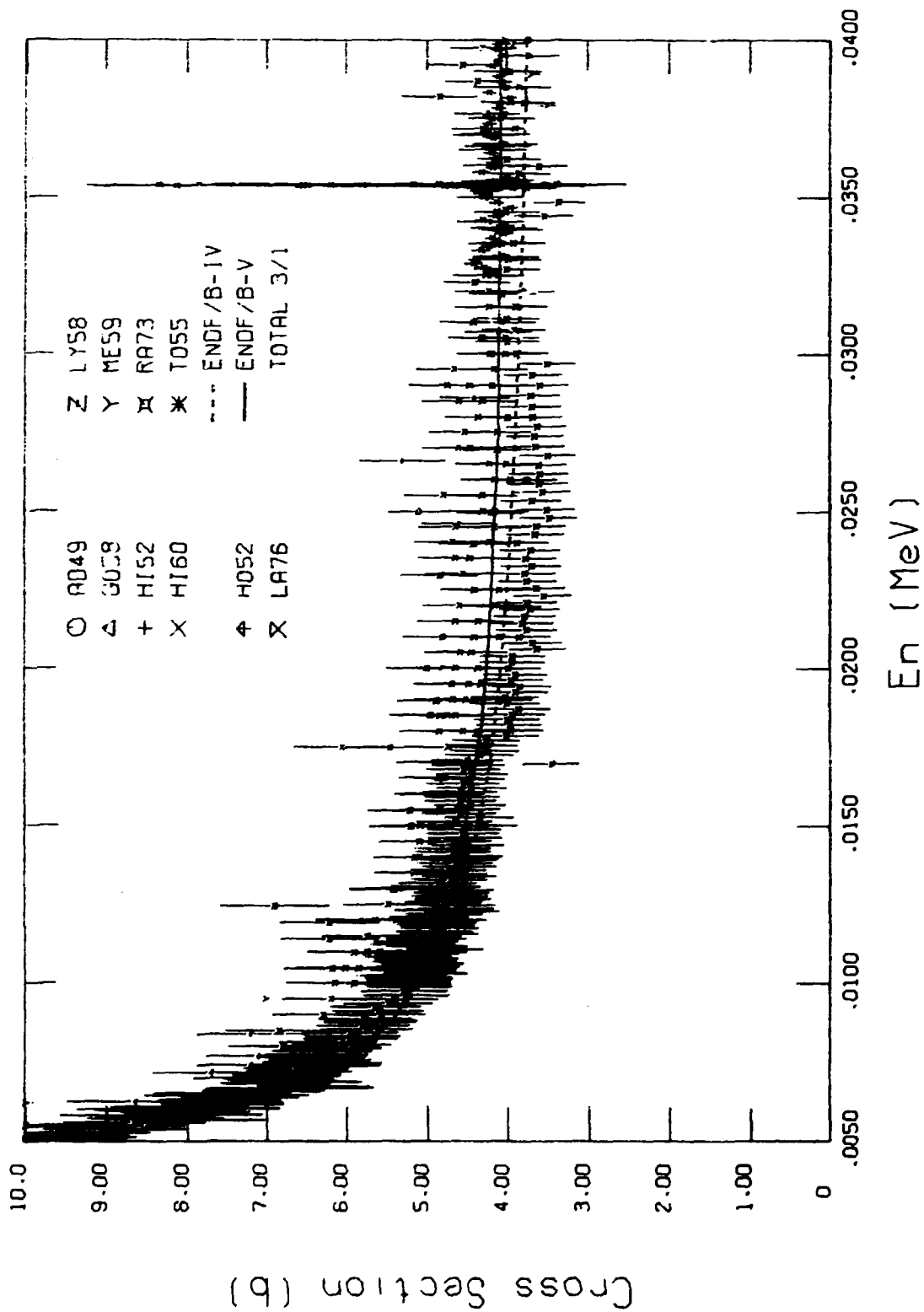


Fig. 6. Comparison of V4 and V5 total cross section with available data.

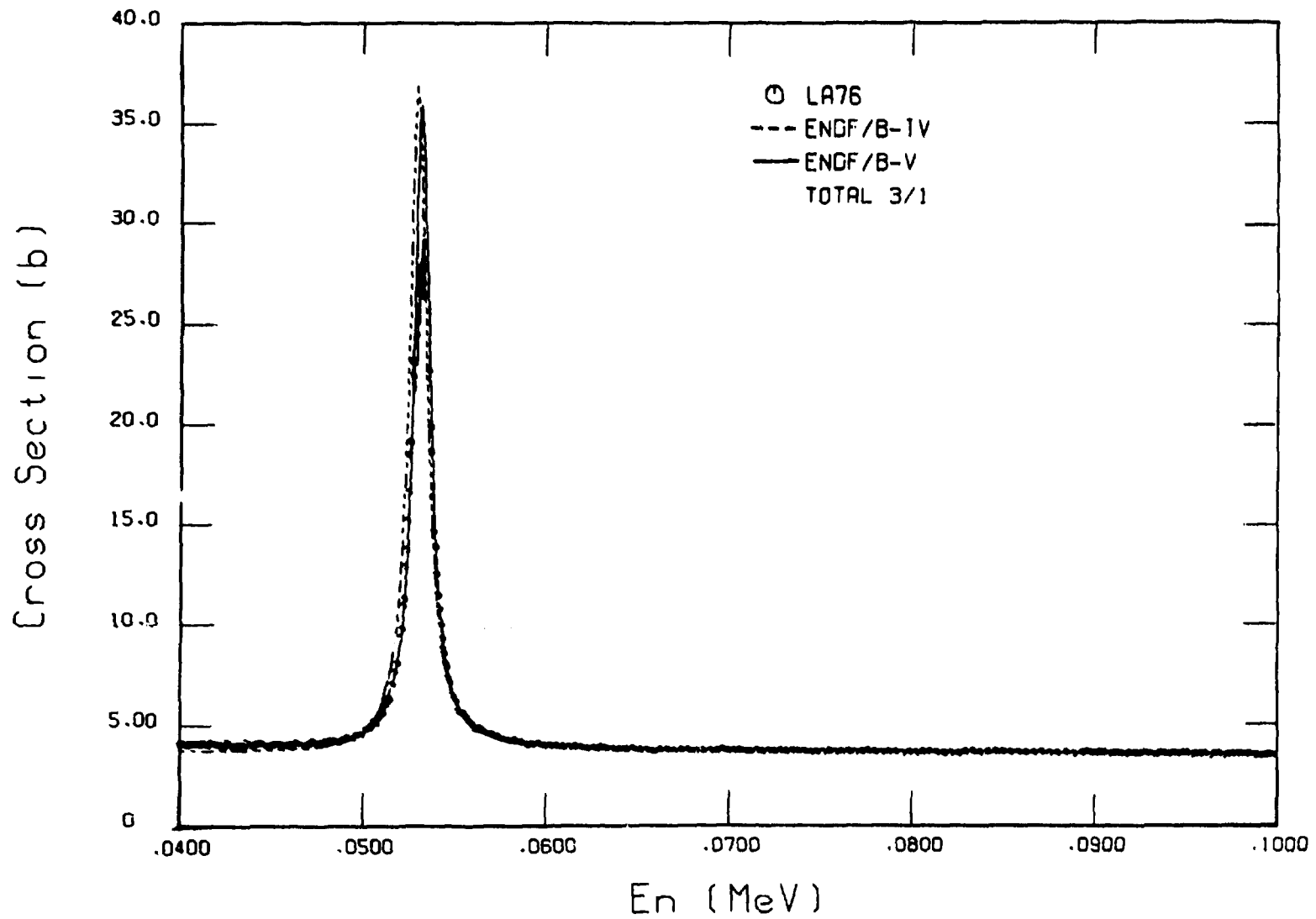


Fig. 7. Comparison of V4 and V5 total cross section with data of LA76.

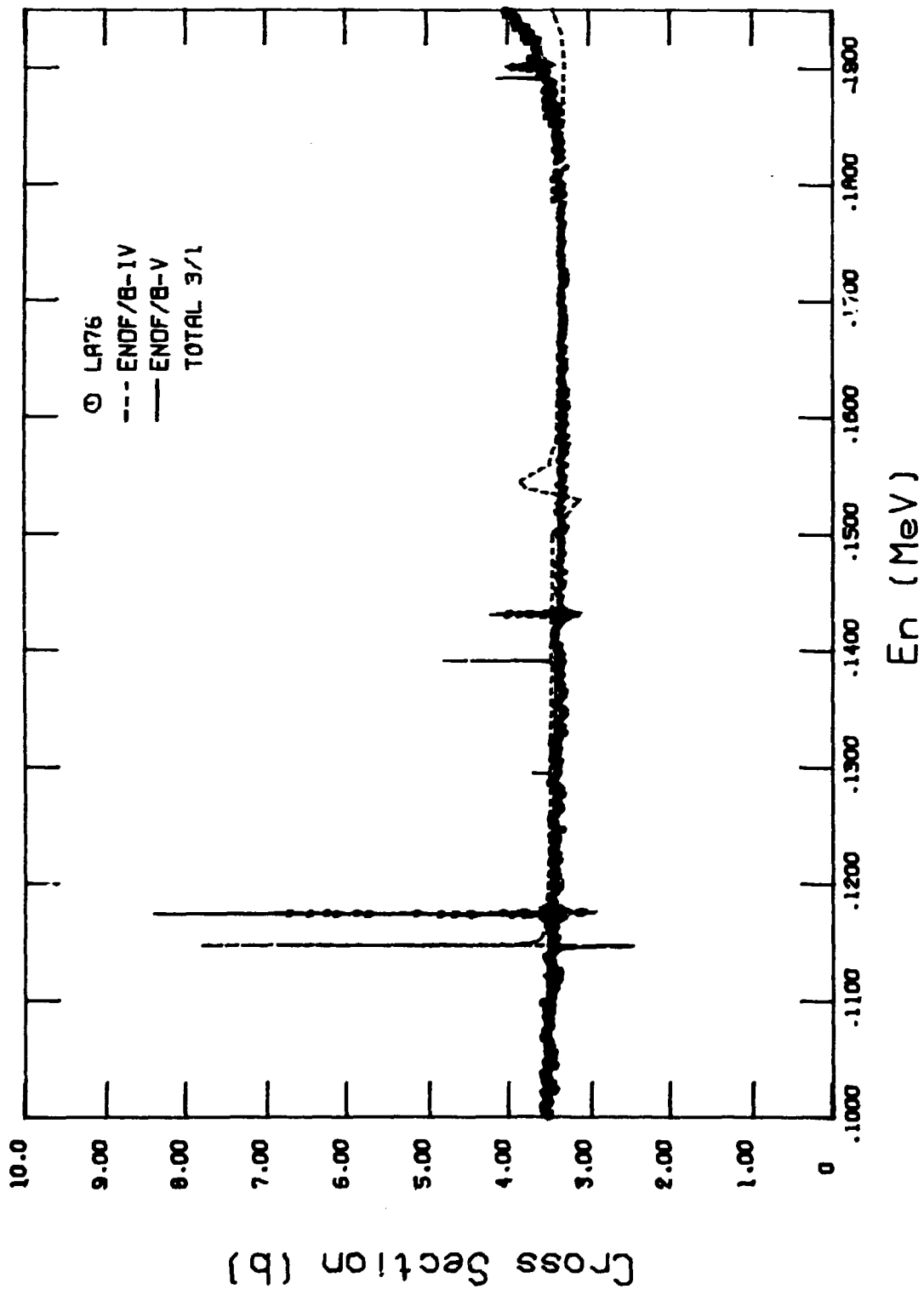


Fig. 8. Comparison of V4 and V5 total cross section with data of LA76.

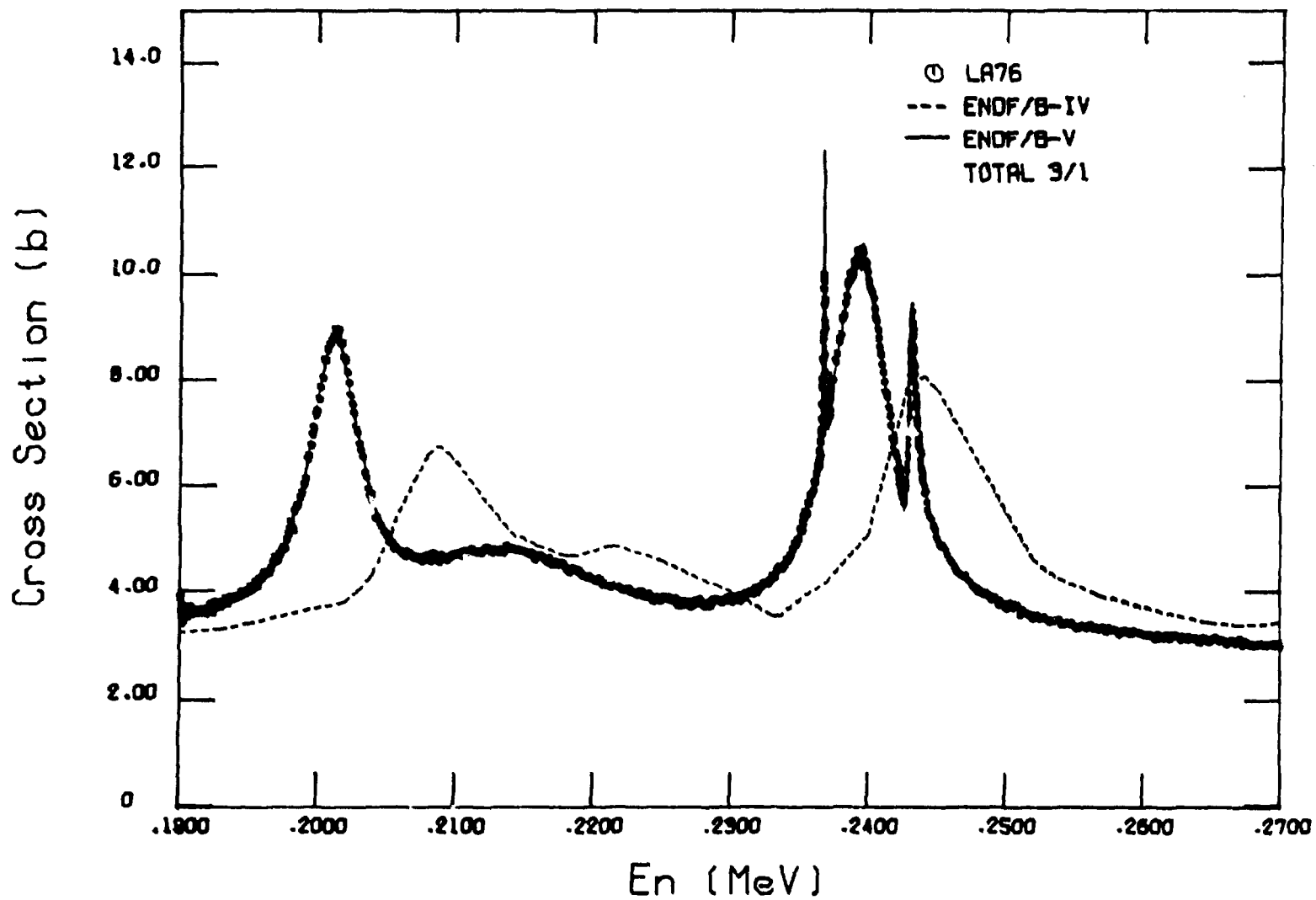


Fig. 9. Comparison of V4 and V5 total cross section with data of LA76.

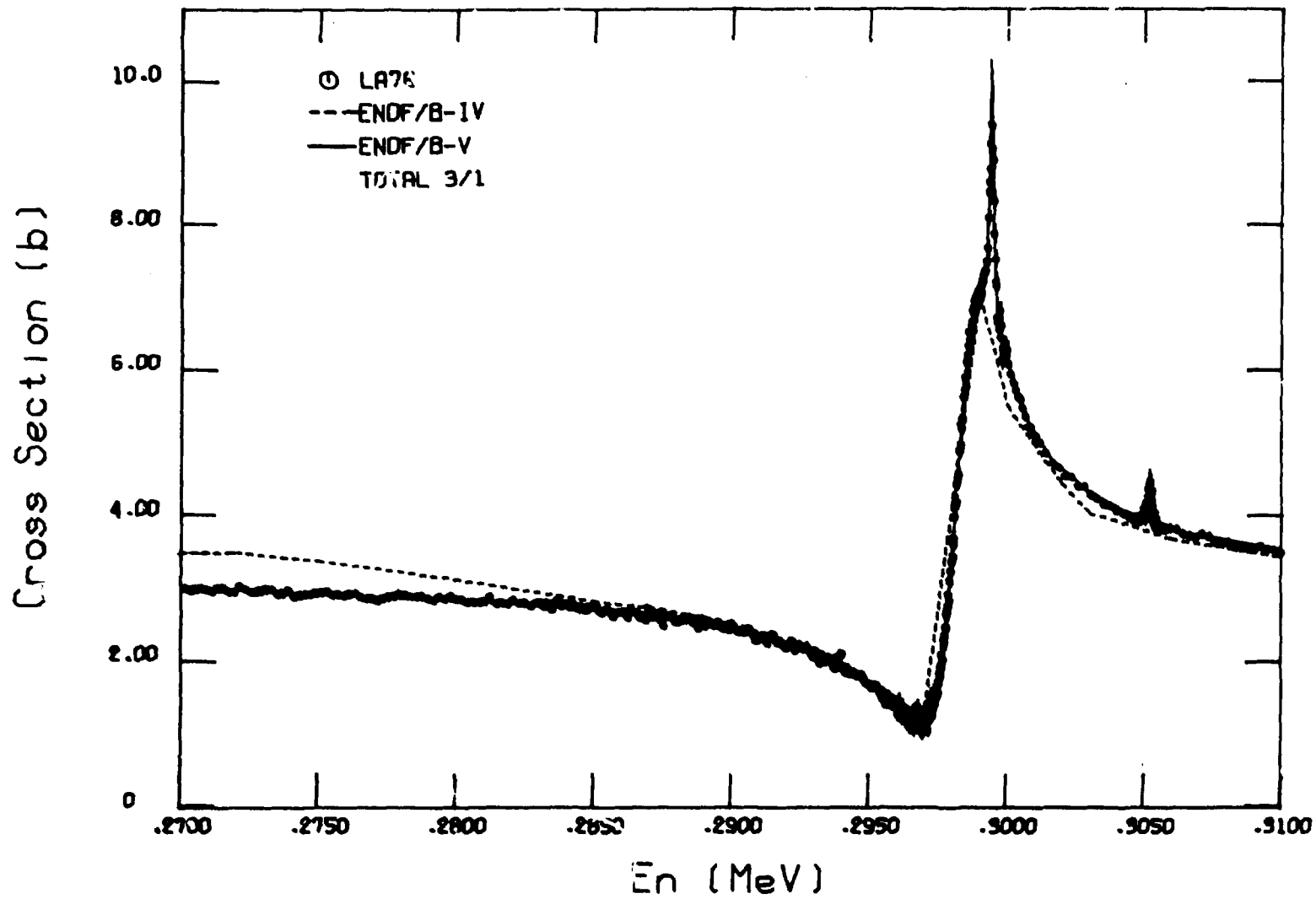


Fig. 10. Comparison of V4 and V5 total cross section with data of LA76.

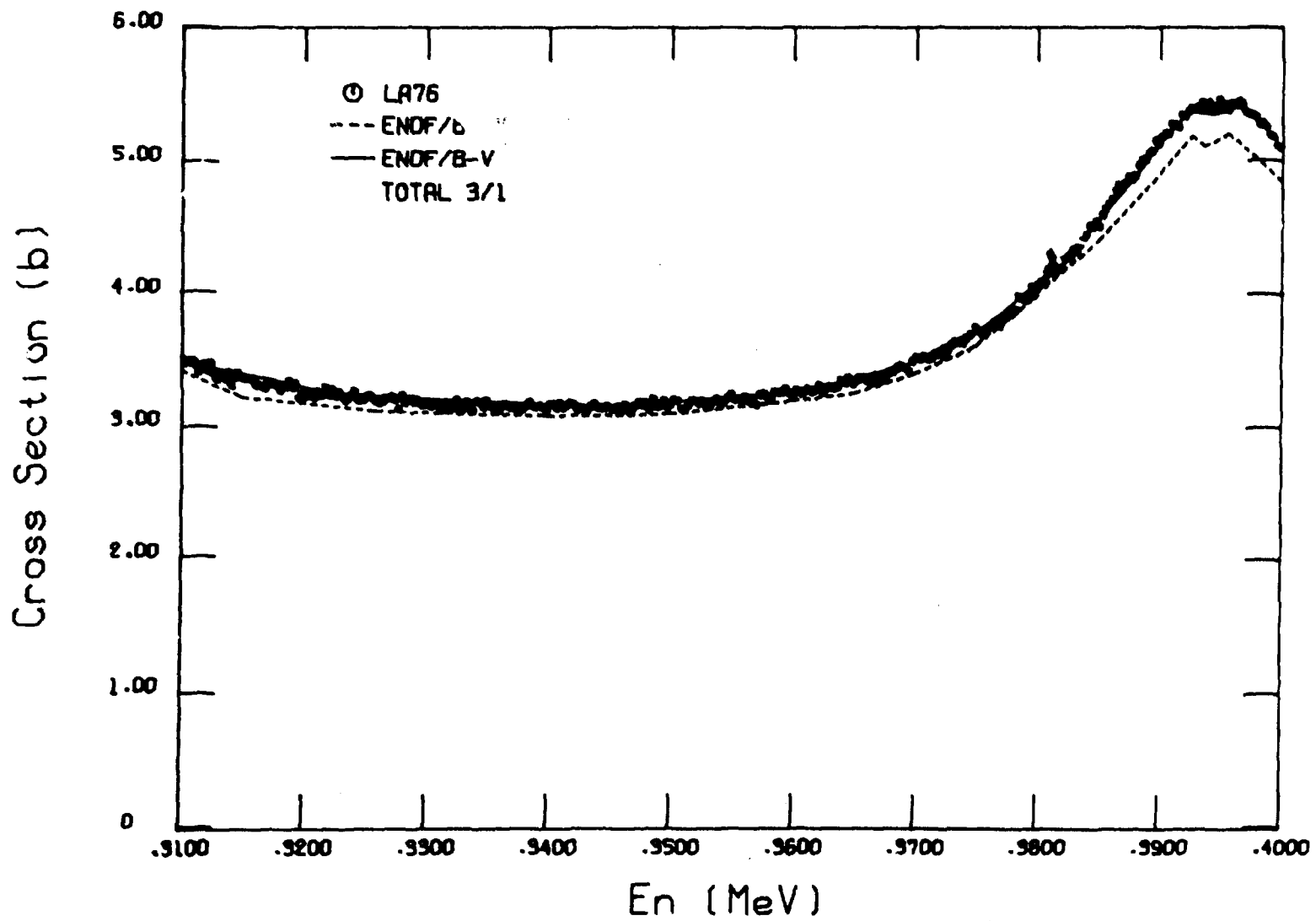


Fig. 11. Comparison of V4 and V5 total cross section with data of LA76.

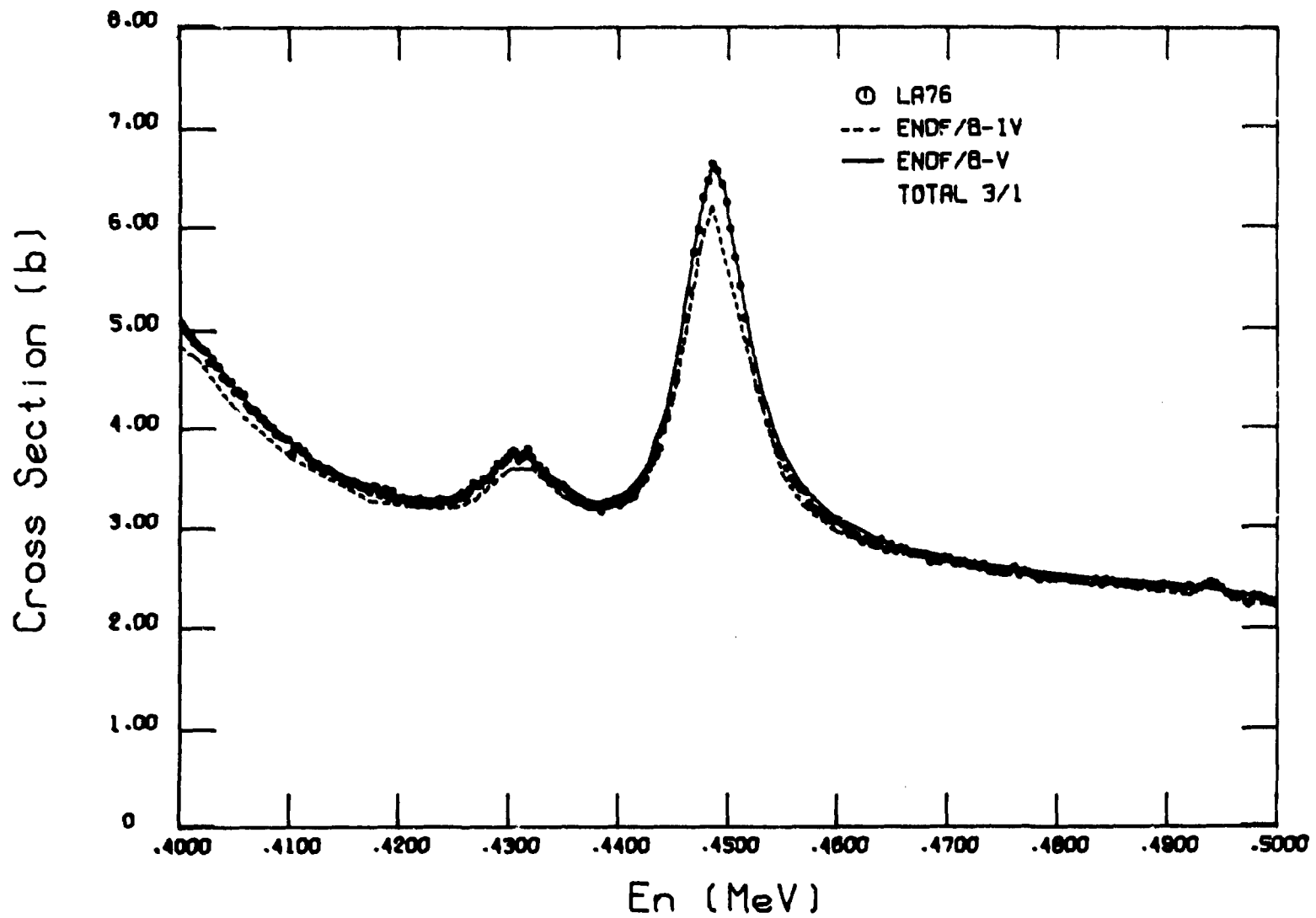


Fig. 12. Comparison of V4 and V5 total cross section with data of LA76.

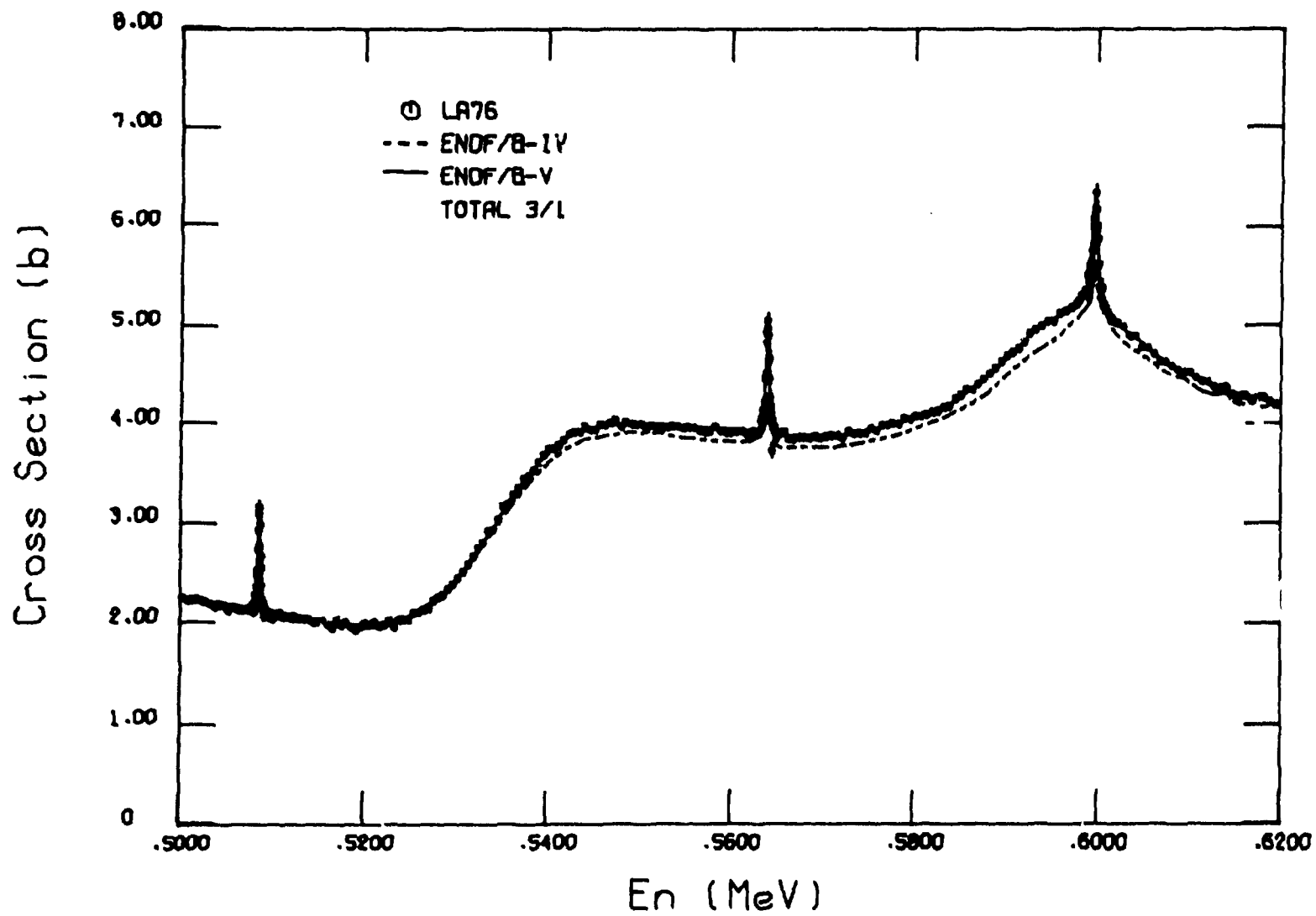


Fig. 13. Comparison of V4 and V5 total cross section with data of LA76.

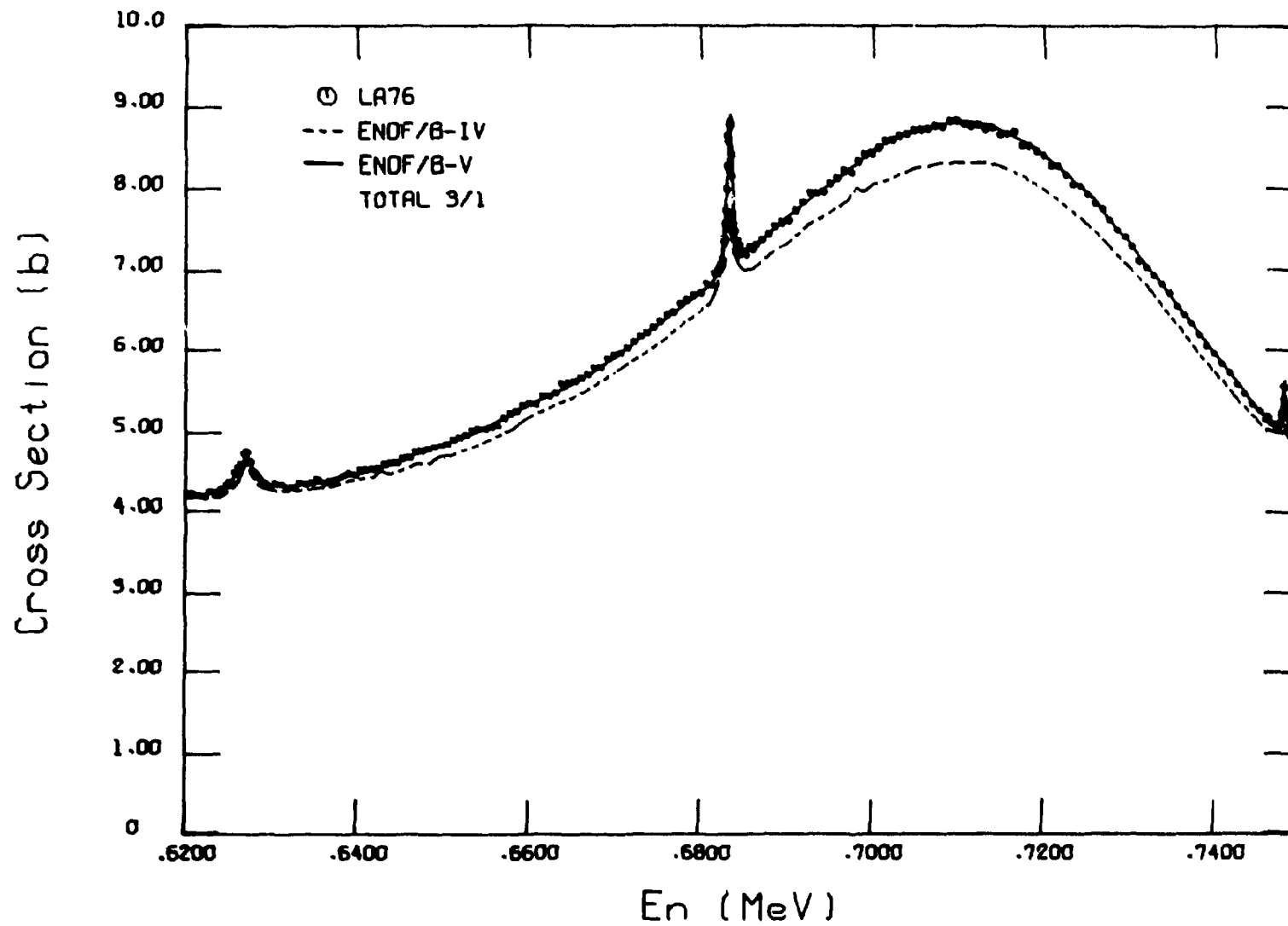


Fig. 14. Comparison of V4 and V5 total cross section with data of LA76.

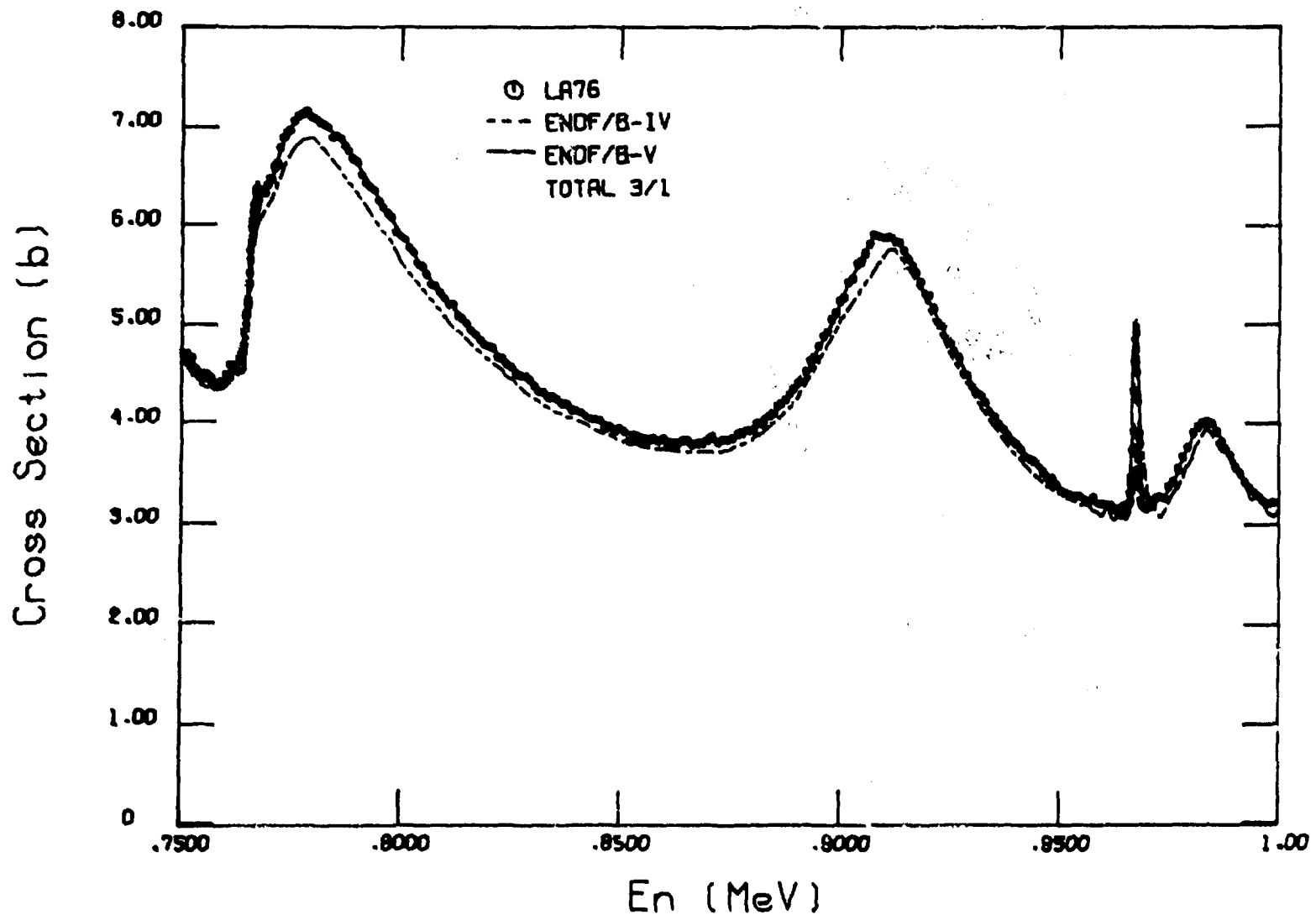


Fig. 15. Comparison of V4 and V5 total cross section with data of LA76.

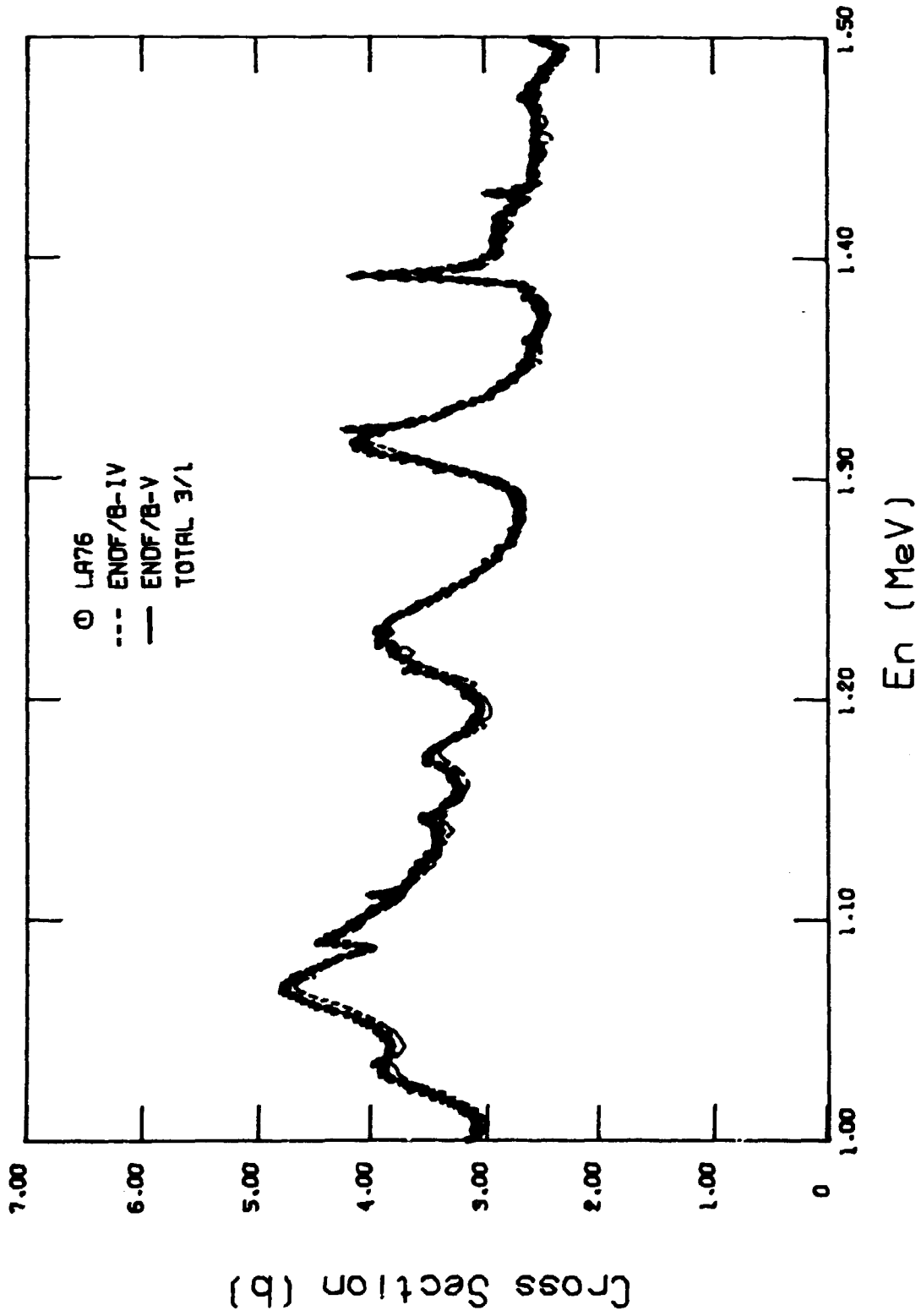


Fig. 16. Comparison of V4 and V5 total cross section with data of LA76.

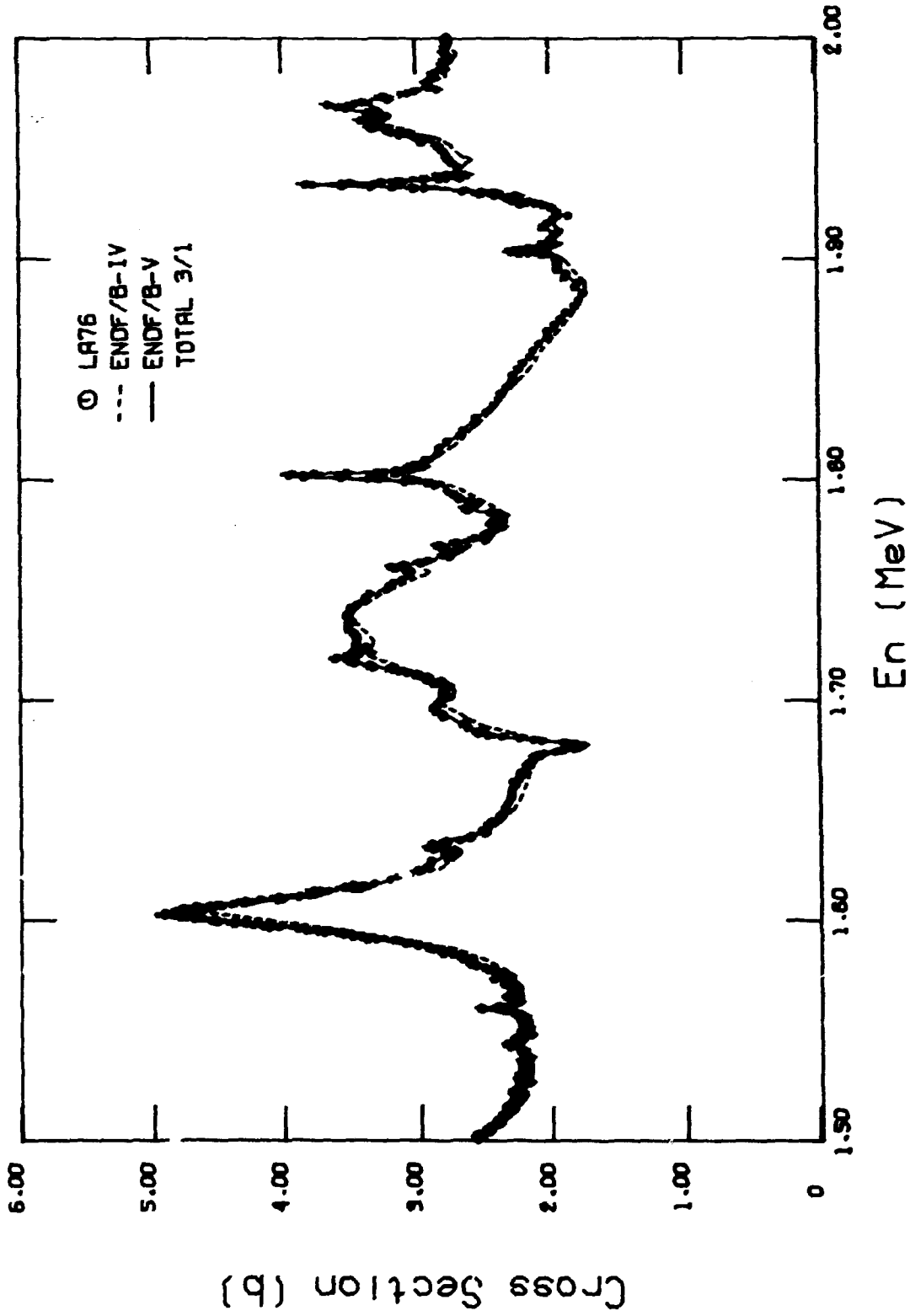


Fig. 17. Comparison of V4 and V5 total cross section with data of LA76.

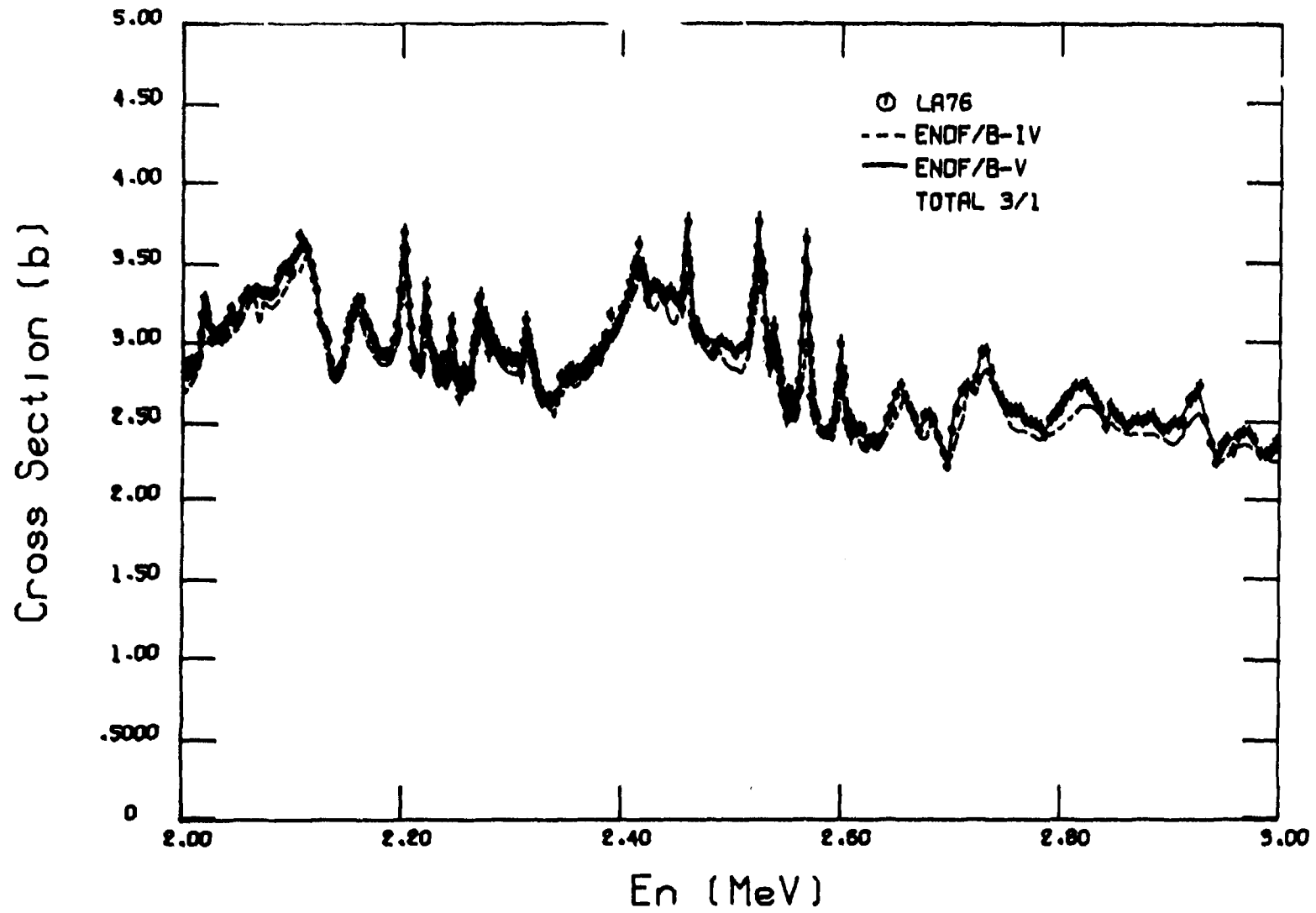


Fig. 18. Comparison of V4 and V5 total cross section with data of LA76.

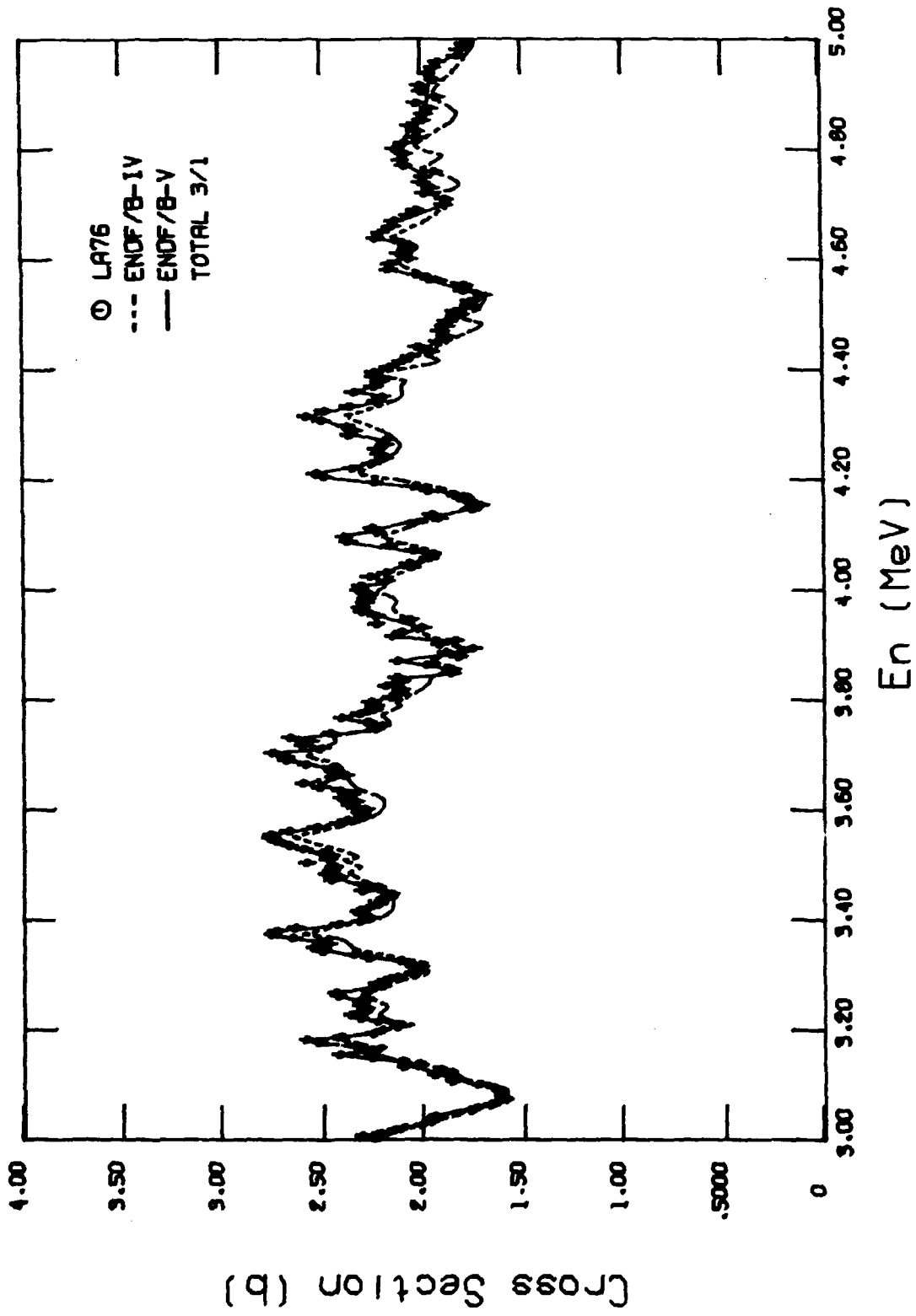


Fig. 19 Comparison of V4 and V5 total cross section with data of LA76.

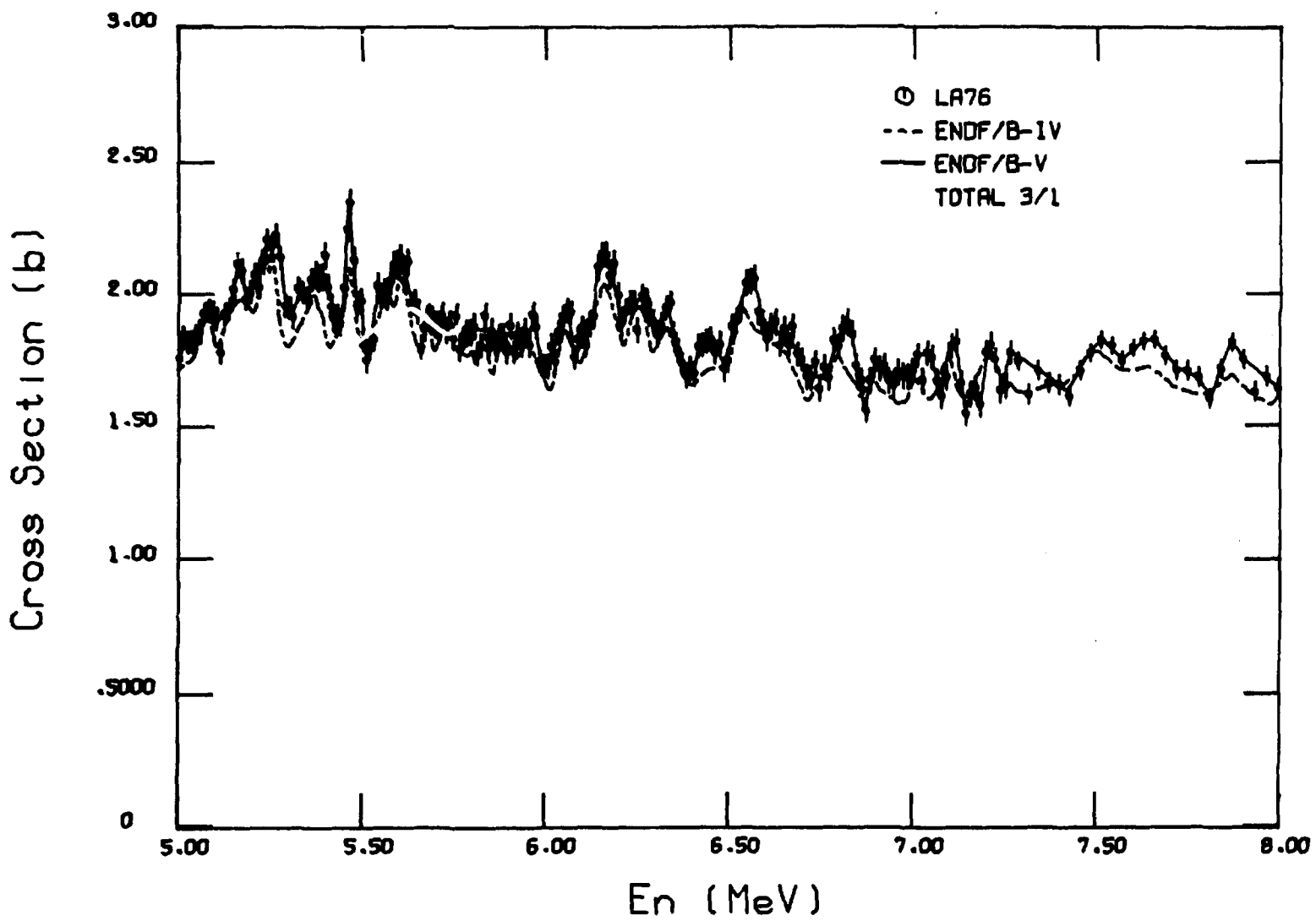


Fig. 20. Comparison of V4 and V5 total cross section with data of LA76.

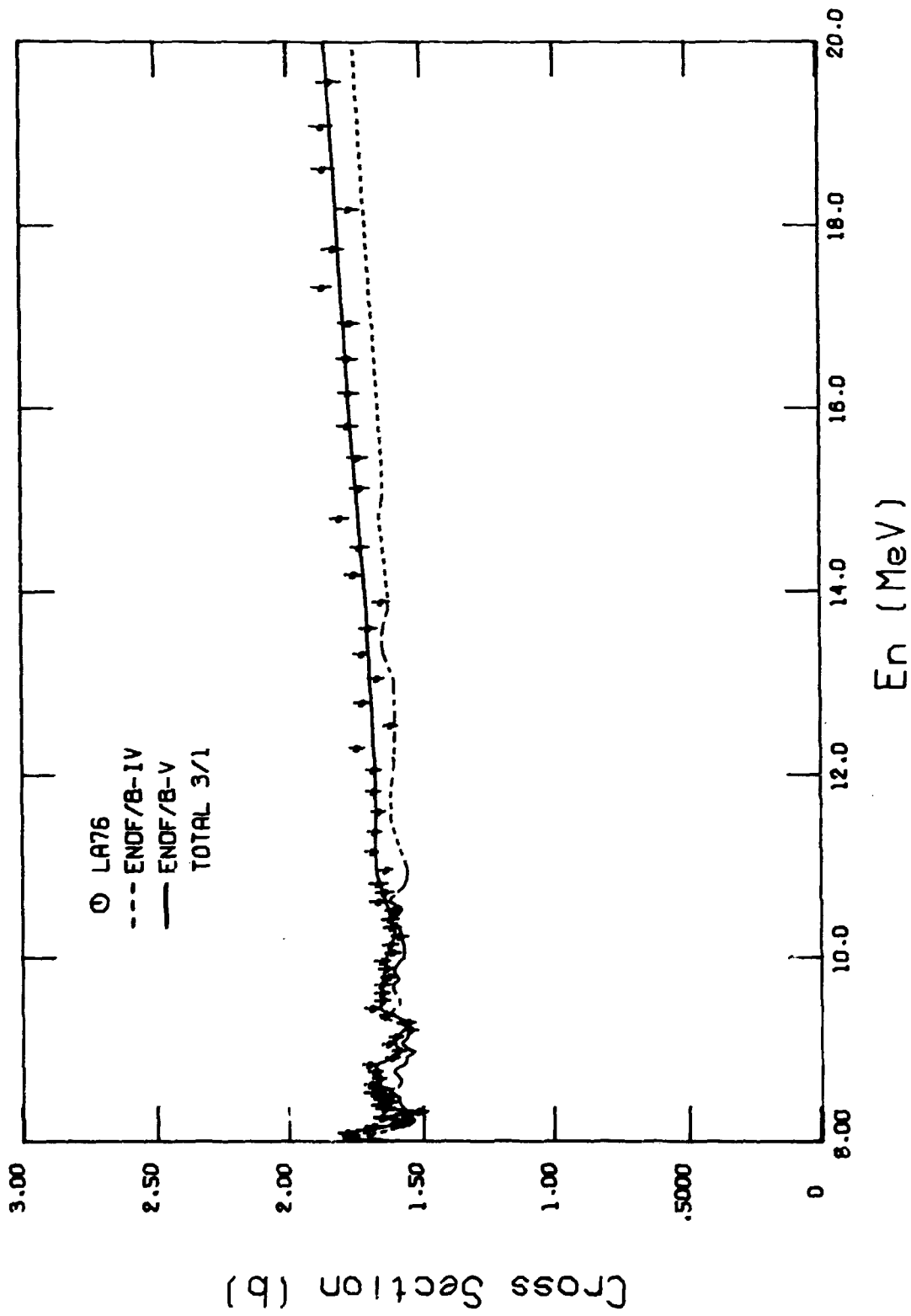


Fig. 21. Comparison of V4 and V5 total cross section with data of LA76.

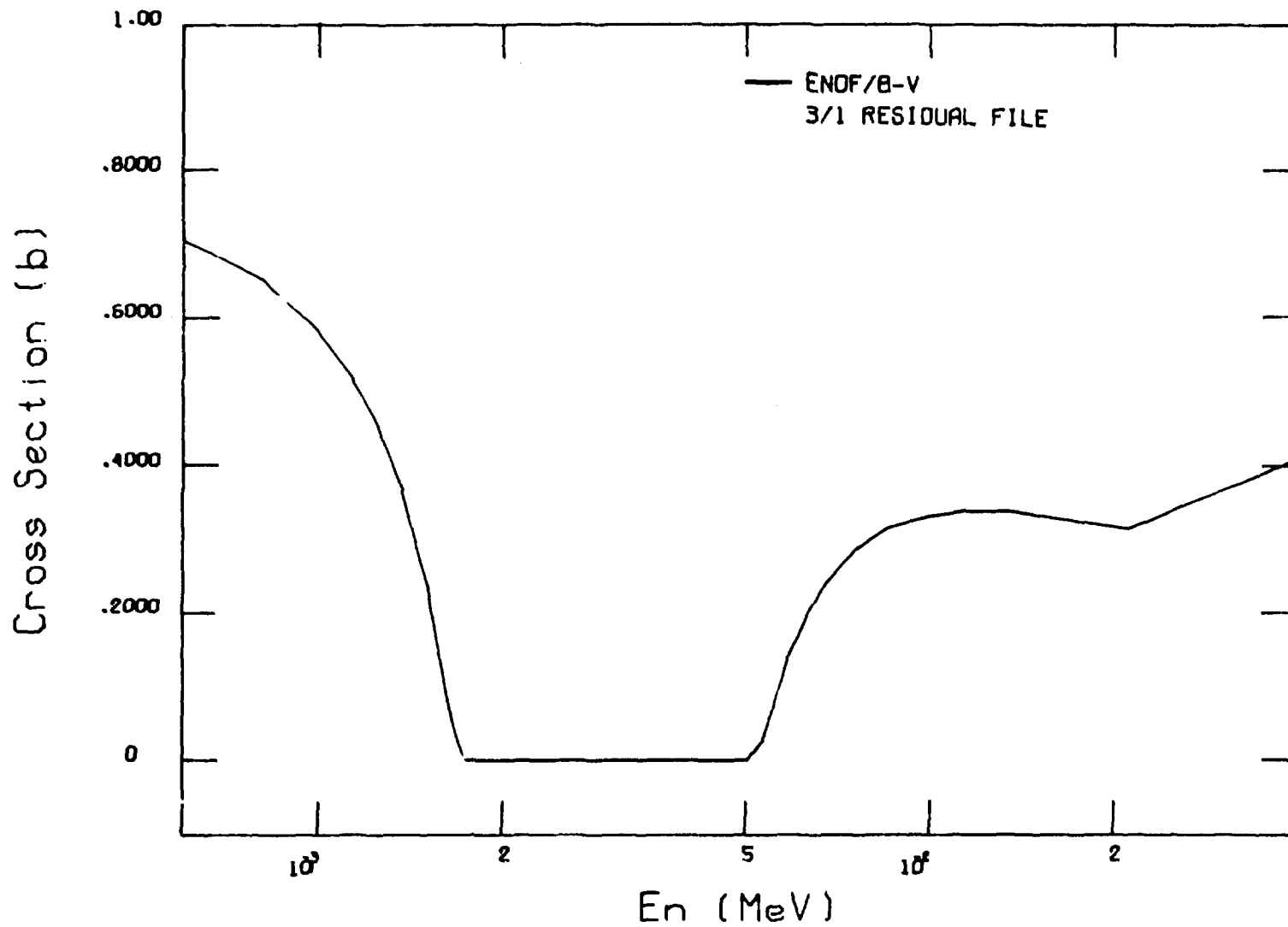


Fig. 22. Smooth background total cross section from 600 eV to 40 keV.

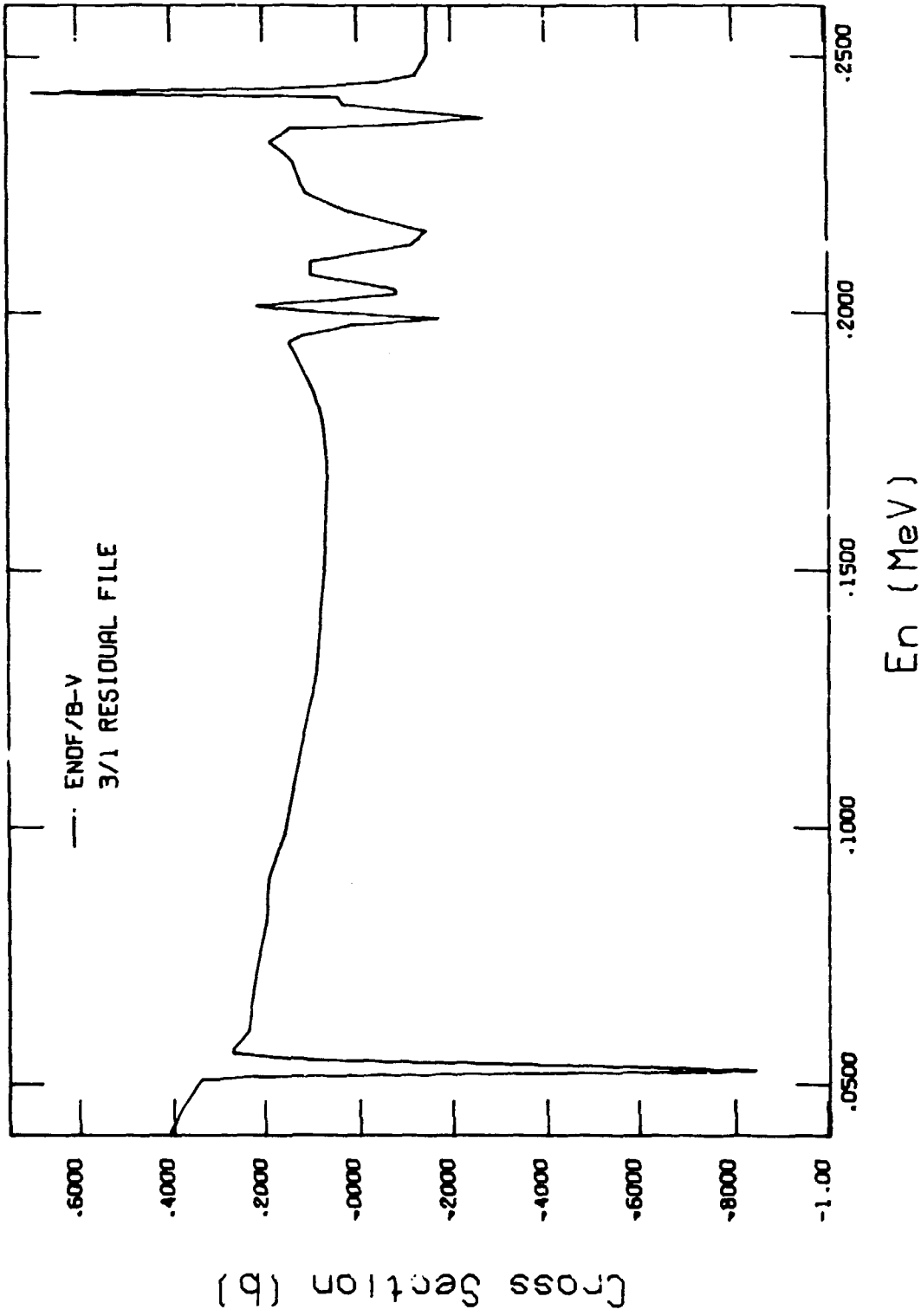


Fig. 23. Smooth background total cross section from 40 keV to 260 keV.

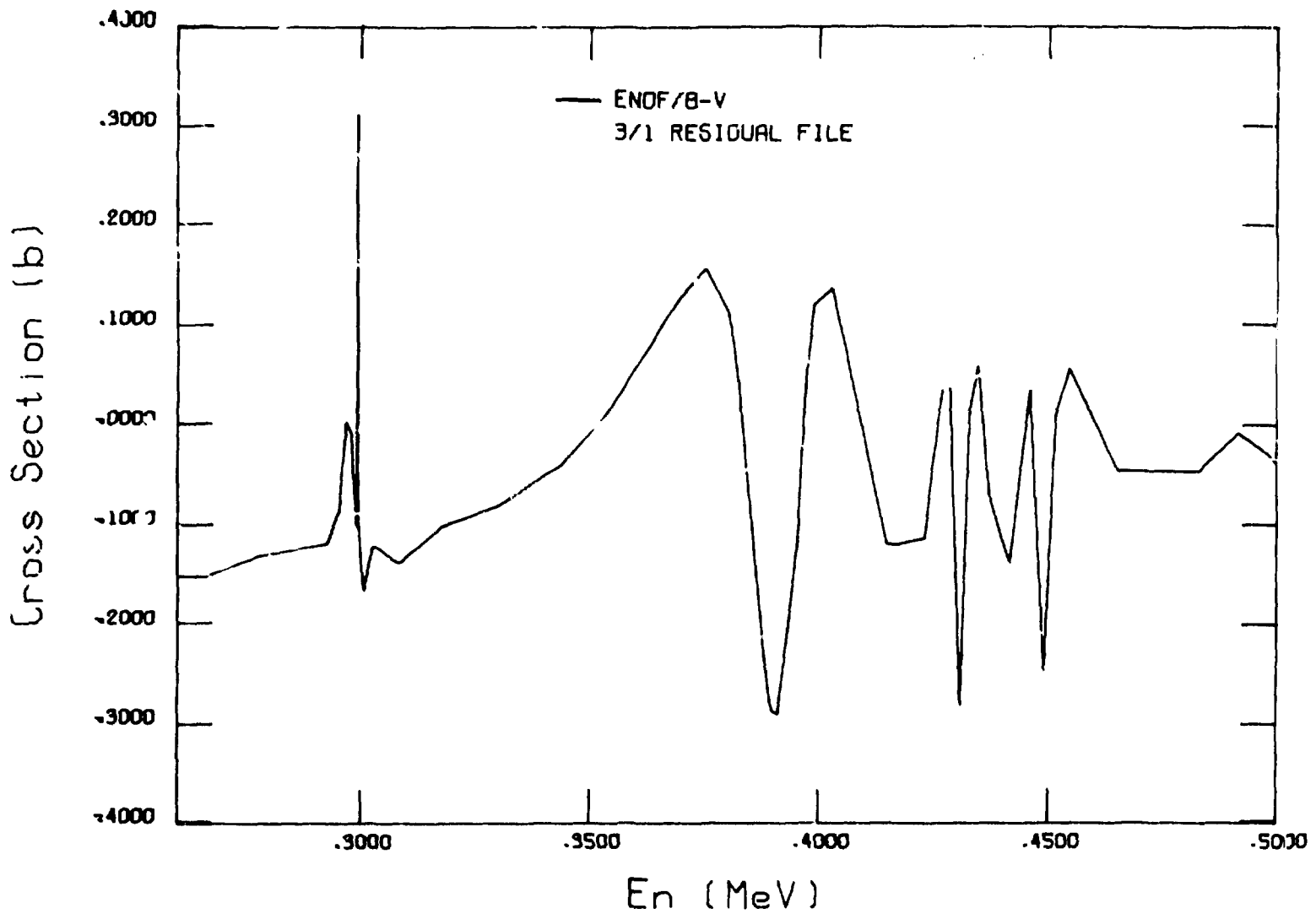


Fig. 24. Smooth background total cross section from 260 to 500 keV.

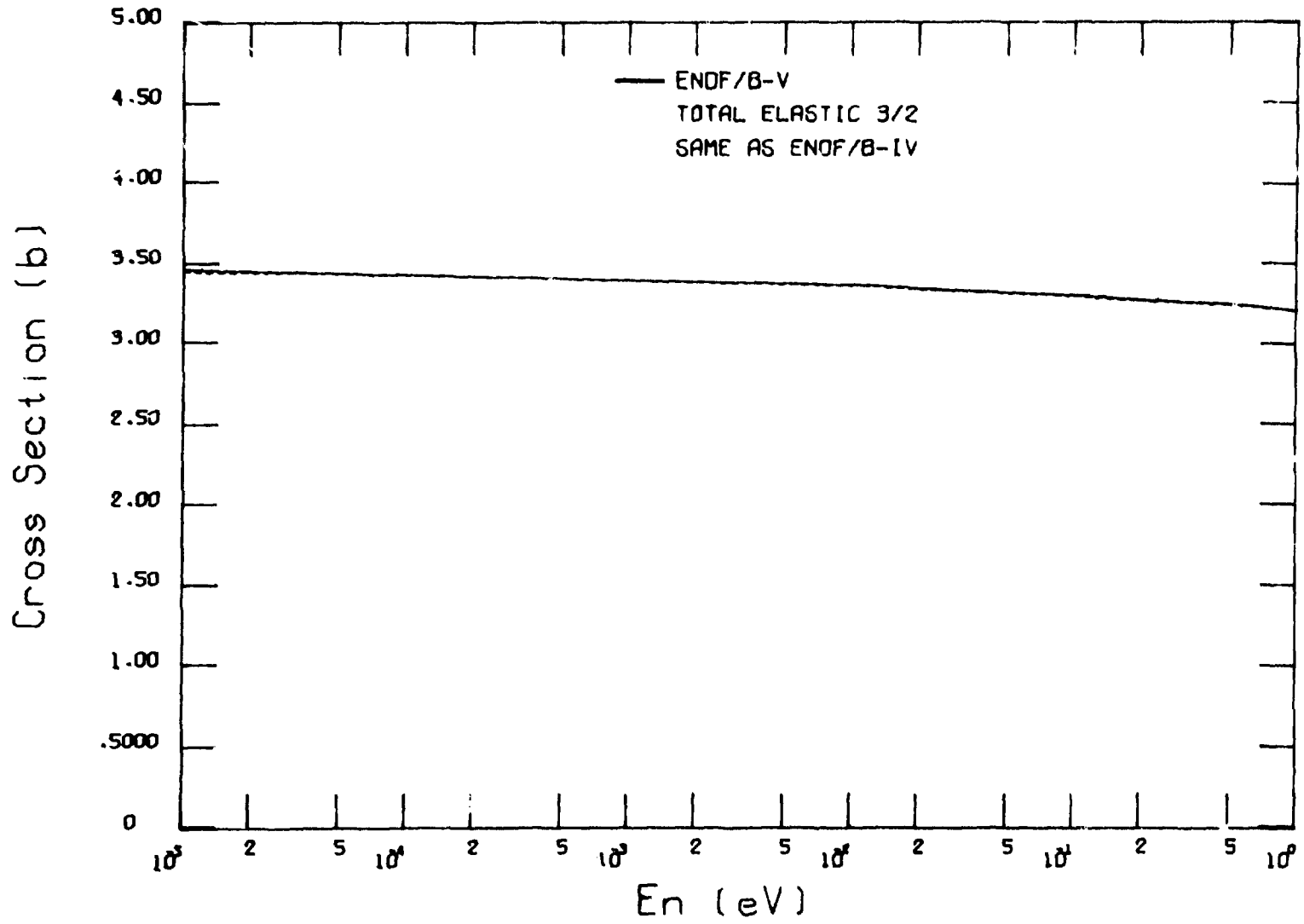


Fig. 25. Comparison of V4 and V5 total elastic cross section from  $10^{-5}$  eV to 1 eV.

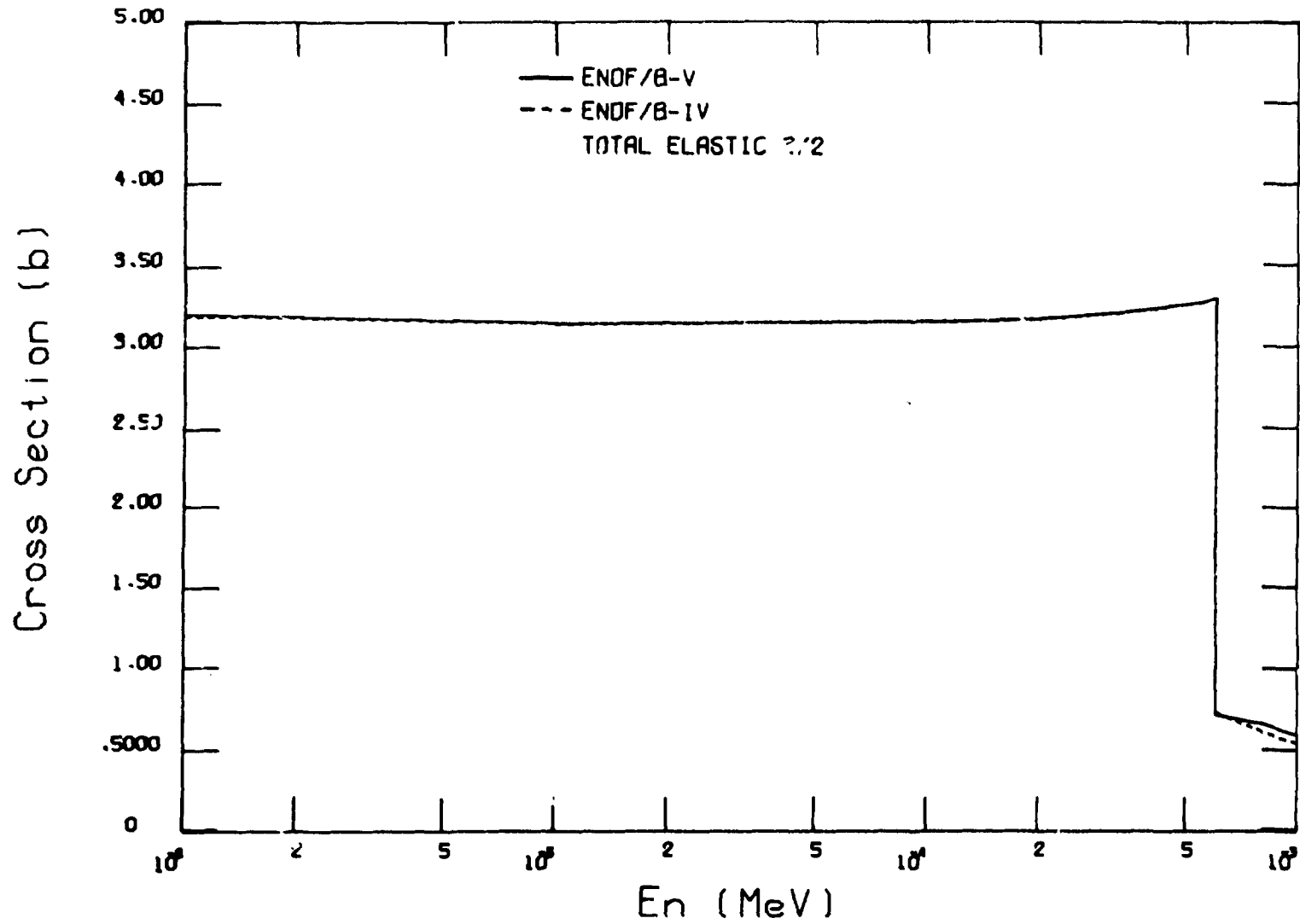


Fig. 26. Comparison of V4 and V5 total elastic cross section from 1 eV to 1 keV.

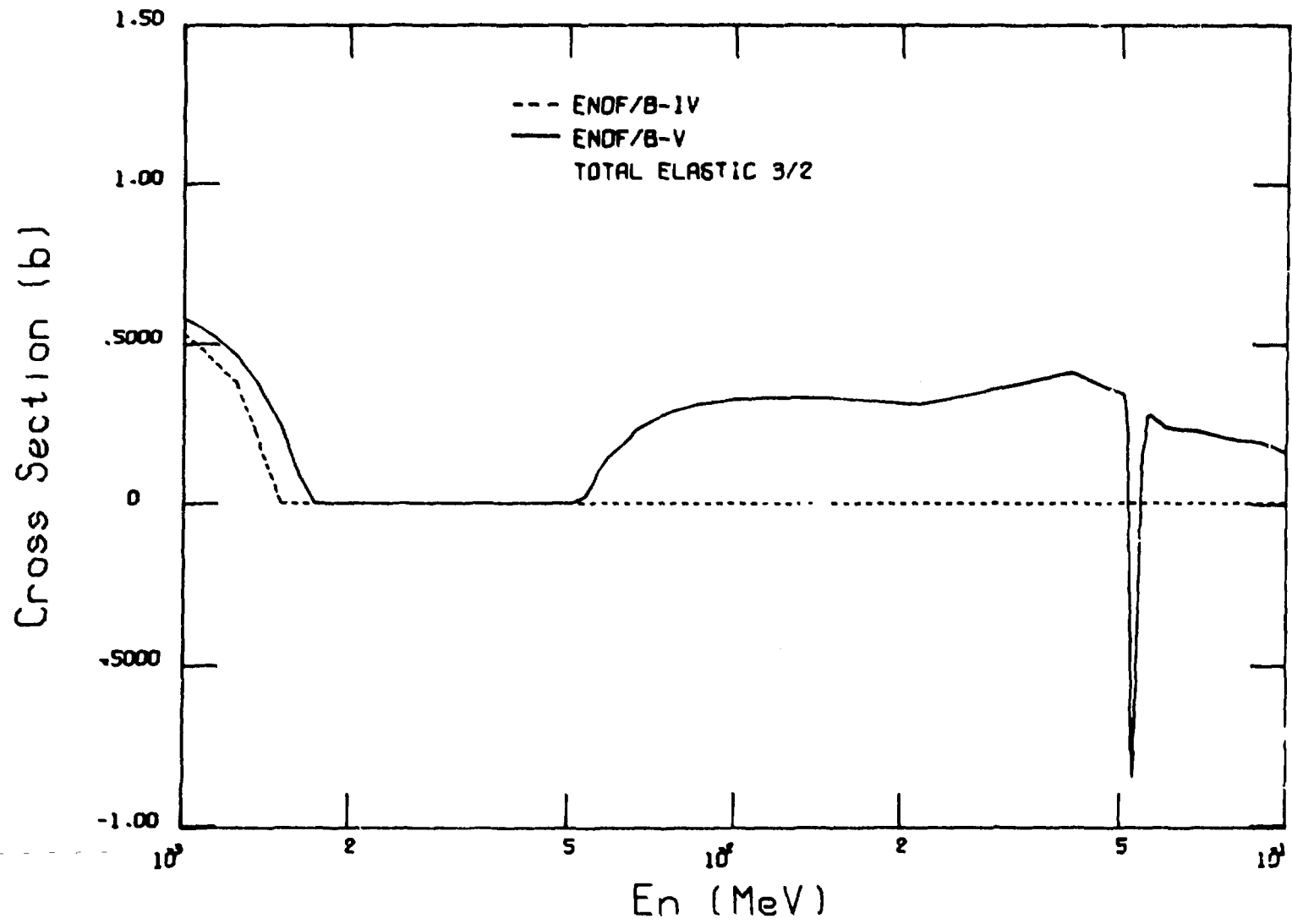


Fig. 27. Comparison of V4 and V5 total elastic cross section from 1 keV to 100 keV.

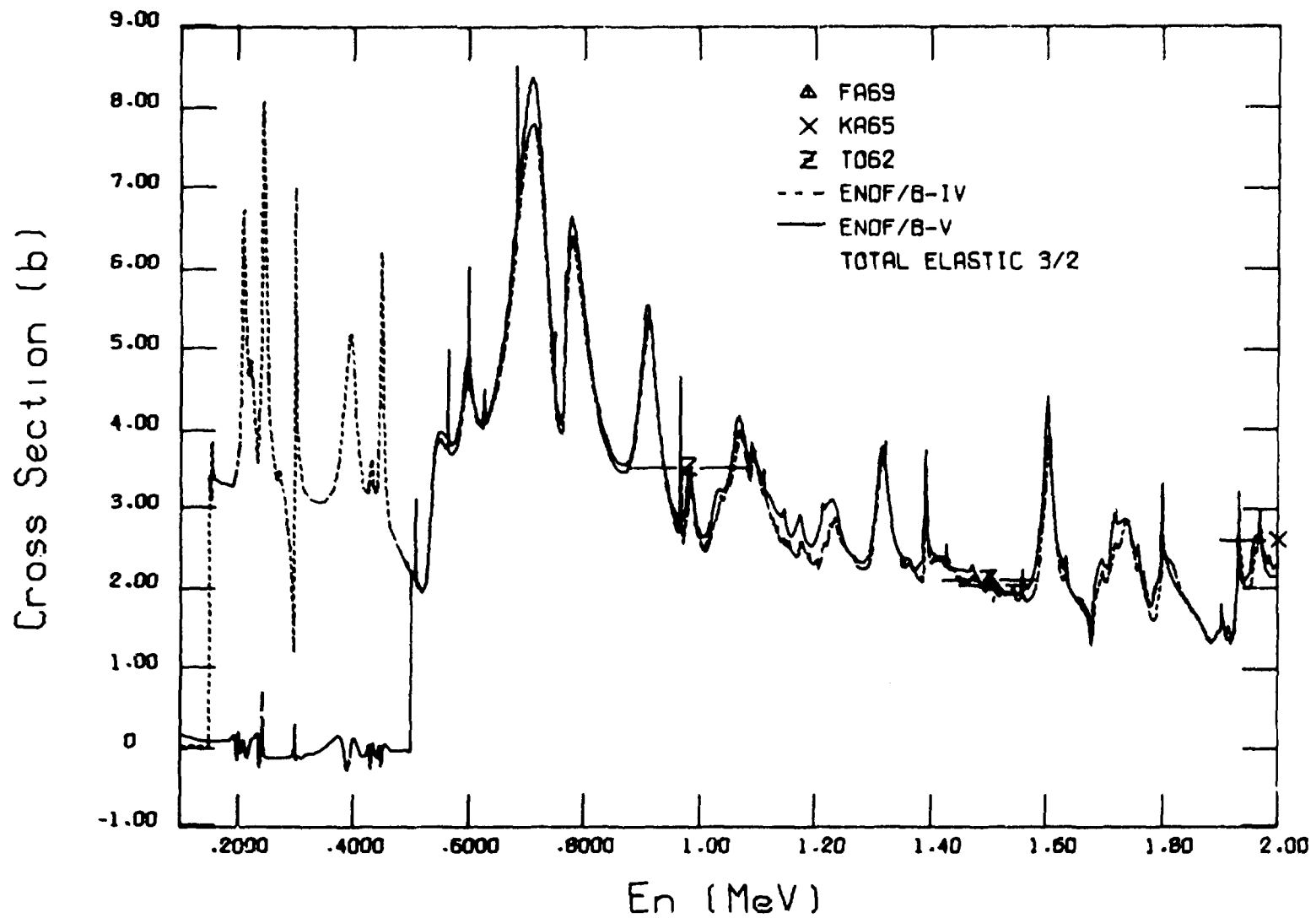


Fig. 28. Comparison of V4 and V5 total elastic cross section from 100 keV to 2 MeV with data of FA69 KA65 and T062.

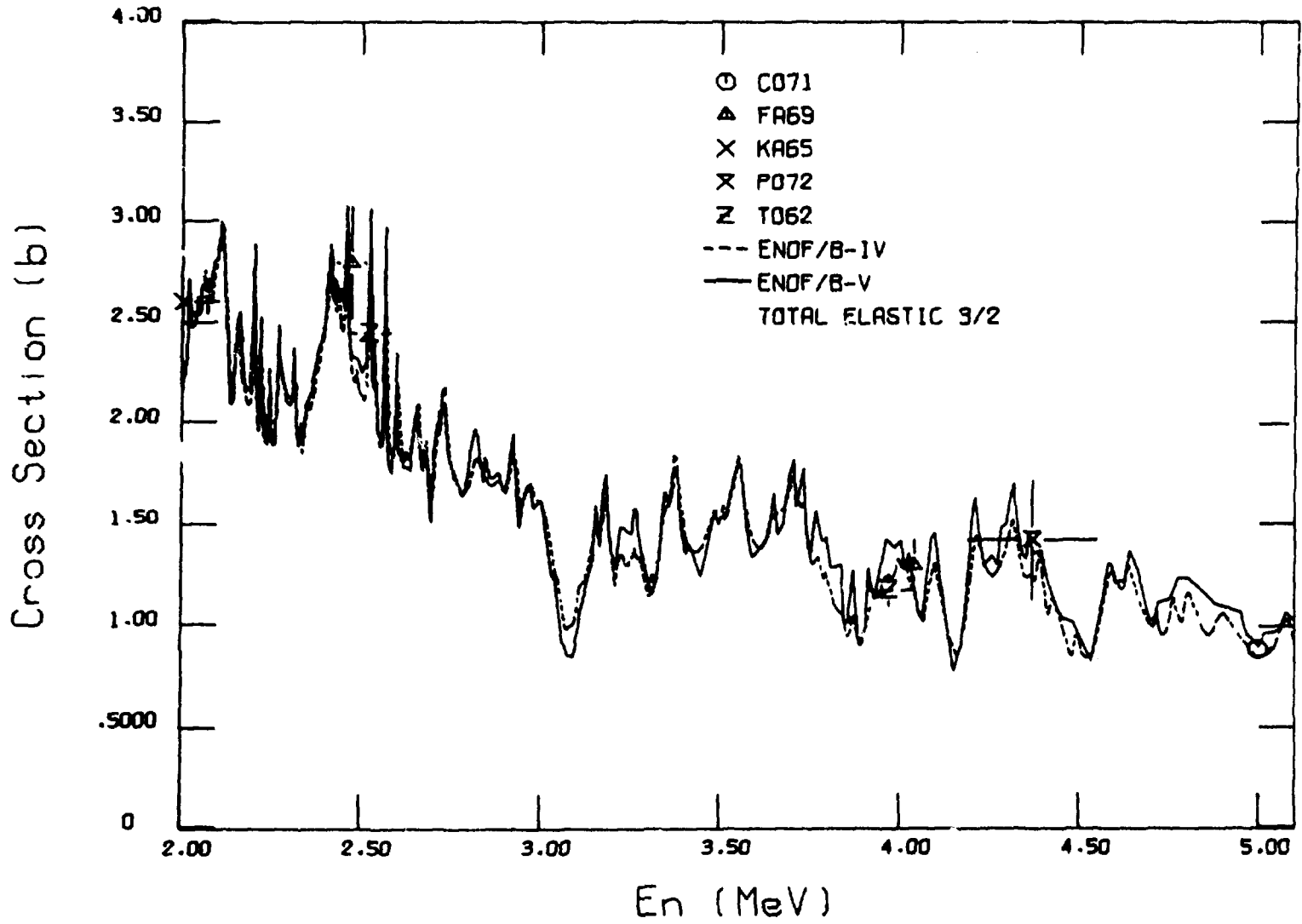


Fig. 29. Comparison of V4 and V5 total elastic cross section from 2.0 to 5.1 MeV with available data.

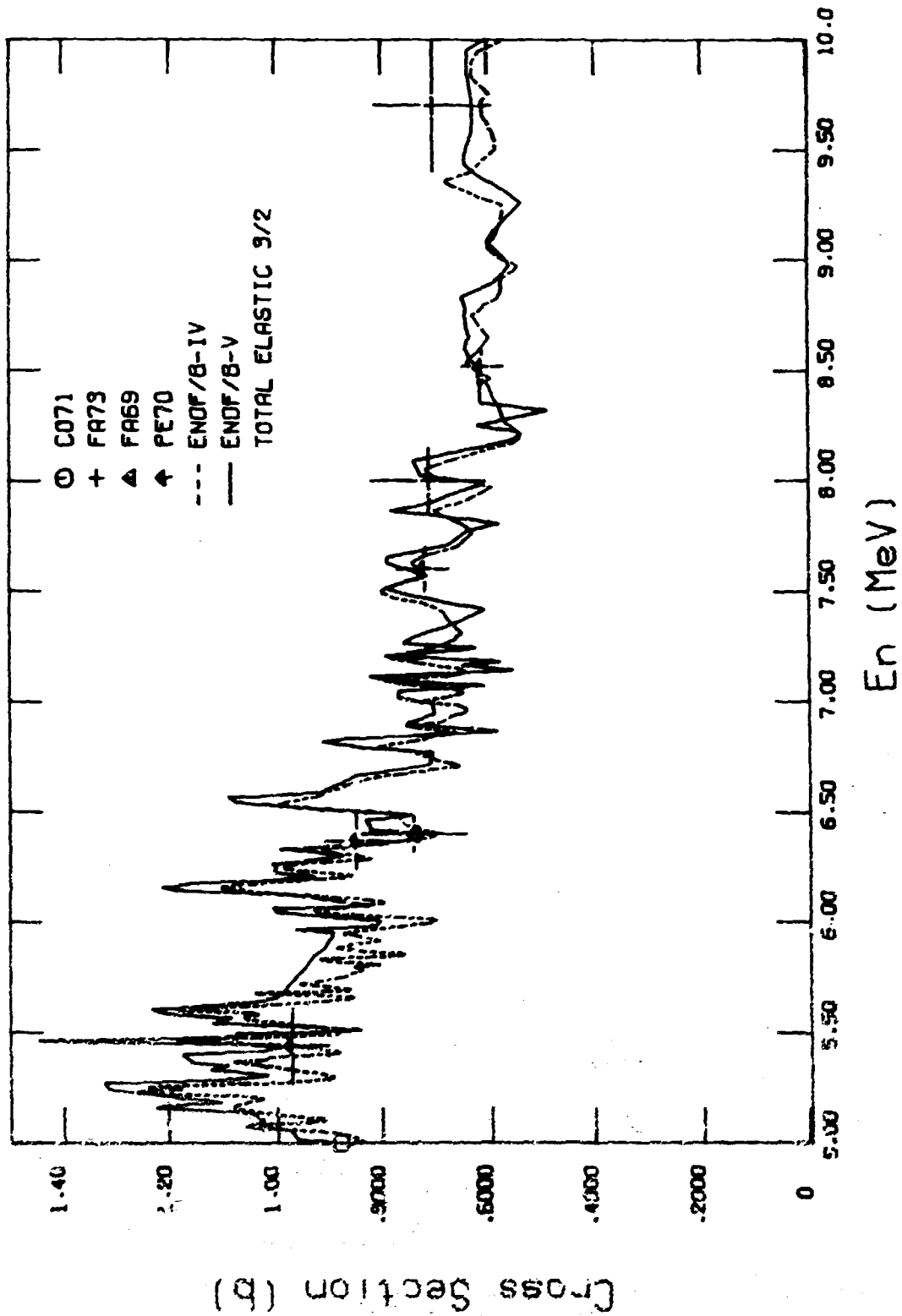


Fig. 30. Comparison of V4 and V5 total elastic cross section from 5 to 10 MeV with available data.

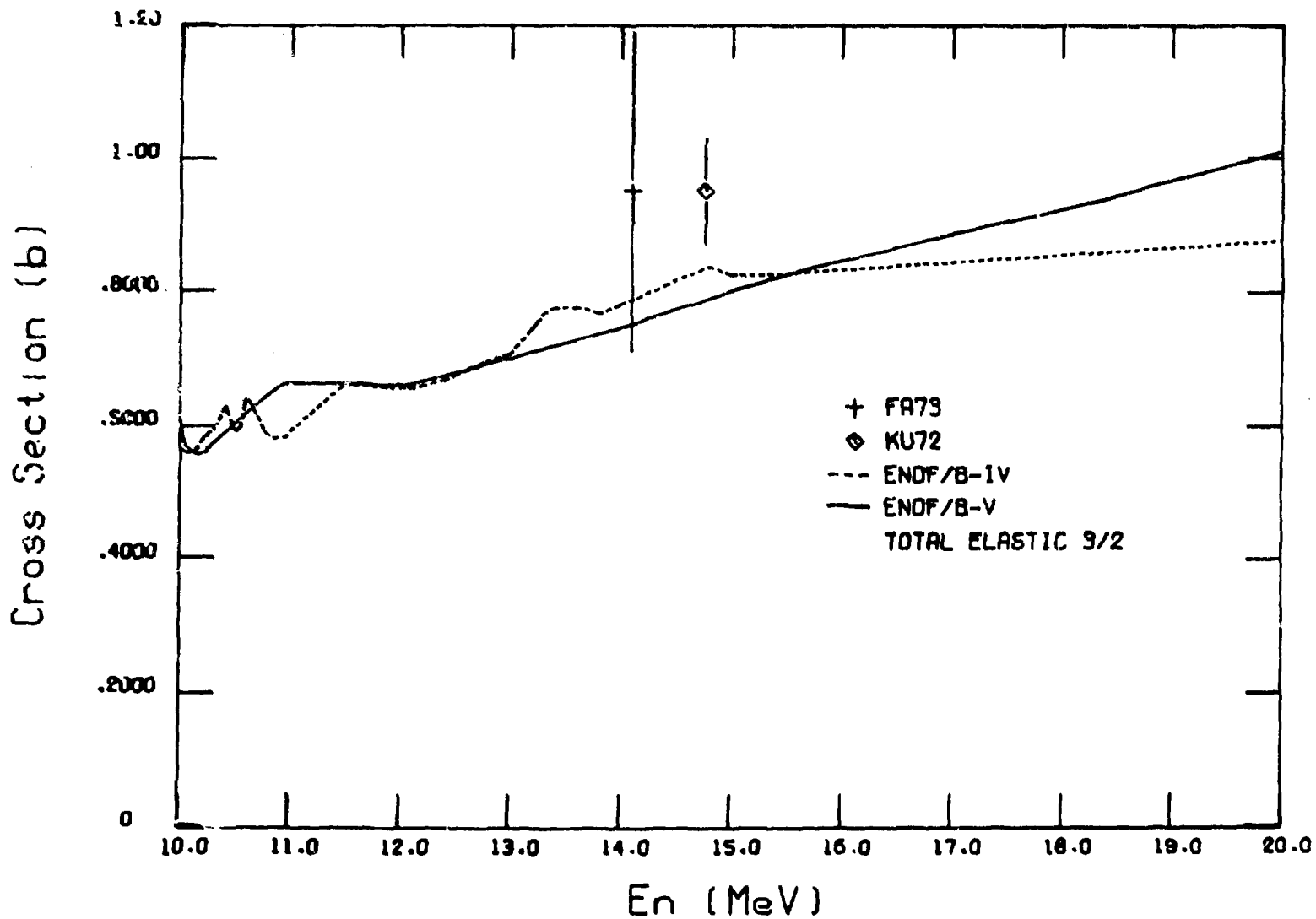


Fig. 31. Comparison of V4 and V5 total elastic cross section from 10 to 20 MeV with available data.

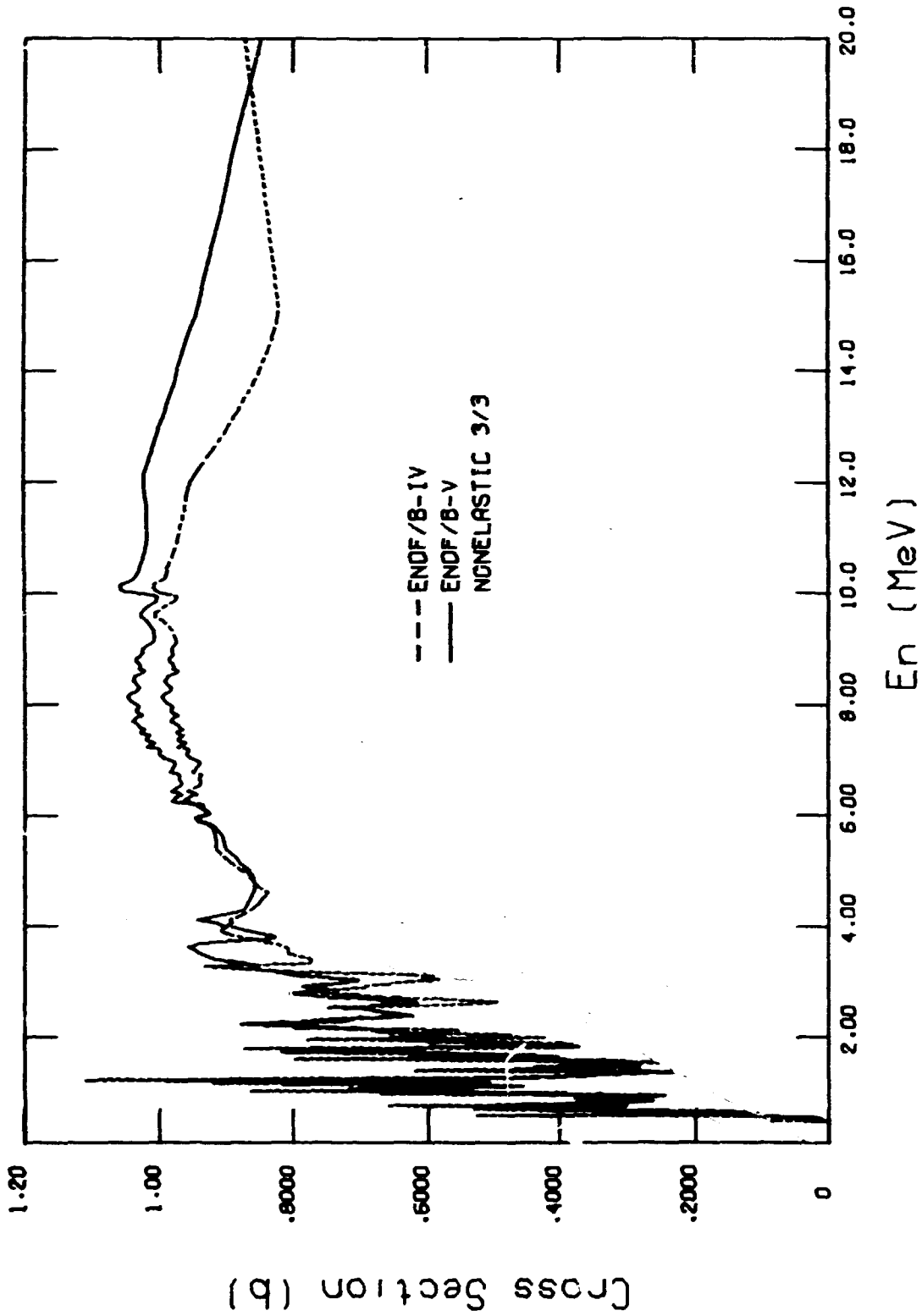


Fig. 32. Comparison of V4 and V5 nonelastic cross sections.

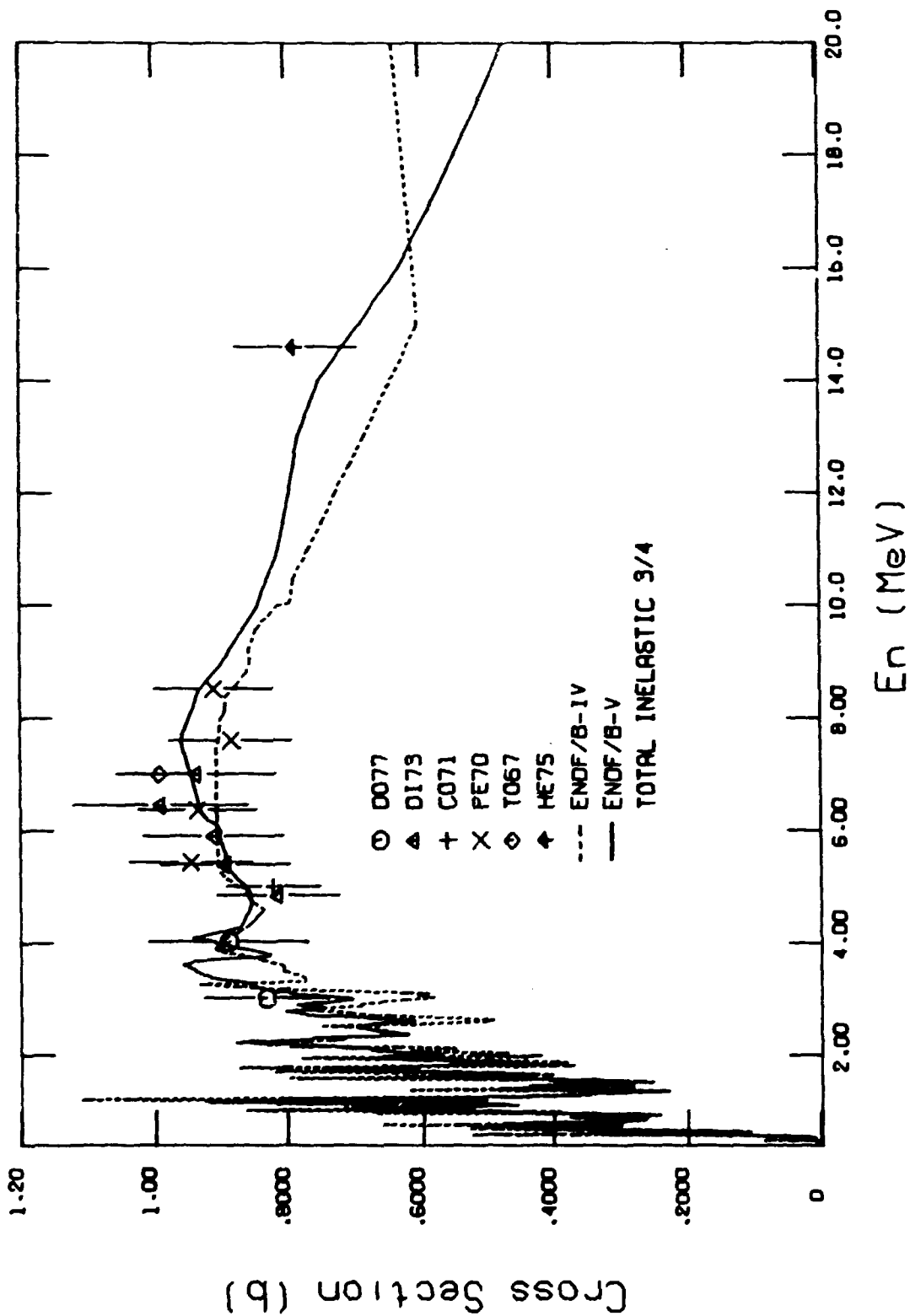


Fig. 33. Comparison of V4 and V5 total inelastic cross sections with available data.

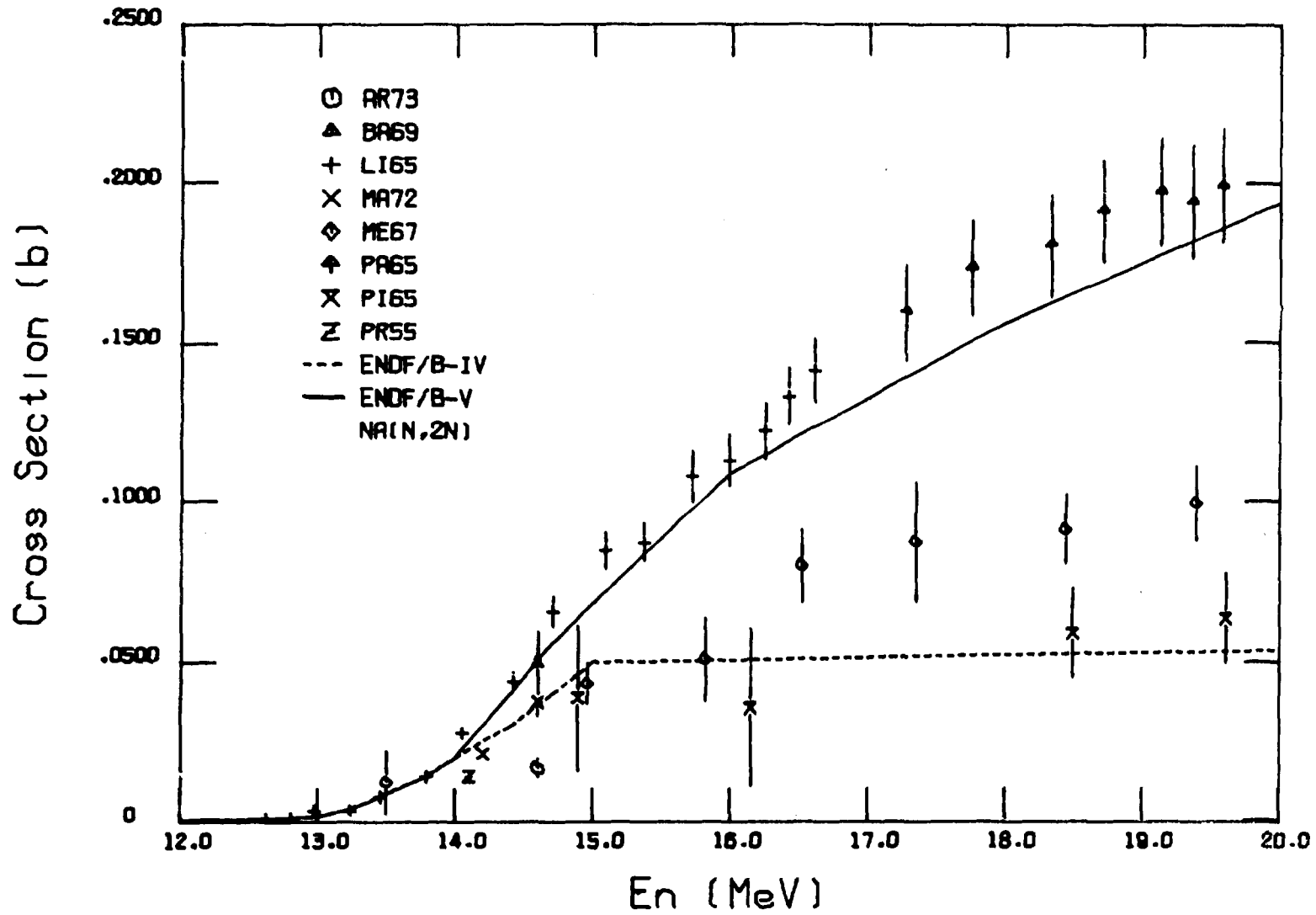


Fig. 34. Comparison of V4 and V5 (n,2n) cross sections with available data.

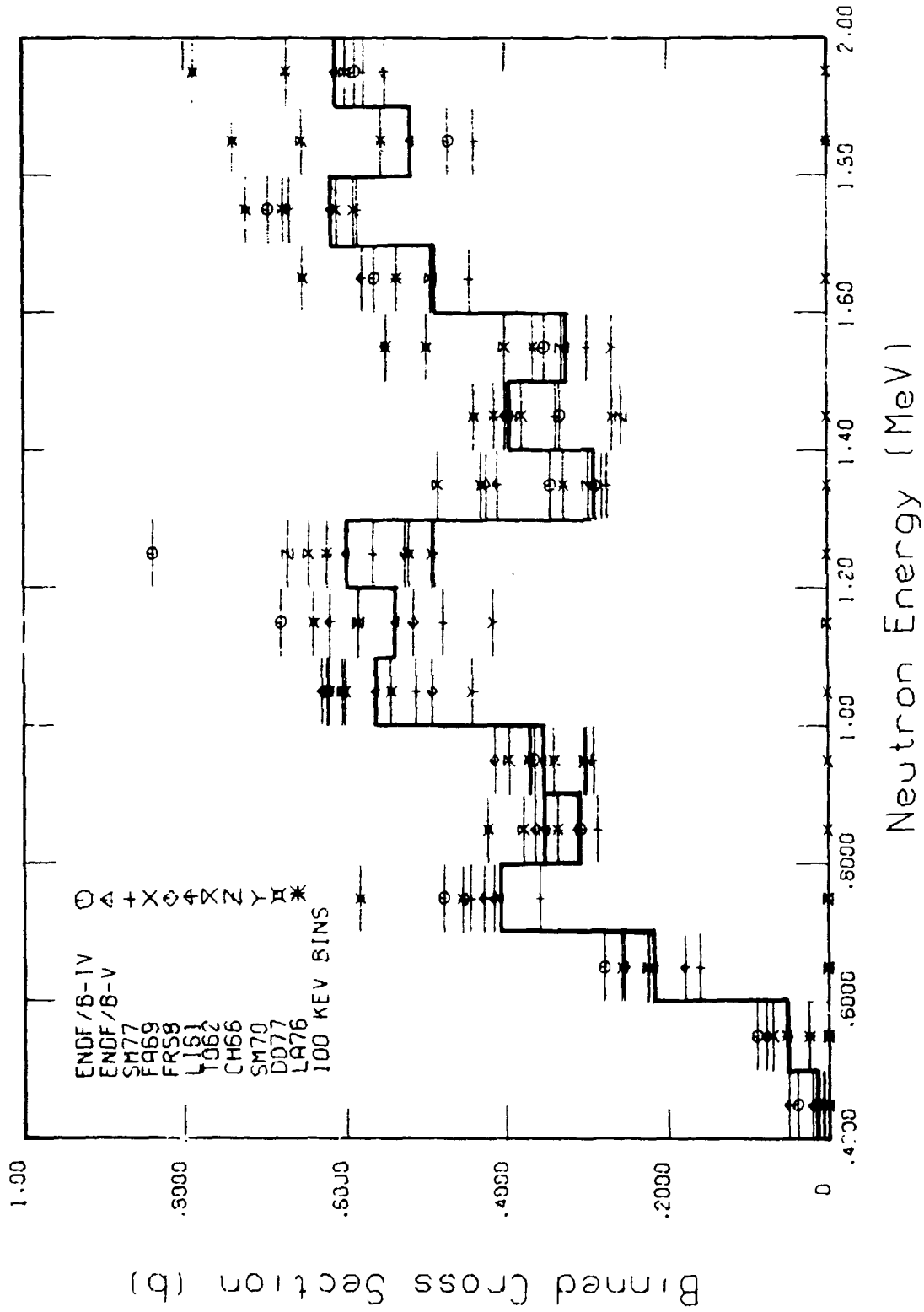


Fig. 35. Comparison of V4 and V5 (n,n') cross sections to .44-Mev level with available data, averaged over 100-keV bins.

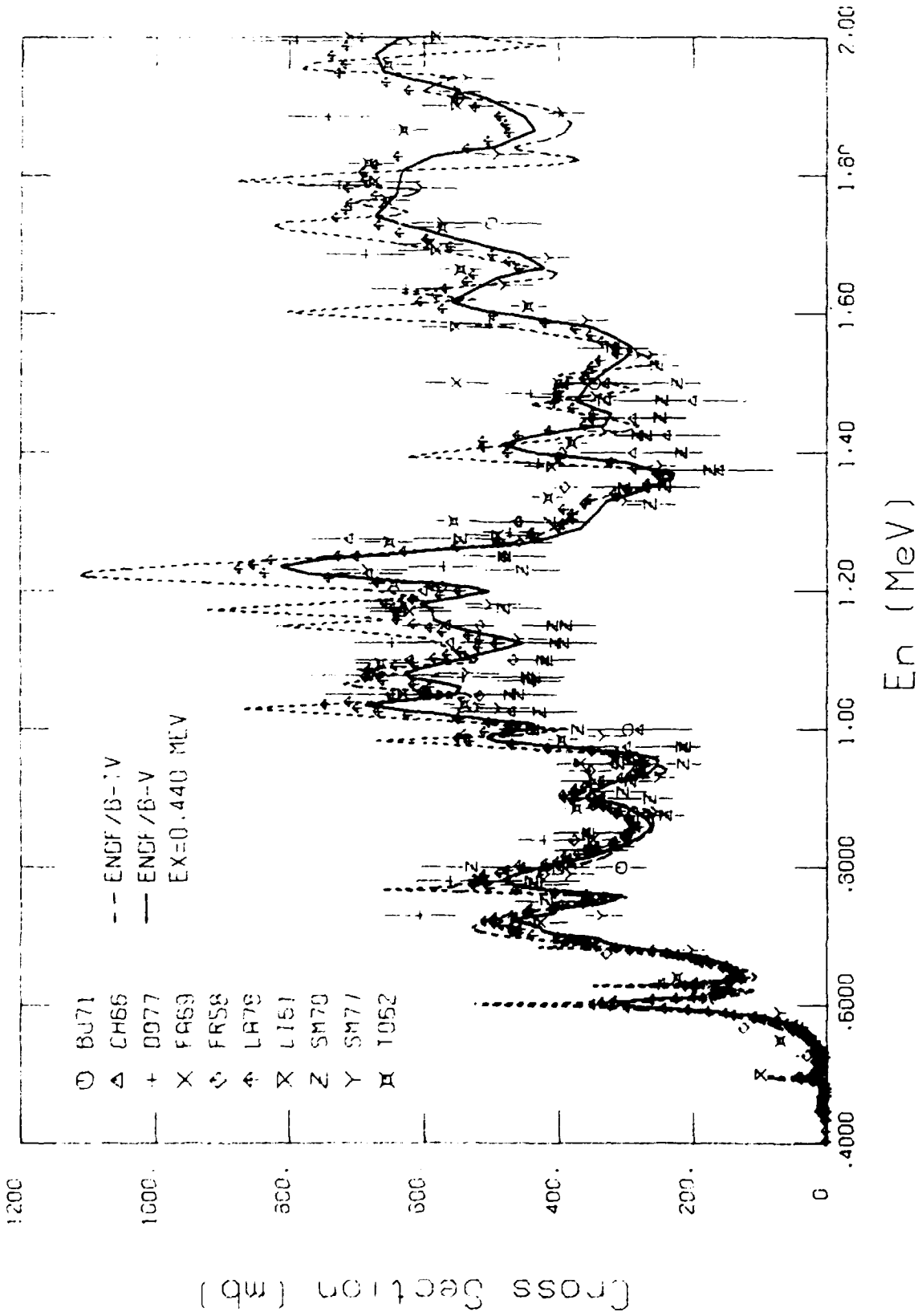


Fig. 36. Comparison of V4 and V5 inelastic scattering to 0.44-MeV level with available data.

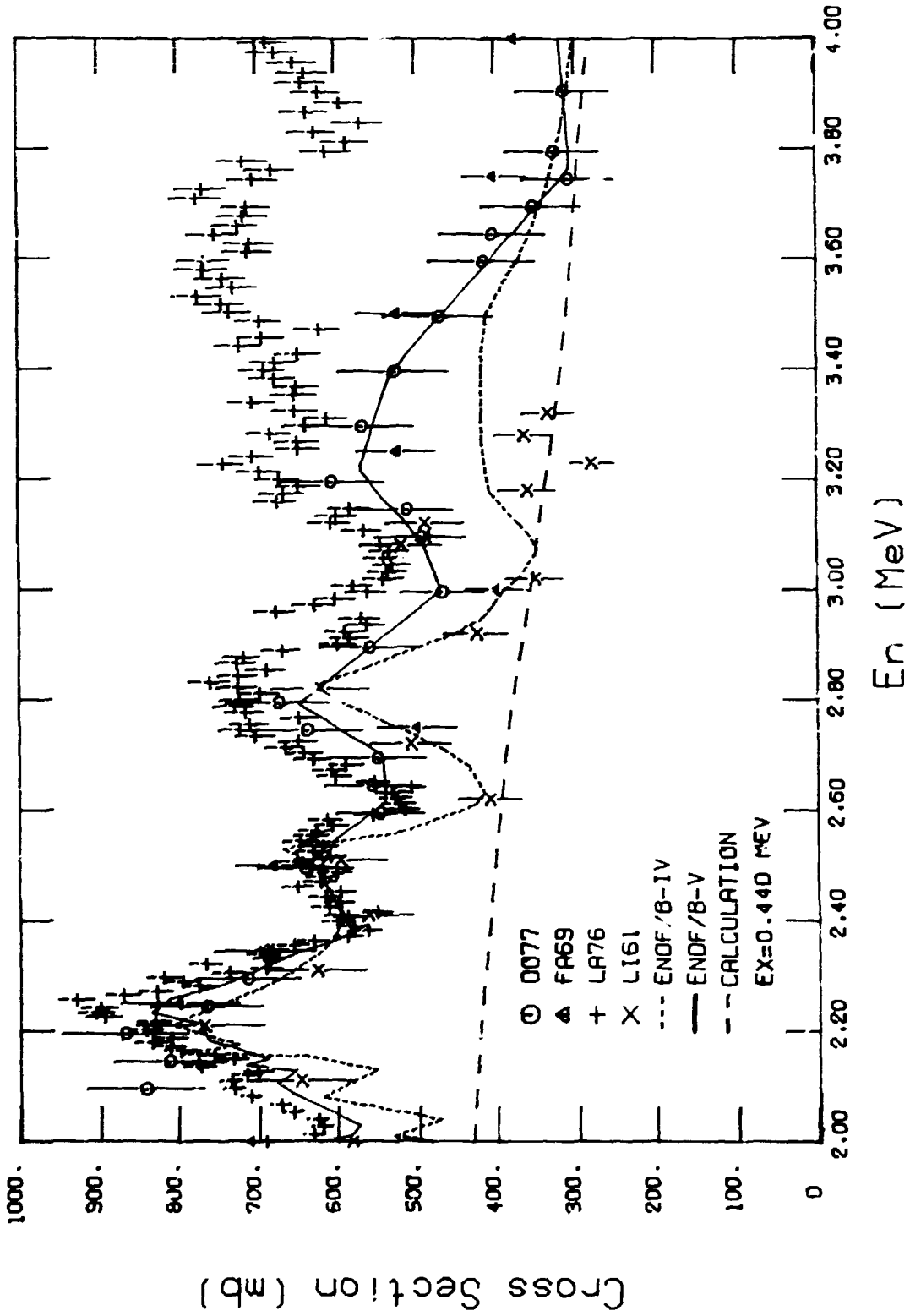


Fig. 37. Comparison of V4 and V5 inelastic scattering to 0.44-MeV level with available data and calculated results.

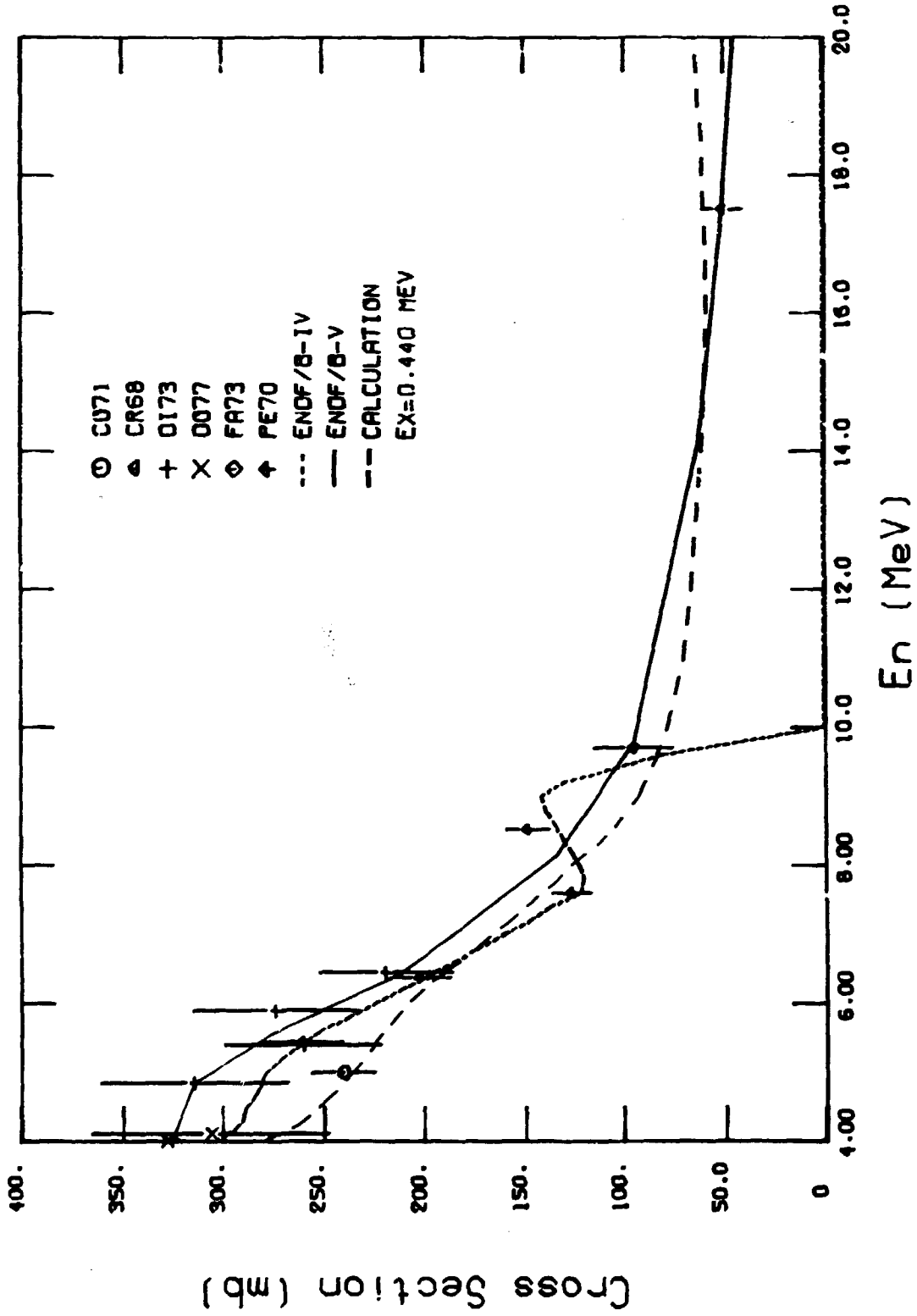


Fig. 38. Comparison of V4 and V5 inelastic scattering to 0.44-MeV level with available data and calculated results.

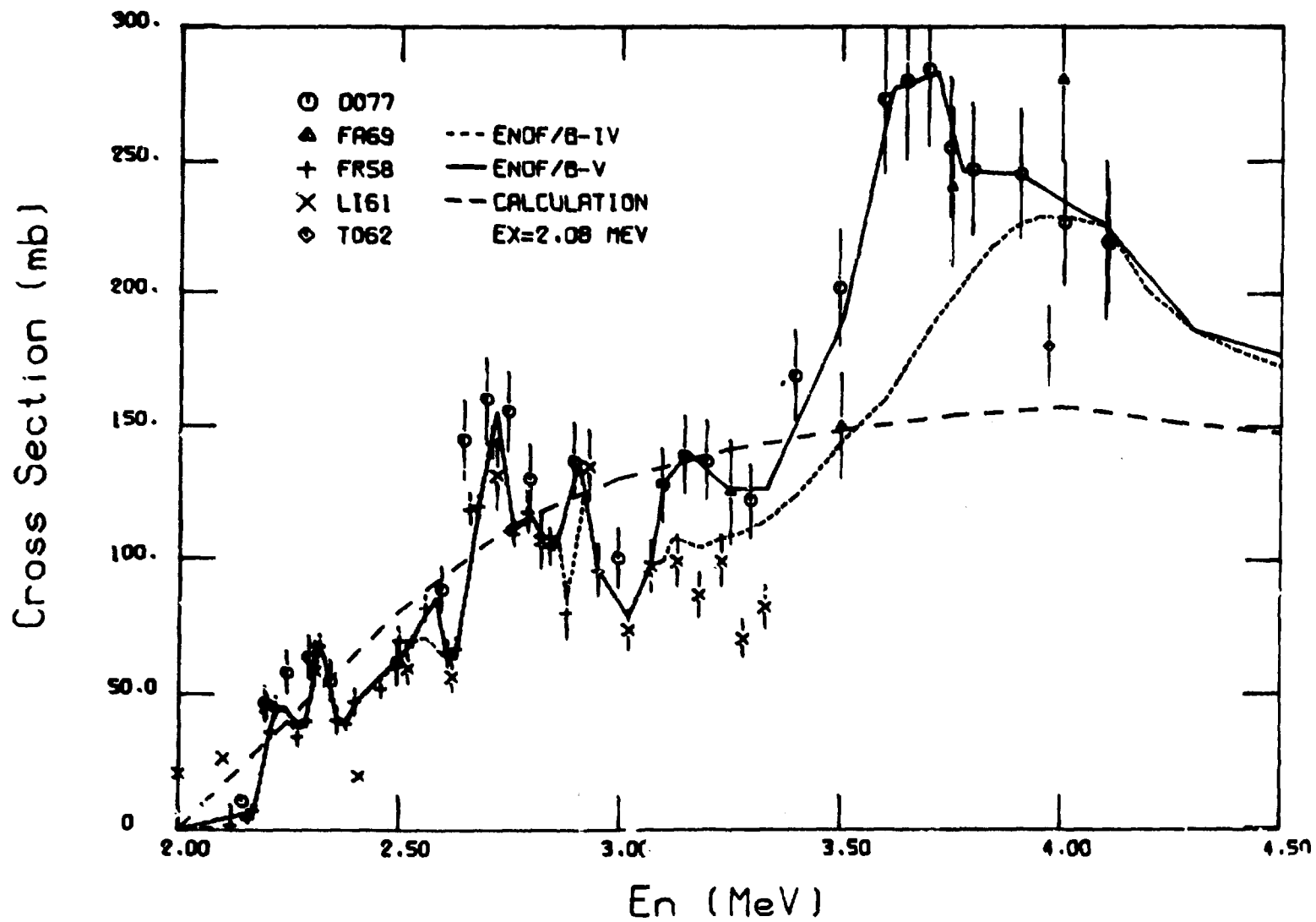


Fig. 39. Comparison of V4 and V5 inelastic scattering to 2.08-MeV level with available data and calculated results.

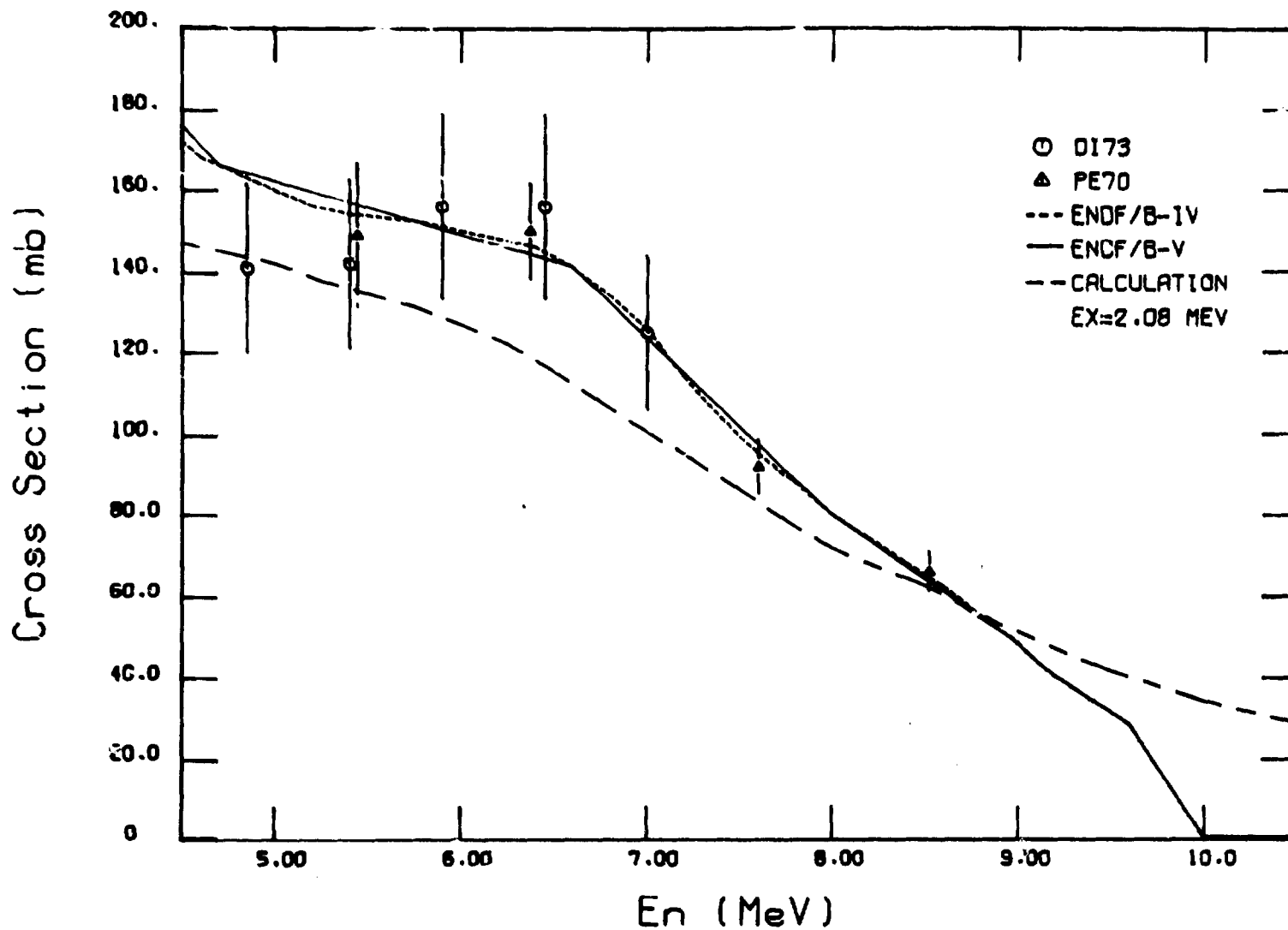


Fig. 40. Comparison of V4 and V5 inelastic scattering to 2.08-MeV level with available data and calculated results.

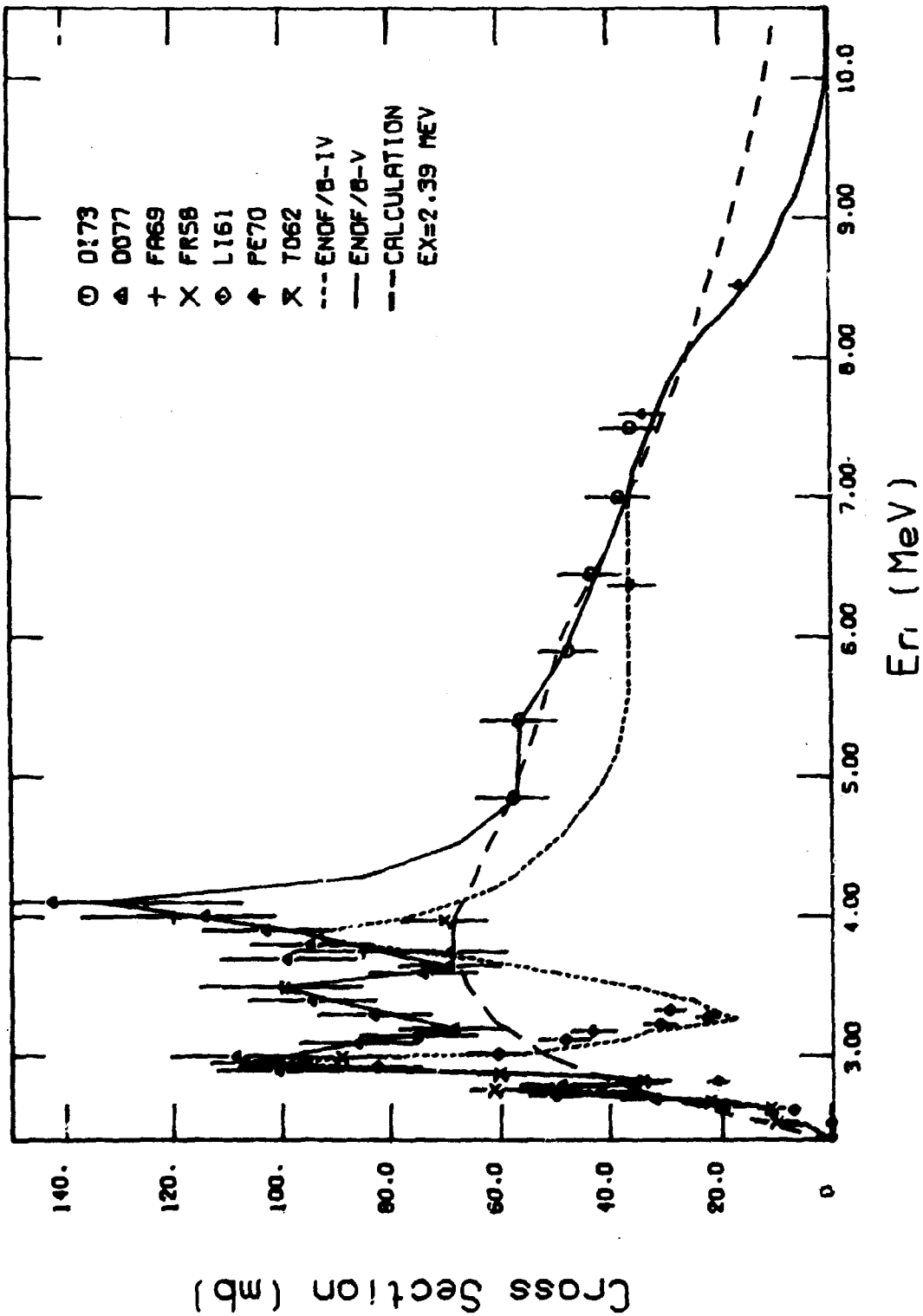


Fig. 41. Comparison of V4 and V5 inelastic scattering to 2.39-MeV level with available data and calculated results.

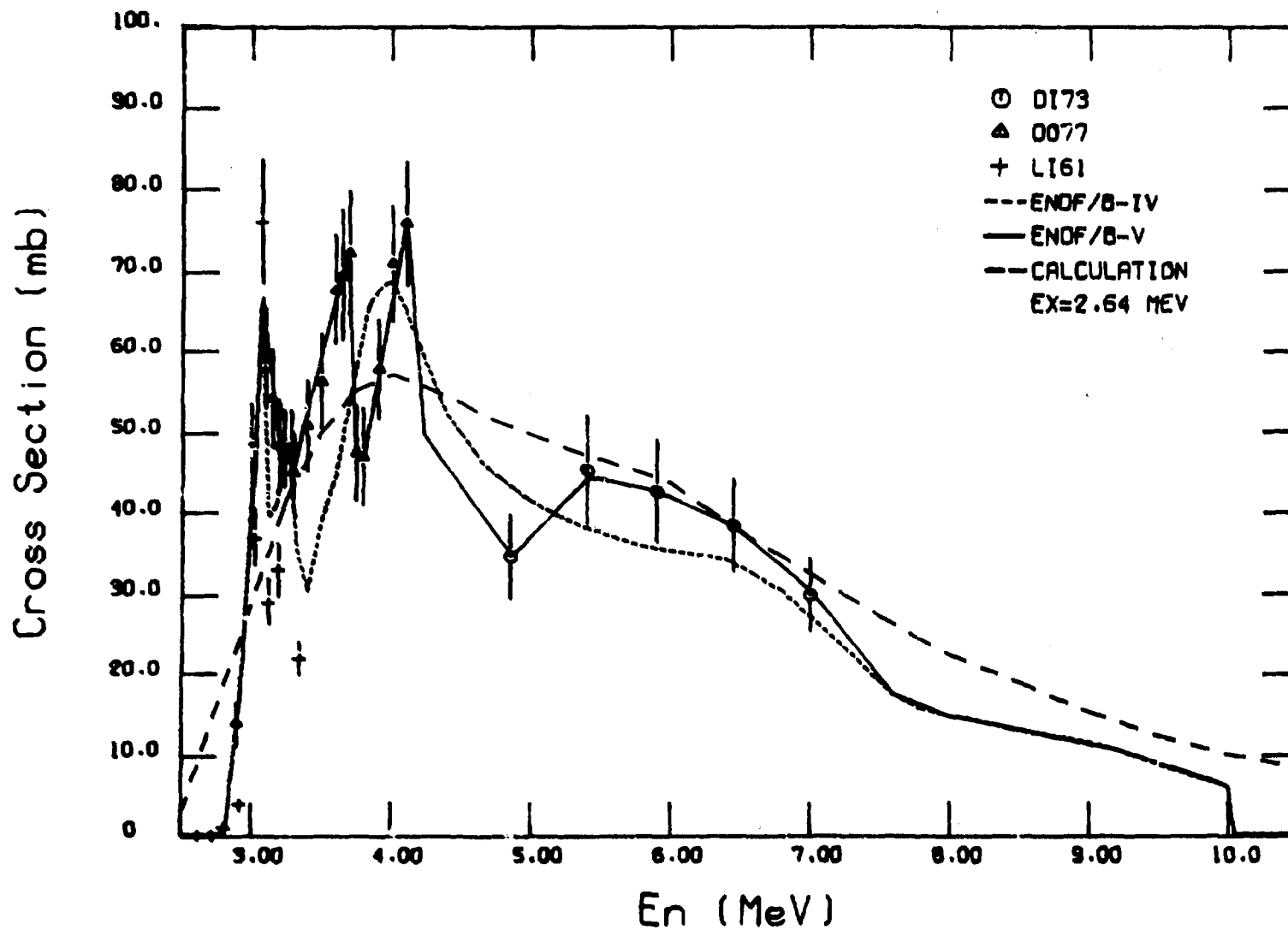


Fig. 42. Comparison of V4 and V5 inelastic scattering to 2.64-MeV level with available data and calculated results.

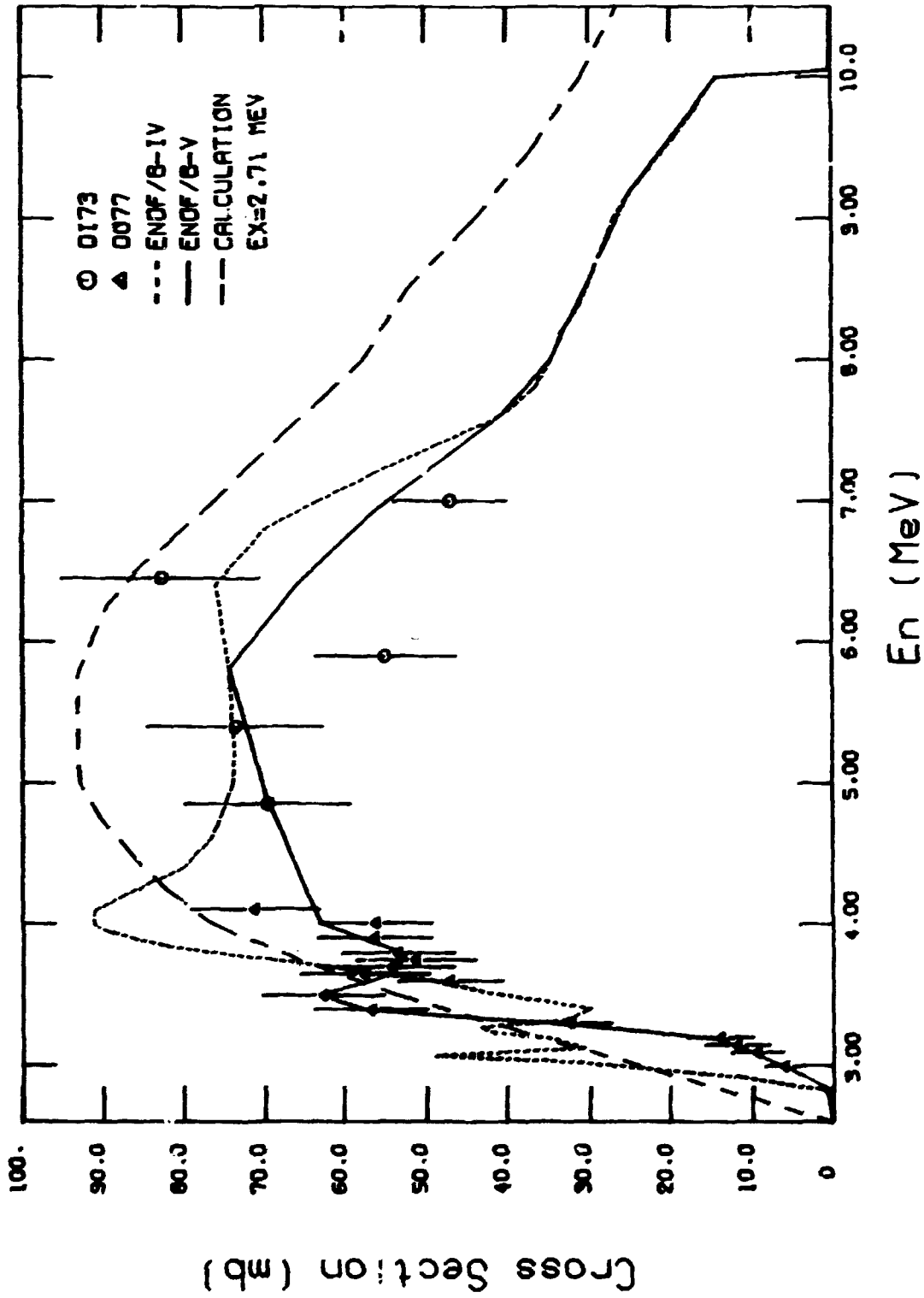


Fig. 43. Comparison of V4 and V5 inelastic scattering to 2.71-MeV level with available data and calculated results.

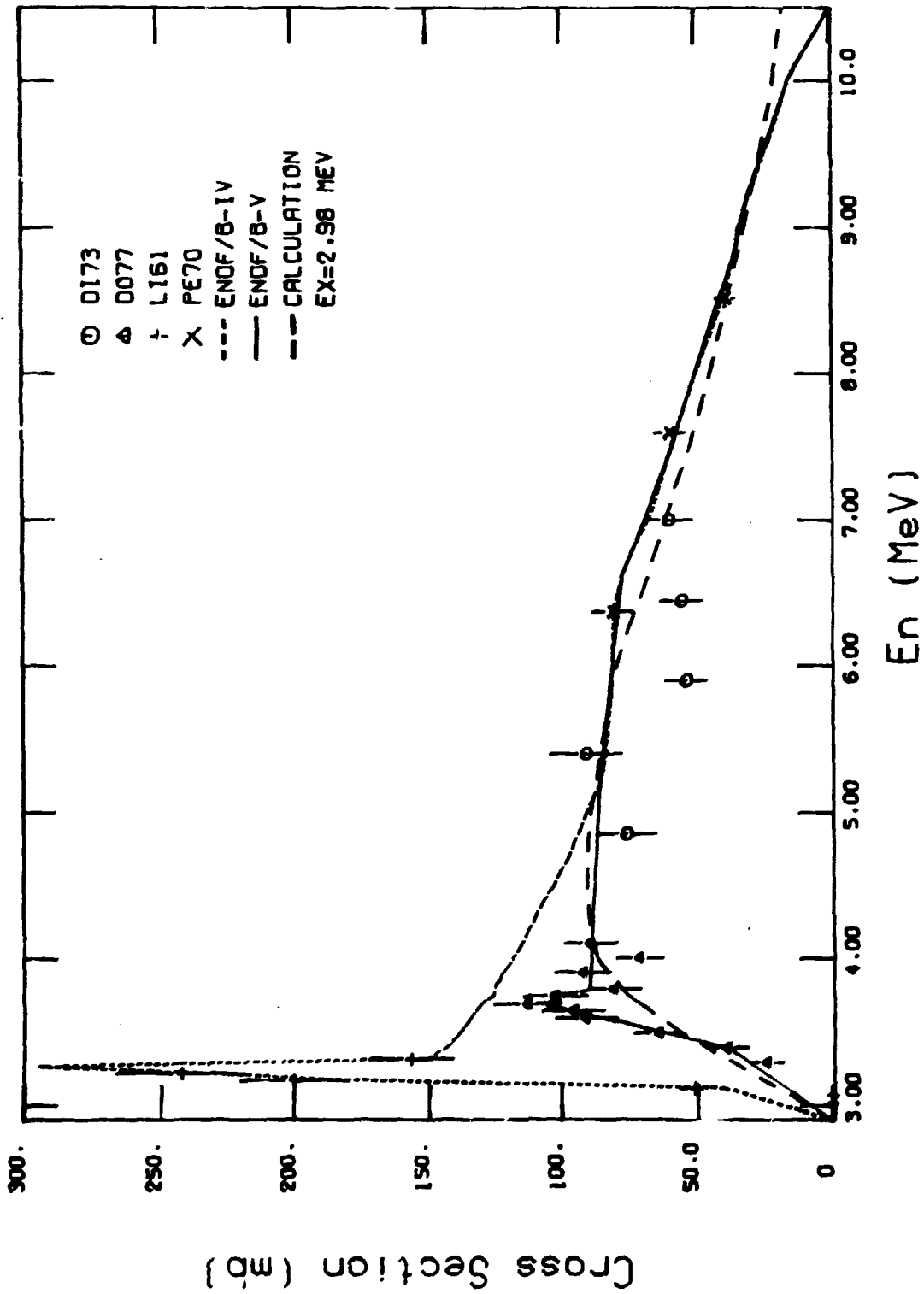


Fig. 44. Comparison of V4 and V5 inelastic scattering to 2.98-MeV level with available data and calculated results.

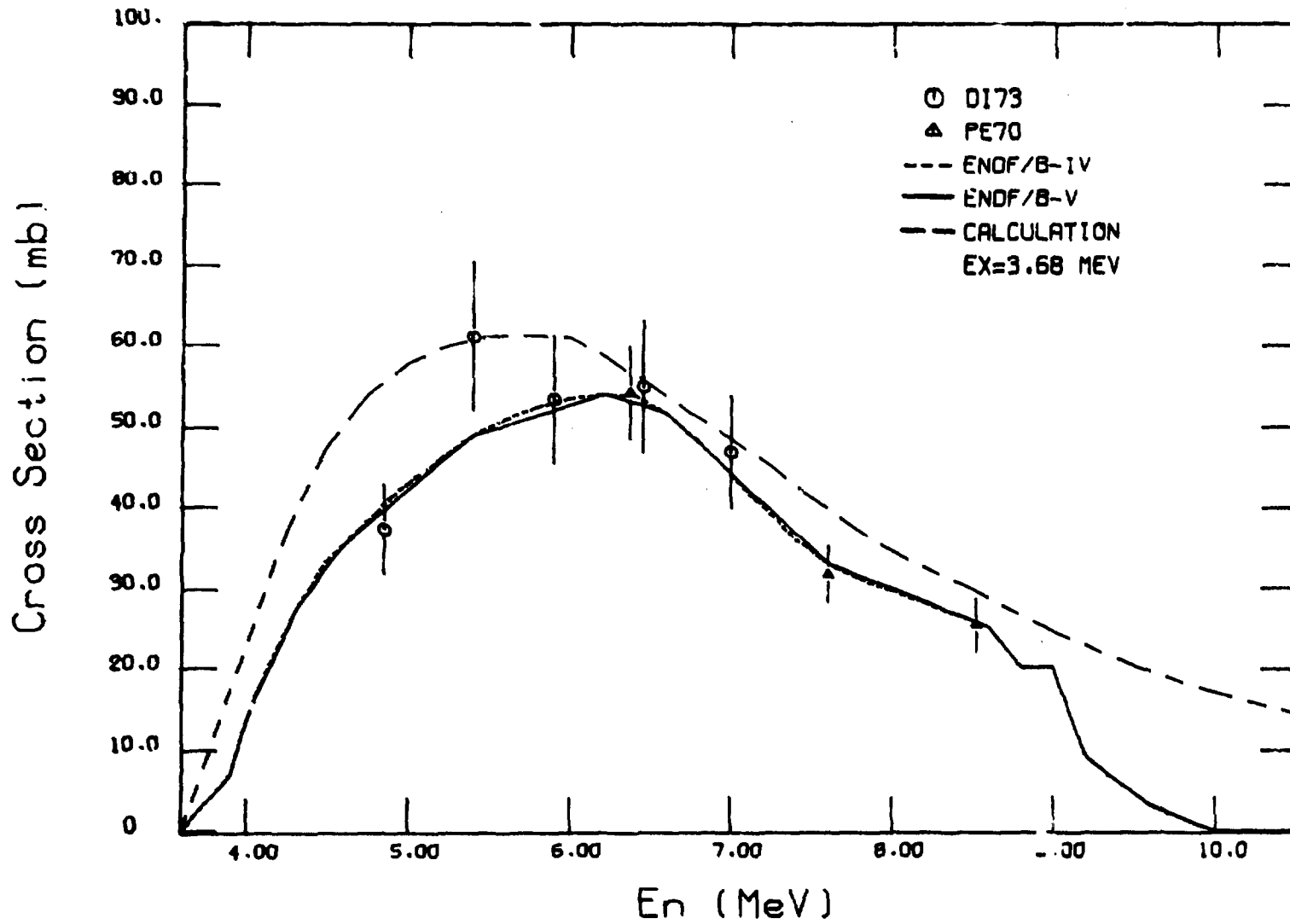


Fig. 45. Comparison of V4 and V5 inelastic scattering to 3.68-MeV level with available data and calculated results.

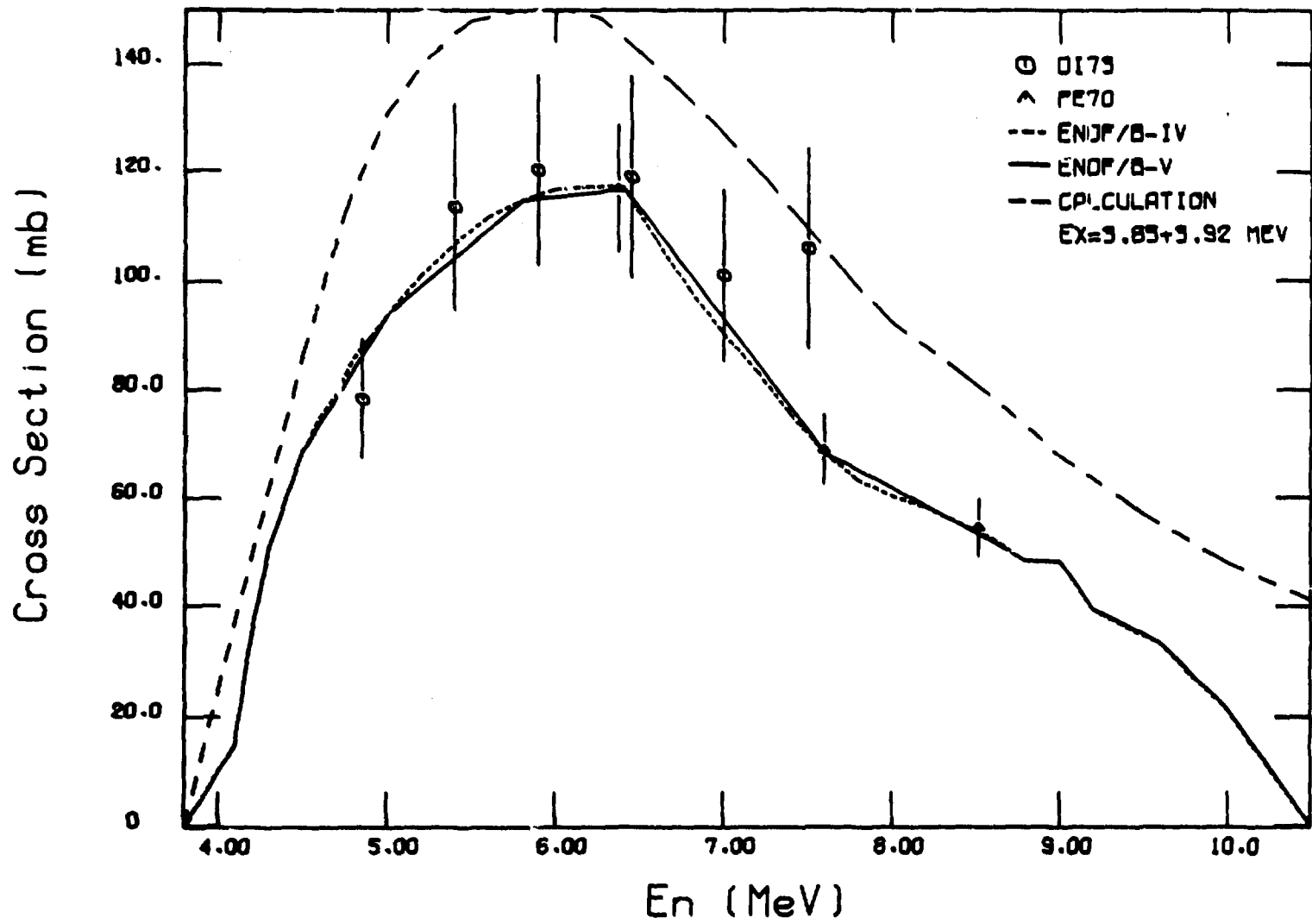


Fig. 46. Comparison of V4 and V5 inelastic scattering to 3.85+3.92-MeV levels with available data and calculated results.

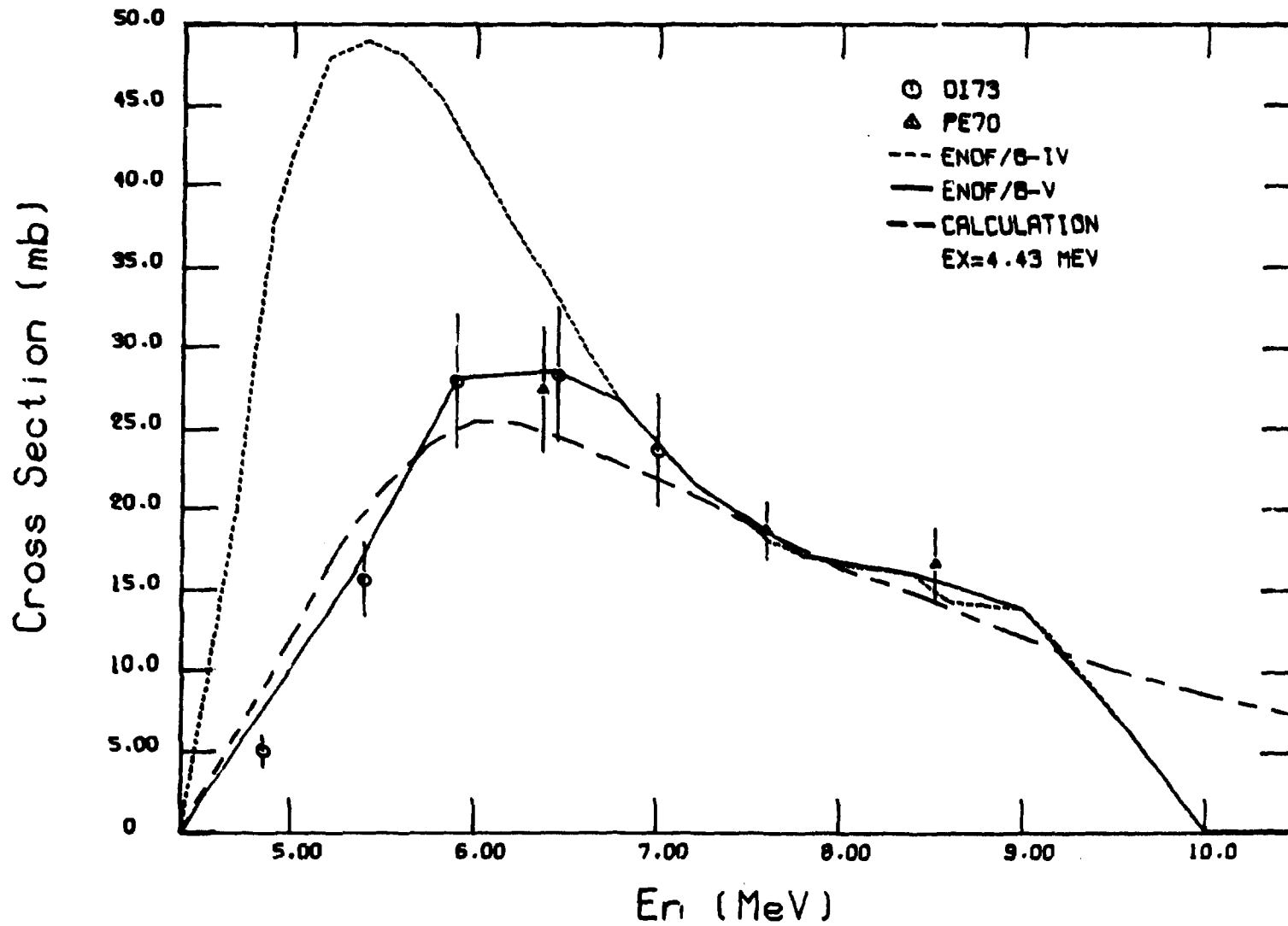


Fig. 47. Comparison of V4 and V5 inelastic scattering to 4.43-MeV level with available data and calculated results.

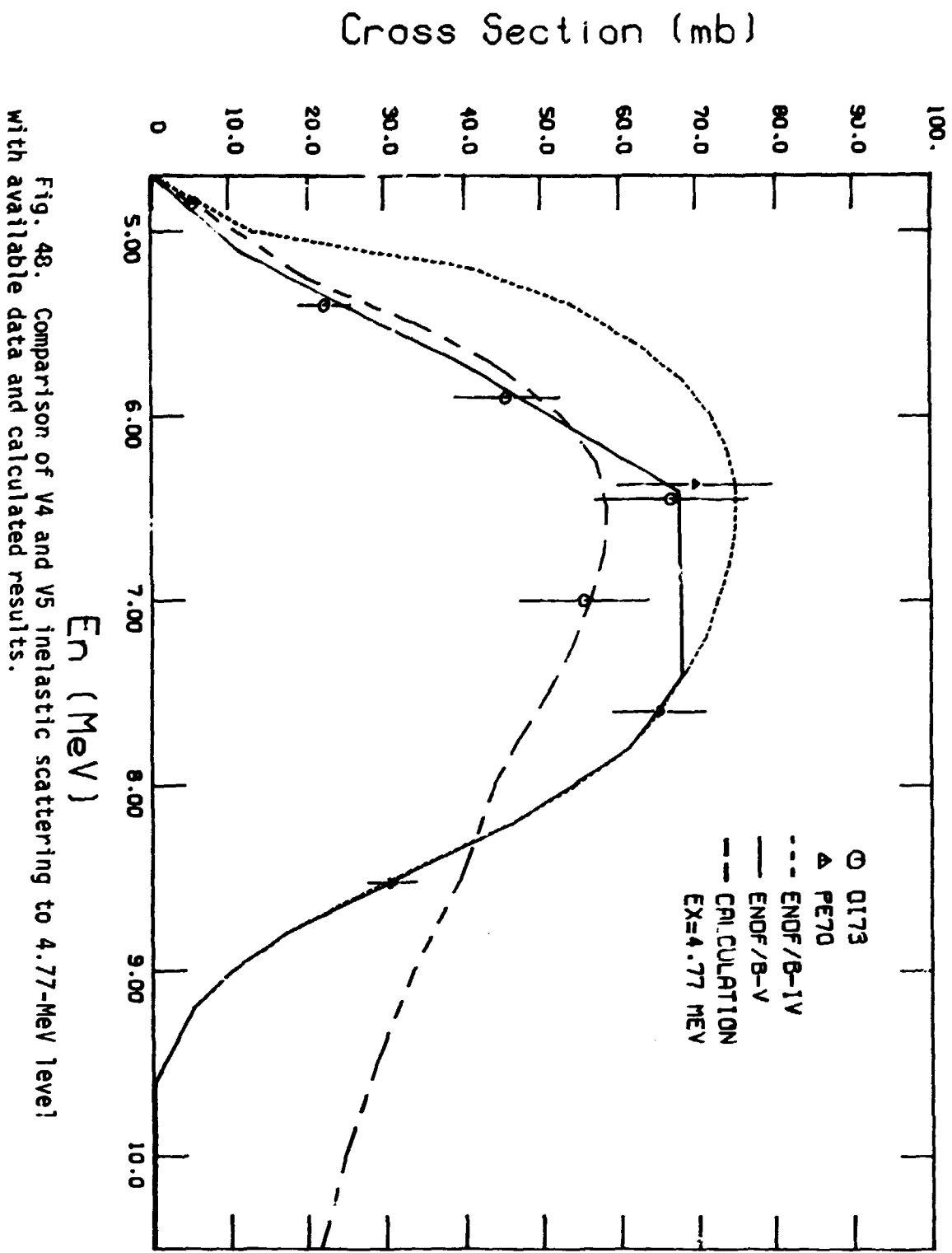


Fig. 48. Comparison of V4 and V5 inelastic scattering to 4.77-MeV level with available data and calculated results.

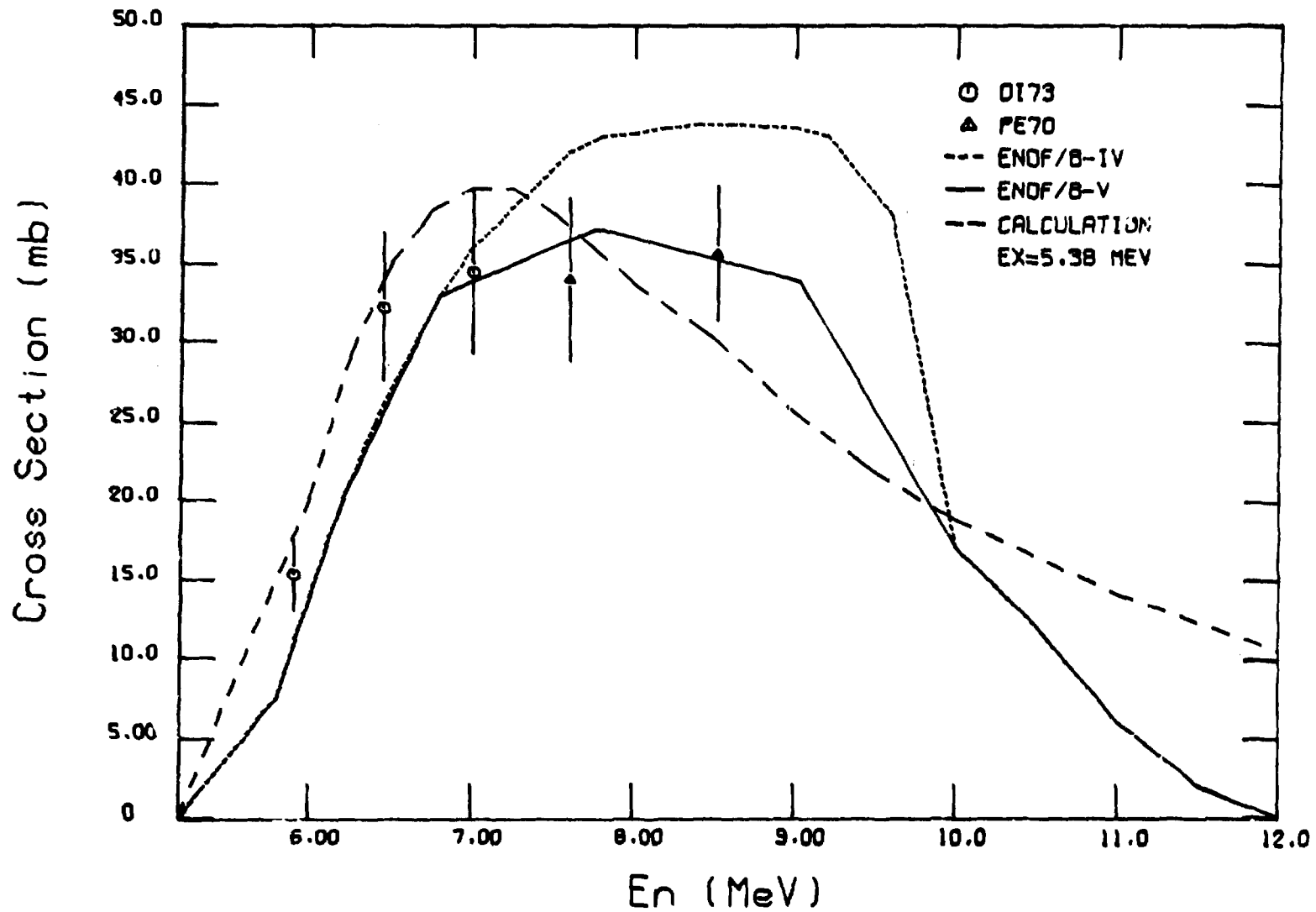


Fig. 49. Comparison of V4 and V5 inelastic scattering to 5.38-MeV level with available data and calculated results.

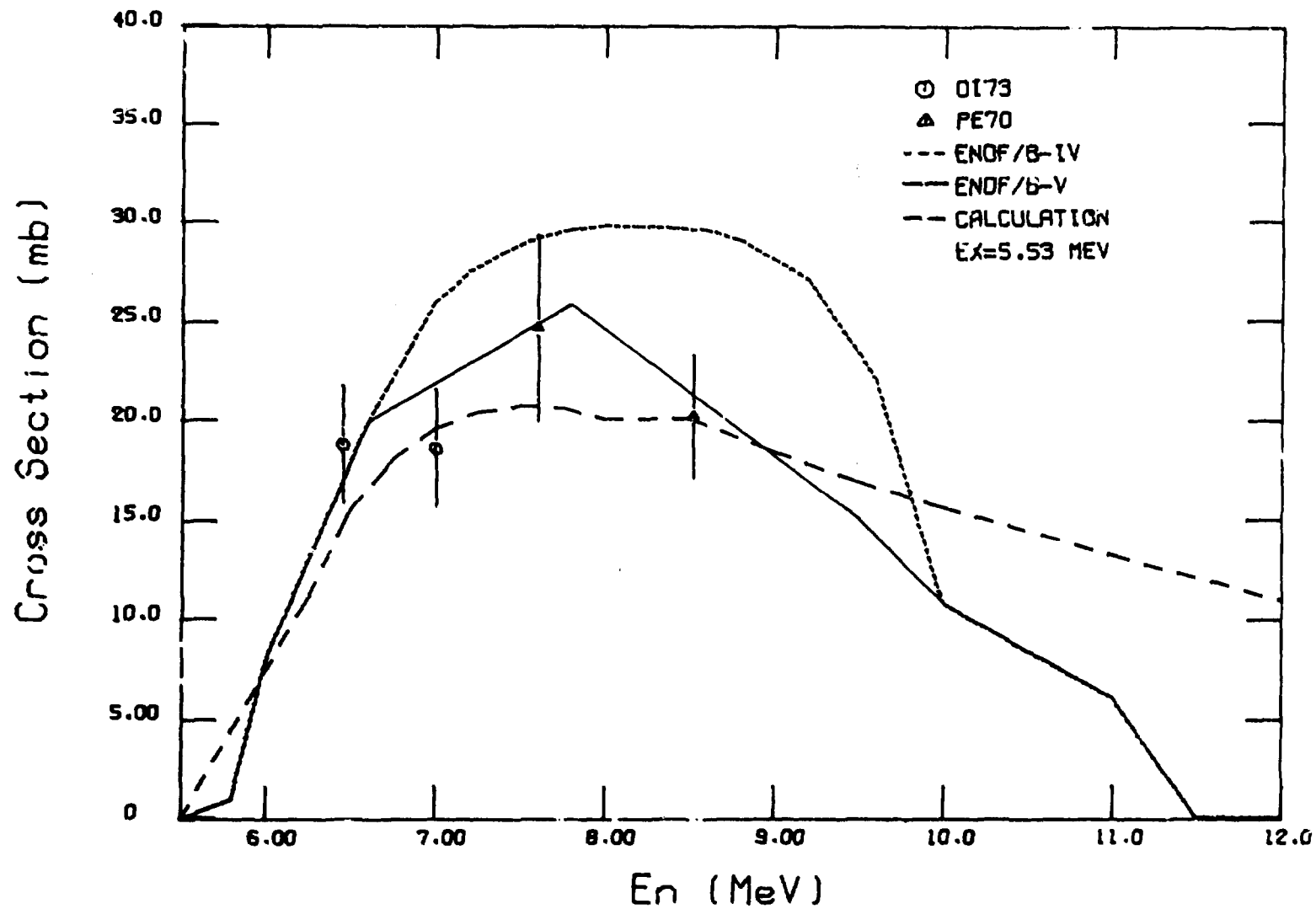


Fig. 50. Comparison of V4 and V5 inelastic scattering to 5.53-MeV level with available data and calculated results.

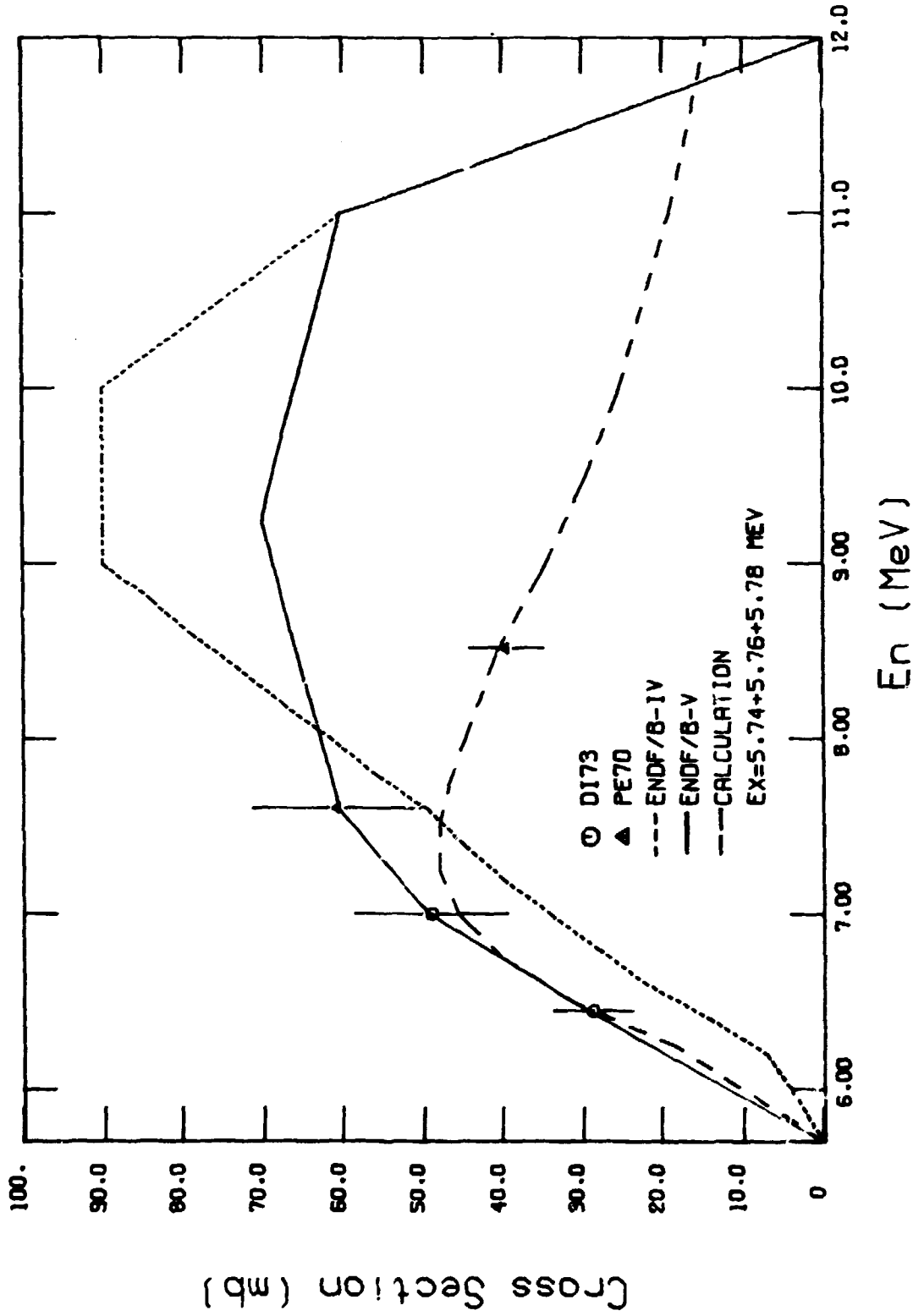


Fig. 51. Comparison of V4 and V5 inelastic scattering to 5.74+5.76+5.78-MeV levels with available data and calculated results.

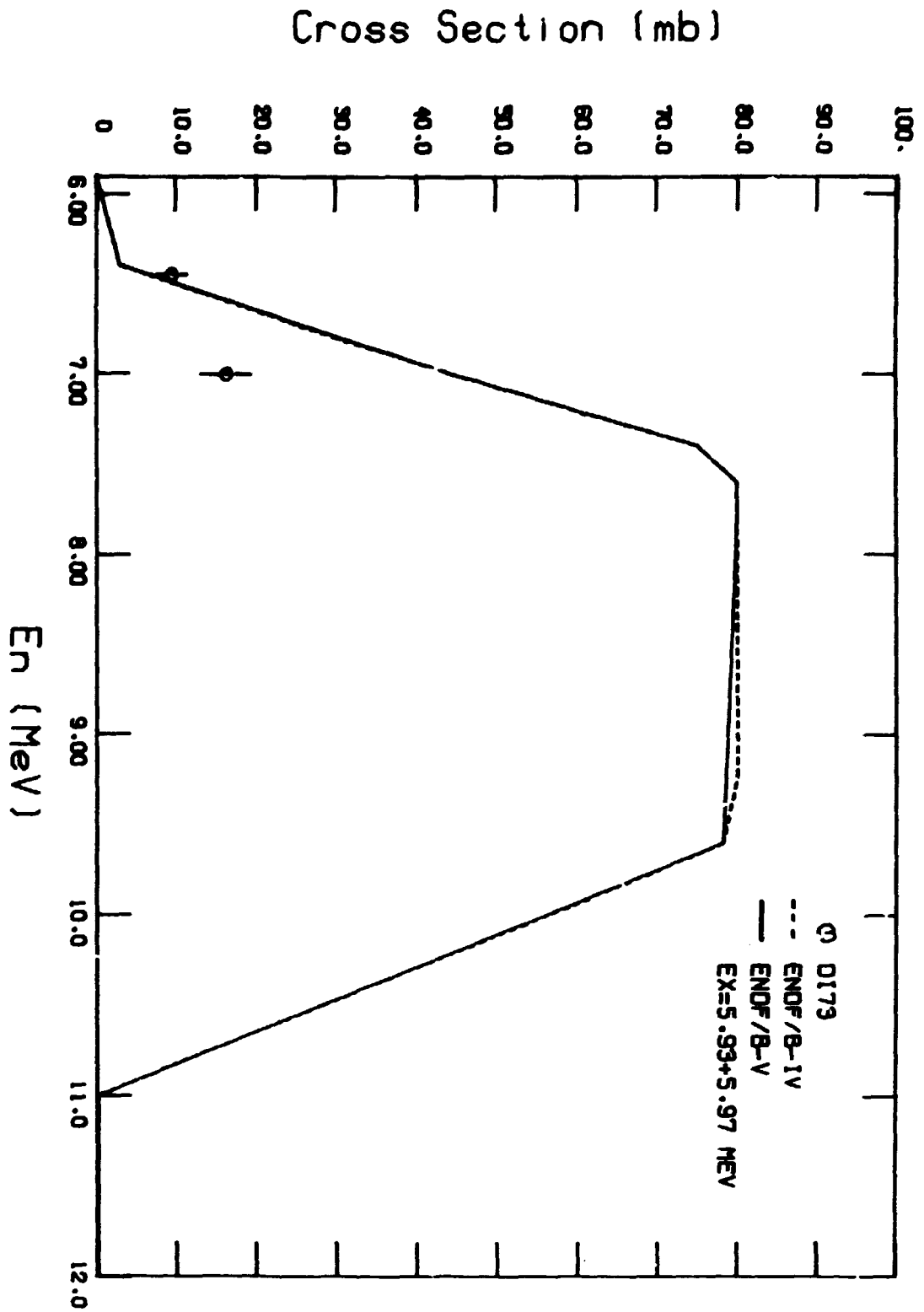


Fig. 52. Comparison of V4 and V5 inelastic scattering to 5.93+5.97-MeV level.

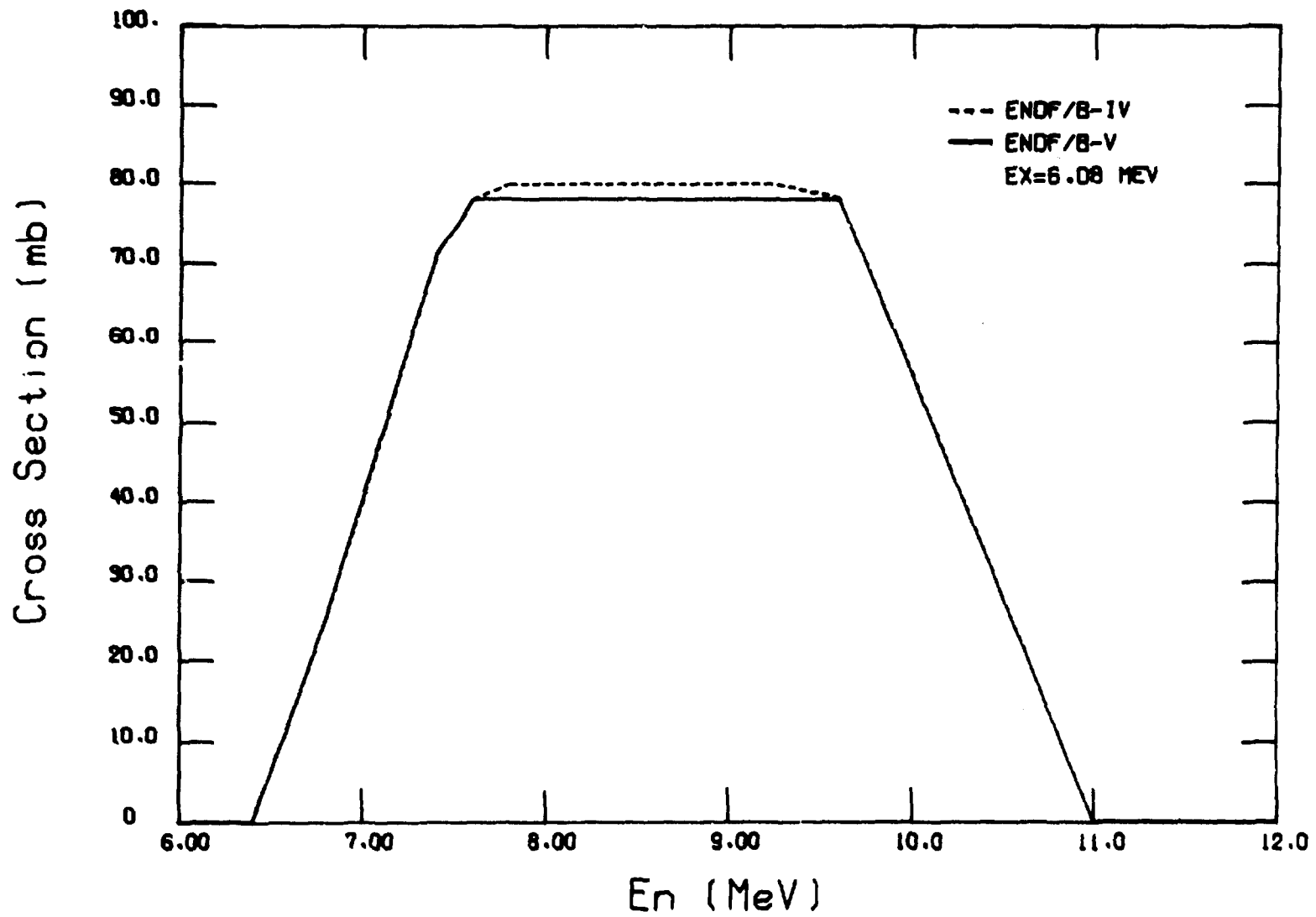


Fig. 53. Comparison of V4 and V5 inelastic scattering to 6.08-MeV level.

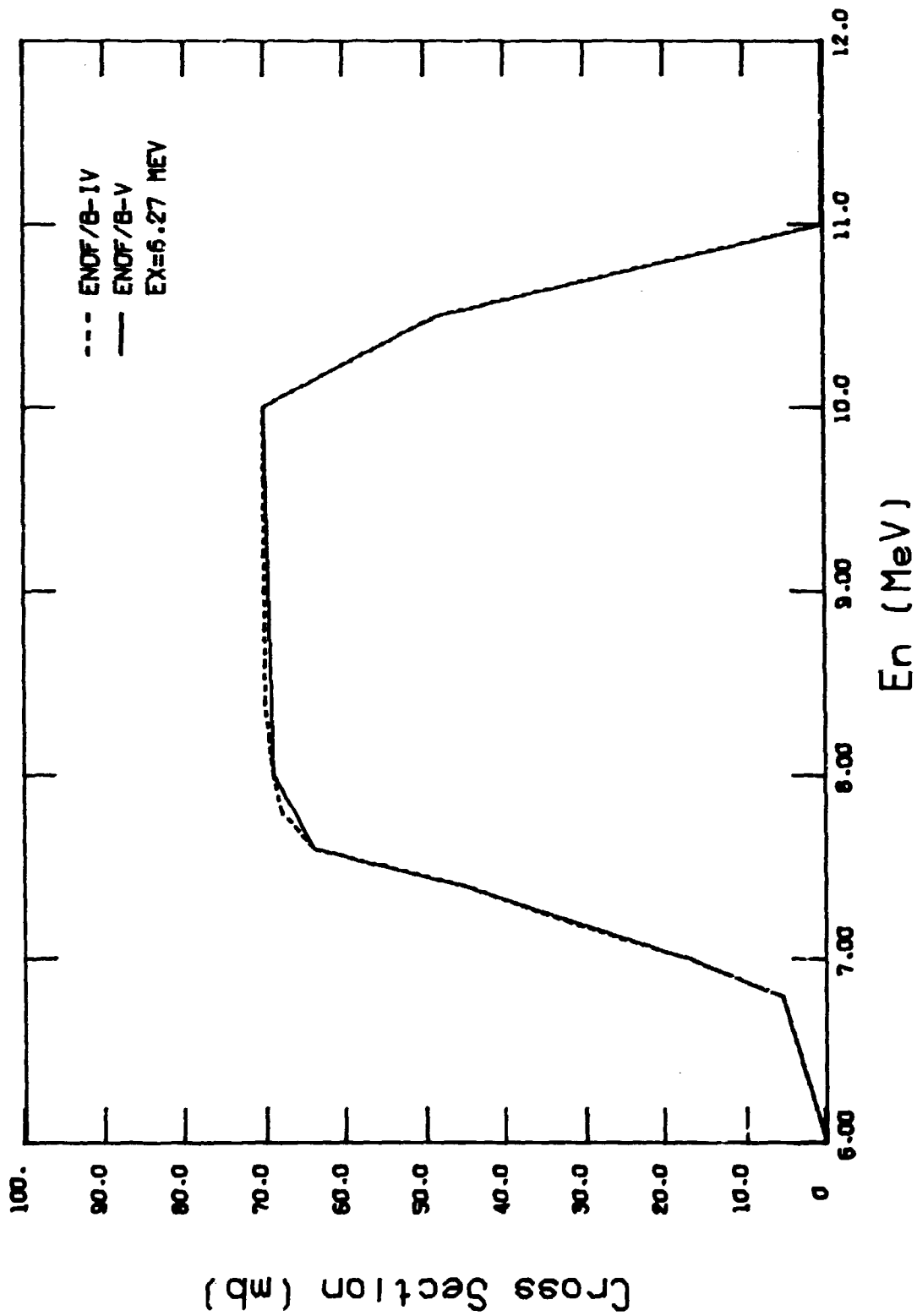


Fig. 54. Comparison of V4 and V5 inelastic scattering to 6.27-MeV level.

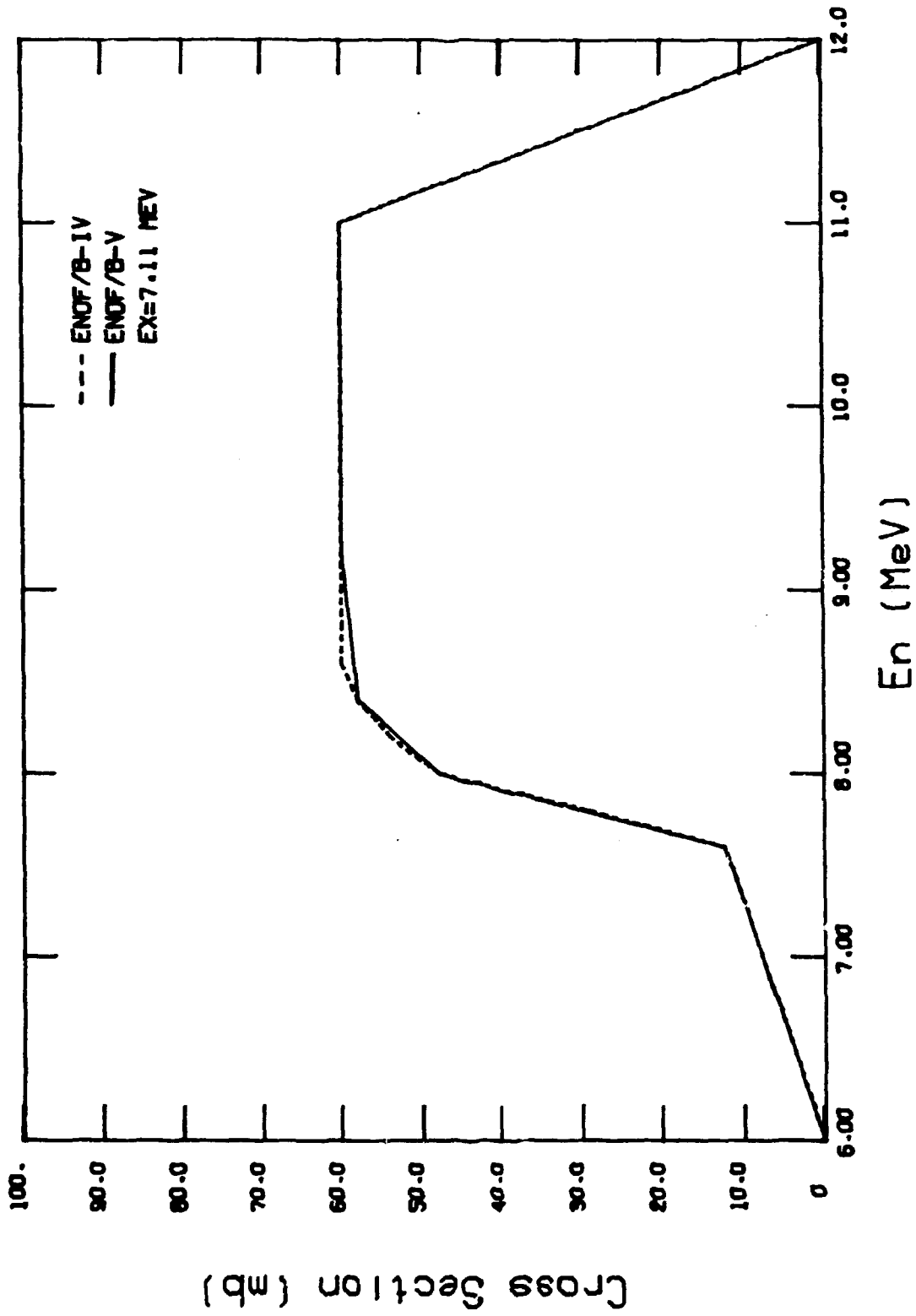


Fig. 55. Comparison of V4 and V5 inelastic scattering to 7.11-MeV level.

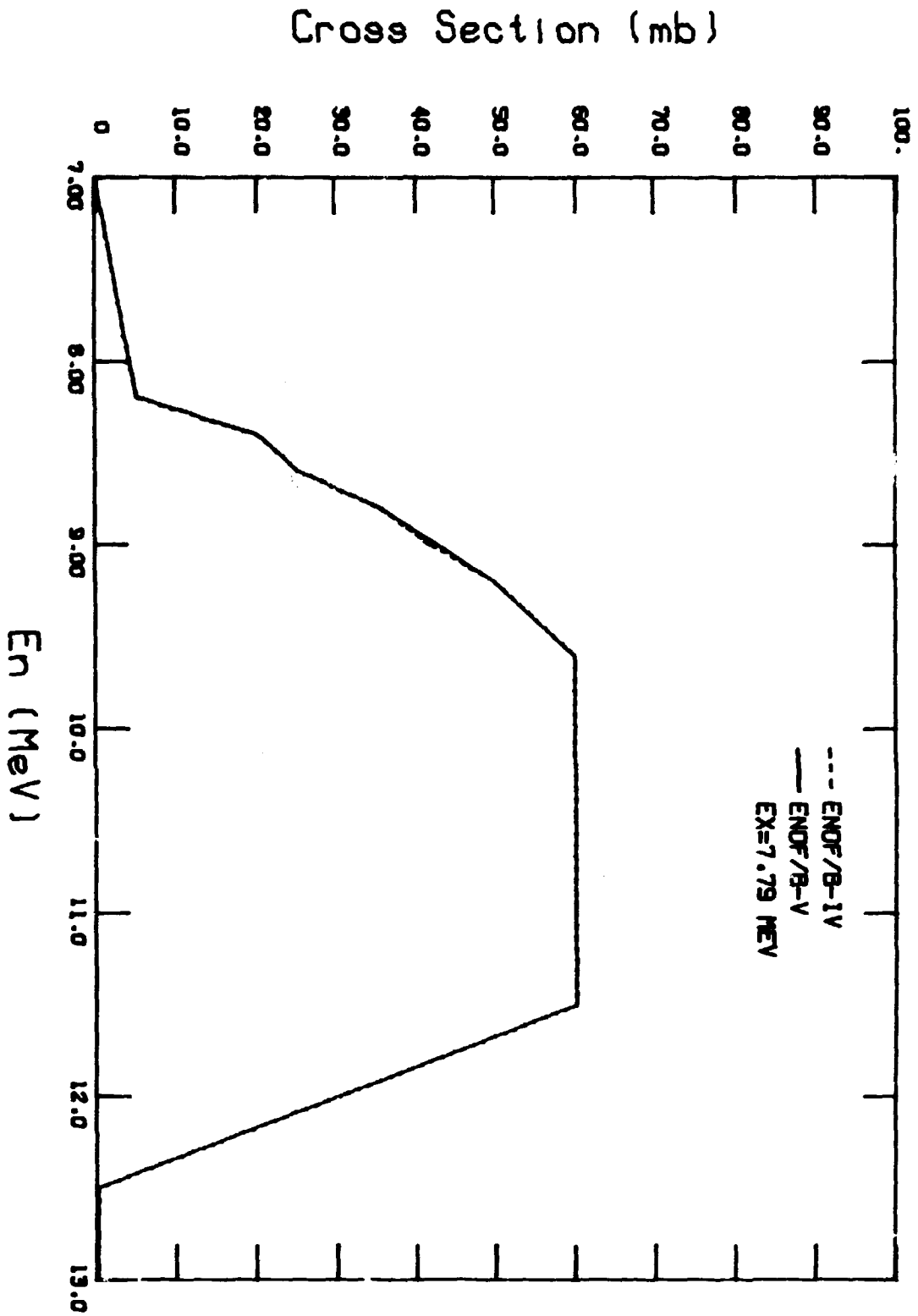


Fig. 56. Comparison of V4 and V5 inelastic scattering to 7.79-MeV level.

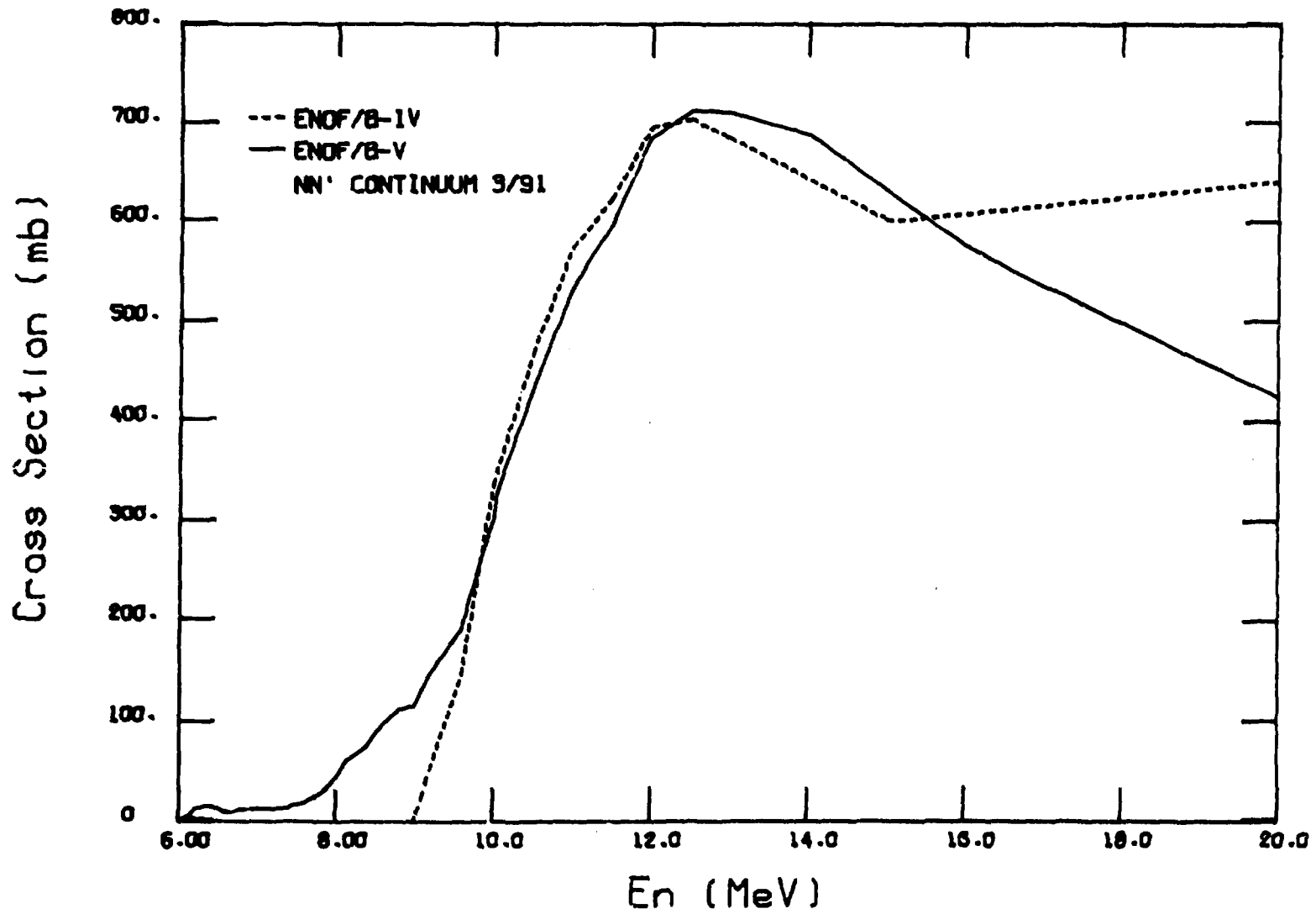


Fig. 57. Comparison of V4 and V5 inelastic scattering to the continuum.

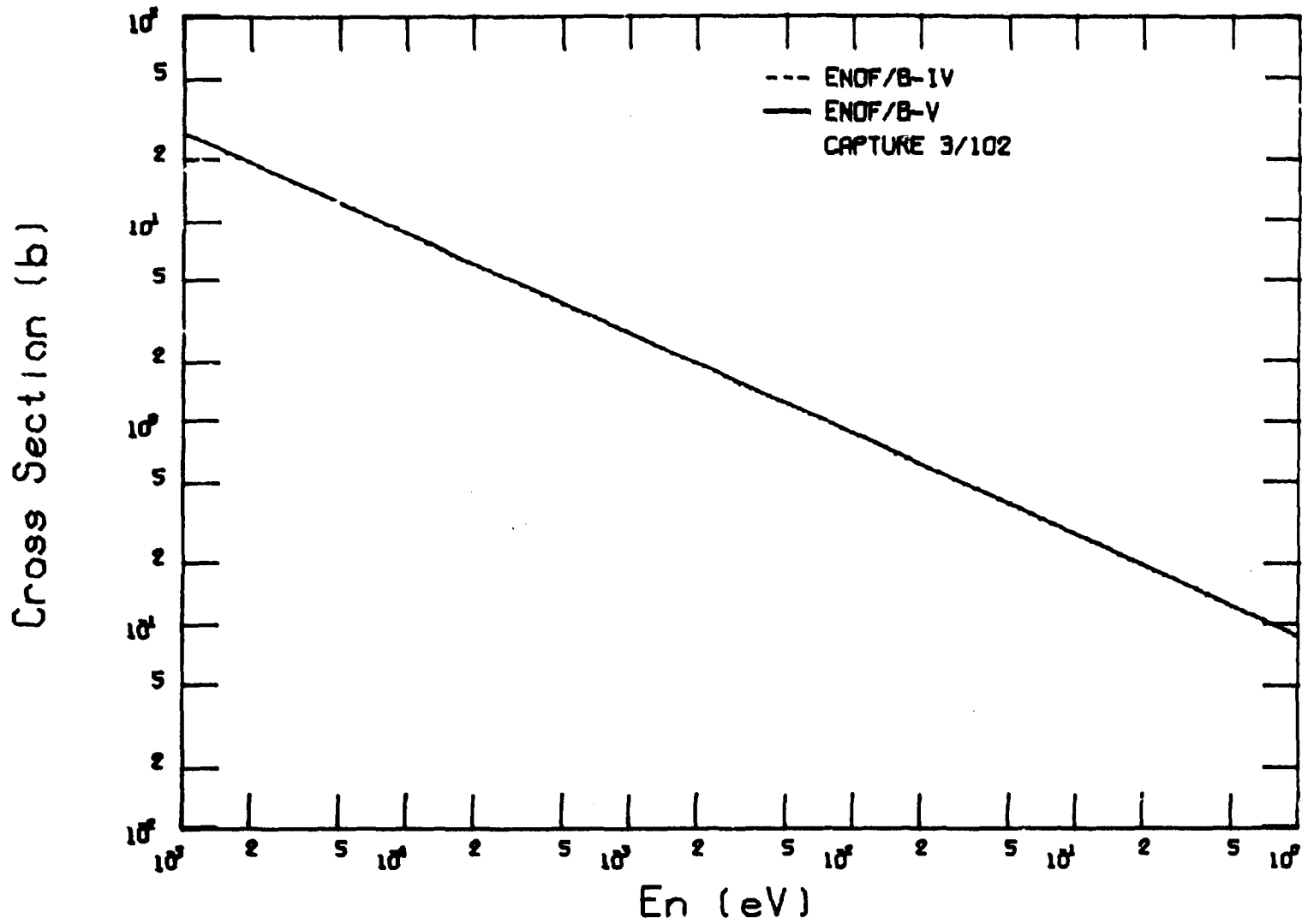


Fig. 58. Comparison of V4 and V5 capture cross sections.

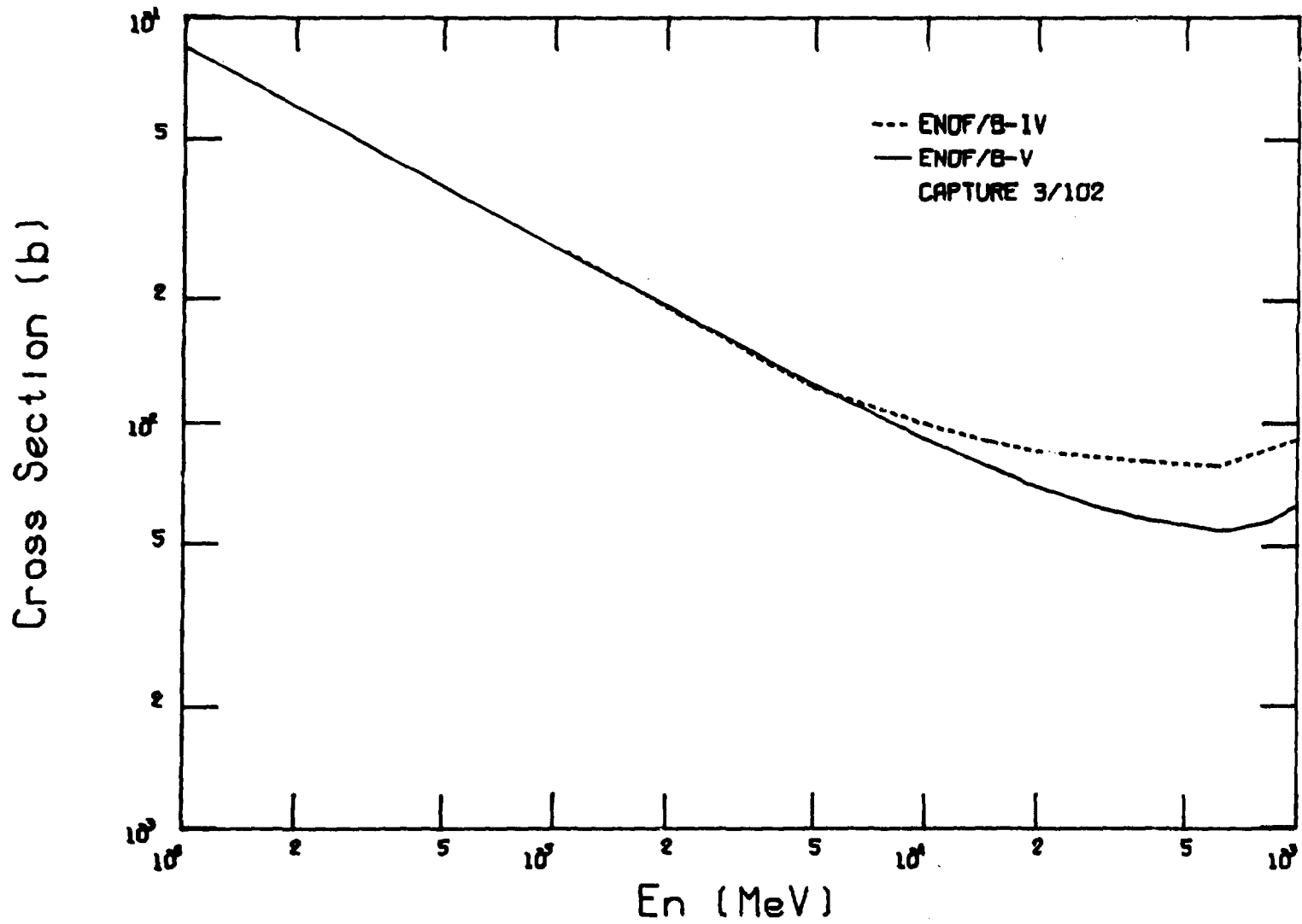


Fig. 59. Comparison of V4 and V5 capture cross sections.

# Cross Section (b)

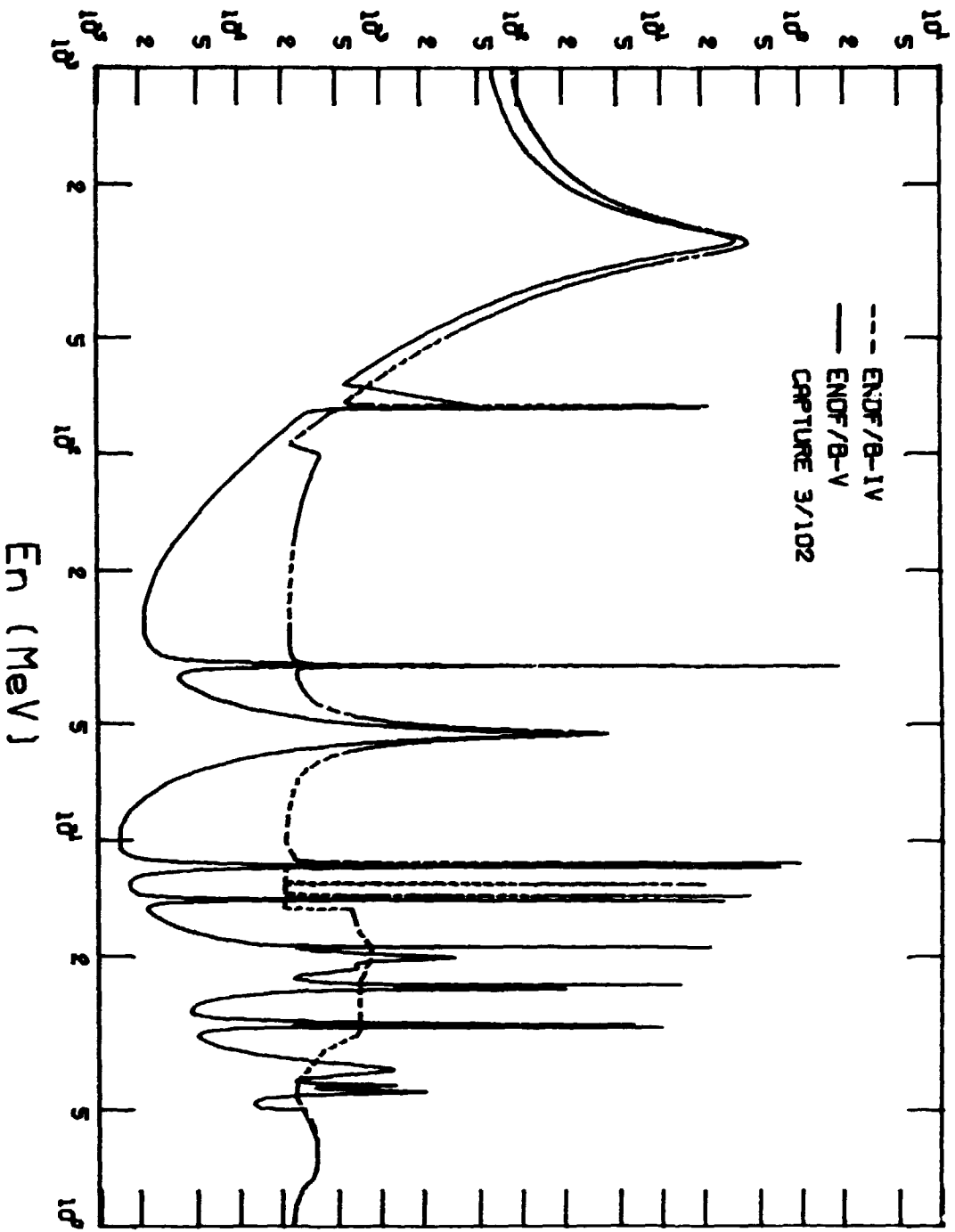


Fig. 60. Comparison of V4 and V5 capture cross sections.

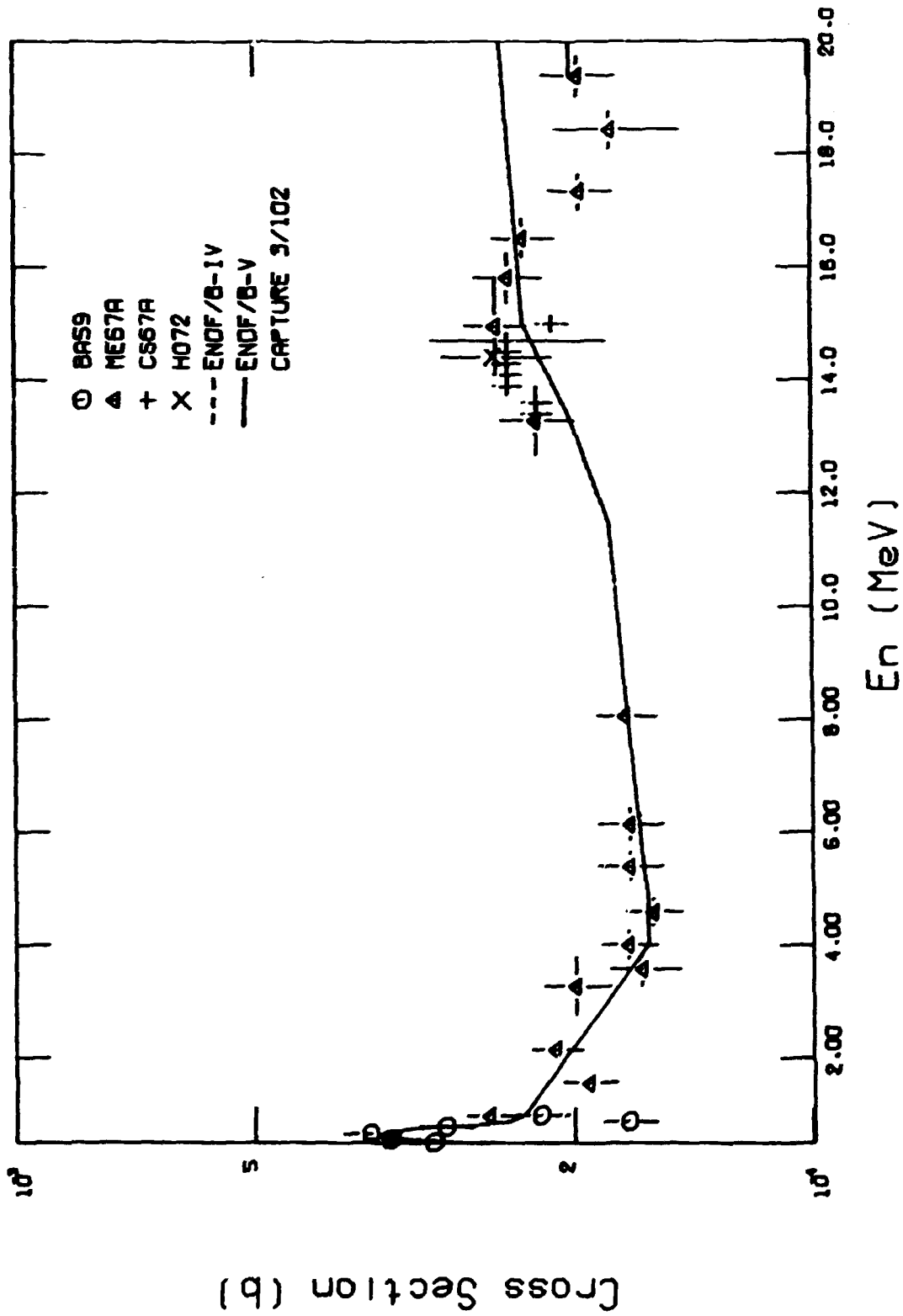


Fig. 61. Comparison of V4 and V5 capture cross sections with available data.

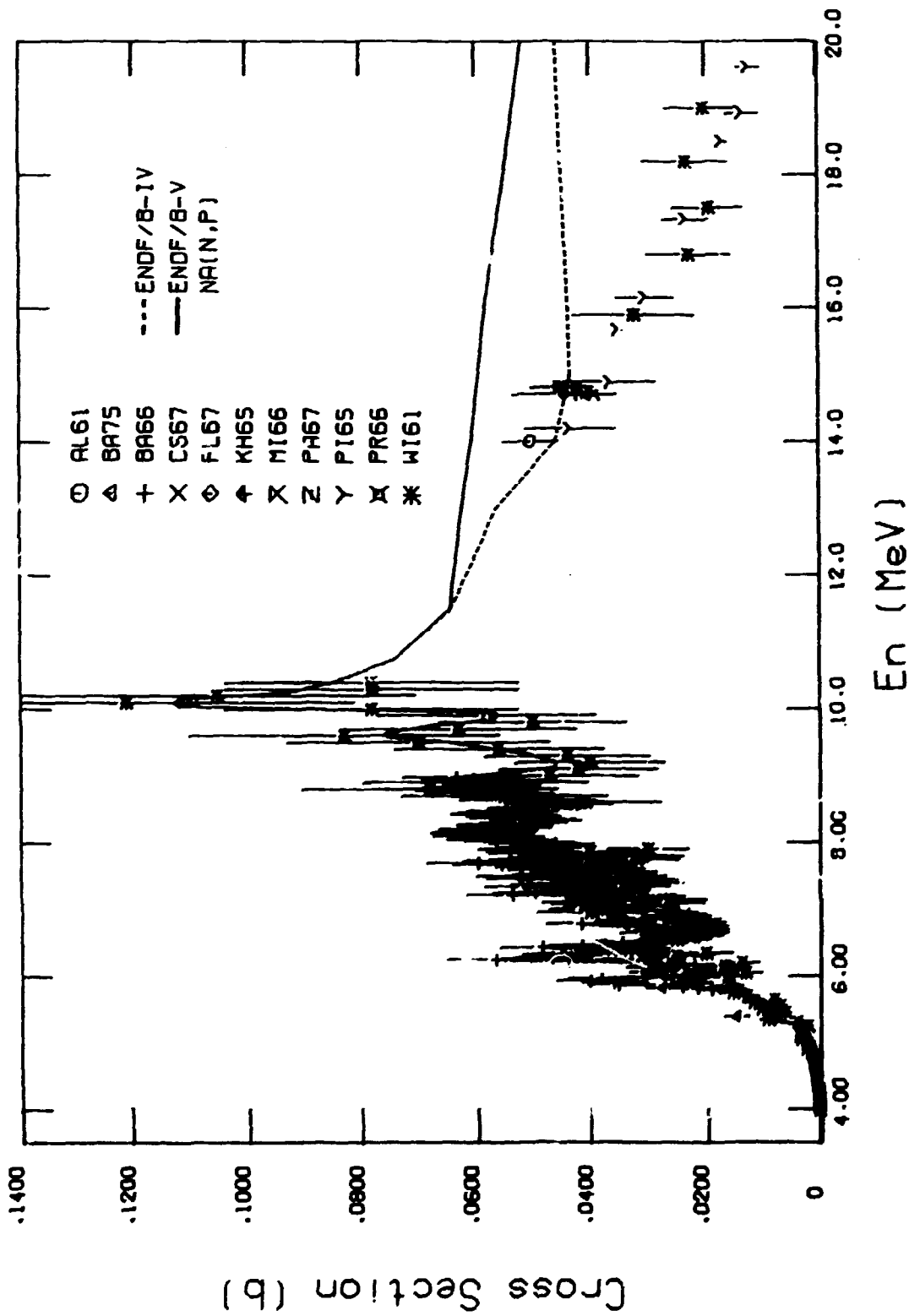


Fig. 62. Comparison of V4 and V5 (n,p) cross sections with available data.

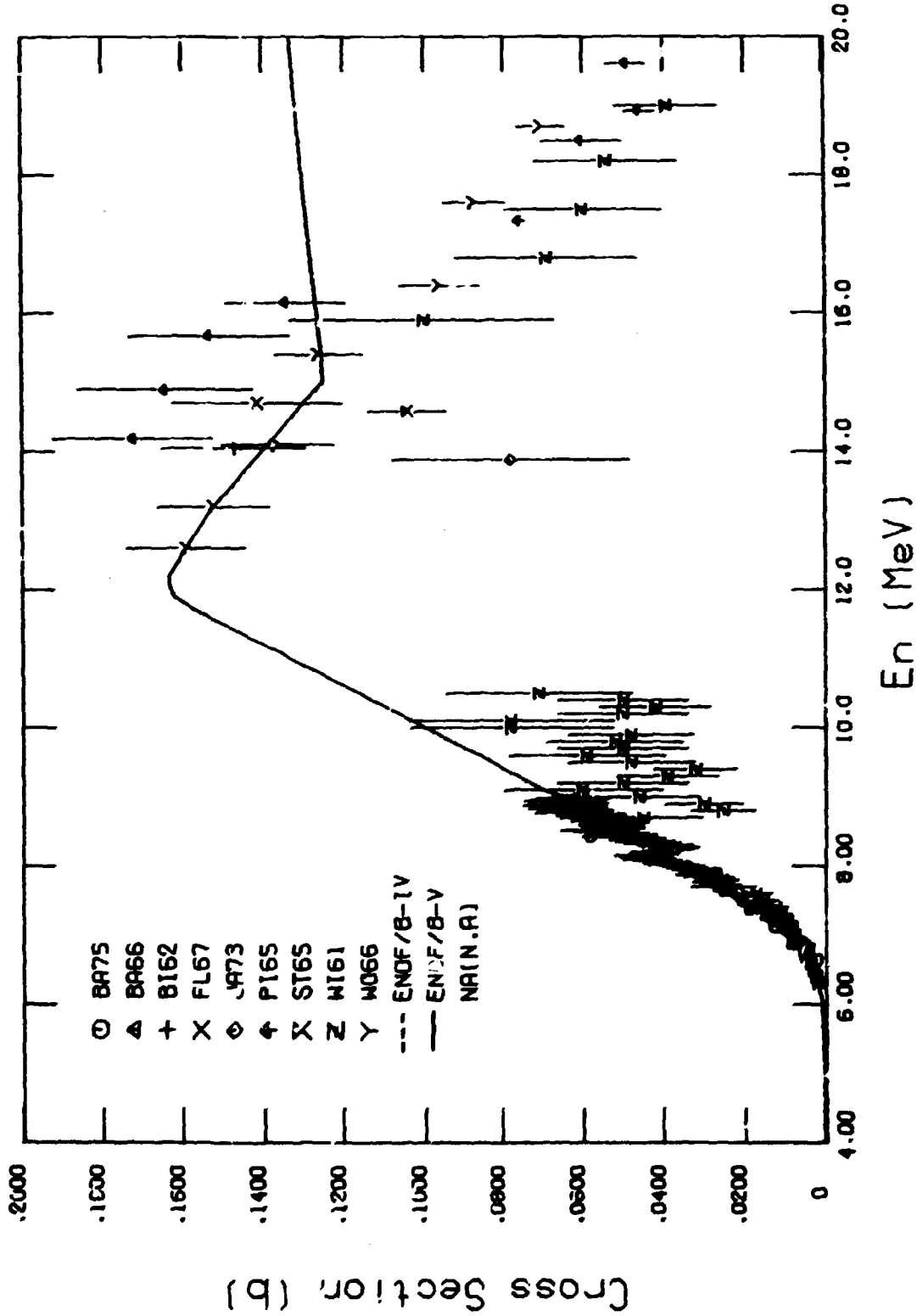


Fig. 63. Comparison of V4 and V5 (n,α) cross sections with available data.

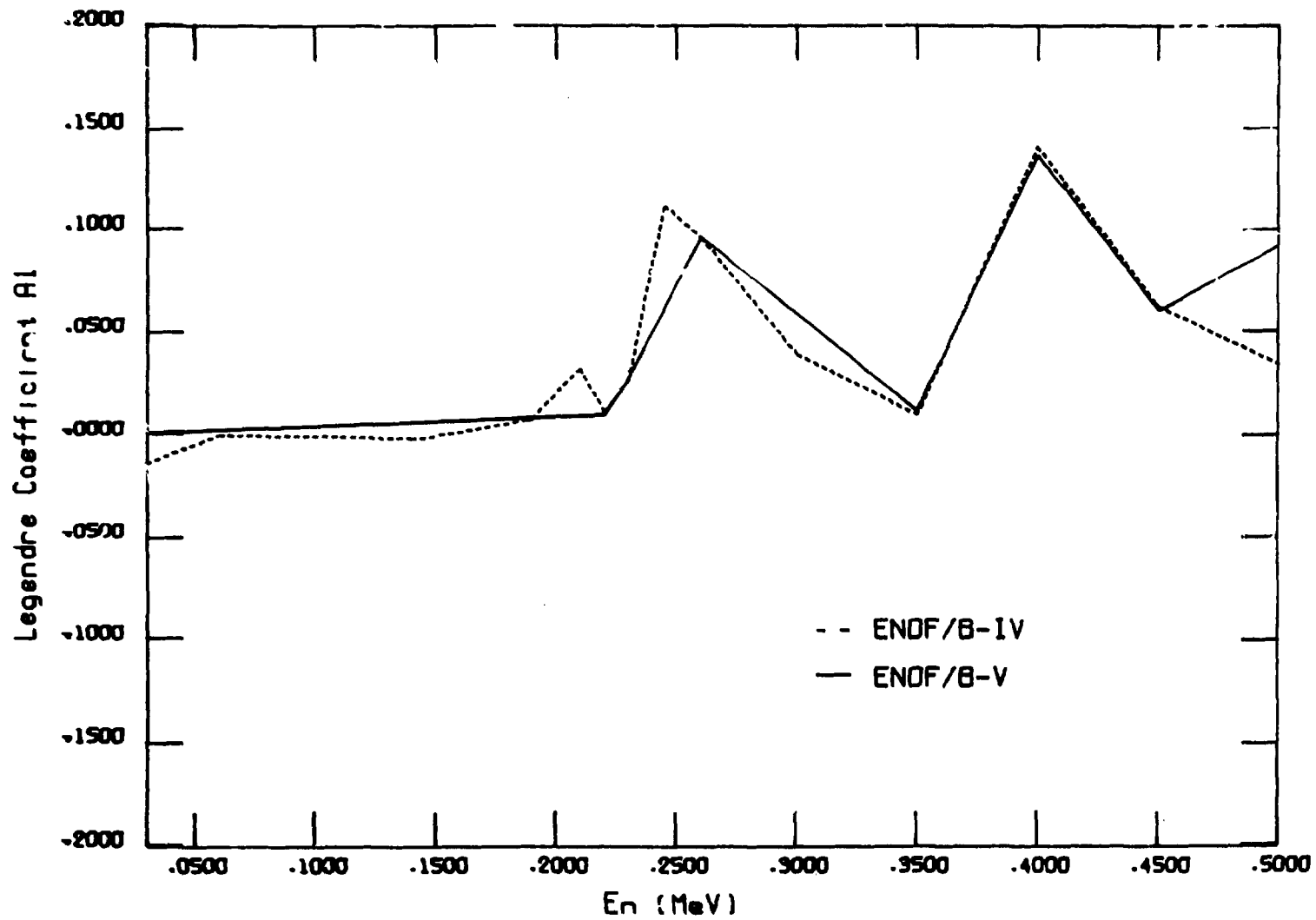


Fig. 64. Comparison of V4 and V5 a<sub>1</sub> Legendre coefficient for elastic scattering from 30-500 keV.

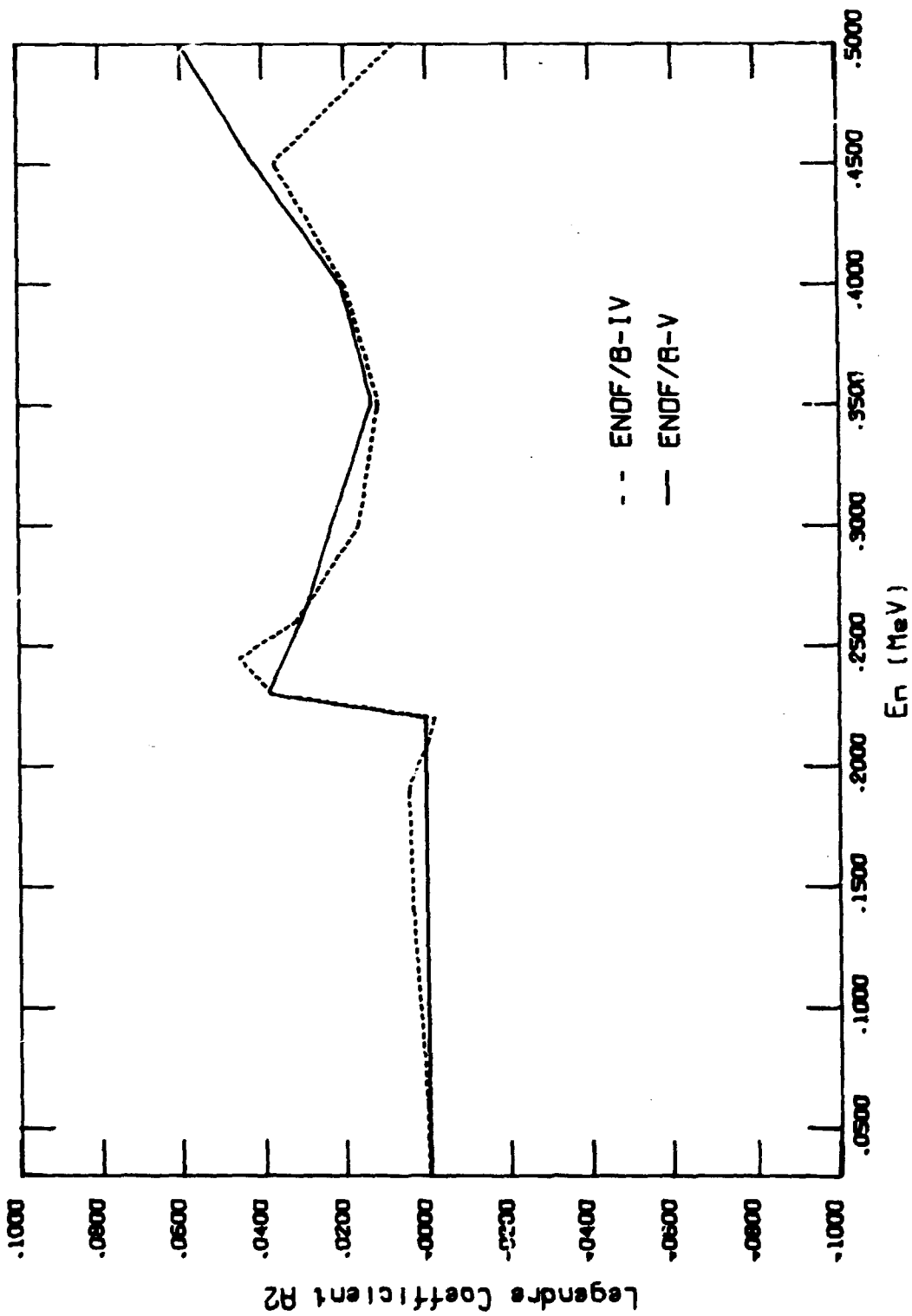


Fig. 65. Comparison of V4 and V5 a<sub>2</sub> Legendre coefficient for elastic scattering from 30-500 keV.

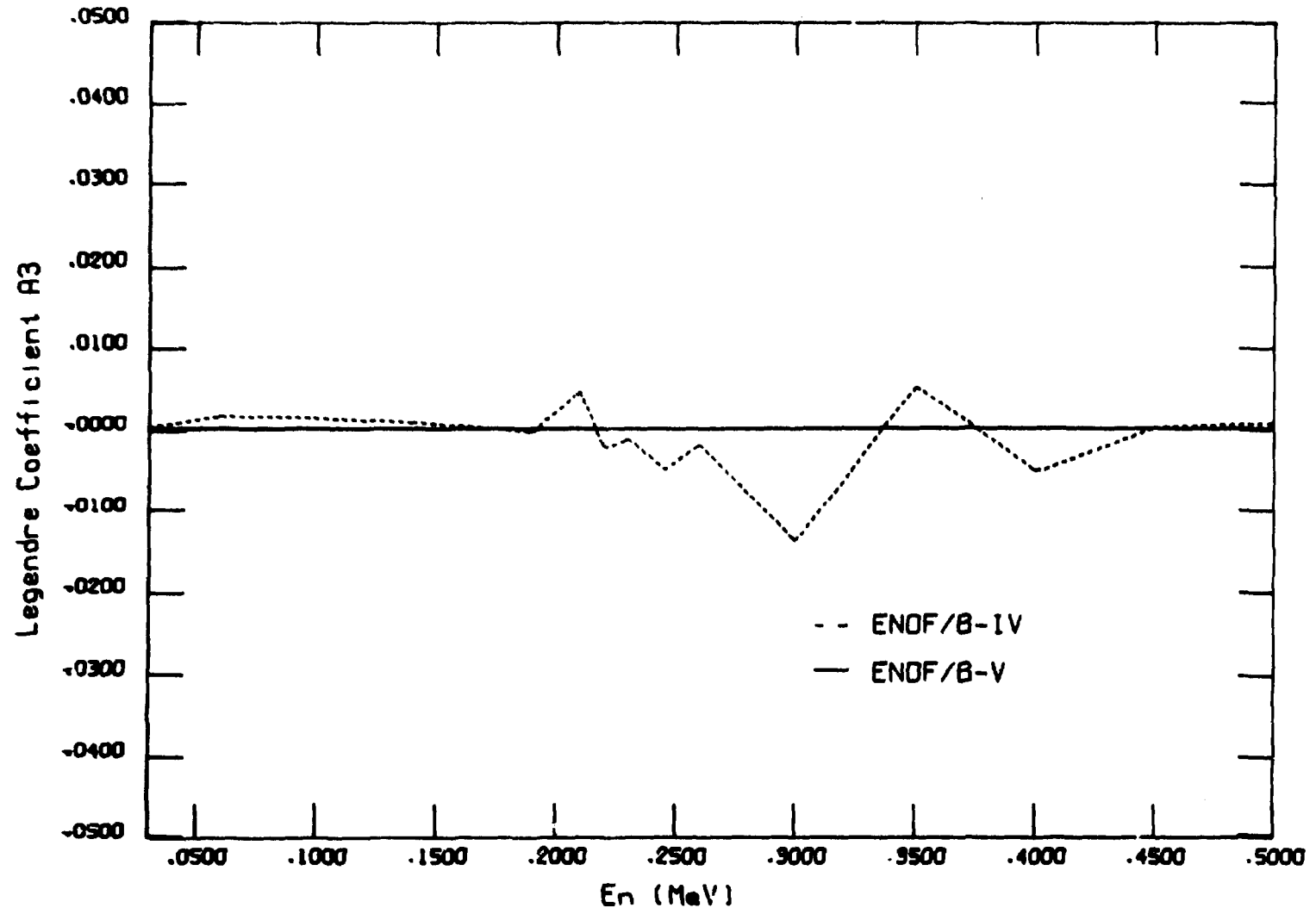


Fig. 66. Comparison of V4 and V5  $a_3$  Legendre coefficient for elastic scattering from 30-500 keV.

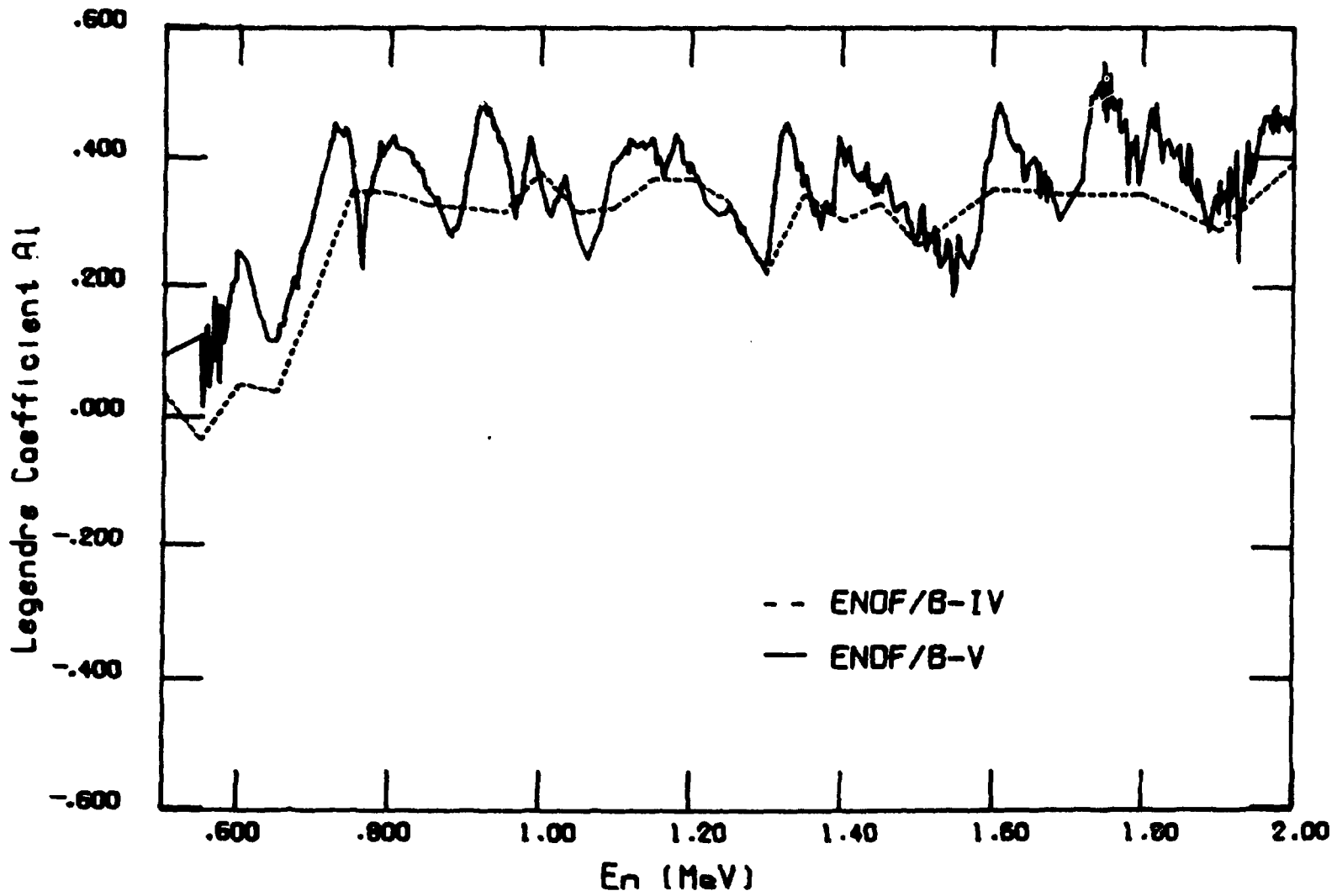


Fig. 67. Comparison of V4 and V5 a<sub>1</sub> Legendre coefficient for elastic scattering from 500 keV to 2 MeV.

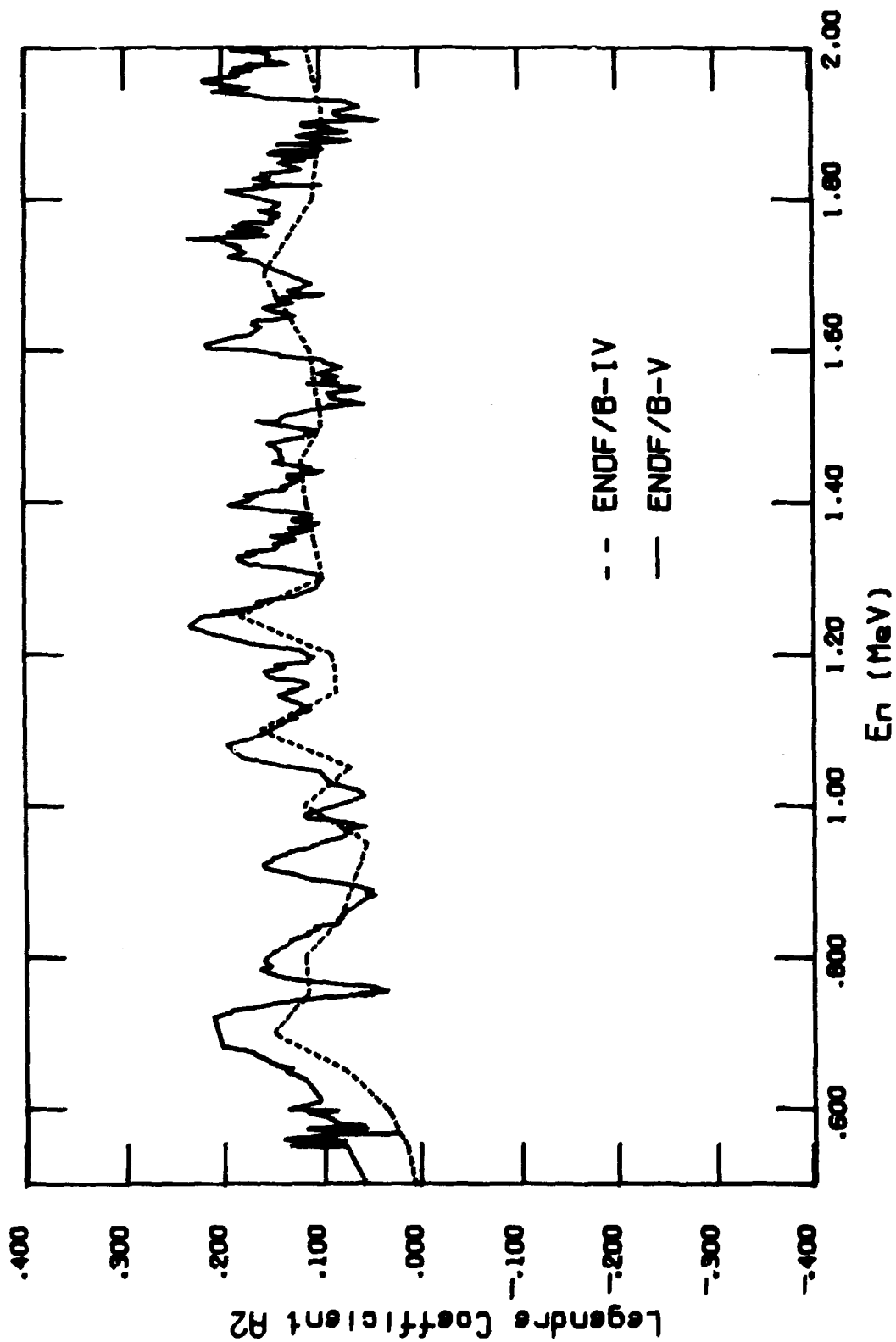


Fig. 68. Comparison of V4 and V5 a<sub>2</sub> Legendre coefficient for elastic scattering from 500 keV to 2 MeV.

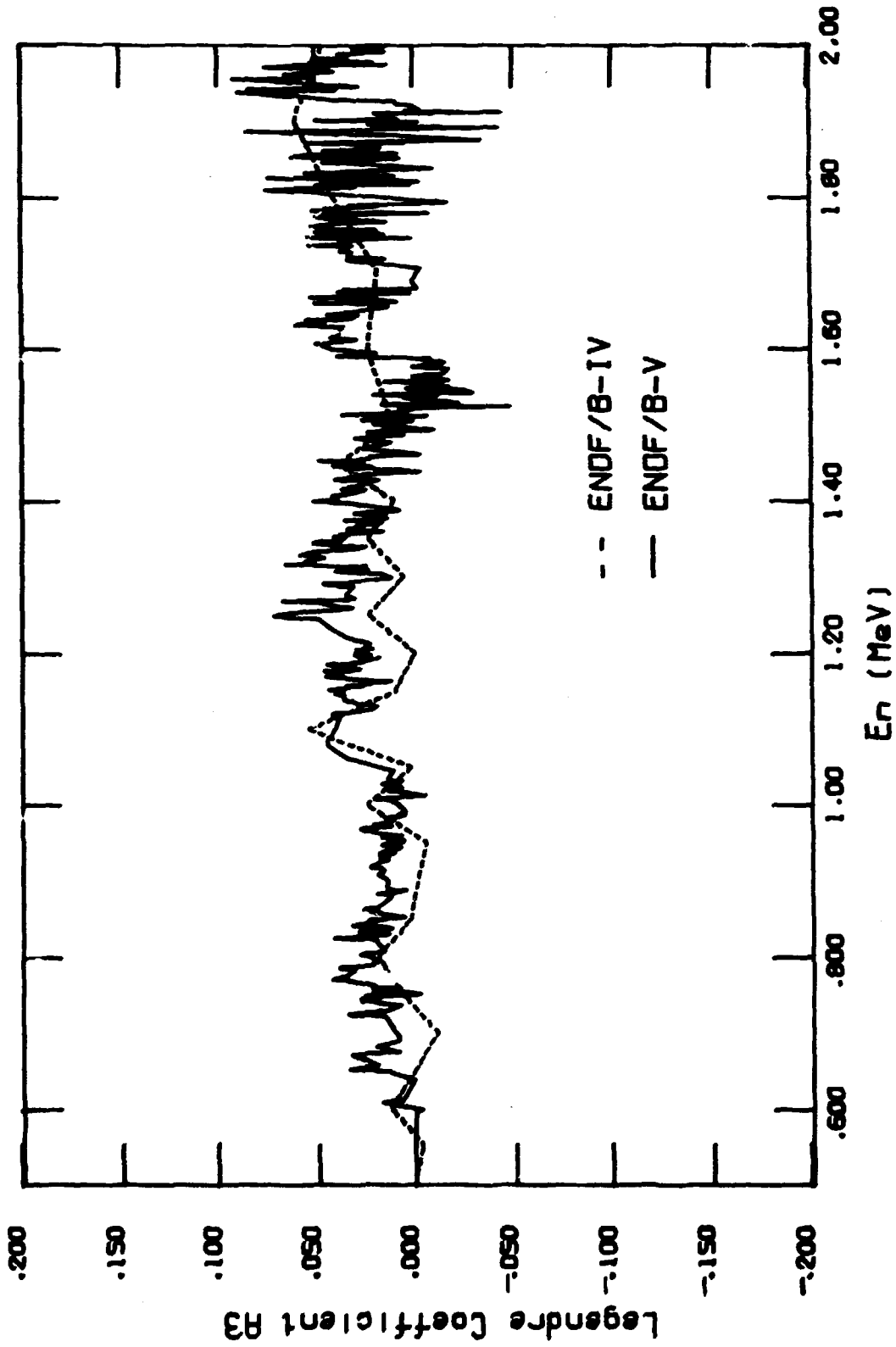


Fig. 69. Comparison of V4 and V5 a<sub>3</sub> Legendre coefficient for elastic scattering from 500 keV to 2 MeV.

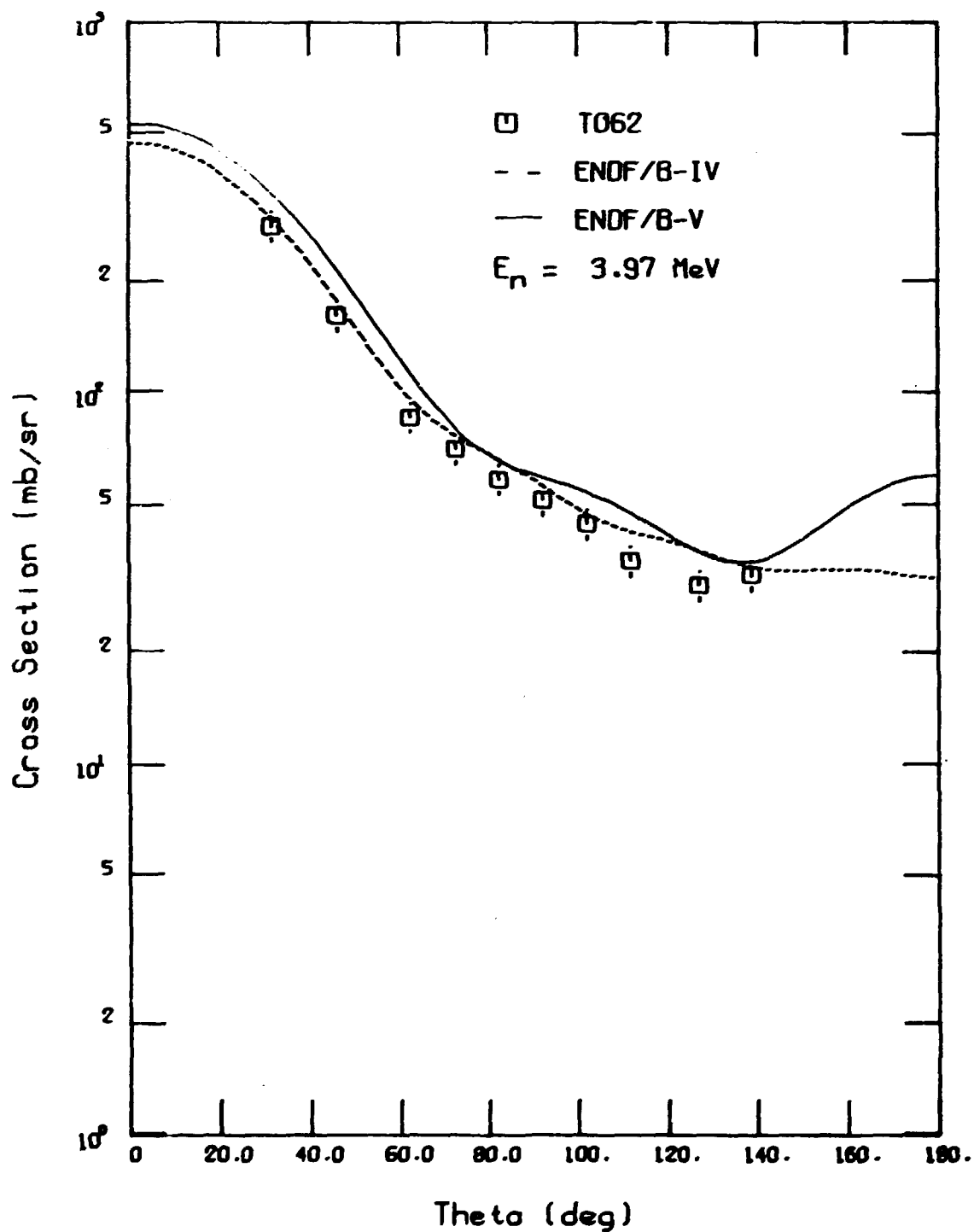


Fig. 70. Comparison of V4 and V5 elastic scattering angular distributions with available data.

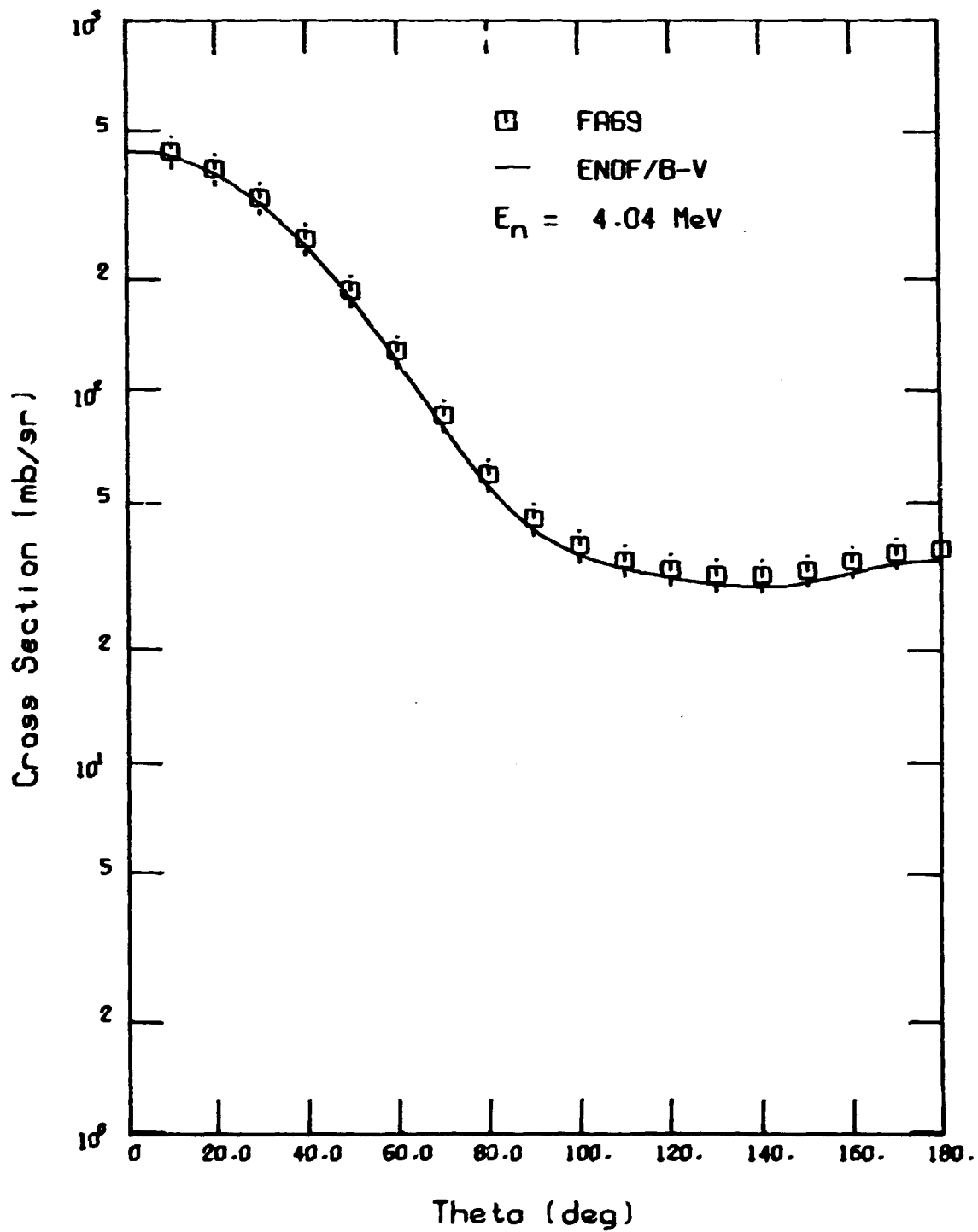


Fig. 71. Comparison of V5 elastic scattering angular distribution with available data.

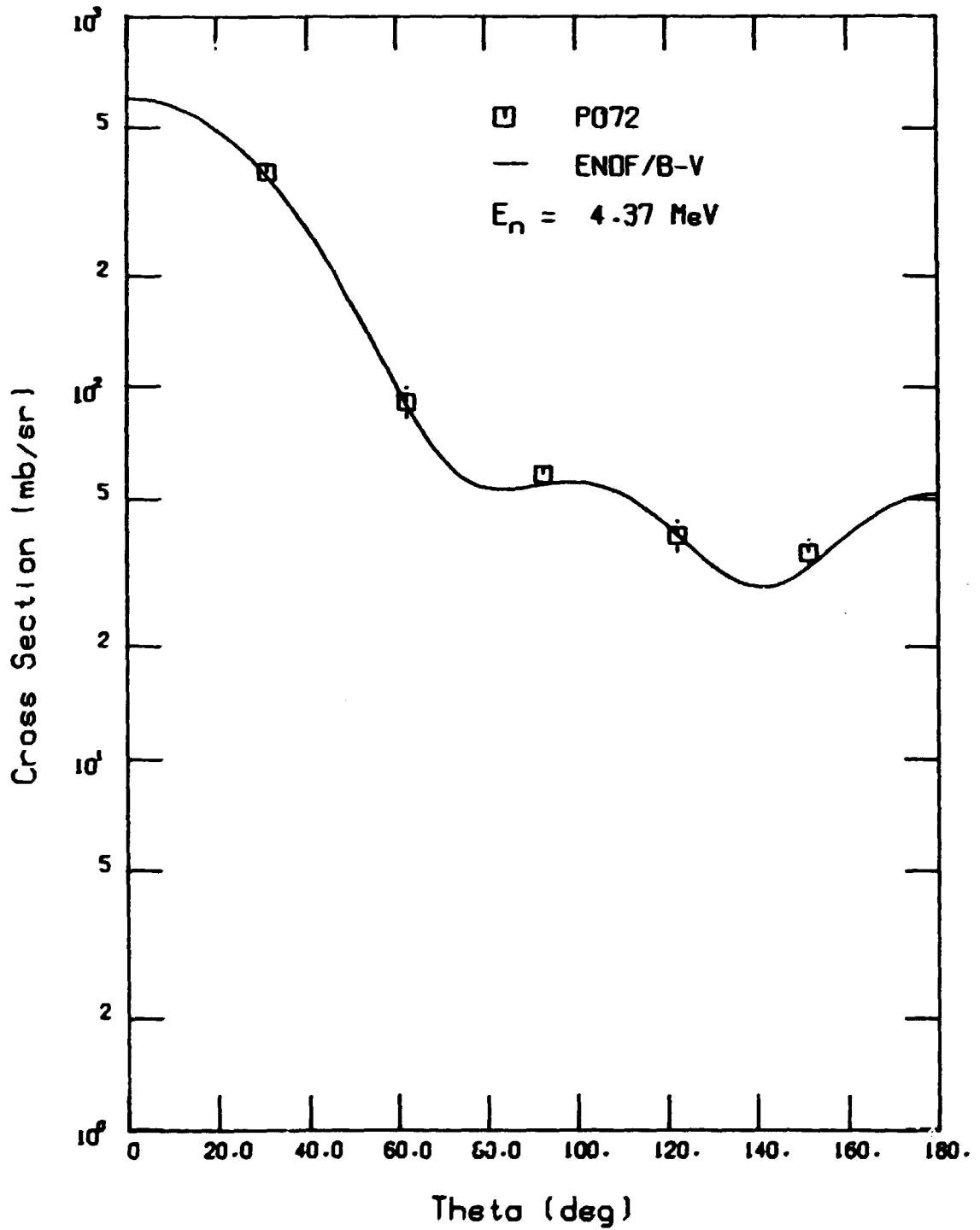


Fig. 72. Comparison of V5 elastic scattering angular distribution with available data.

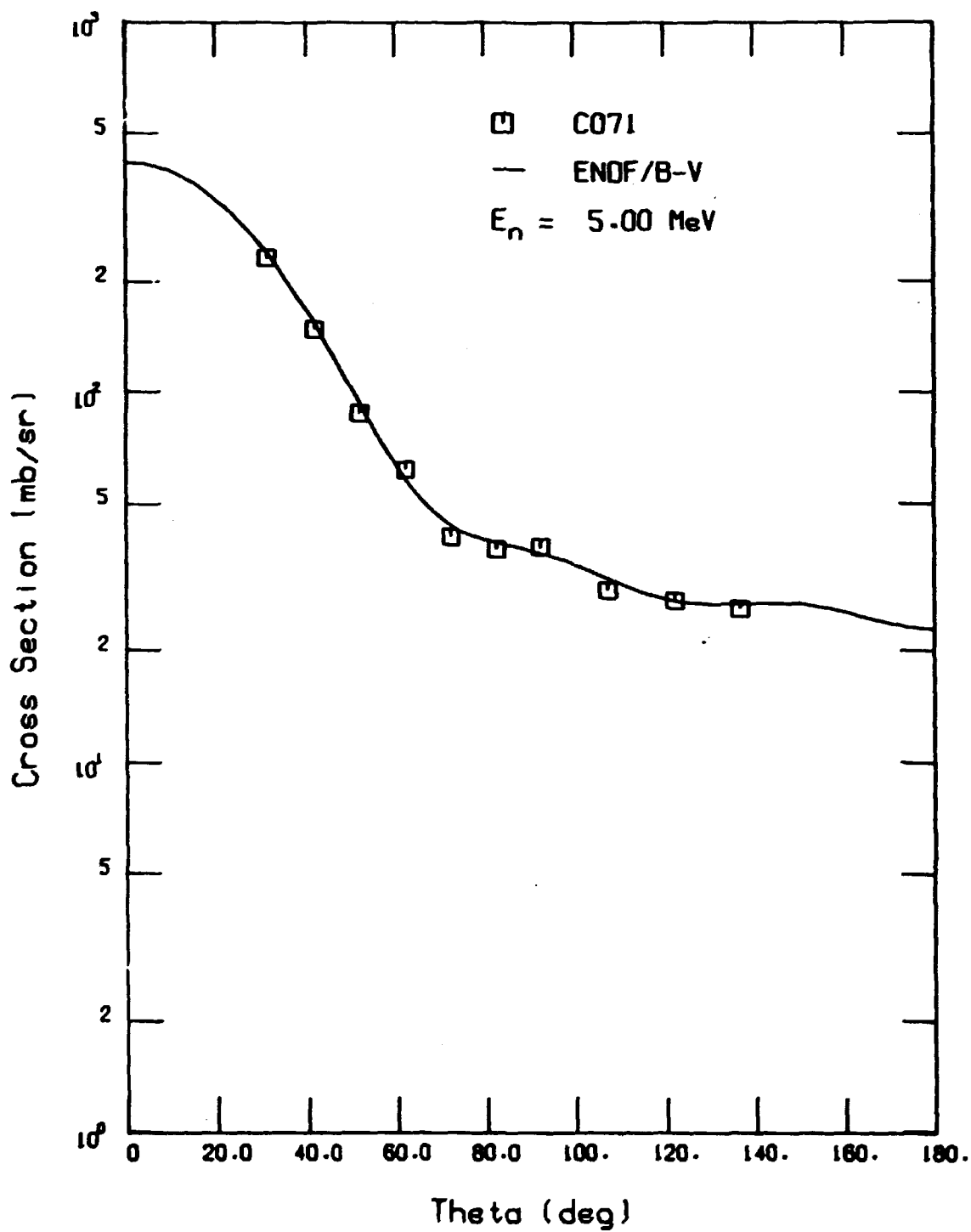


Fig. 73. Comparison of V5 elastic scattering angular distribution with available data.

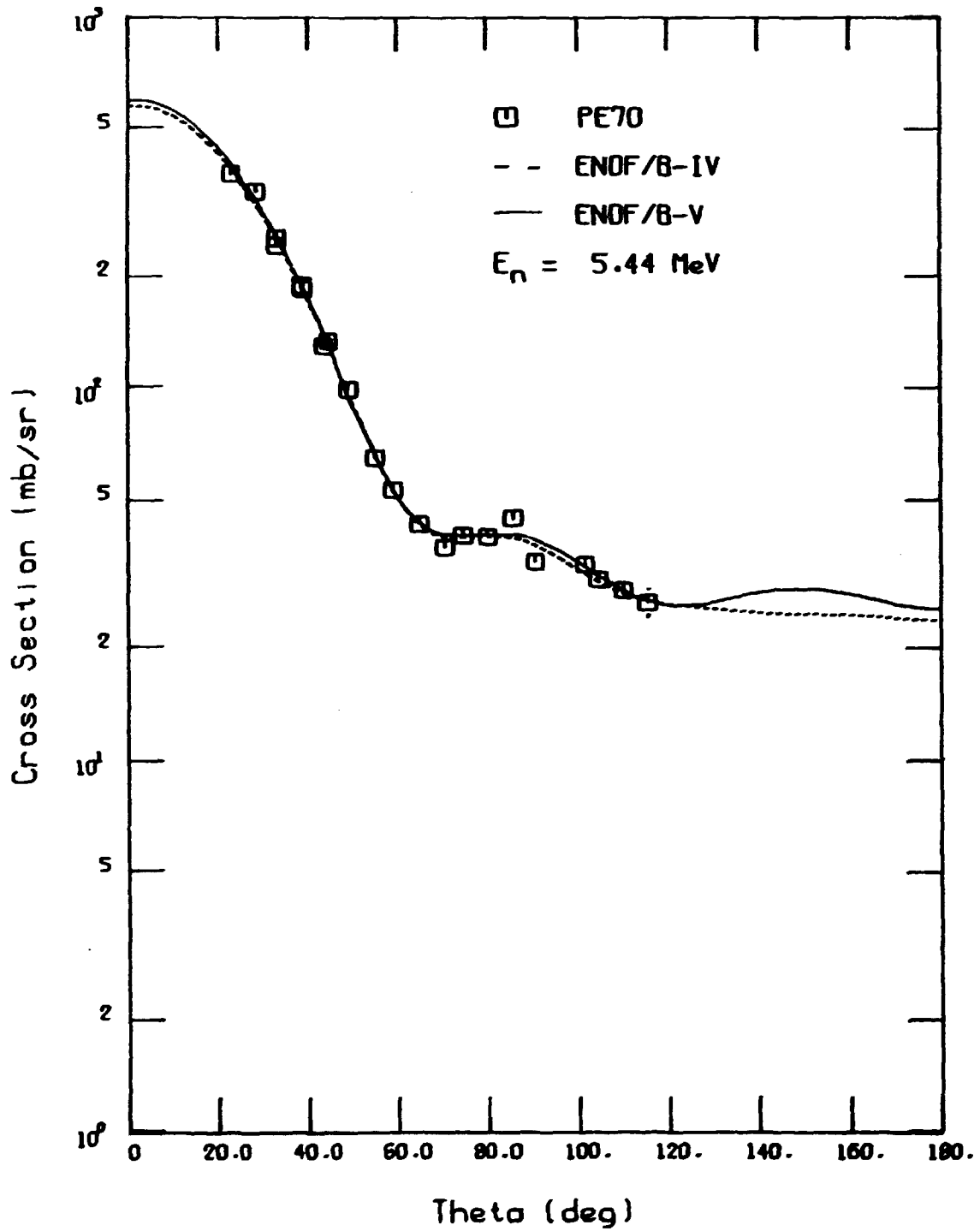


Fig. 74. Comparison of V4 and V5 elastic scattering angular distribution with available data.

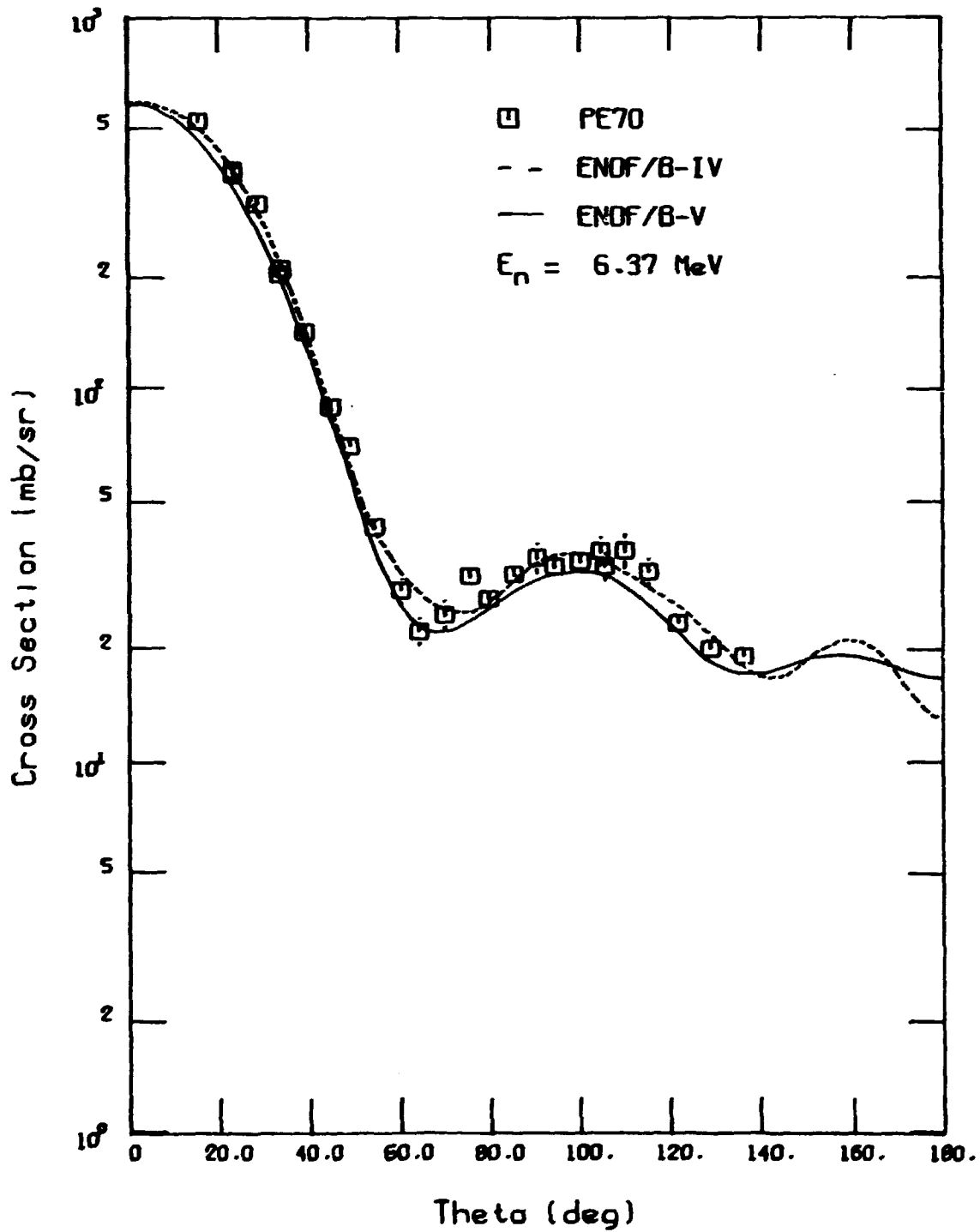


Fig. 75. Comparison of V4 and V5 elastic scattering angular distribution with available data.

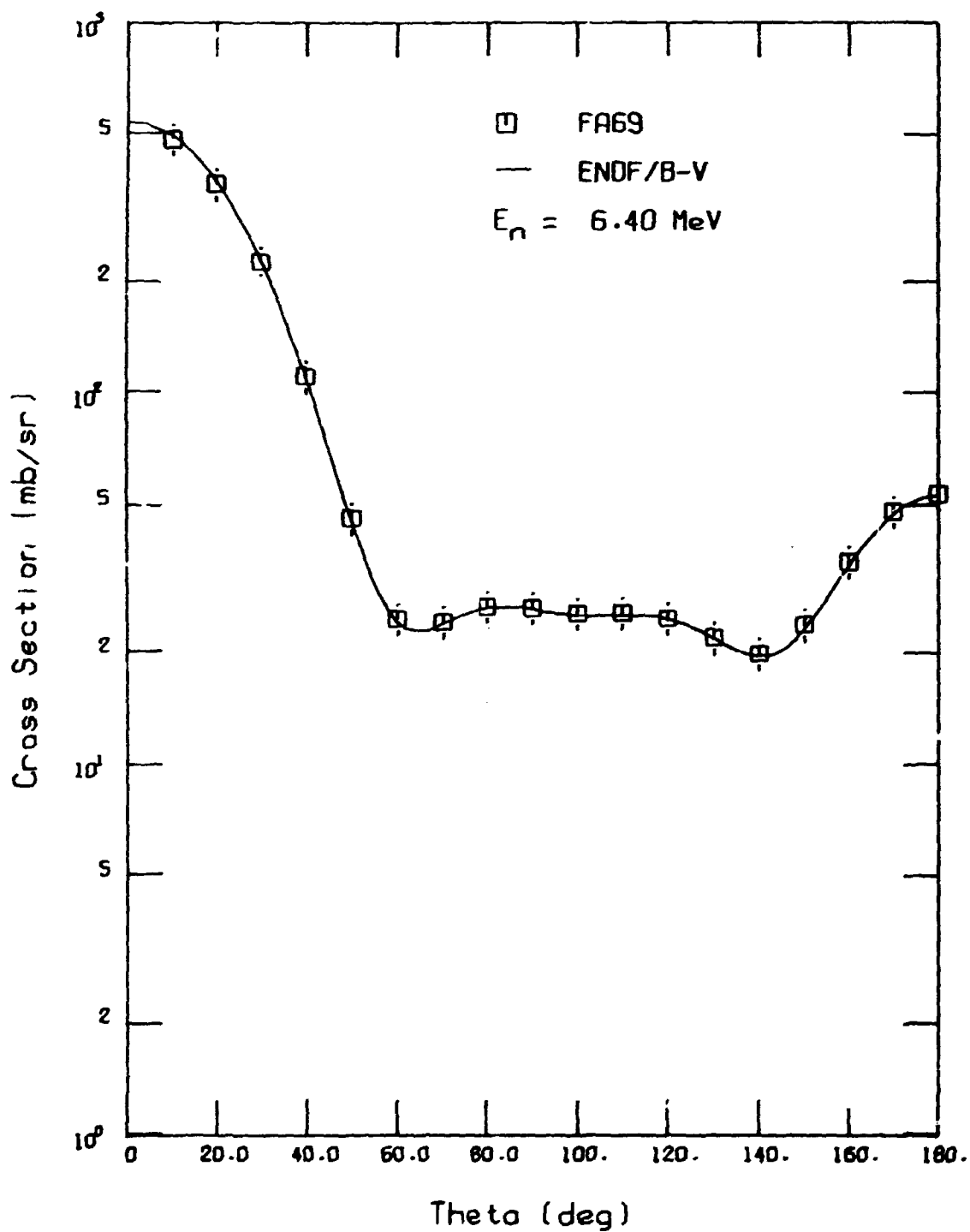


Fig. 76. Comparison of V5 elastic scattering angular distribution with available data.

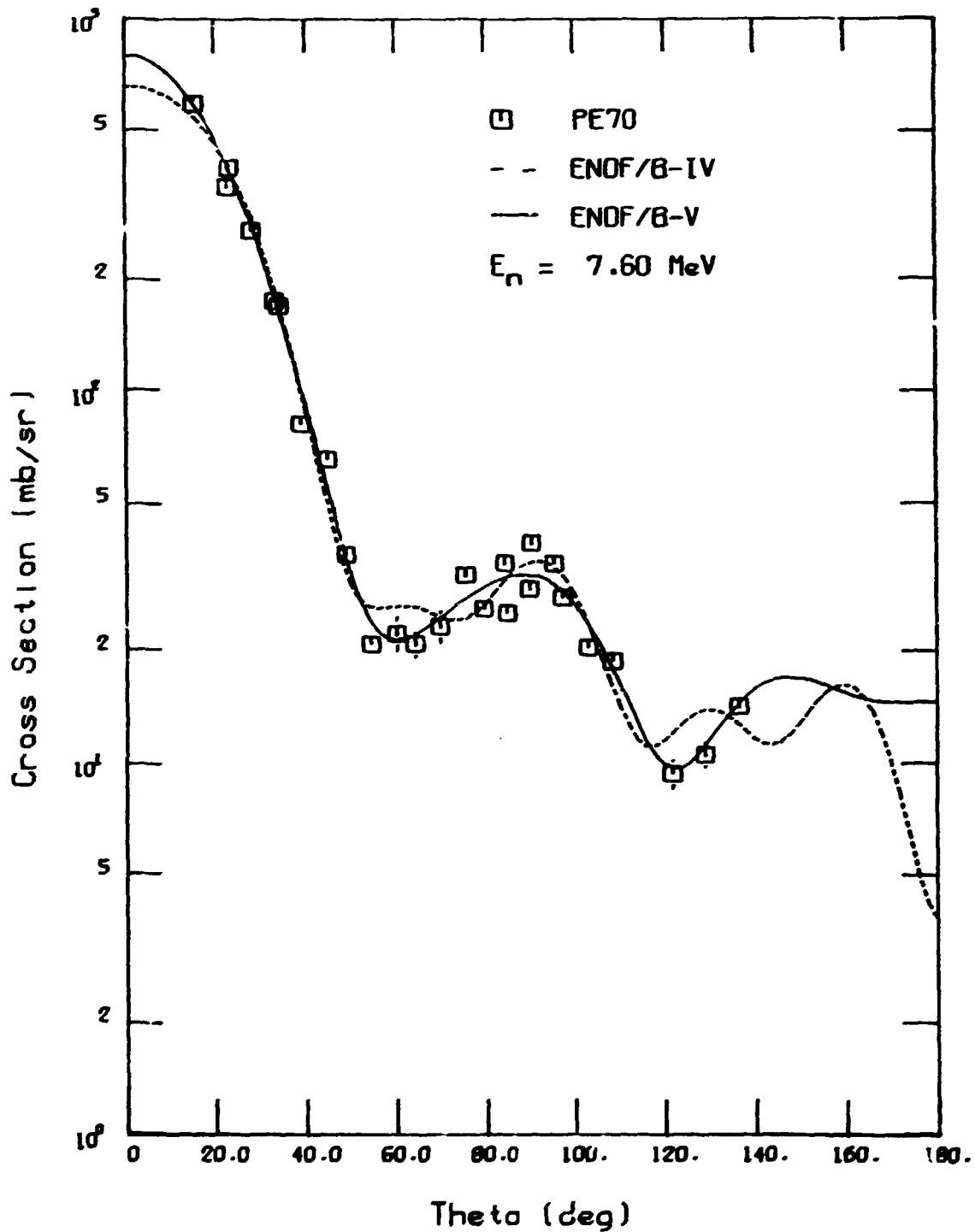


Fig. 77. Comparison of V4 and V5 elastic scattering angular distribution with available data.

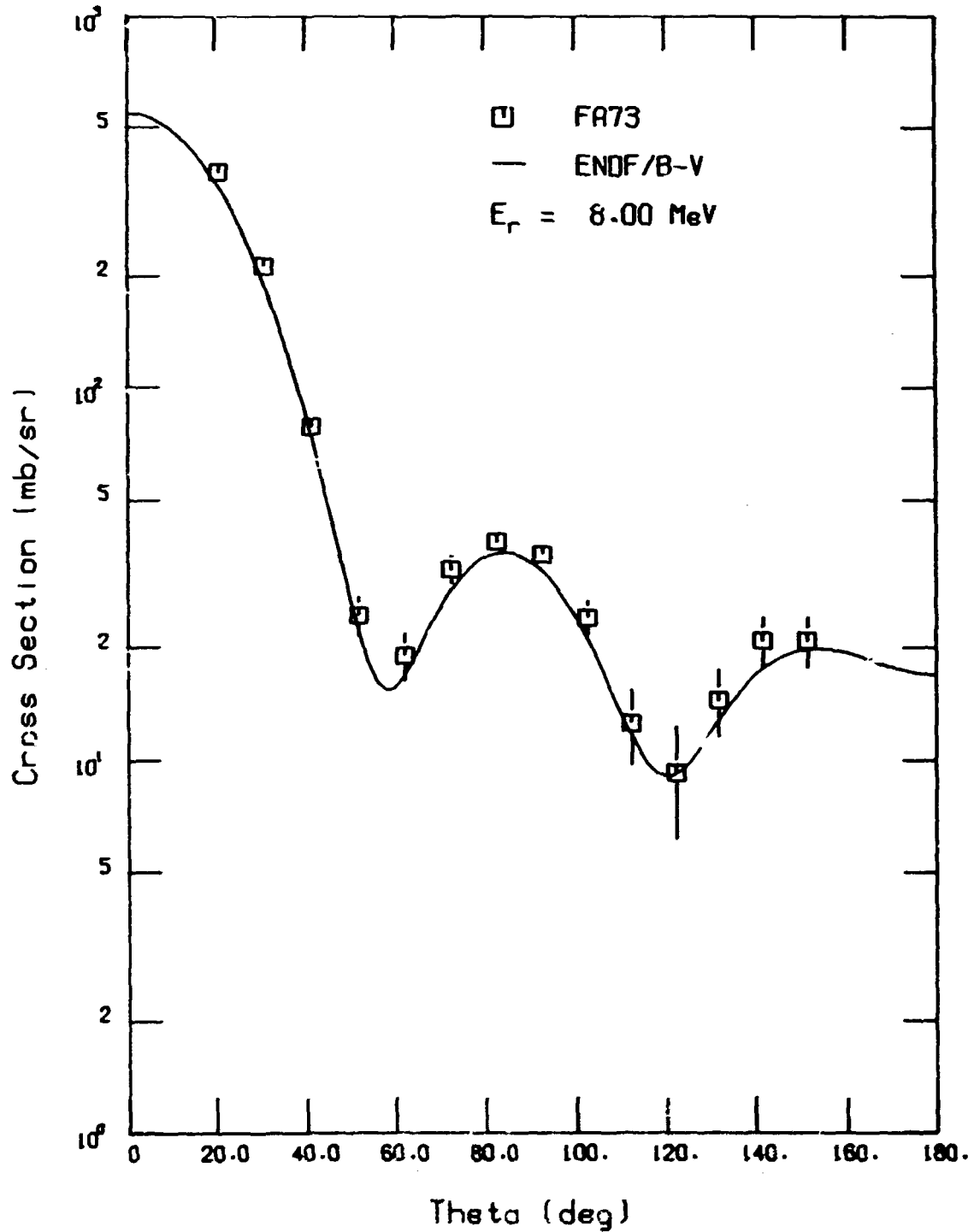


Fig. 78. Comparison of V5 elastic scattering angular distribution with available data.

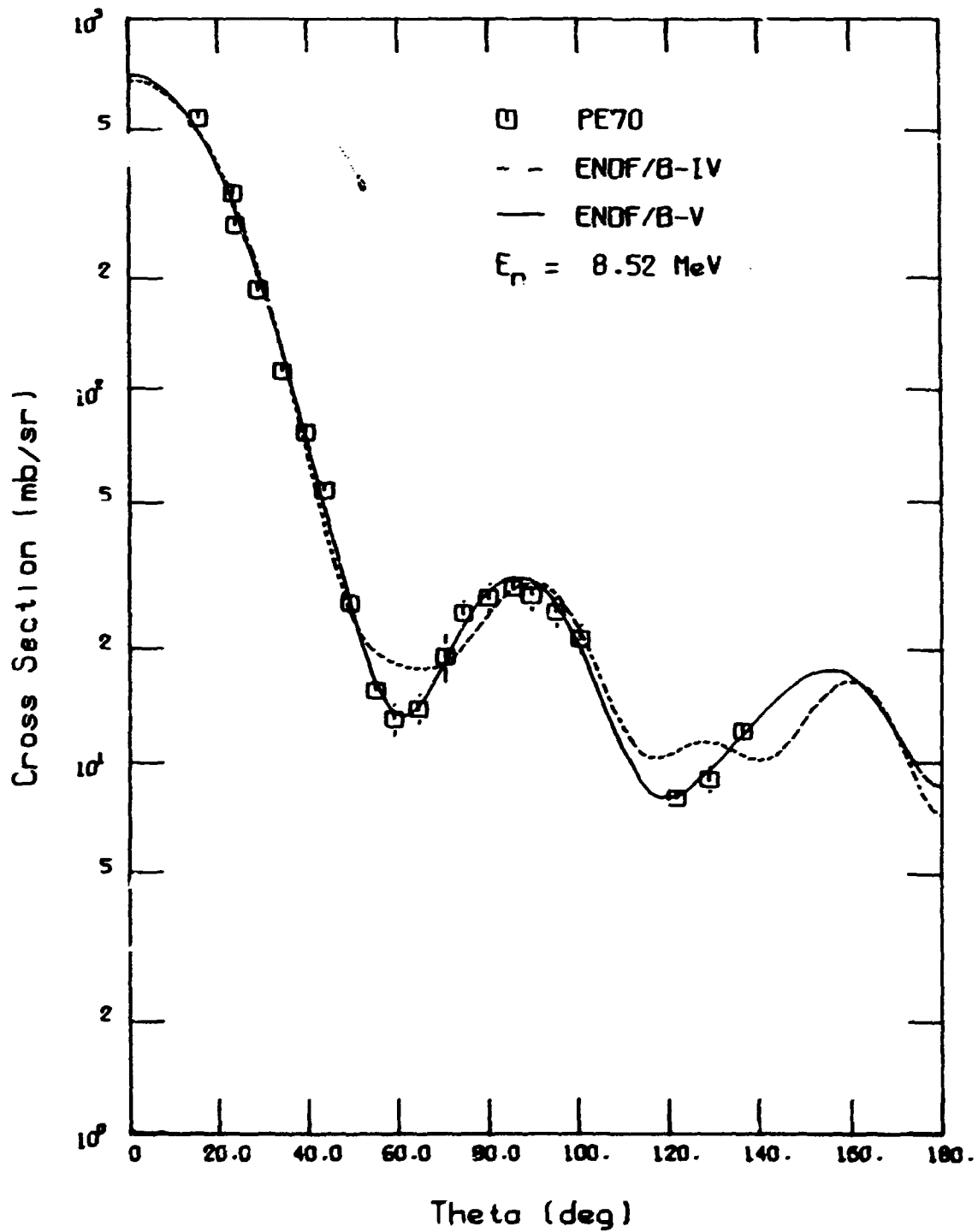


Fig. 79. Comparison of V4 and V5 elastic scattering angular distribution with available data.

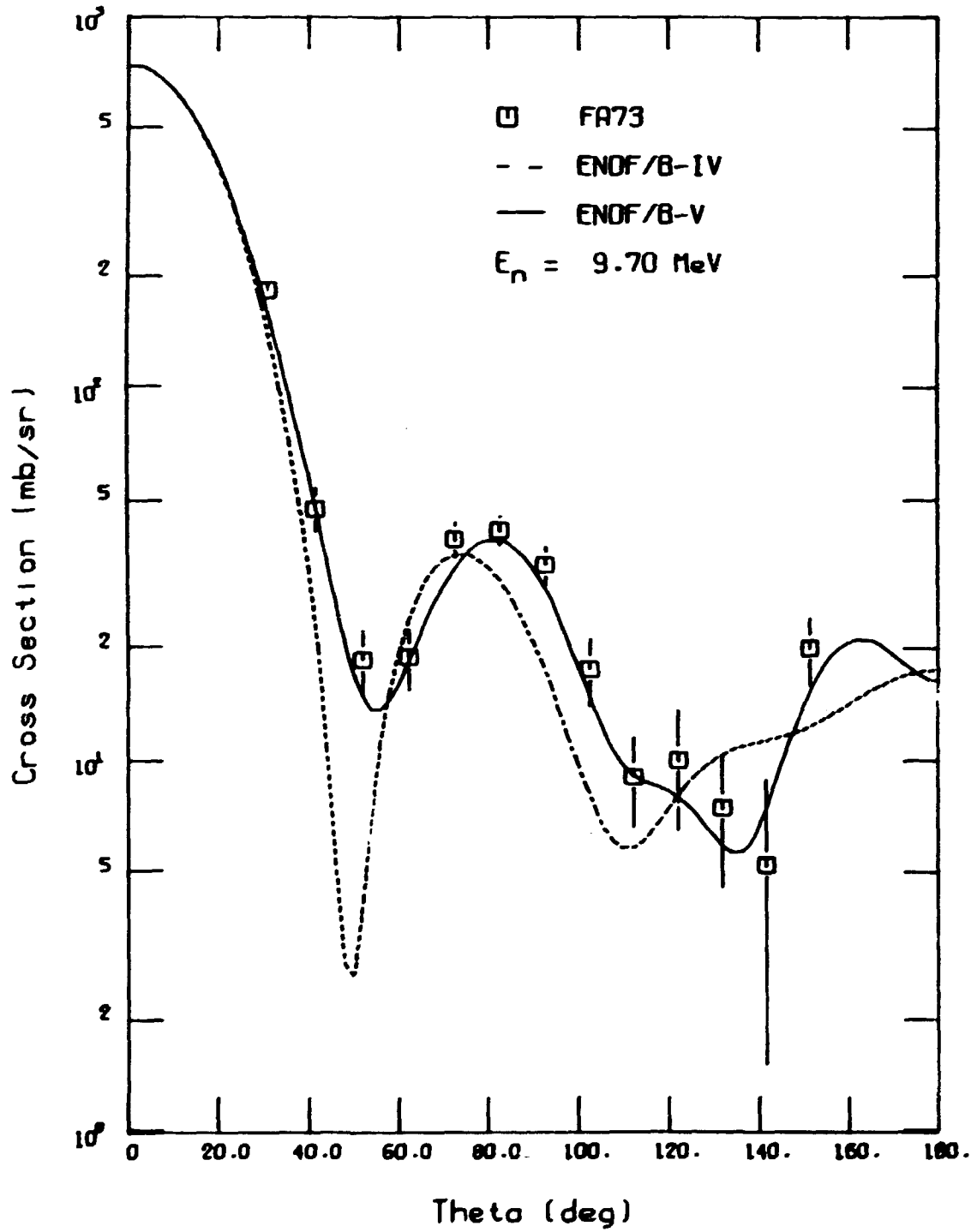


Fig. 80. Comparison of  $V_4$  and  $V_5$  elastic scattering angular distribution with available data.

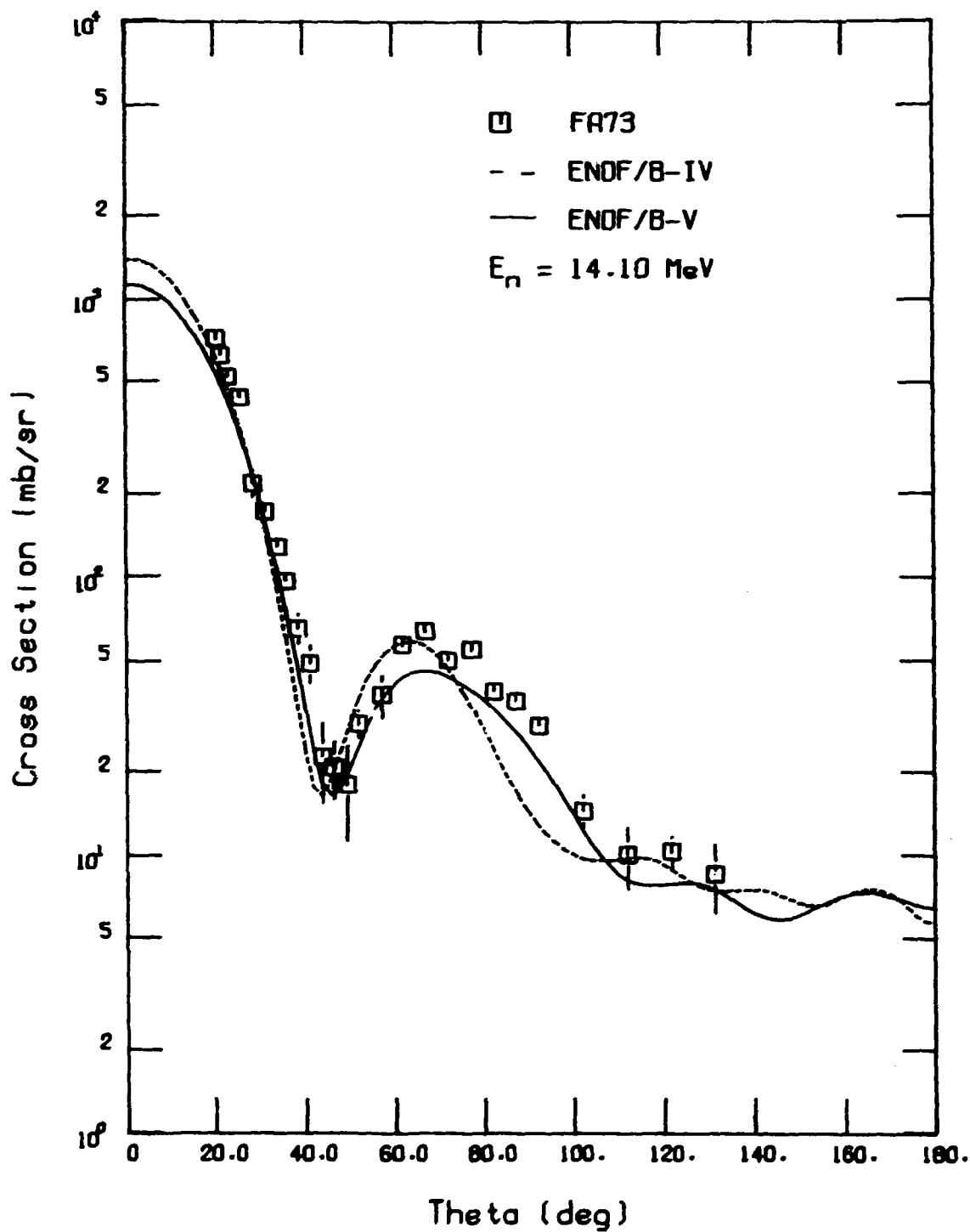


Fig. 81. Comparison of V4 and V5 elastic scattering angular distribution with available data.

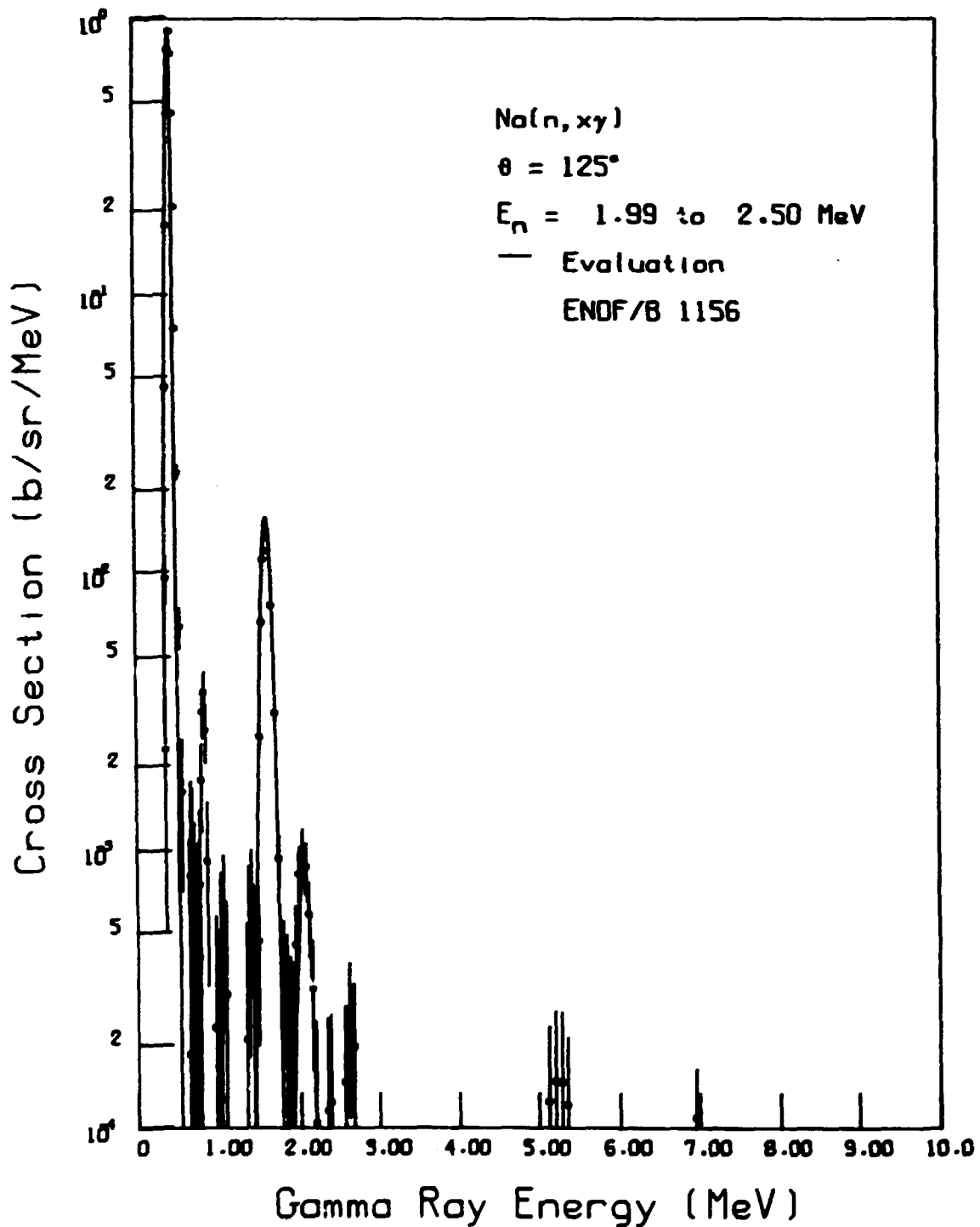


Fig. 82. Comparison of V4 with (n,xy) data of LA78.

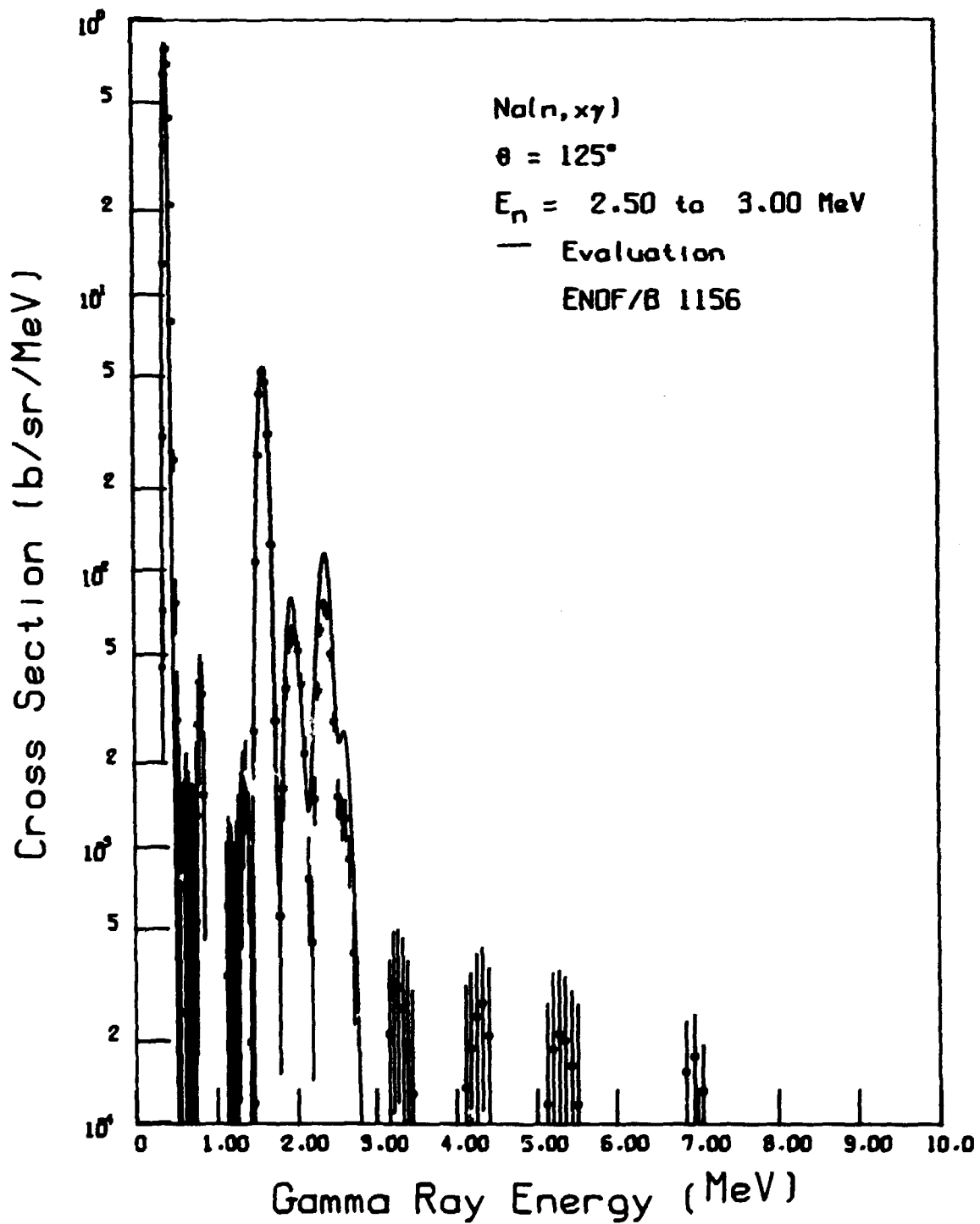


Fig. 83. Comparison of V4 with (n,γ) data of LA78.

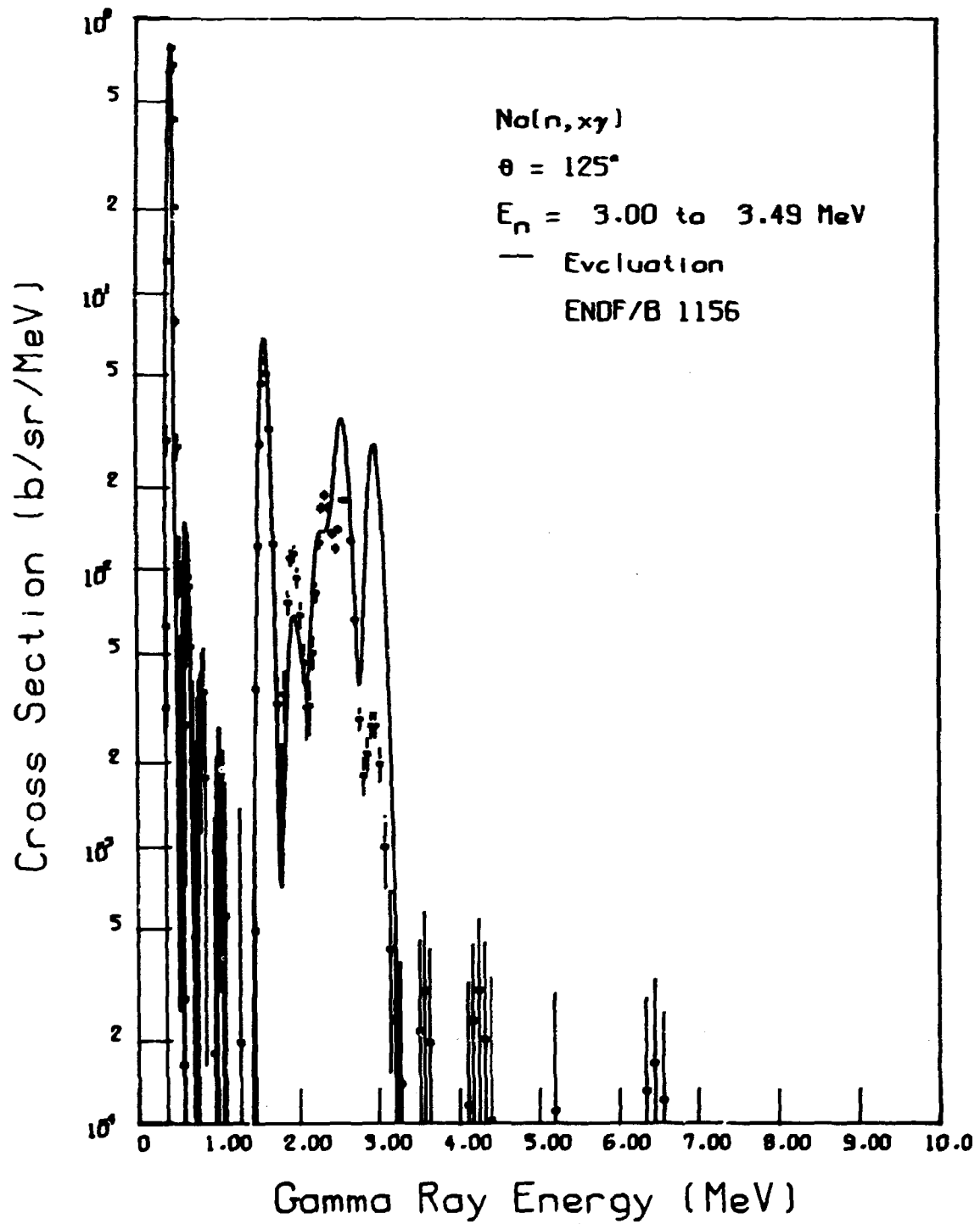


Fig. 84. Comparison of V4 with (n,xy) data of LA78.

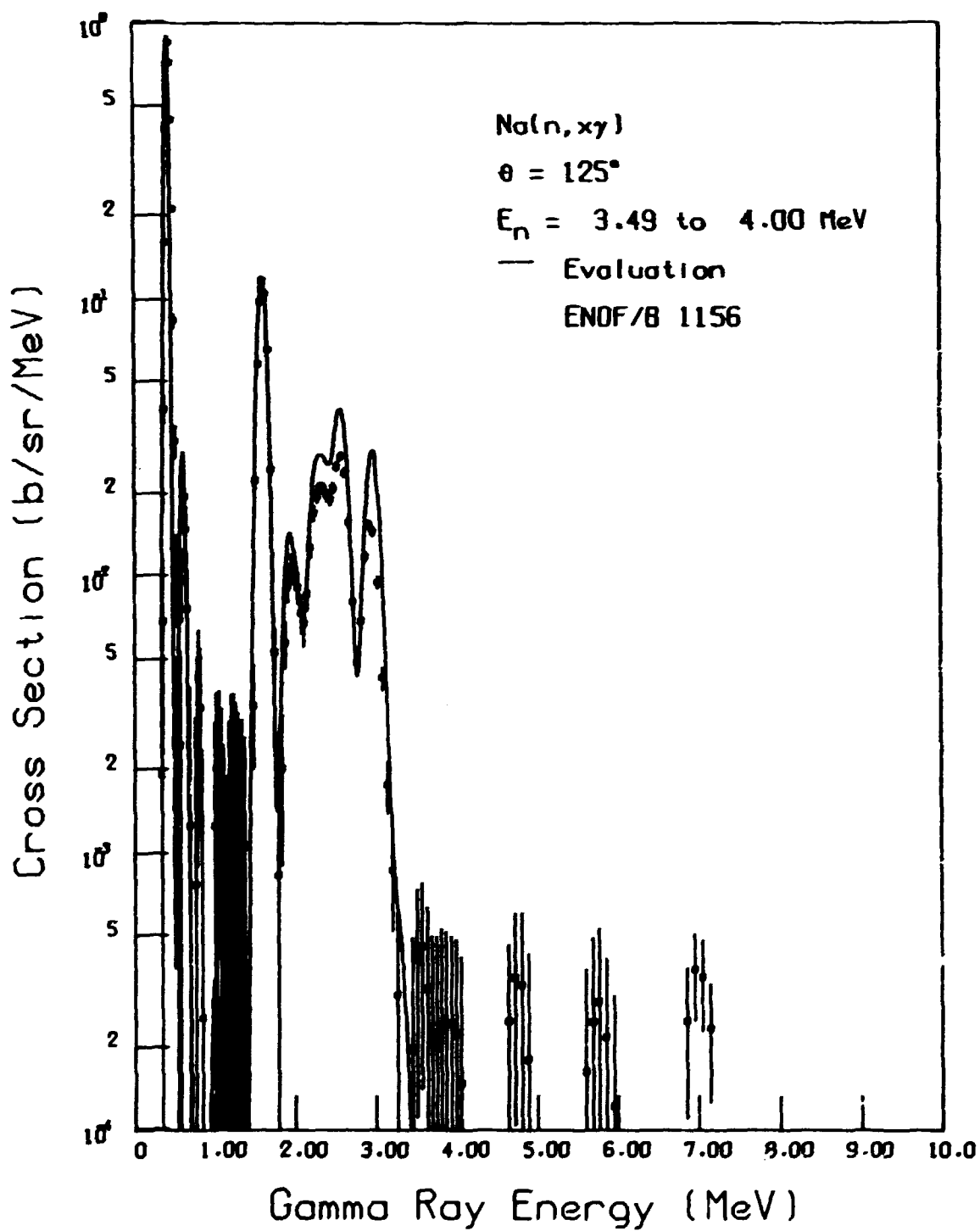


Fig. 85. Comparison of V4 with (n,xy) data of LA78.

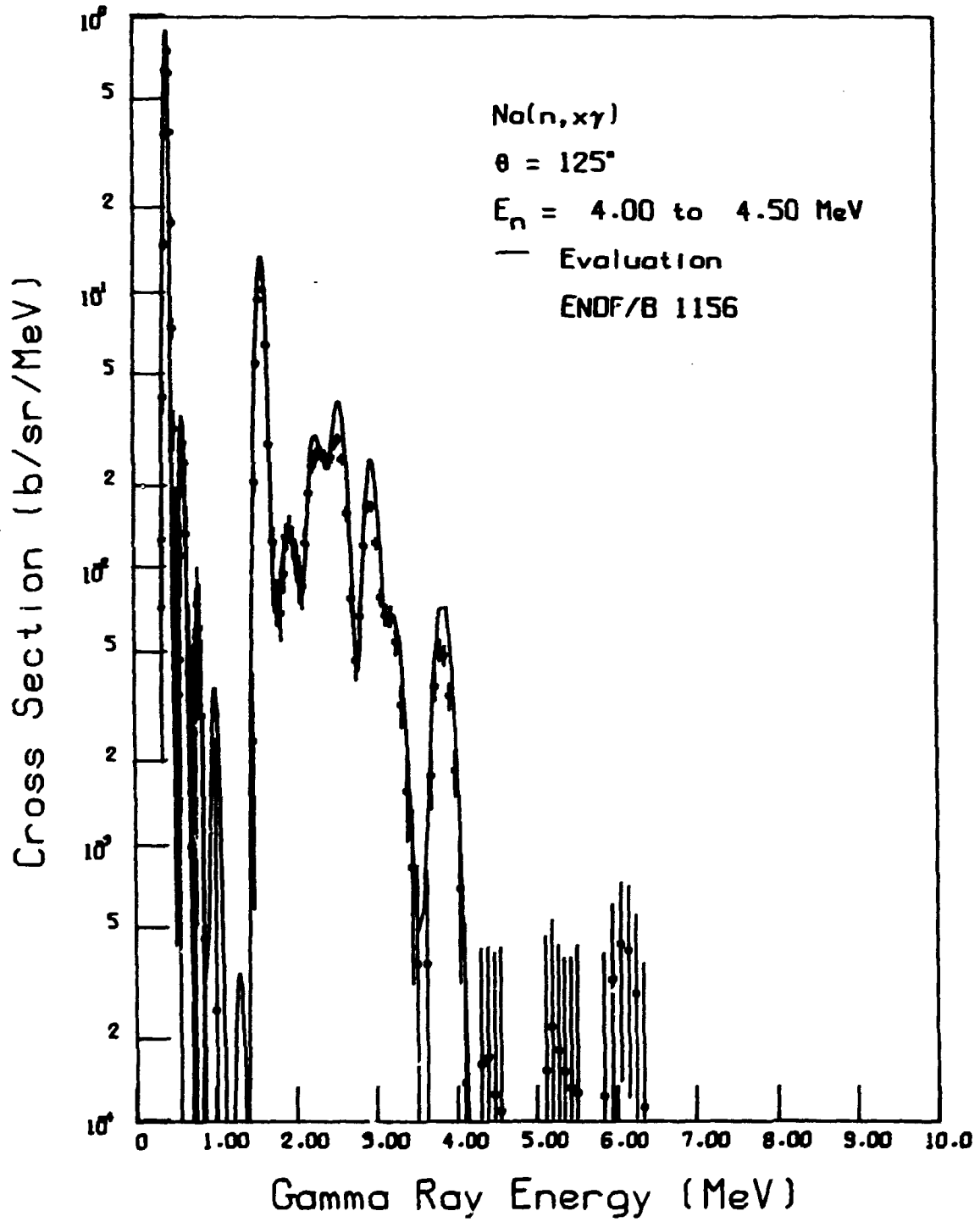


Fig. 86. Comparison of V4 with (n,x $\gamma$ ) data of LA78.

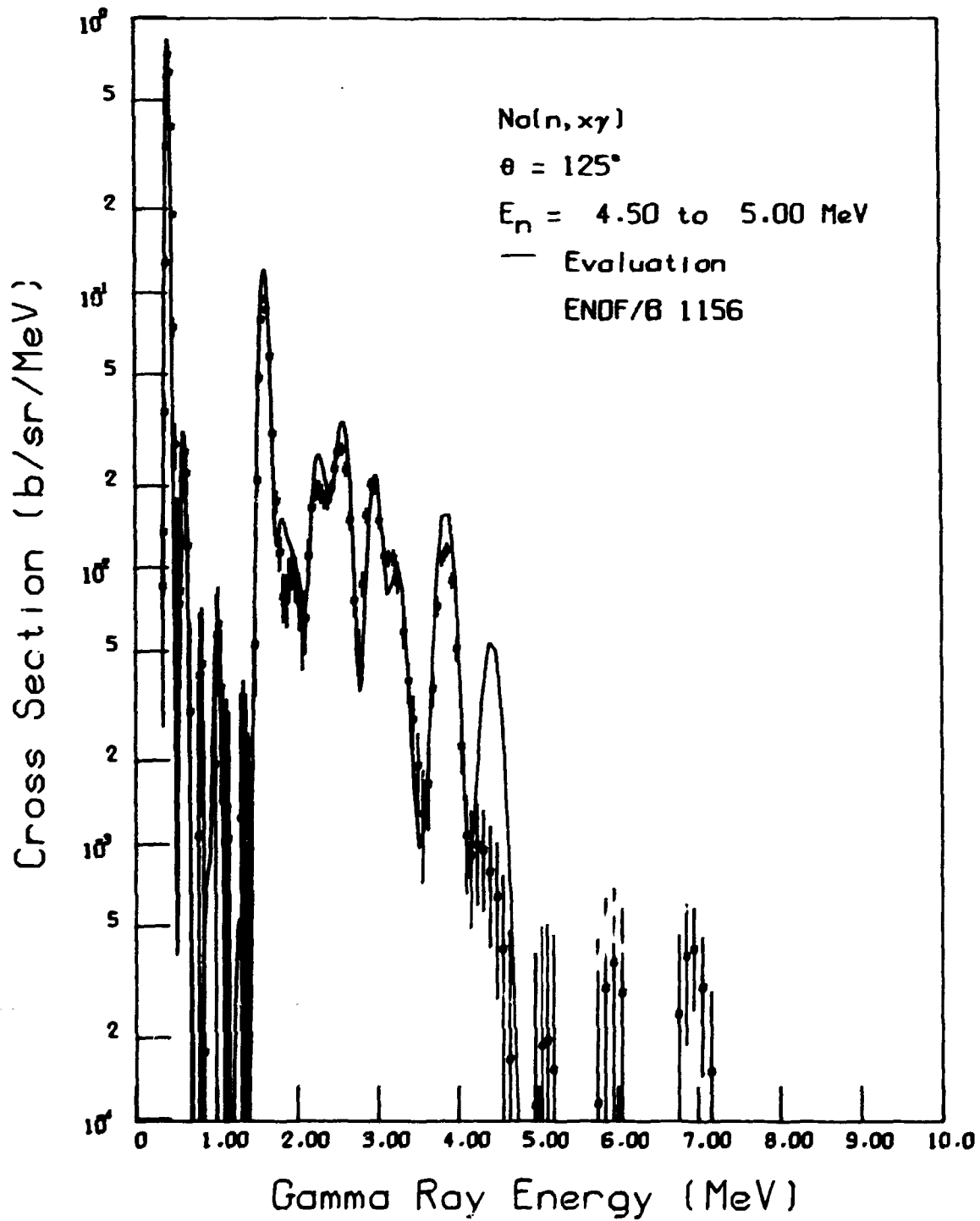


Fig. 87. Comparison of V4 with (n,xy) data of LA78.

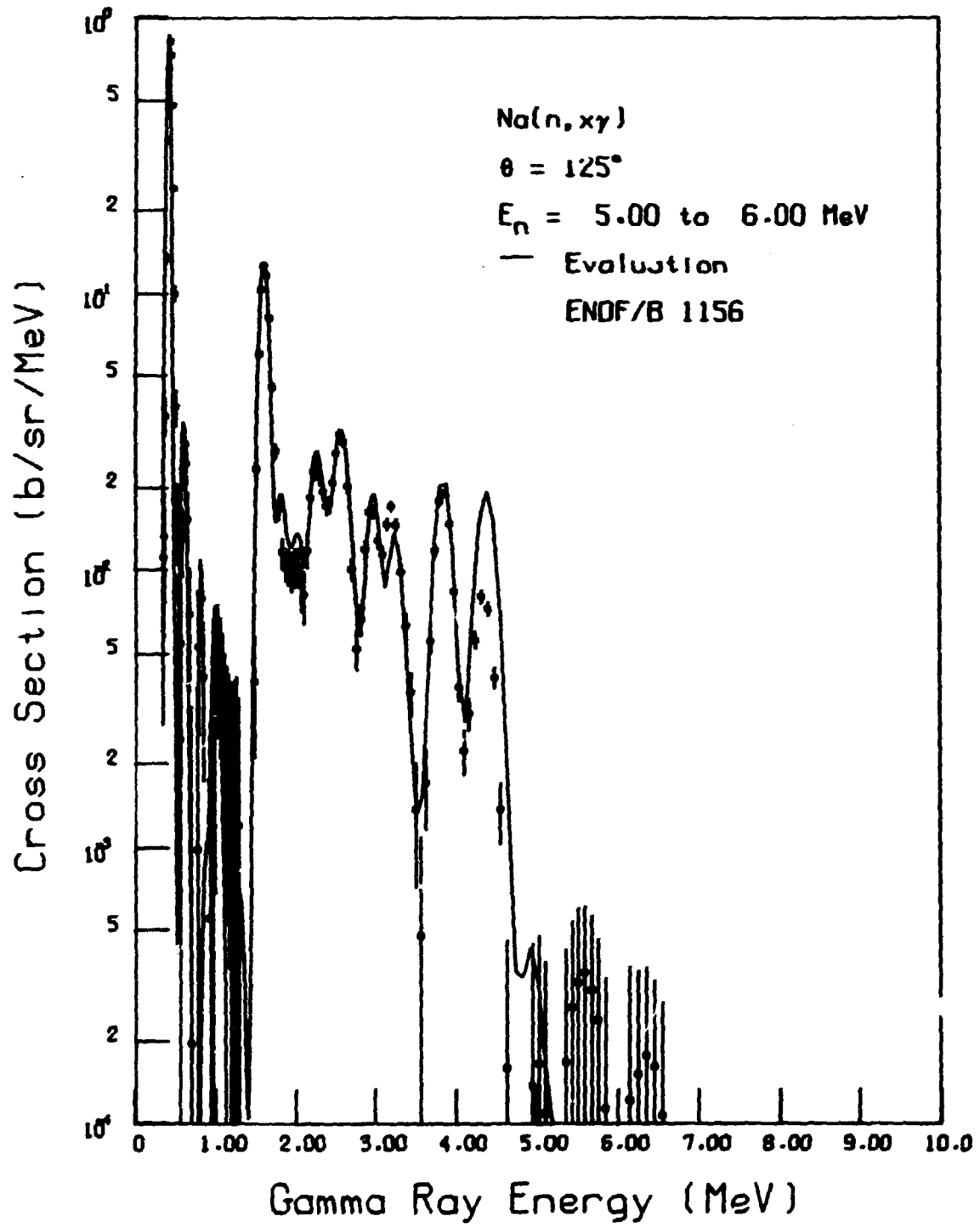


Fig. 88. Comparison of V4 with (n,xy) data of LA78.

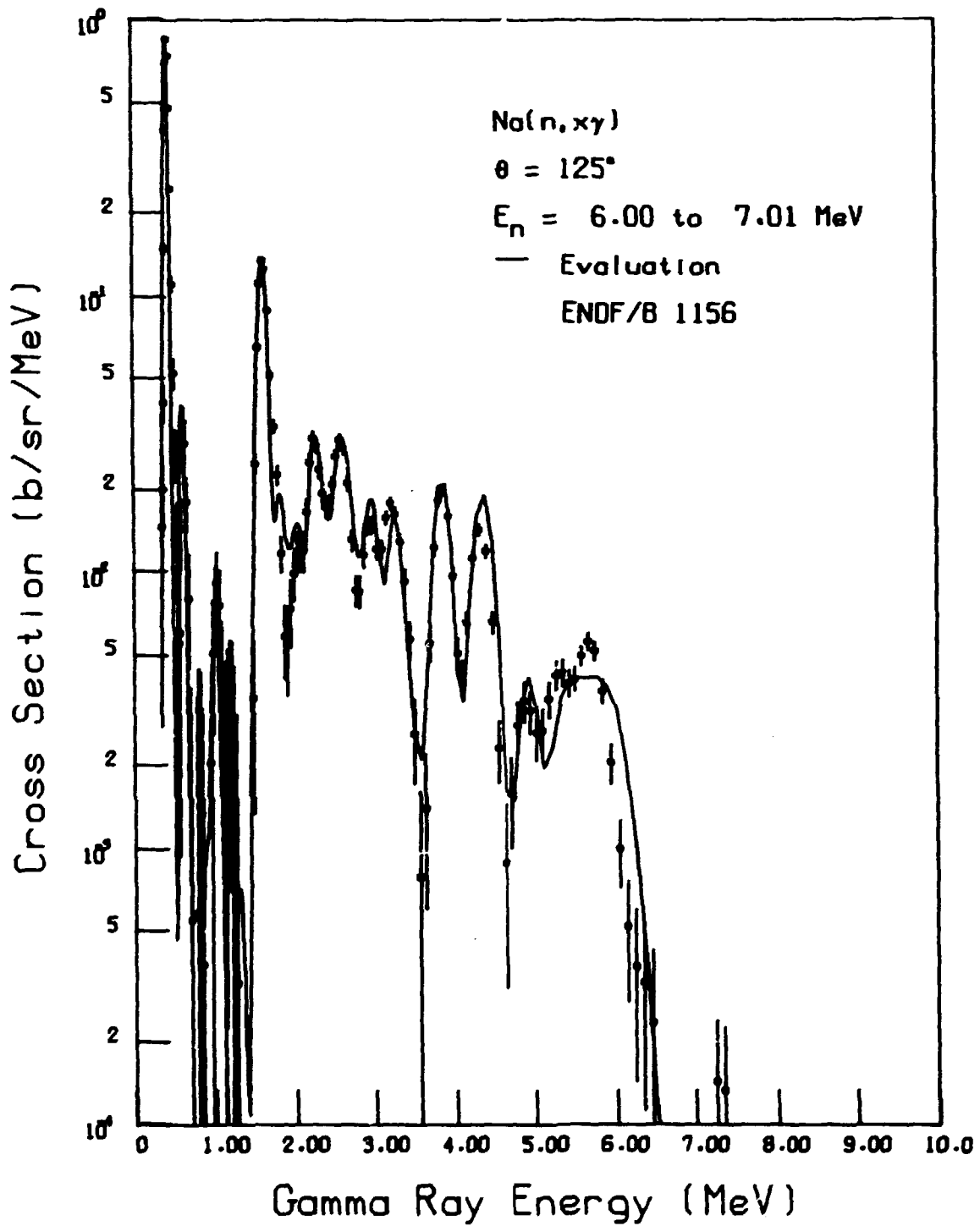


Fig. 89. Comparison of V4 with (n,xy) data of LA78.

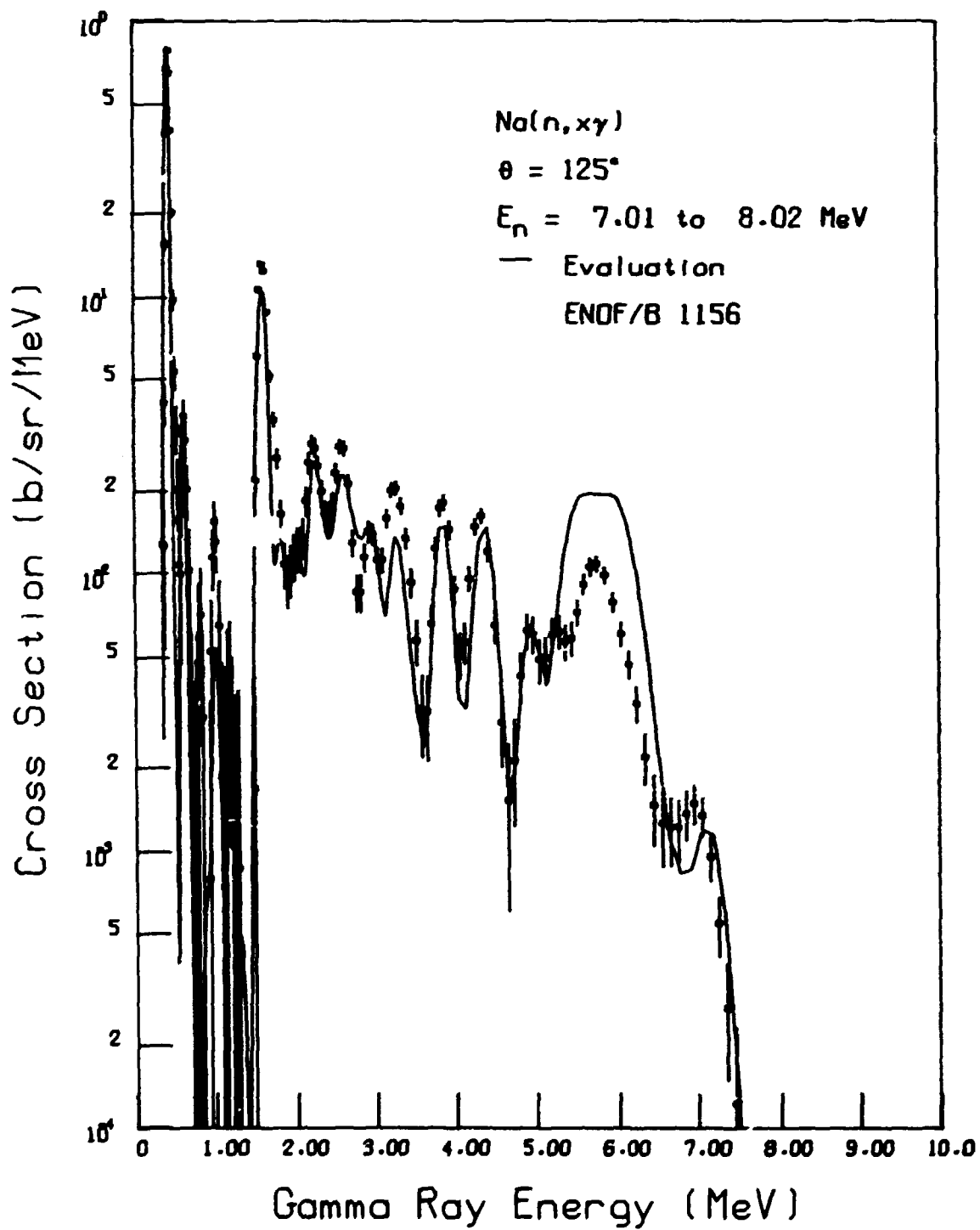


Fig. 90. Comparison of V4 with (n,x $\gamma$ ) data of LA78.

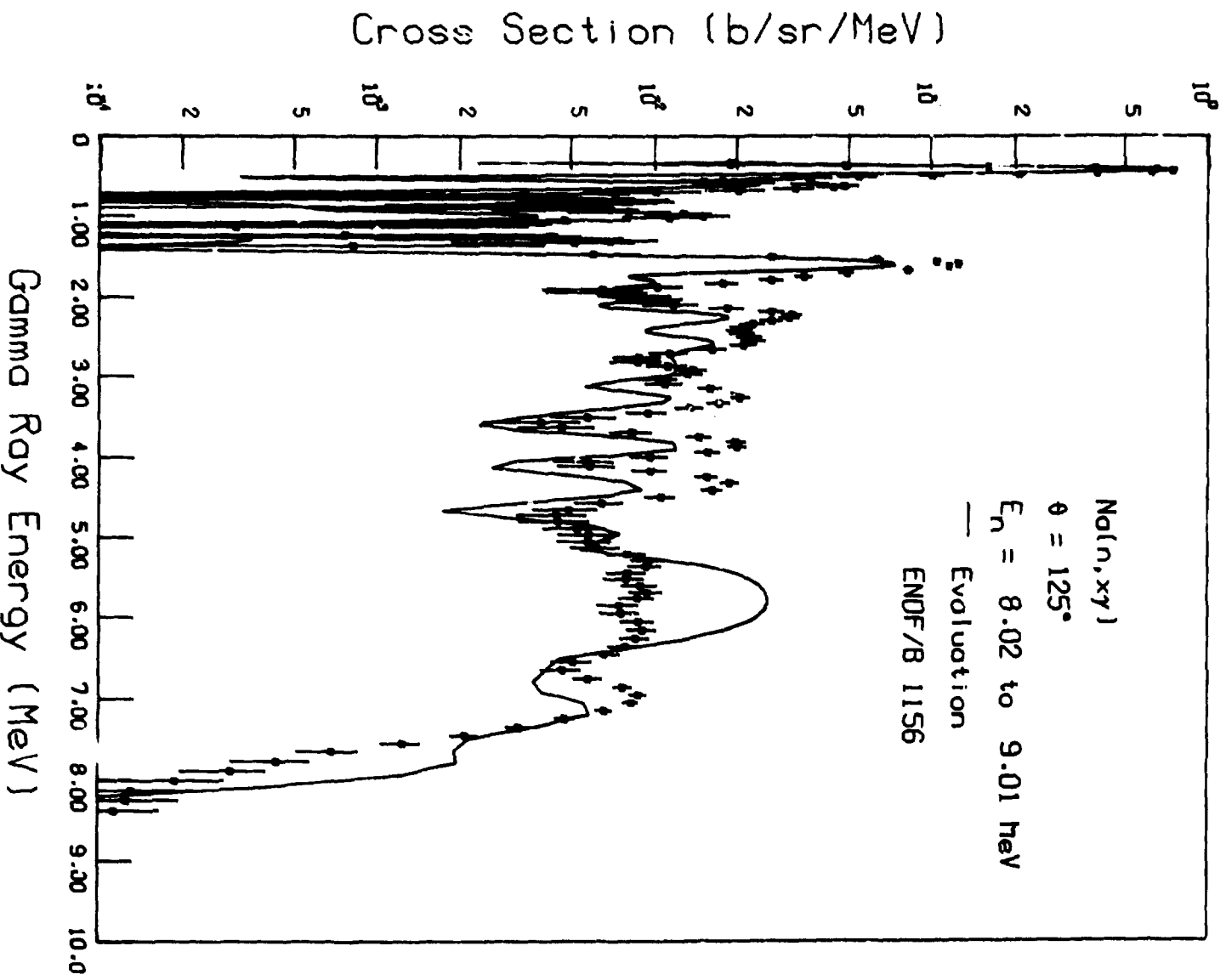


Fig. 91. Comparison of V4 with (n,xy) data of LA78.

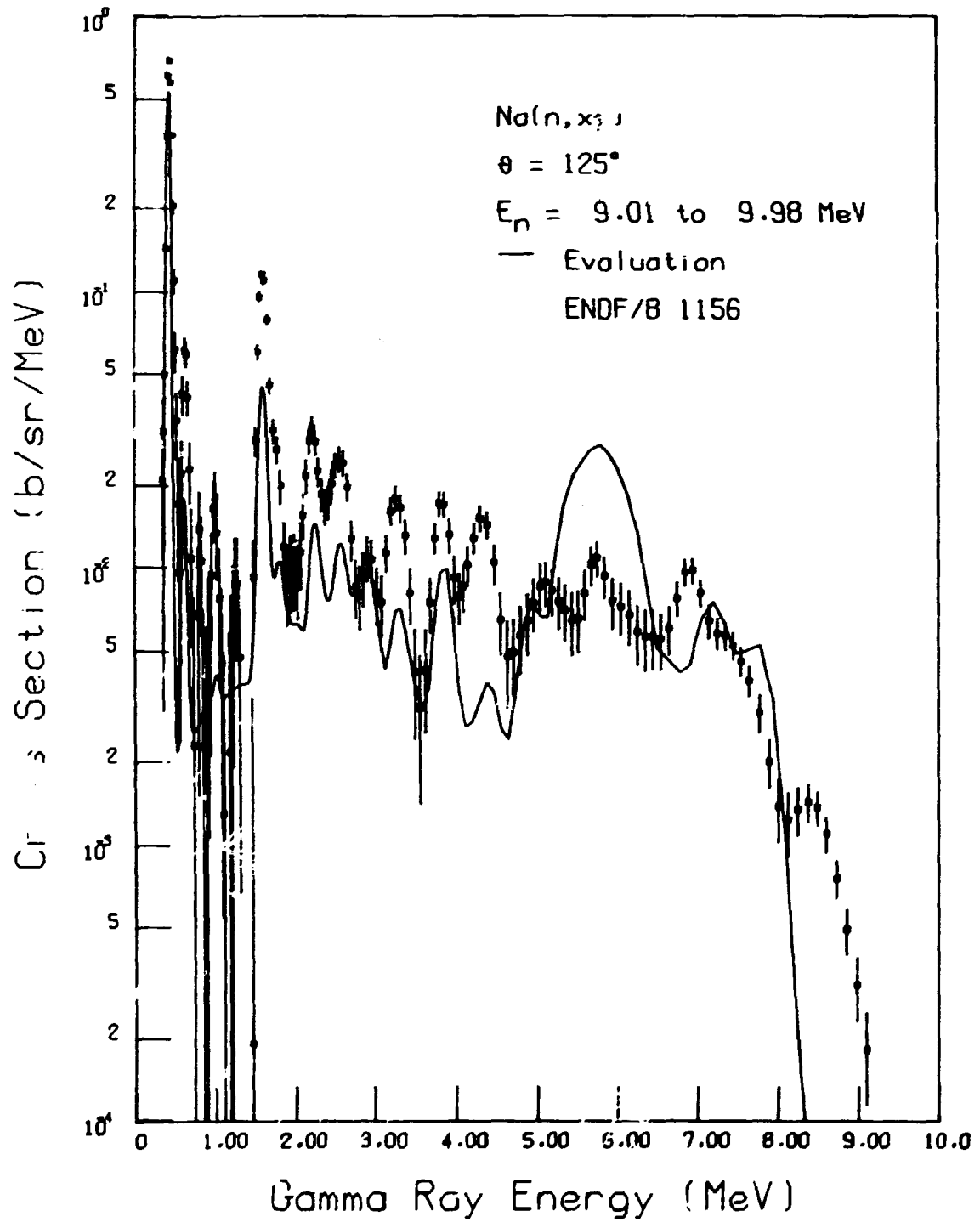


Fig. 92. Comparison of V4 with (n,xy) data of LA78.

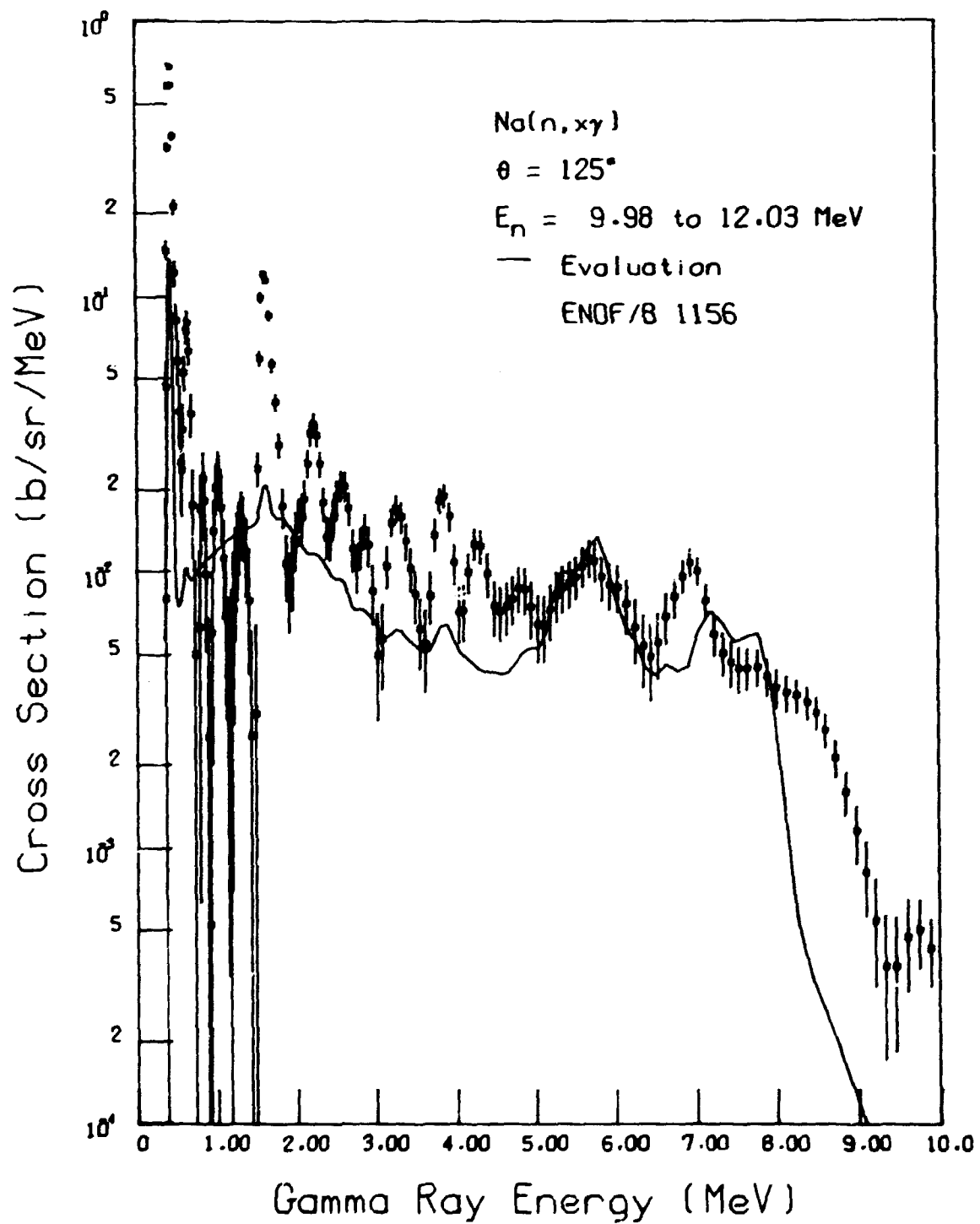


Fig. 93. Comparison of V4 with (n,x $\gamma$ ) data of LA78.

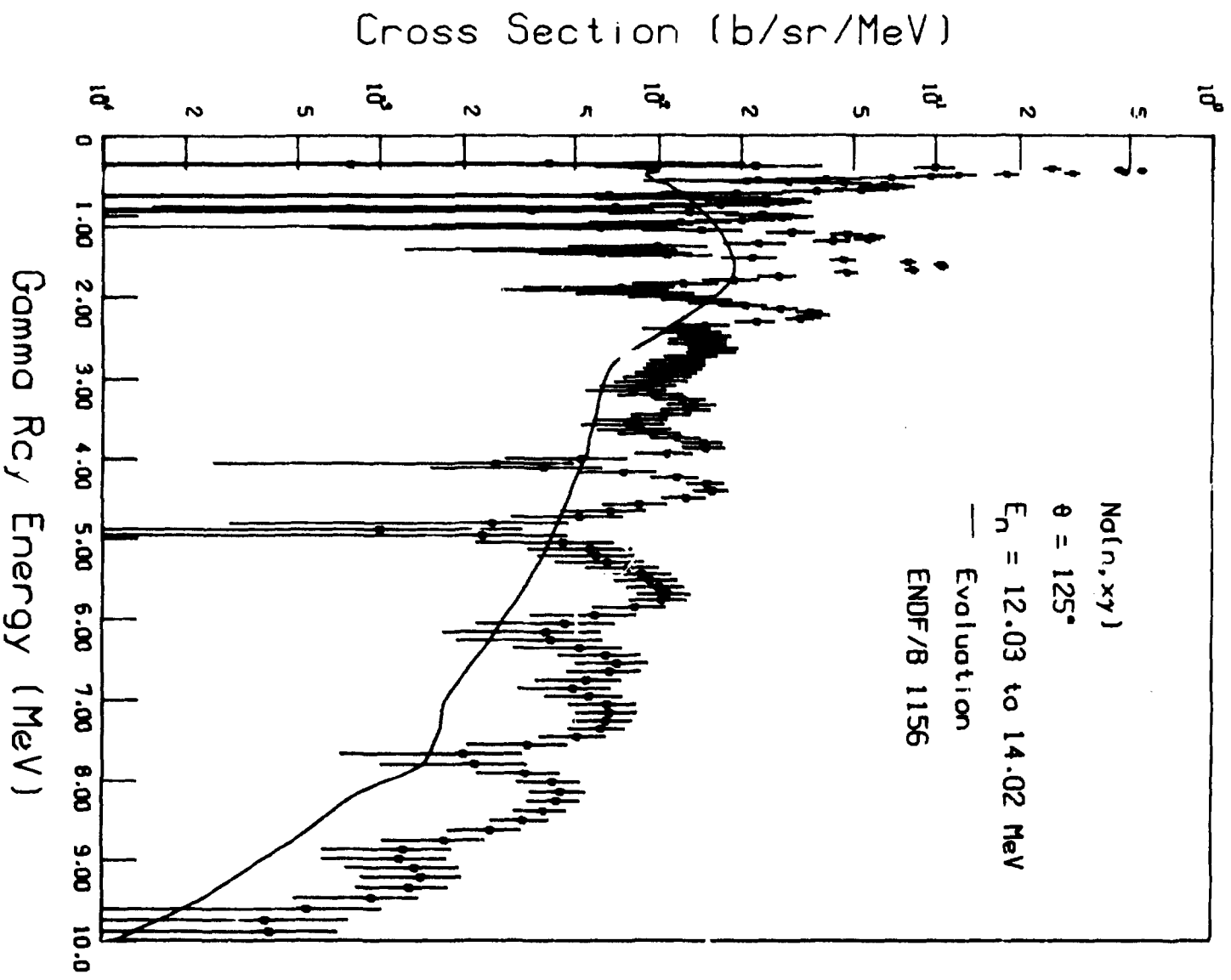


Fig. 94. Comparison of V4 with (n,xy) data of LA78.

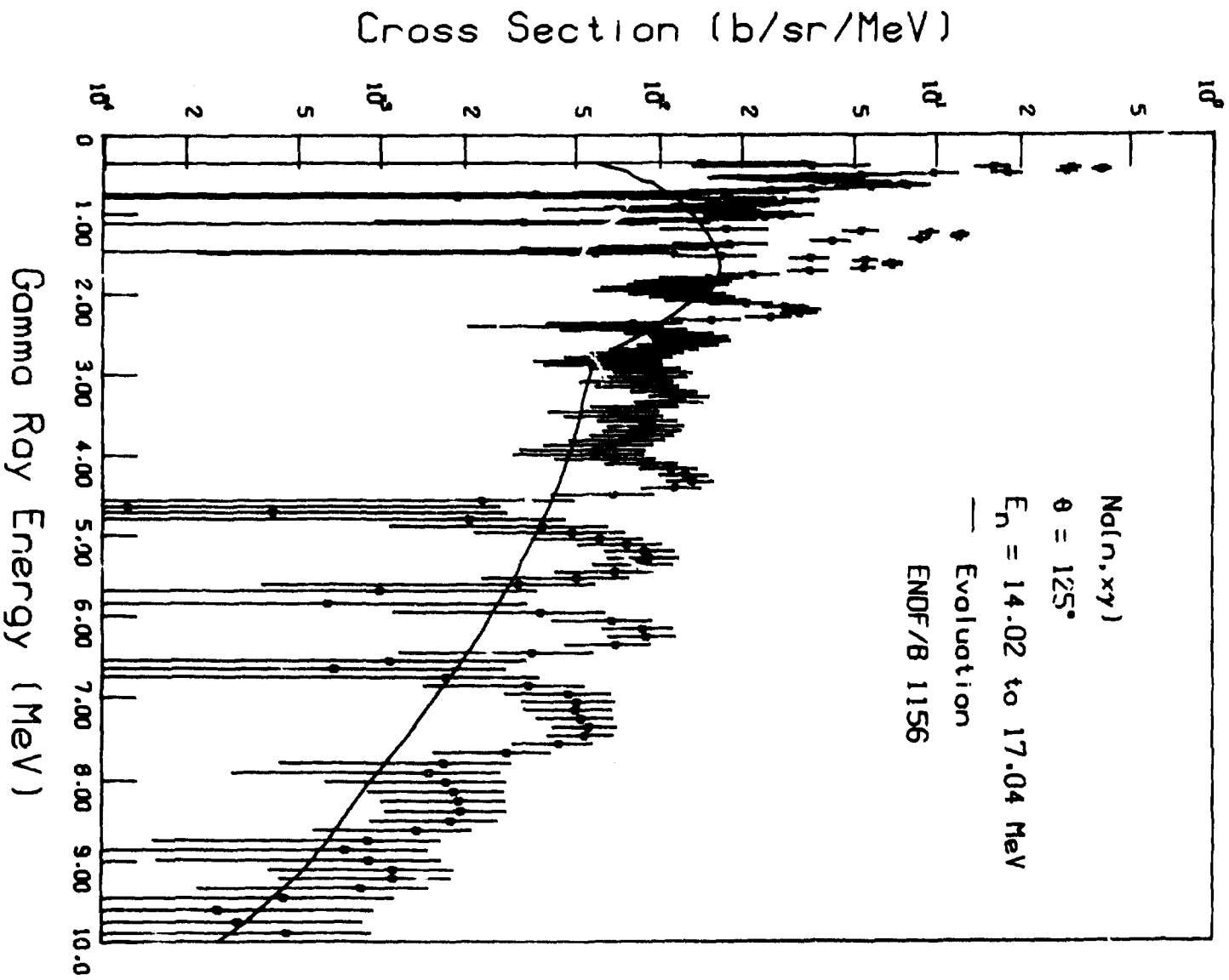


Fig. 95. Comparison of V4 with (n,xy) data of LA78.

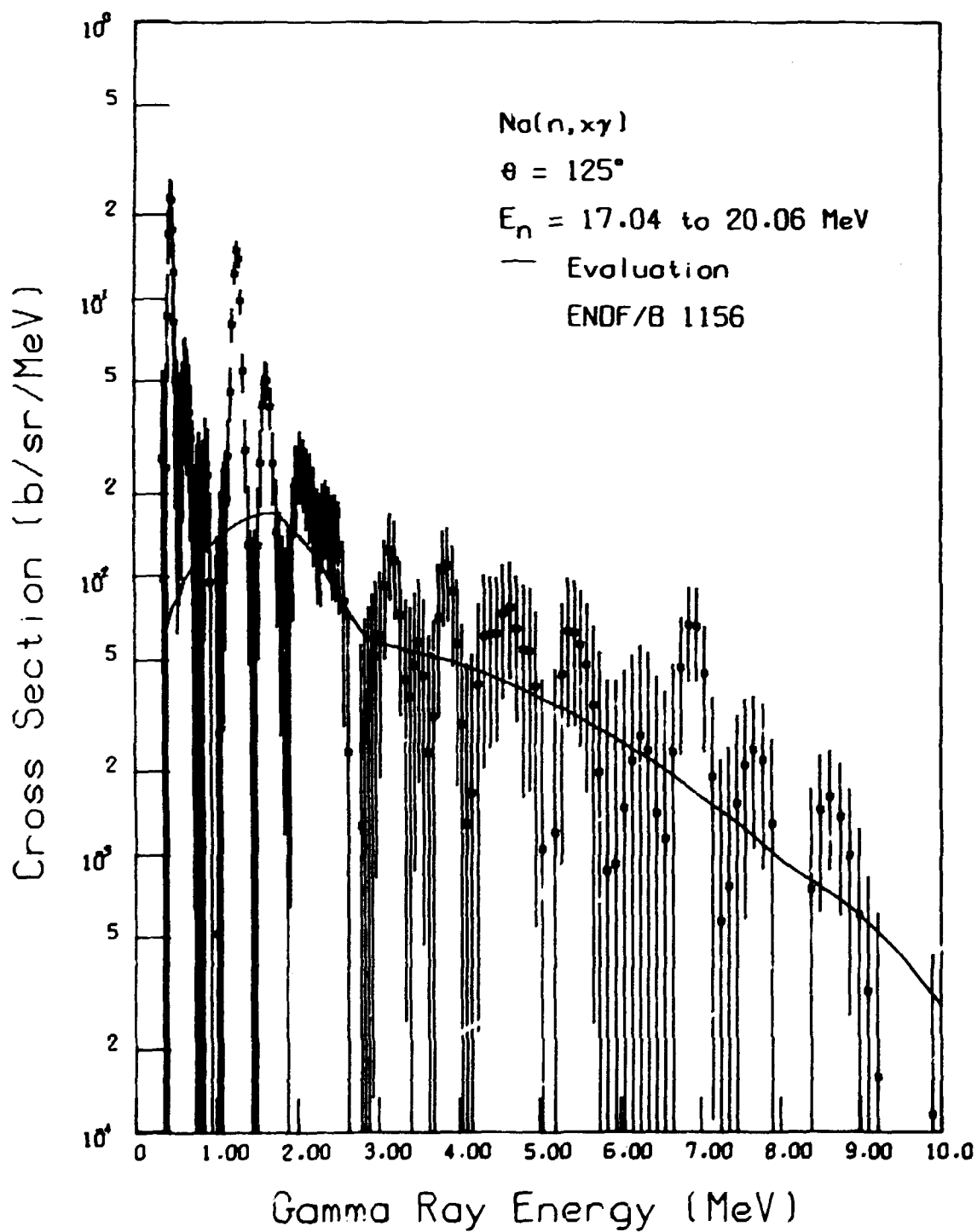


Fig. 96. Comparison of V4 with (n,γ) data of LA78.

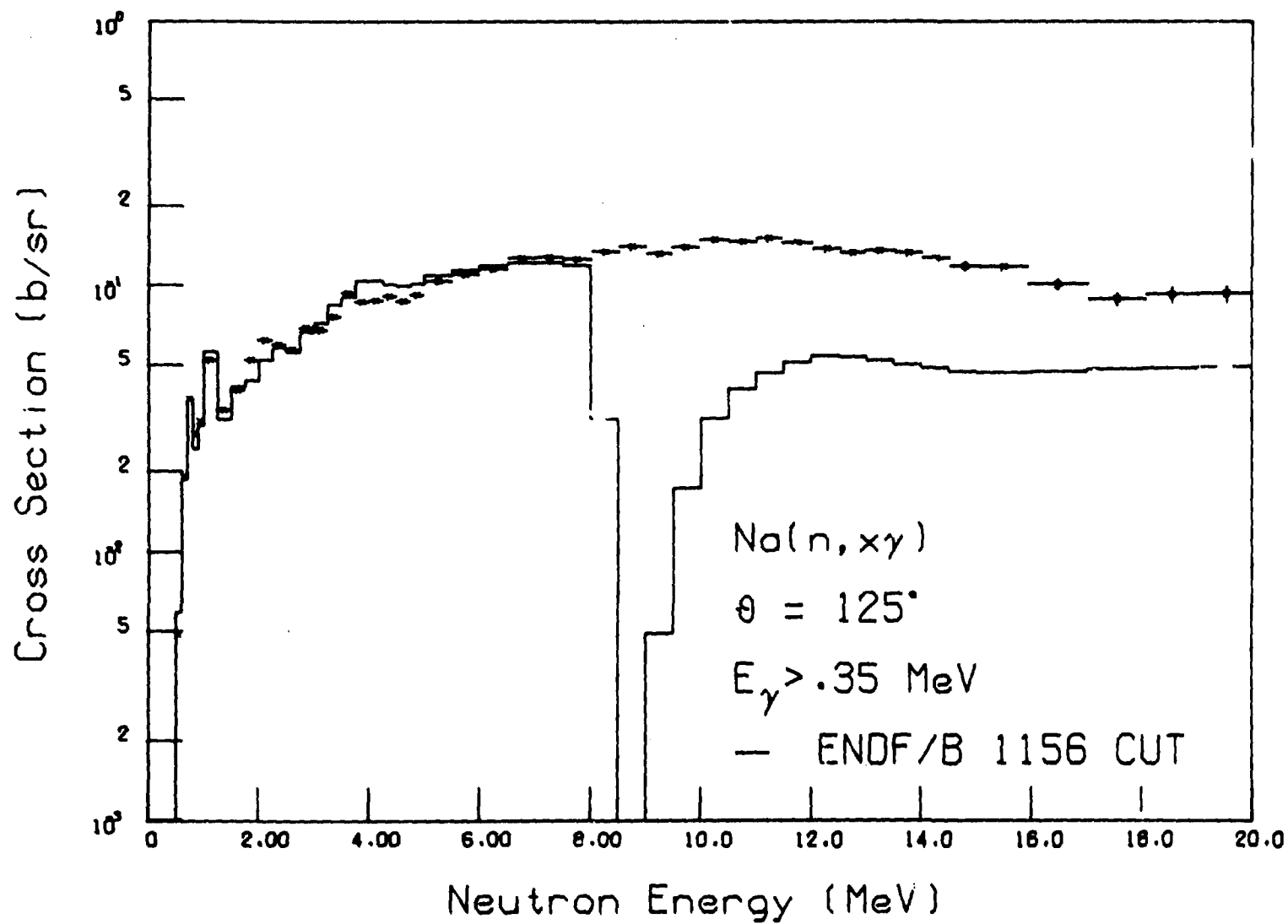


Fig. 97. Total gamma-ray-production cross section of LA78 as a function of neutron energy, compared with the cutoff V4 evaluation. See text for discussion of this point.

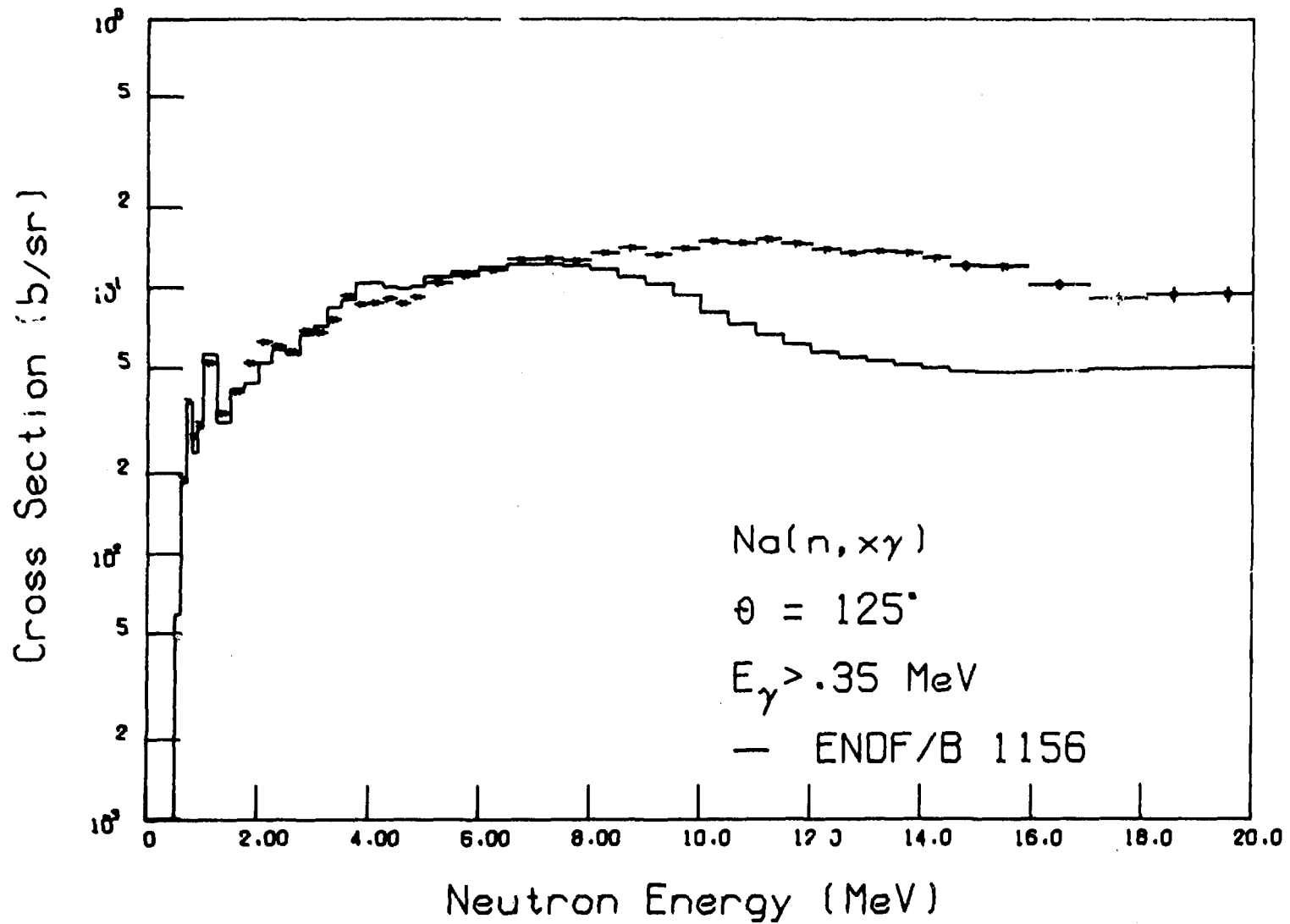


Fig. 98. Same as Fig. 97, except evaluation is shown without processing code cutoff on neutron energy.

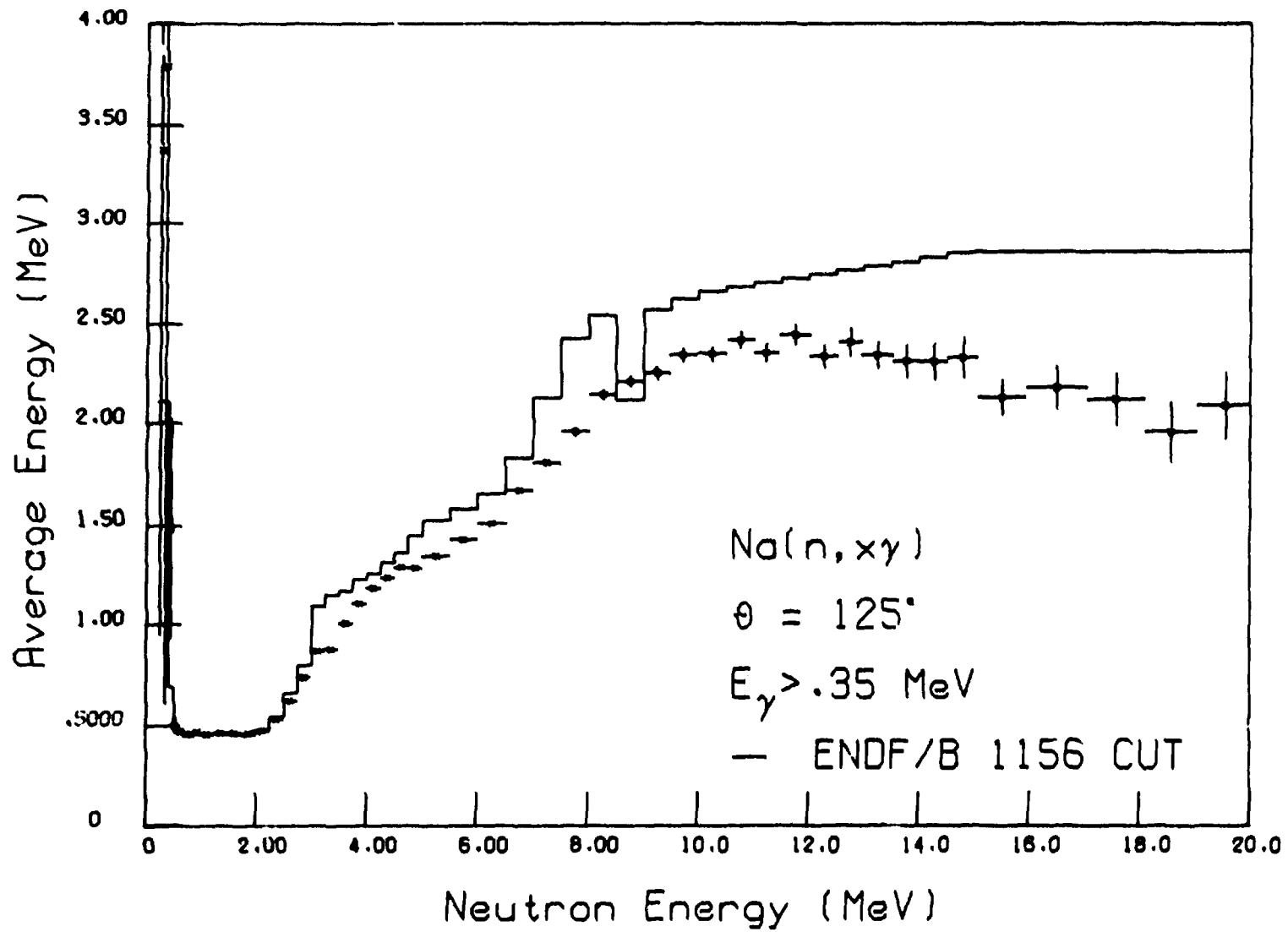


Fig. 99. Average secondary gamma-ray energy of LA78 as a function of neutron energy, compared with the cutoff V4 evaluation. See text for discussion.

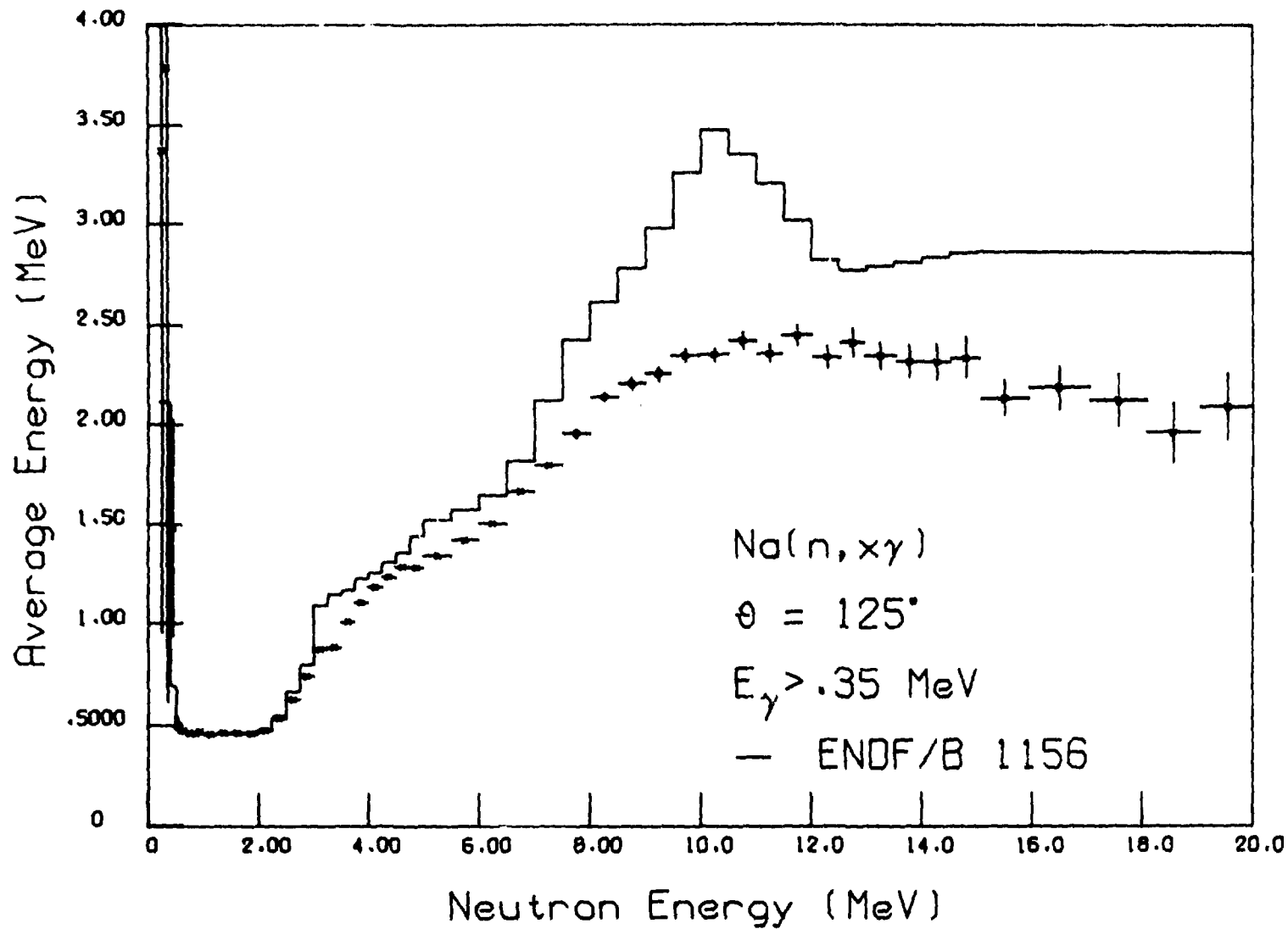


Fig. 100. Same as Fig. 990, except V4 evaluation is shown without processing code cutoff on neutron energy.

# Total Cross Section (b)

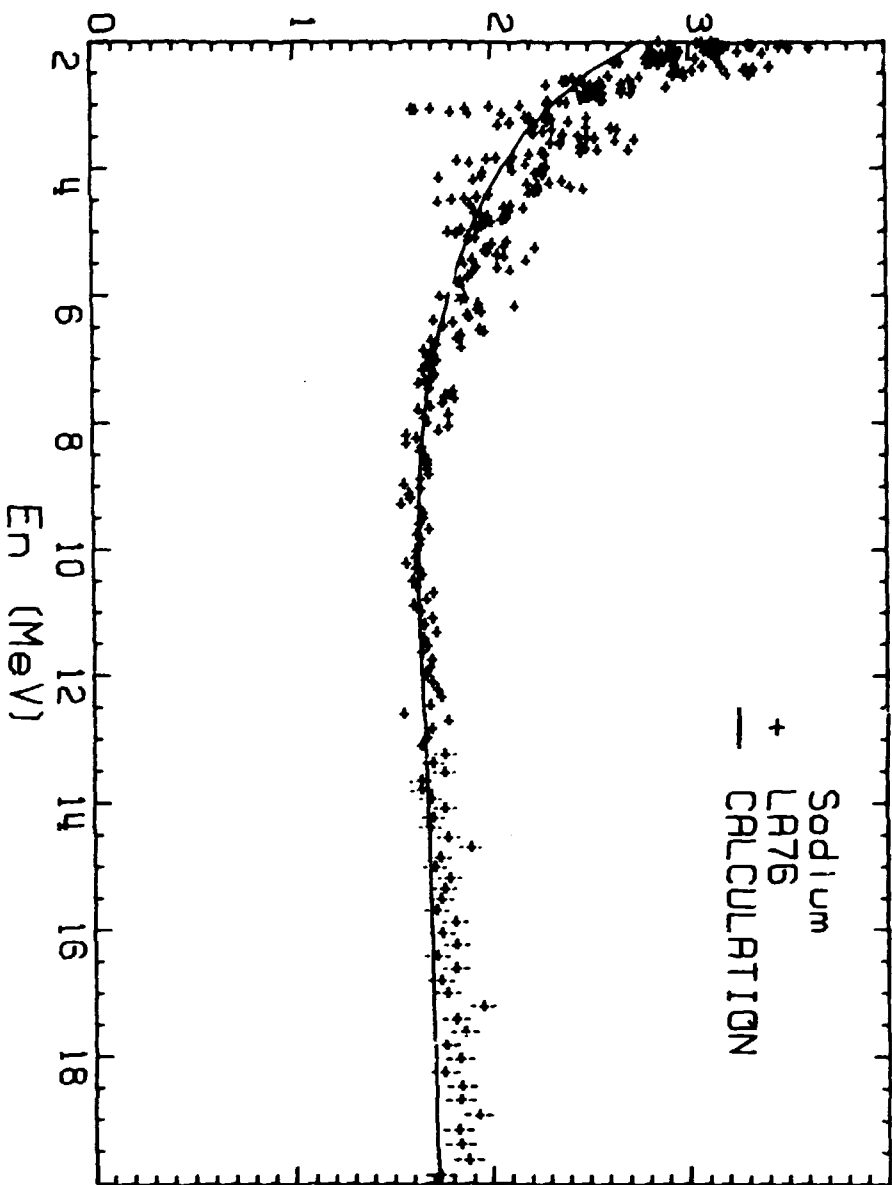


Fig. 101. Comparison of total cross section from optical model with data of Ref. LA76.

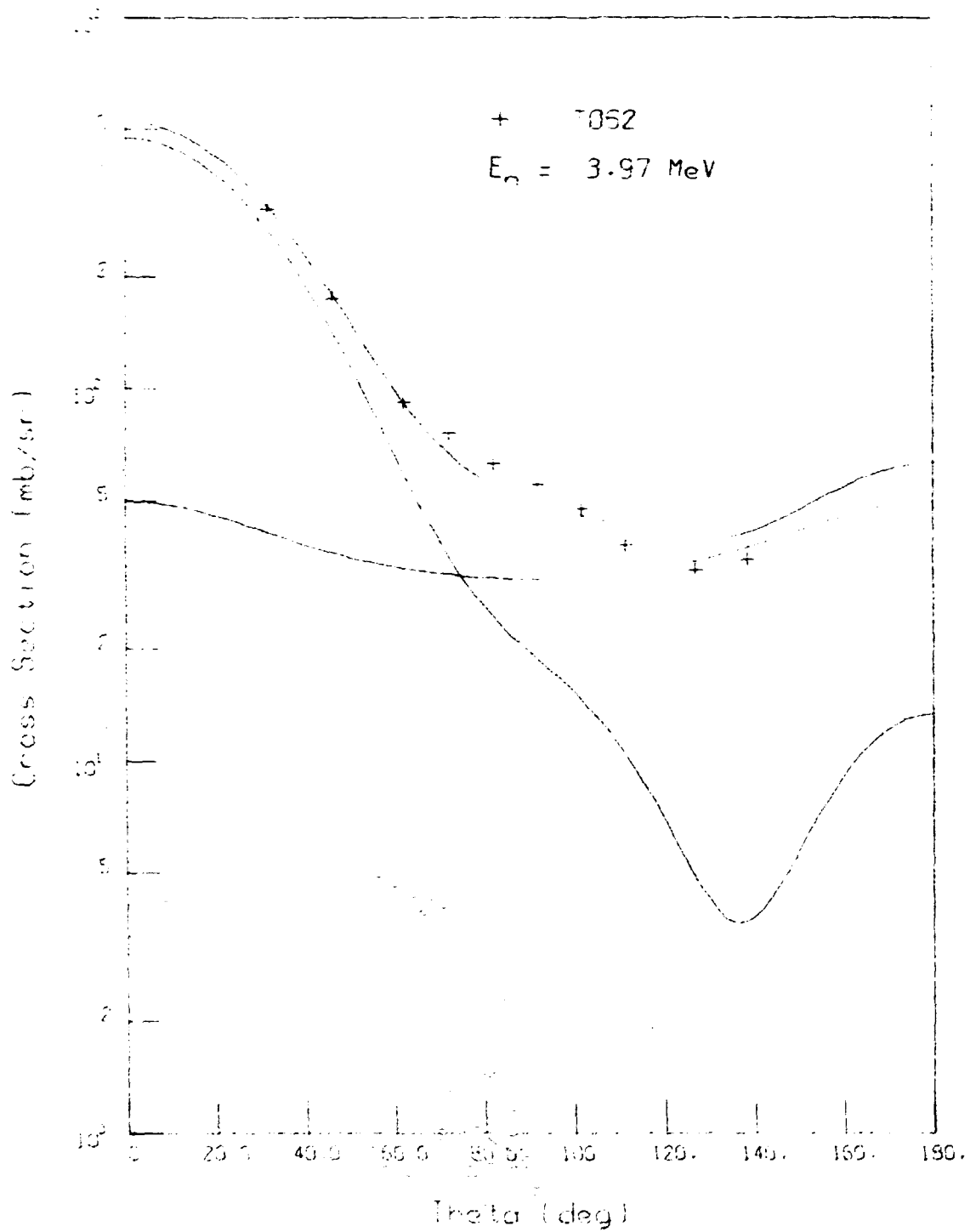


Fig. 102. Comparison of final optical model fit with data of Ref. T062. The compound and shape elastic are summed to give the total elastic.

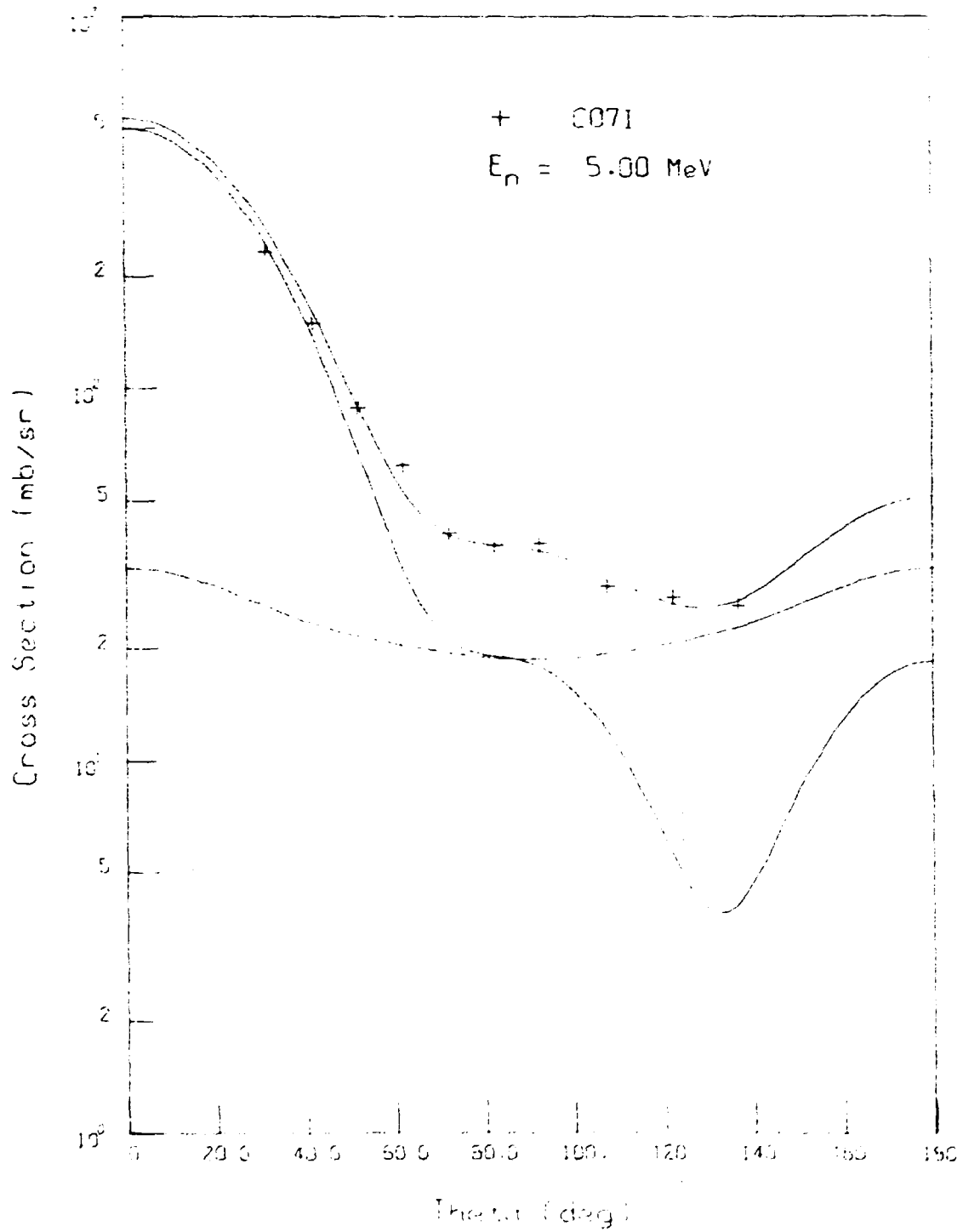


Fig. 103. Comparison of final optical model fit with data of Ref. C071. The compound and shape elastic are summed to give the total elastic.

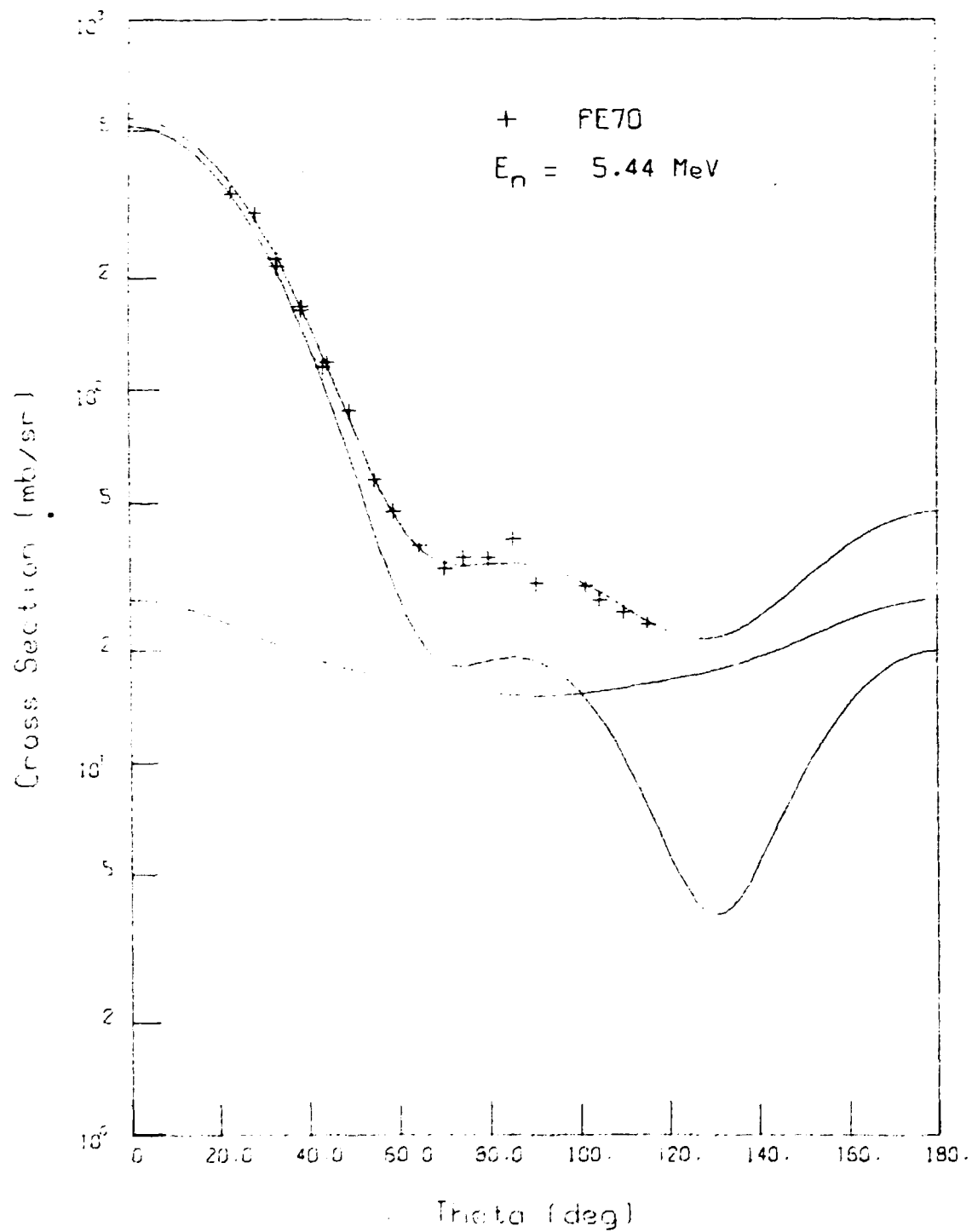


Fig. 104. Comparison of final optical model fit with data of Ref. PE70. The compound and shape elastic are summed to give the total elastic.

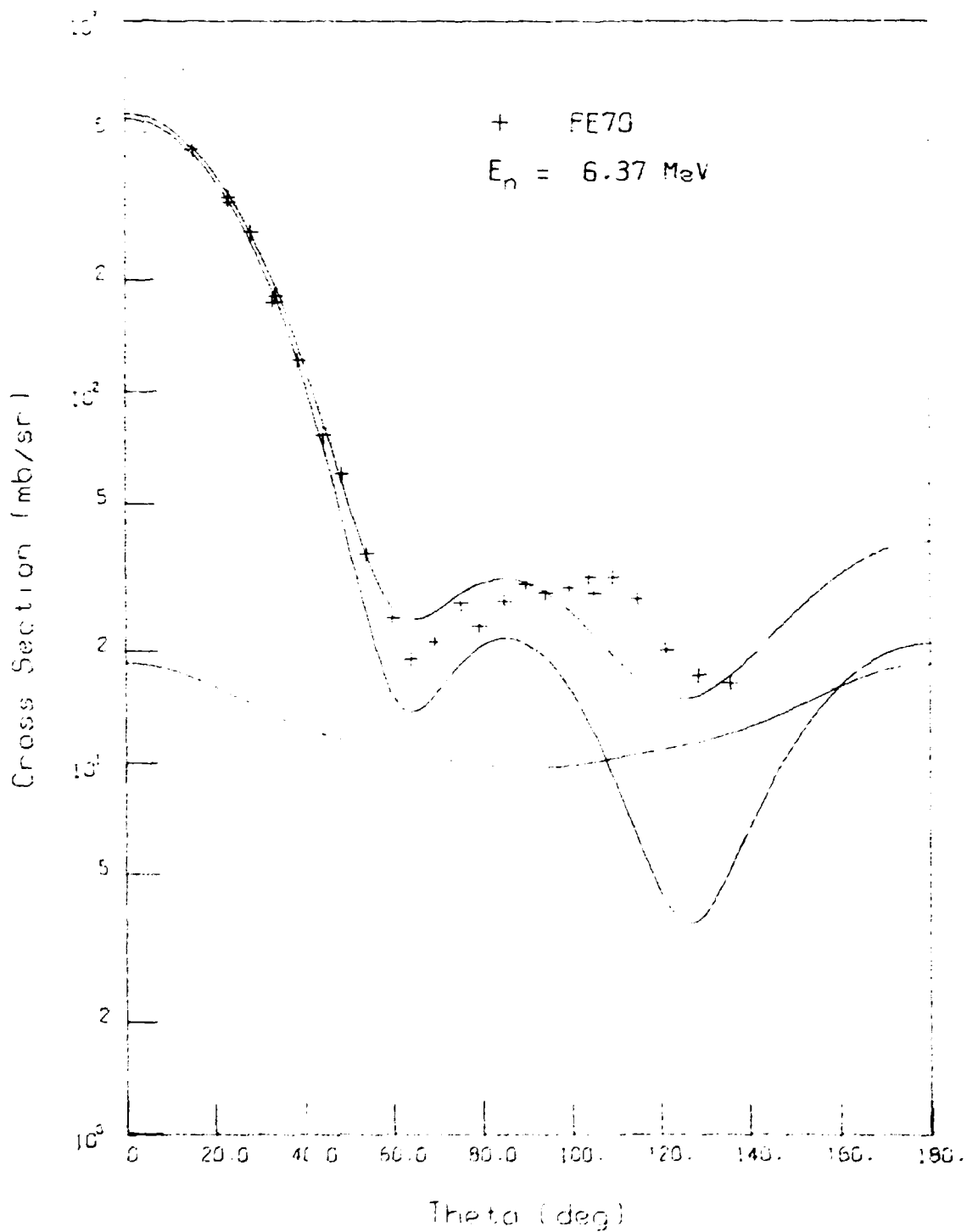


Fig. 105. Comparison of final optical model fit with data of Ref. PE70. The compound and shape elastic are summed to give the total elastic.

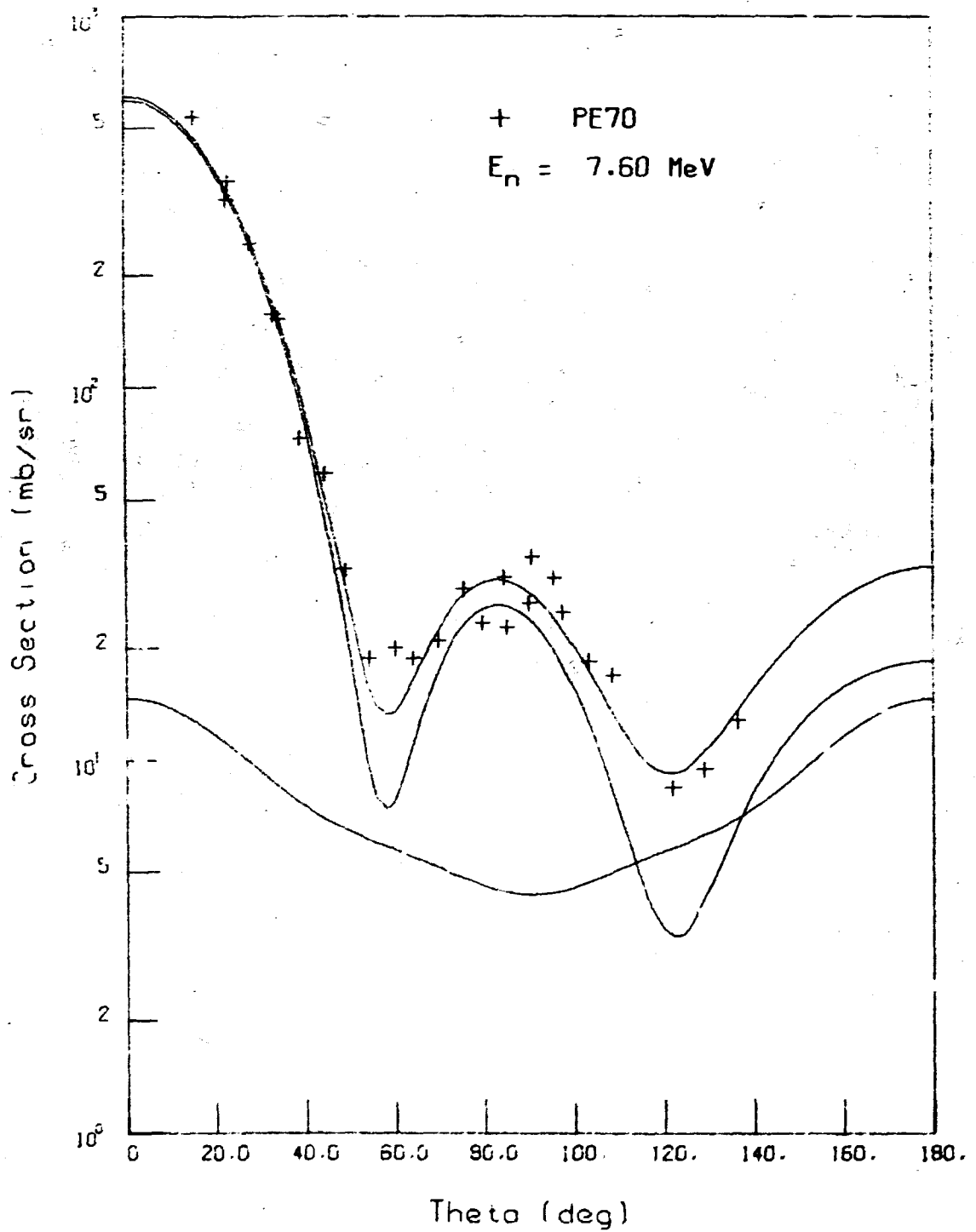


Fig. 106. Comparison of final optical model fit with data of Ref. P170. The compound and shape elastic are summed to give the total elastic.

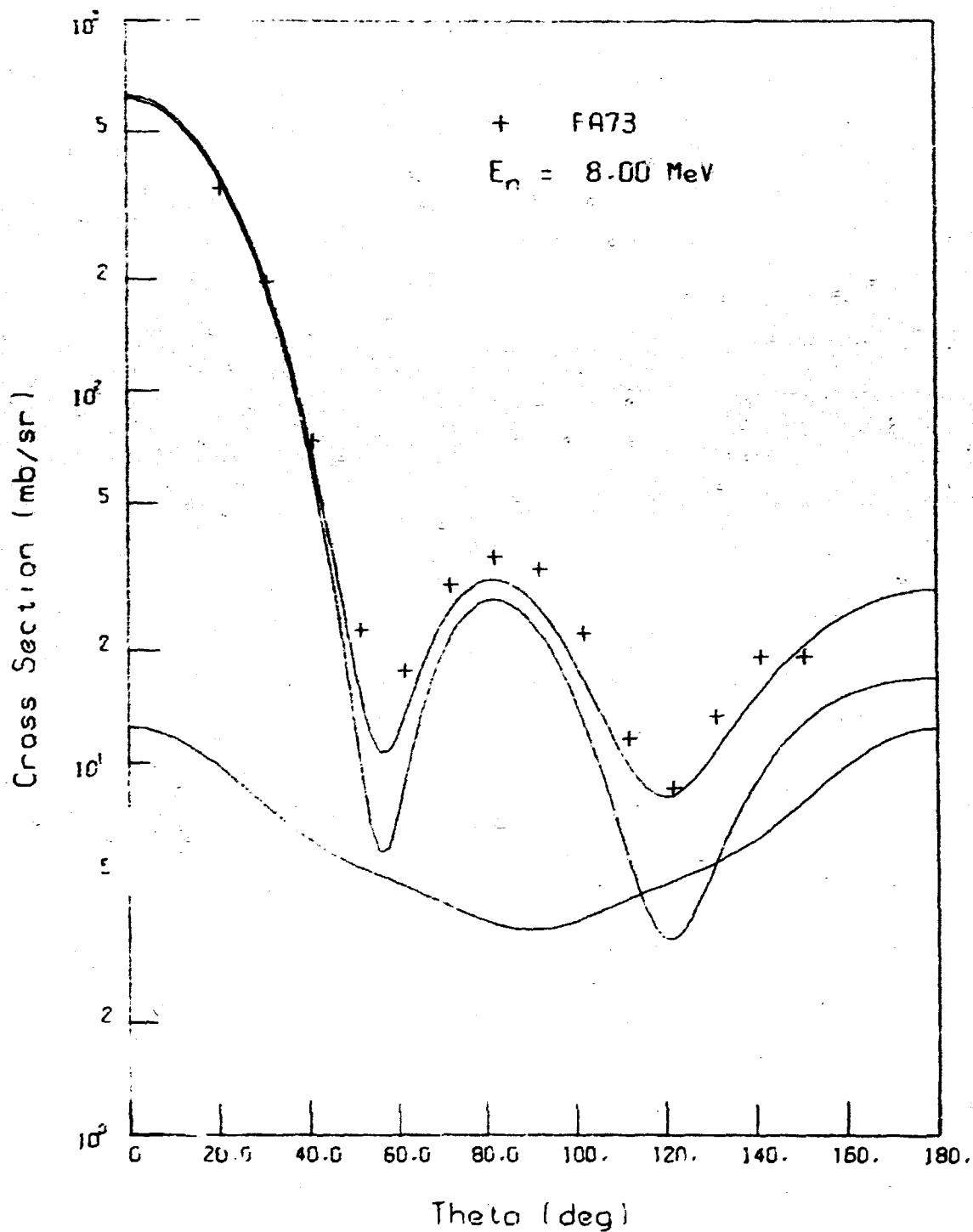


Fig. 107. Comparison of final optical model fit with data of Ref. FA73. The compound and shape elastic are summed to give the total elastic.

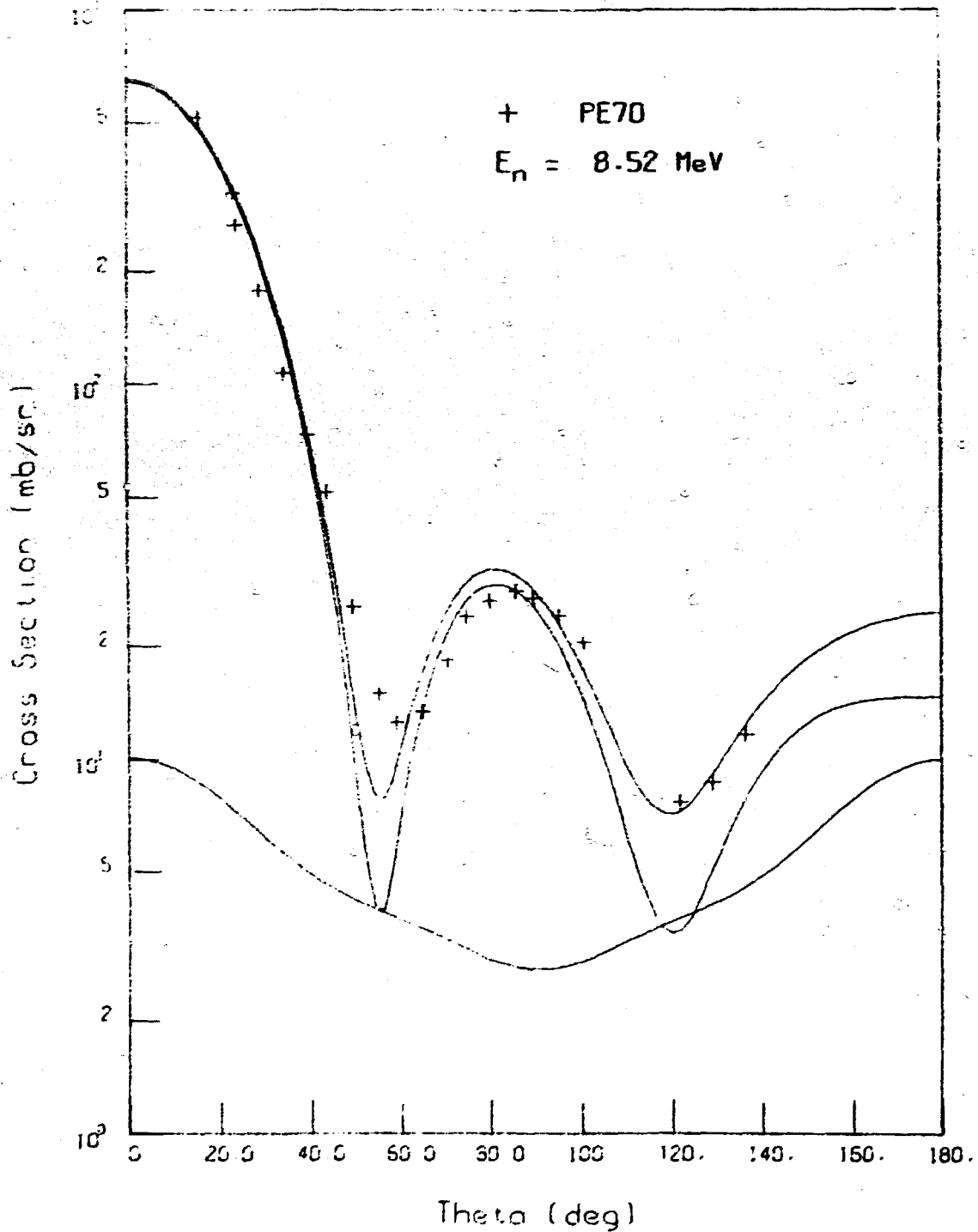


Fig. 108. Comparison of final optical model fit with data of Ref. PE70. The compound and shape elastic are summed to give the total elastic.

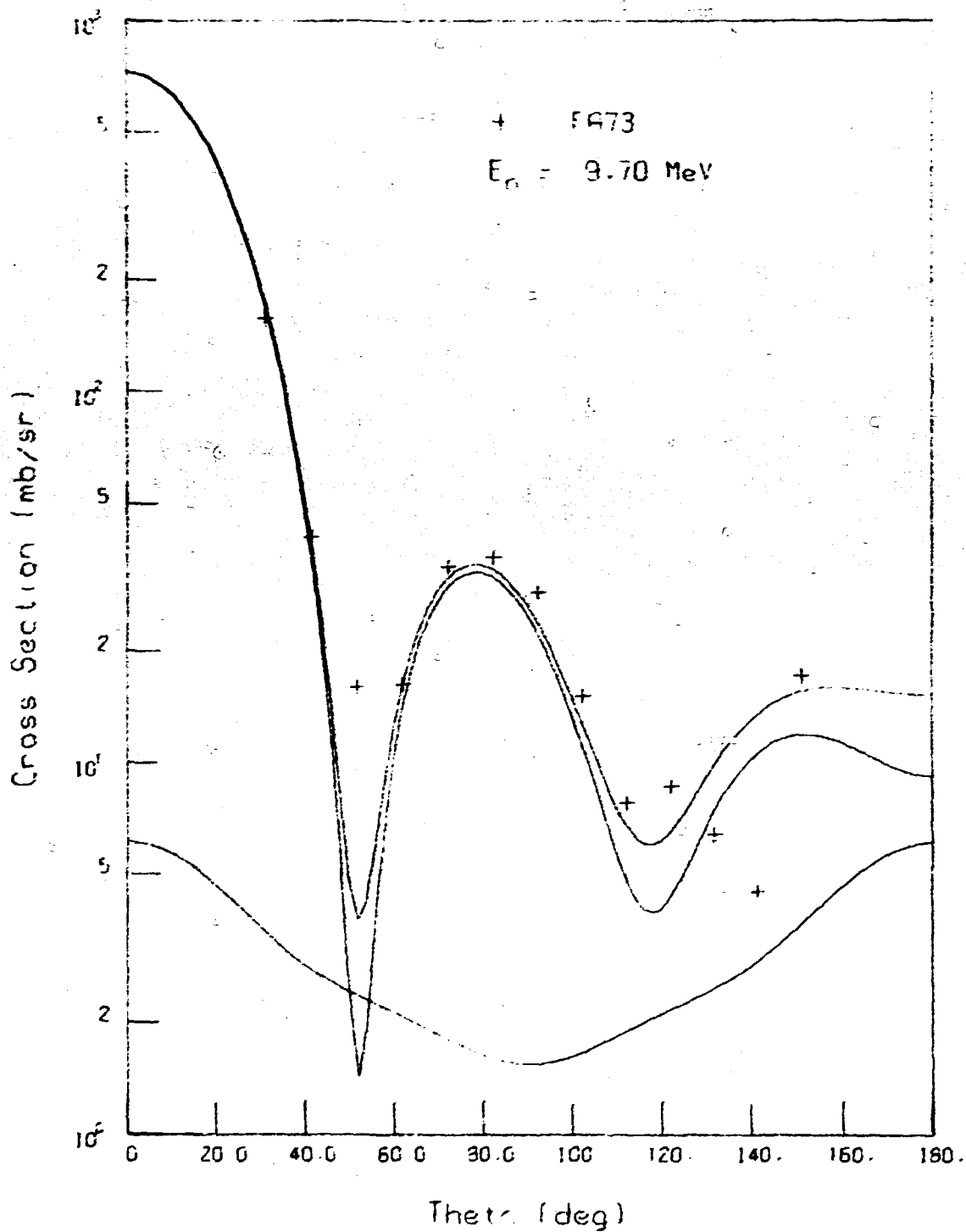


Fig. 109. Comparison of final optical model fit with data of Ref. FA73. The compound and shape elastic are summed to give the total elastic.

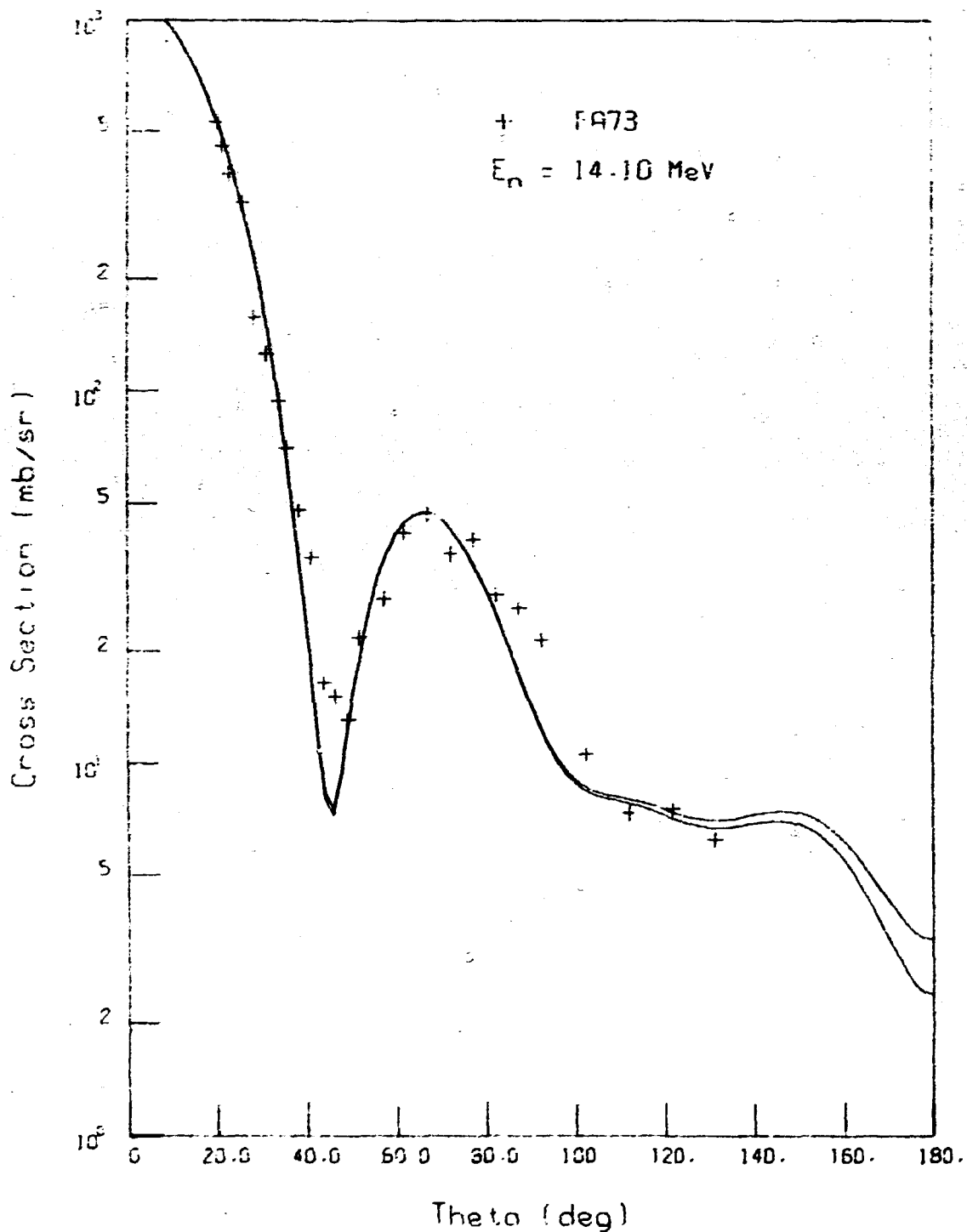


Fig. 110. Comparison of final optical model fit with data of Ref. FA73. The compound and shape elastic are summed to give the total elastic.

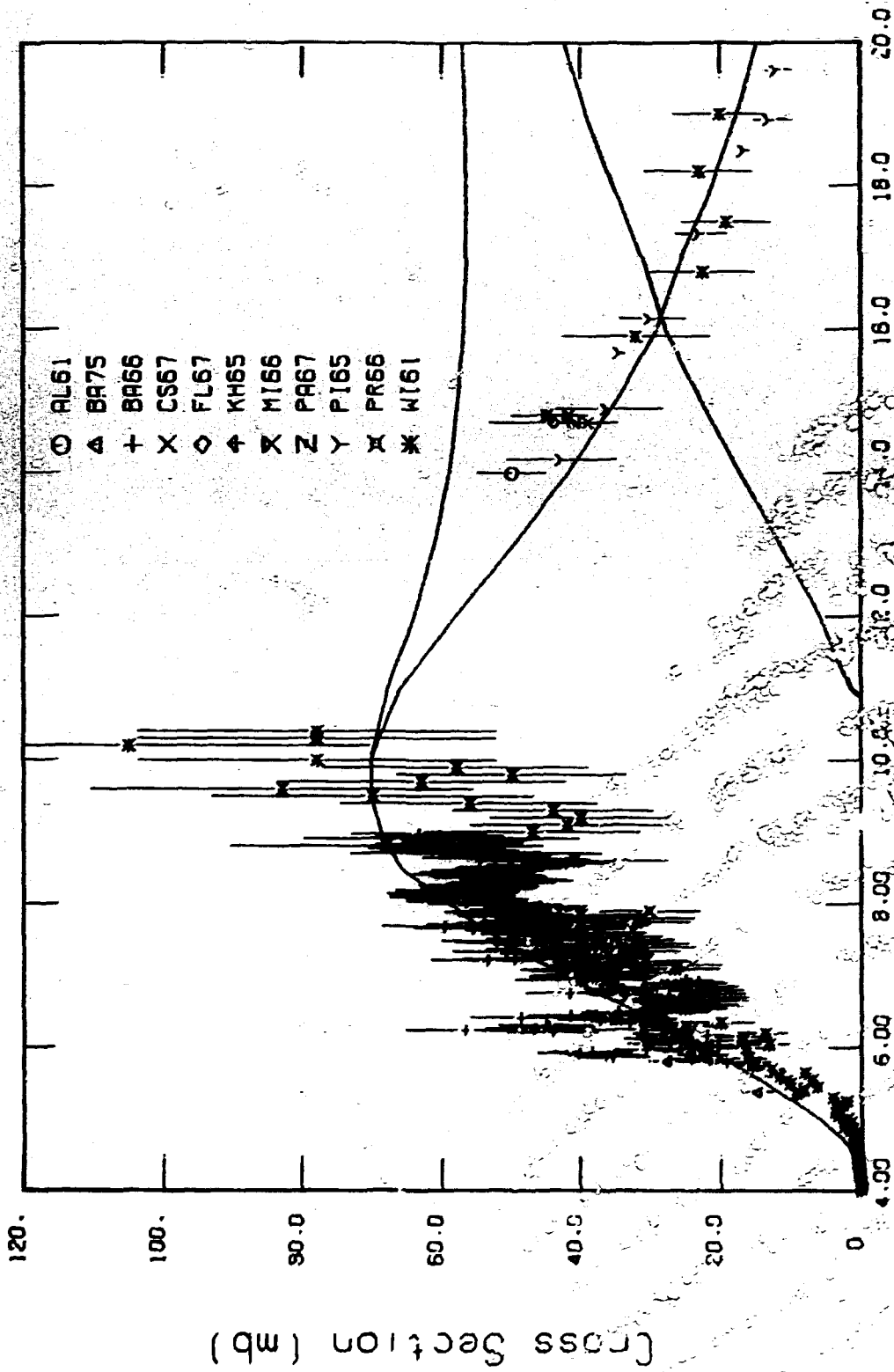


Fig. 111. Comparison of (n,pn) data with calculated results. The (n,pn) contribution (starting at 7.1 MeV) is also shown. The line contains the (n,p) [= (n,p) + (n,pn)] cross section.

# Cross Section (mb)

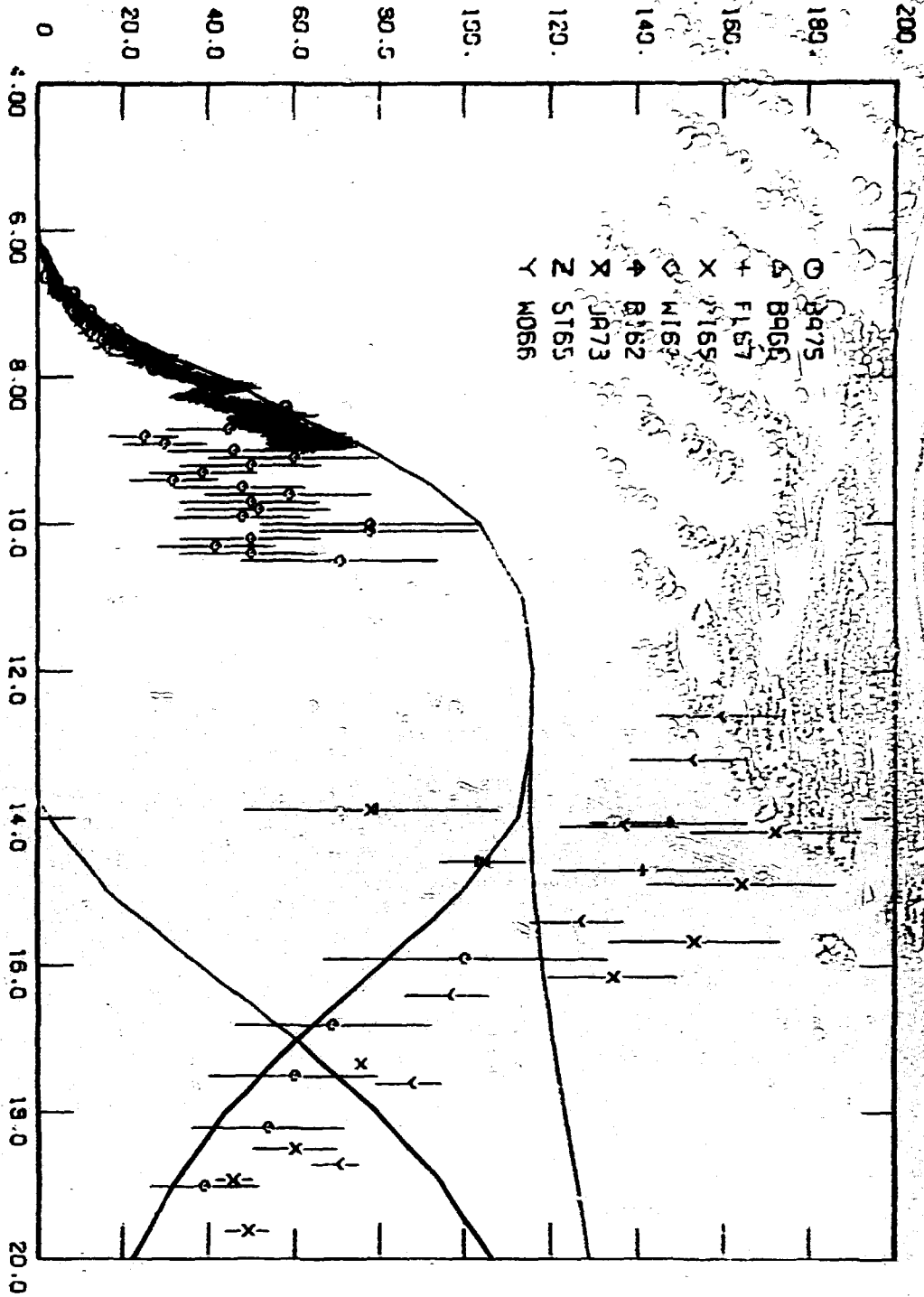


Fig. 112. Comparison of (n,α) data with calculated results. The (n,α) contribution (starting at 14 MeV) is also shown. The file contains the (n,α) [= (n,α) + (n,an)] cross section.

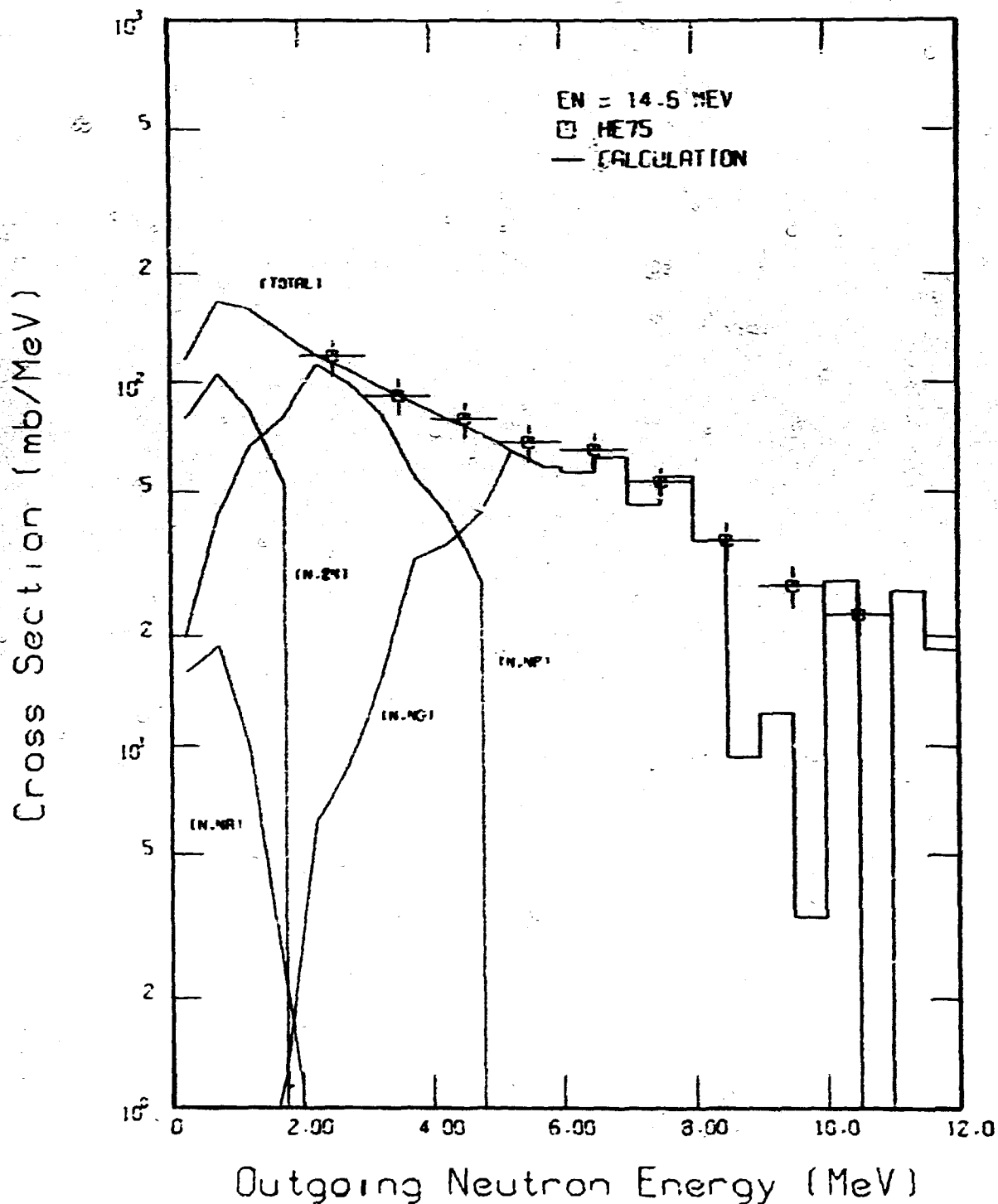


Fig. 113. Comparison of (n,xn) measurement of HE75 with the calculated emission spectrum. Contributions from the various neutron-producing components are also shown, which sum to the total. The curves labeled (n,np) and (n,nα) include the (n,pn) and (n,αn) components, respectively.

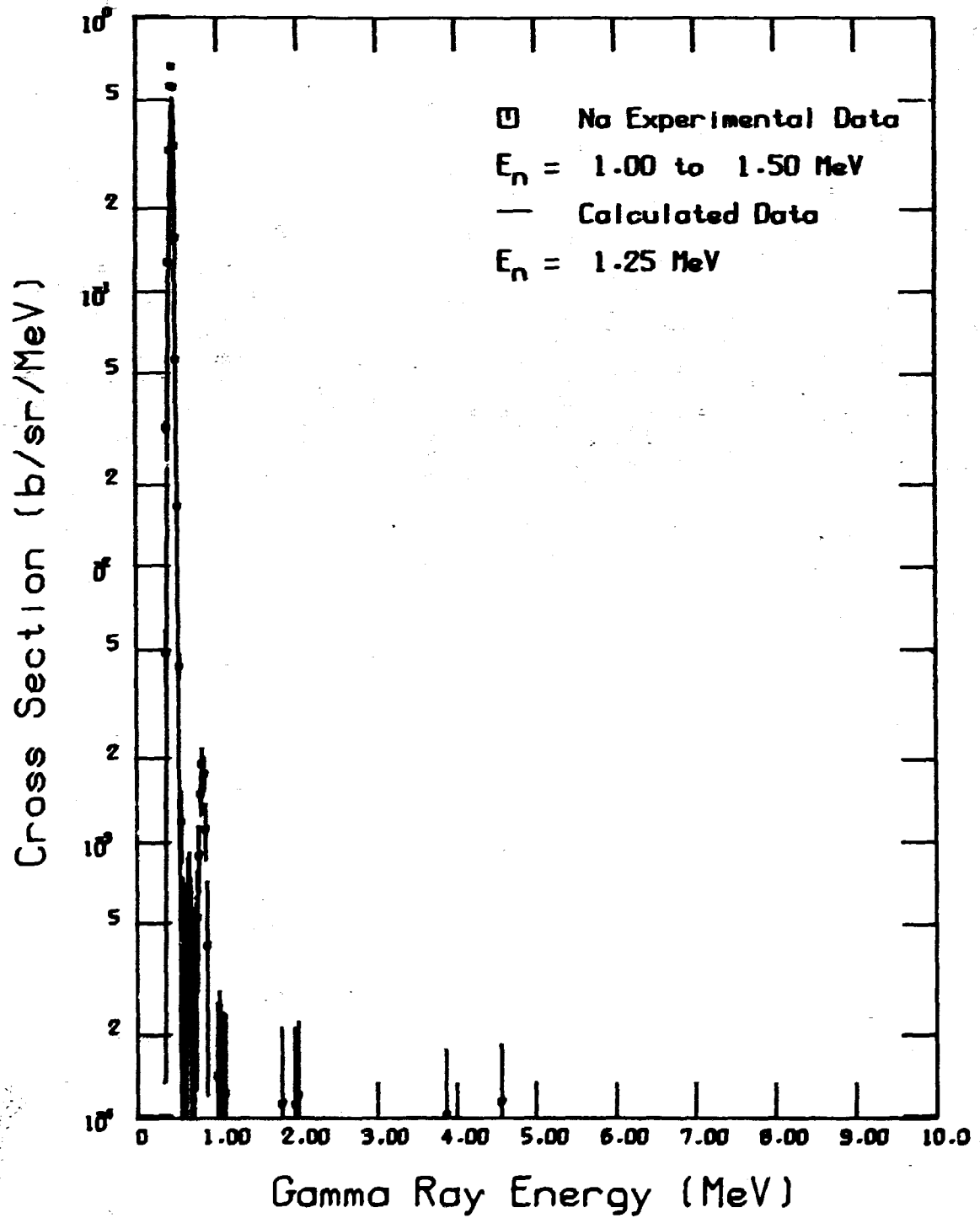


Fig. 114. Comparison of  $(n,\gamma)$  measurement of LA78 with calculated results.



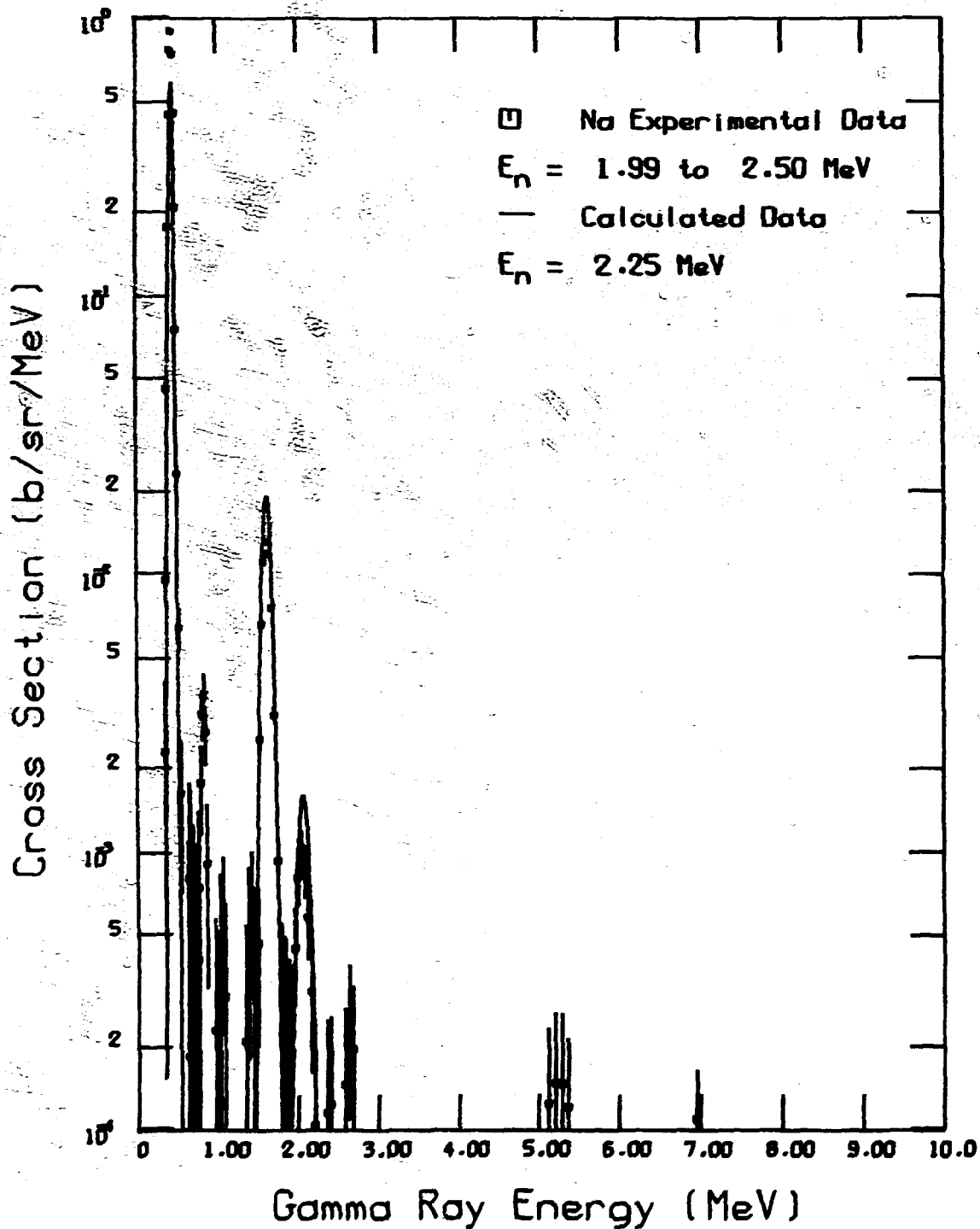


Fig. 116. Comparison of  $(n, x\gamma)$  measurement of LA78 with calculated results.

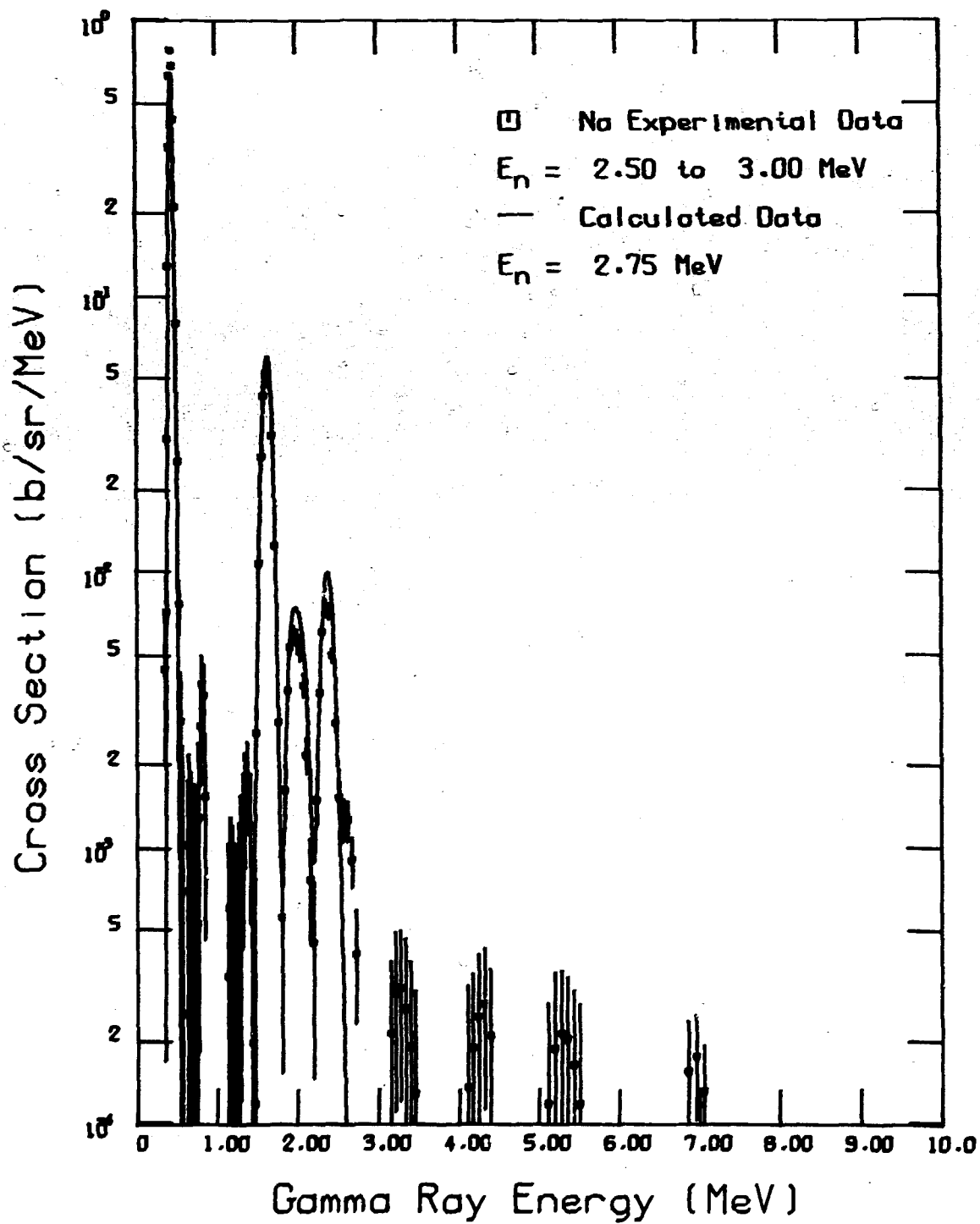


Fig. 117. Comparison of (n,xy) measurement of LA78 with calculated results.

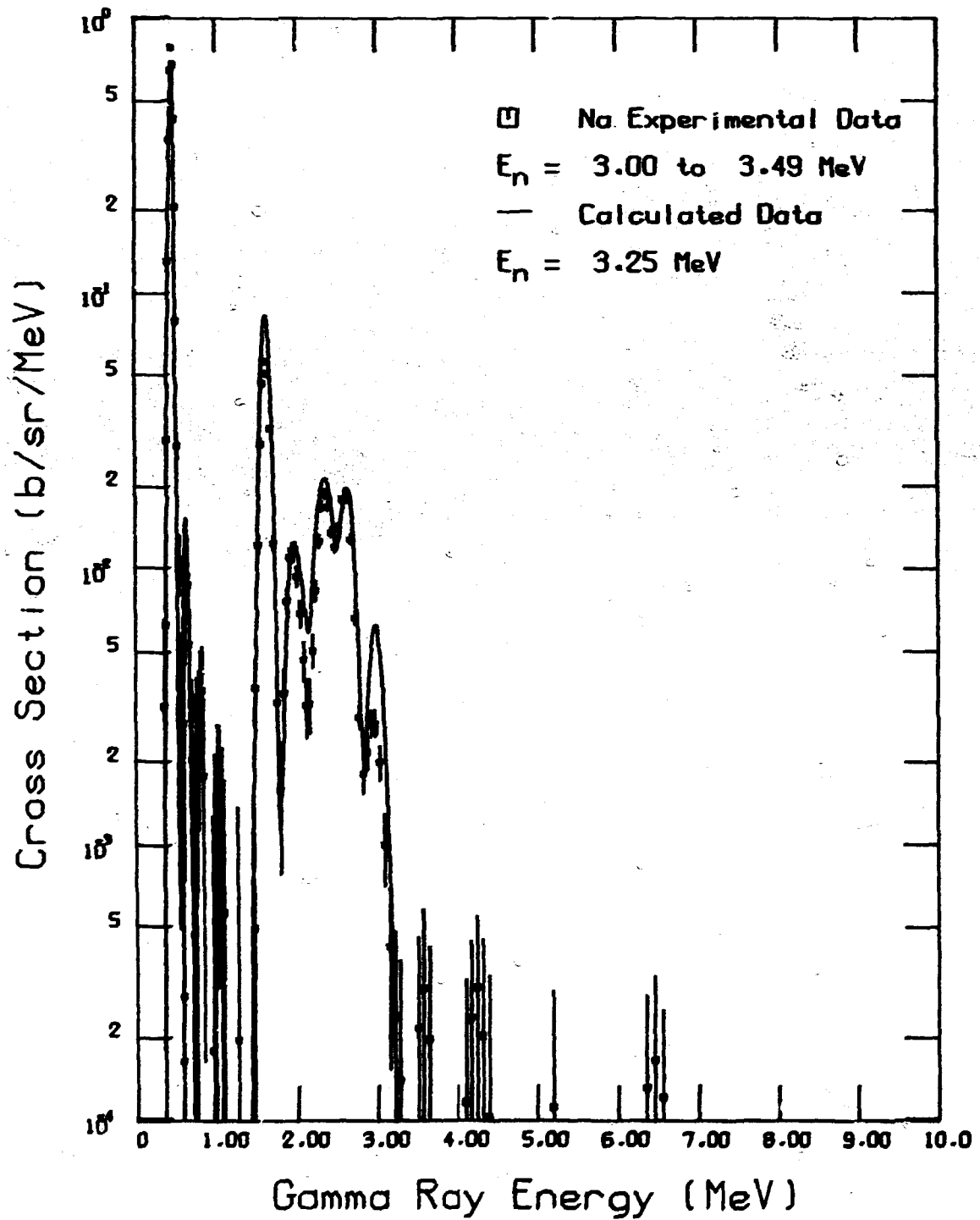


Fig. 118. Comparison of  $(n,xy)$  measurement of LA78 with calculated results.

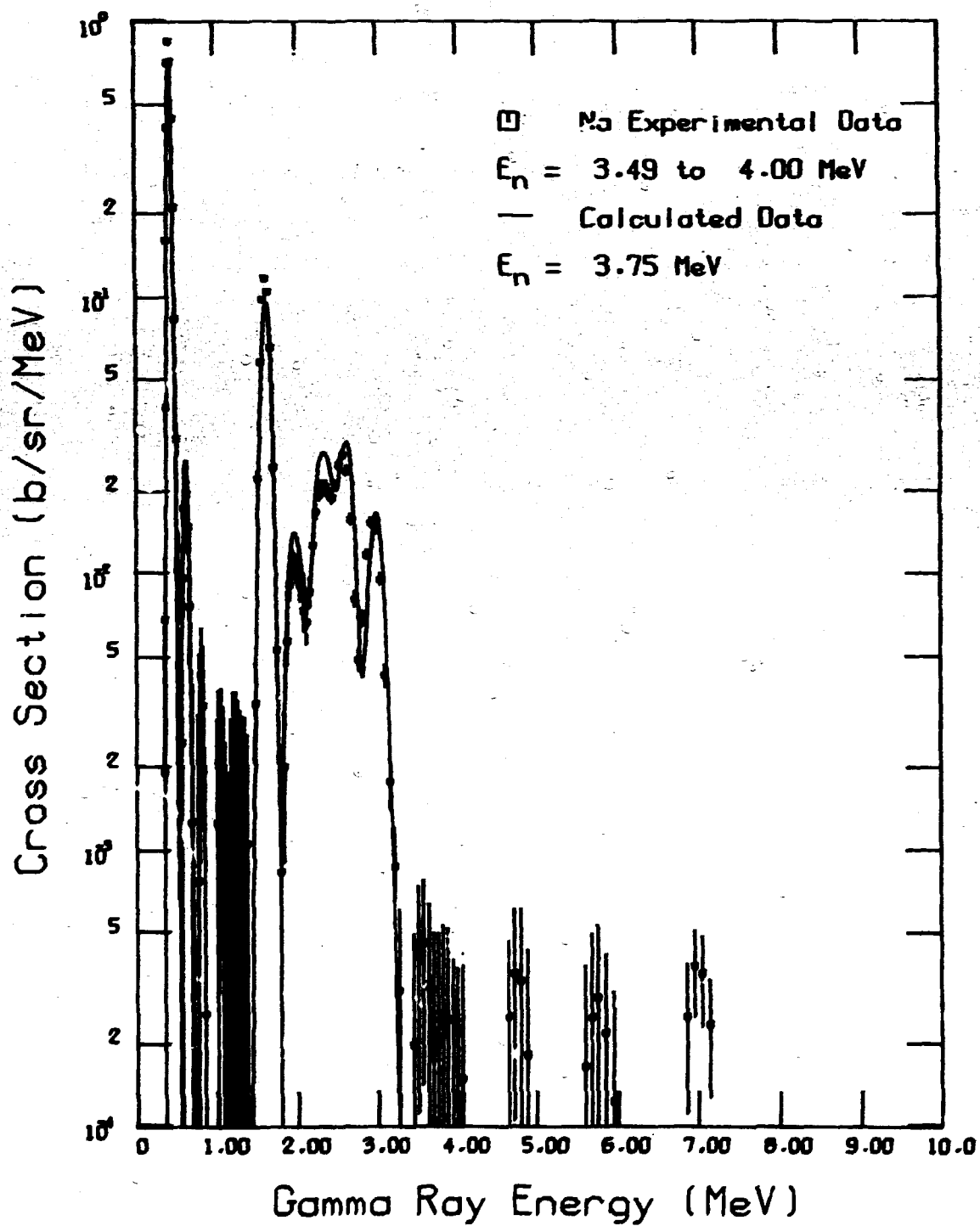


Fig. 119. Comparison of (n,xy) measurement of LA78 with calculated results.

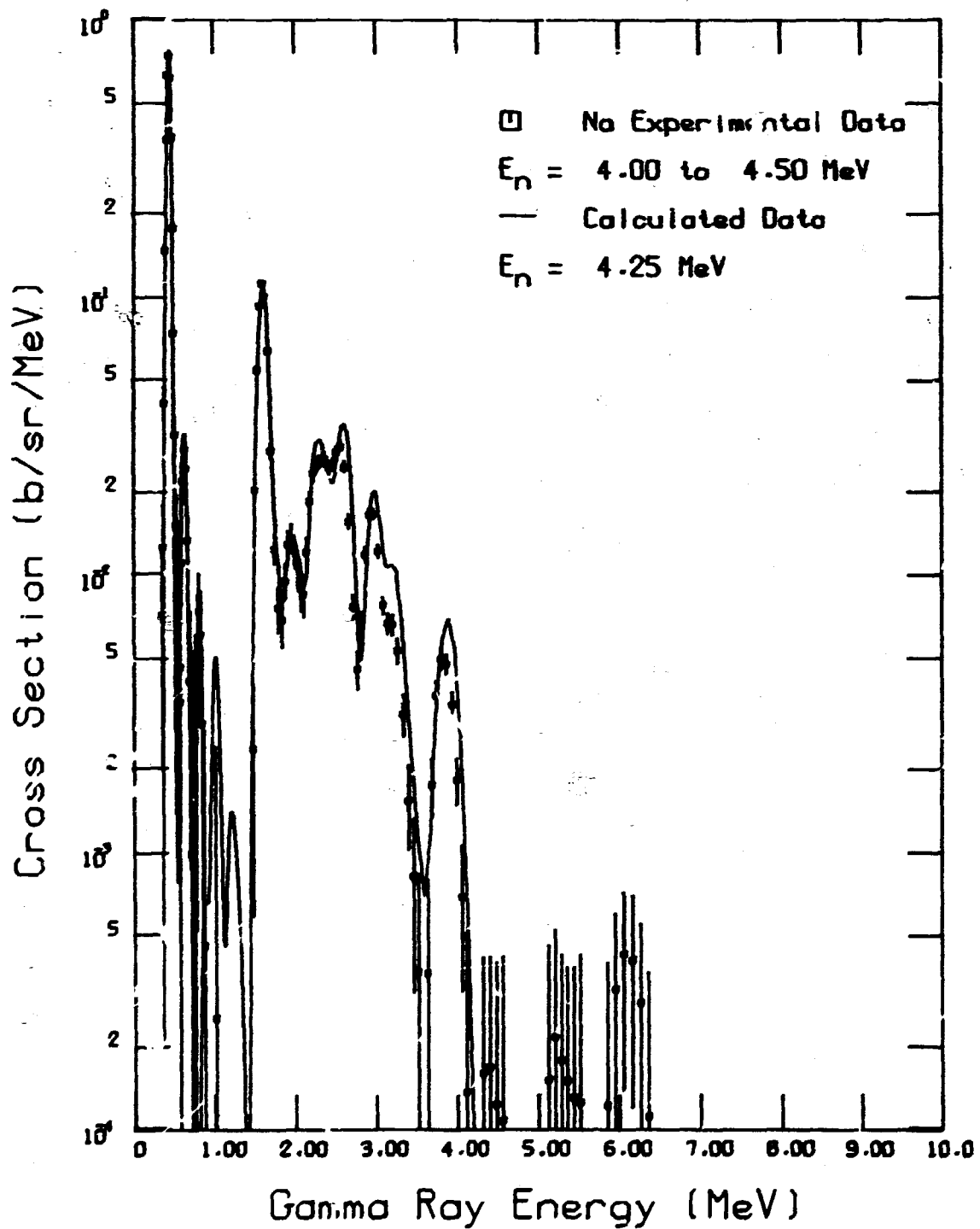


Fig. 120. Comparison of  $(n, x\gamma)$  measurement of LA78 with calculated results.

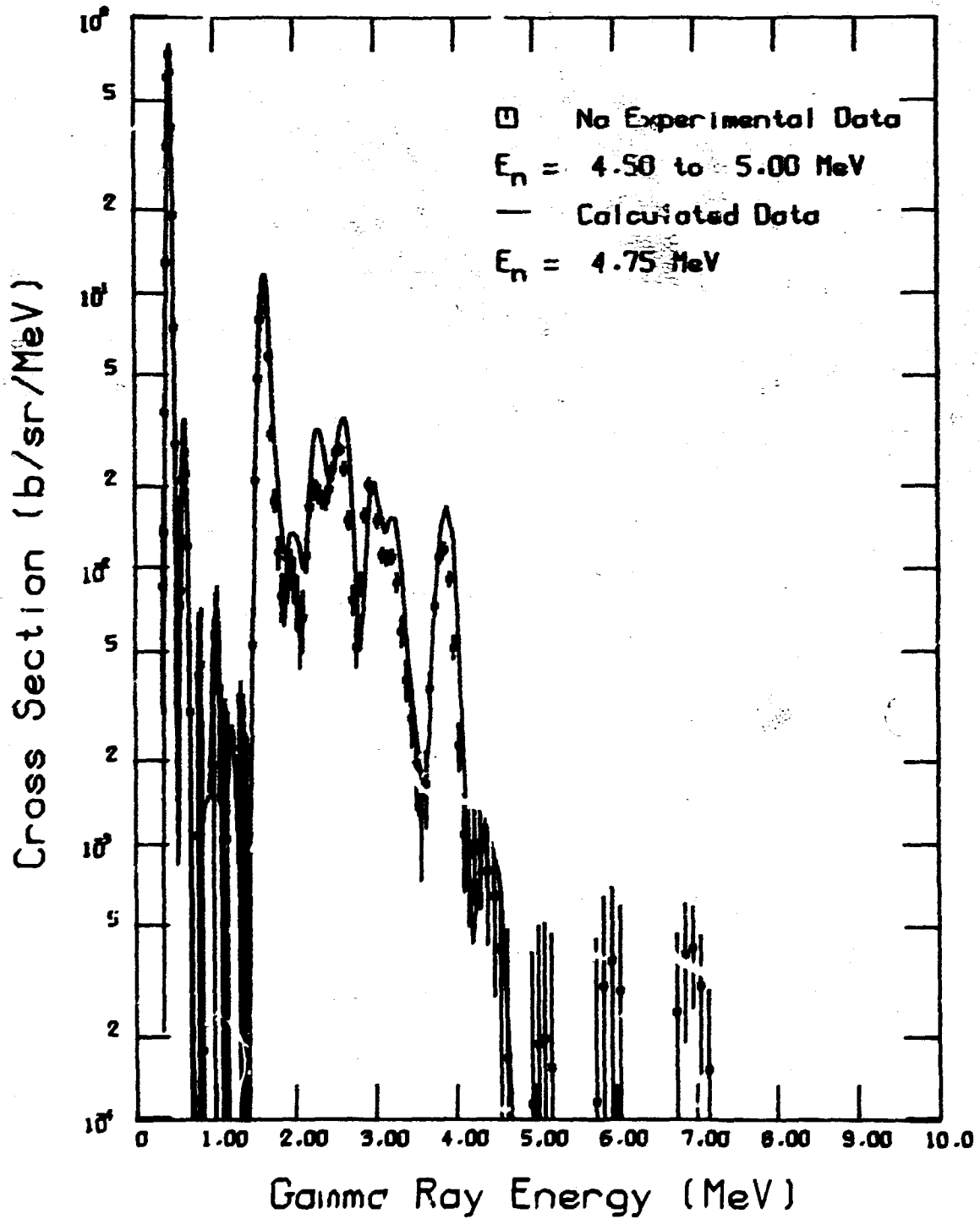


Fig. 121. Comparison of  $(n, \gamma)$  measurement of LA78 with calculated results.

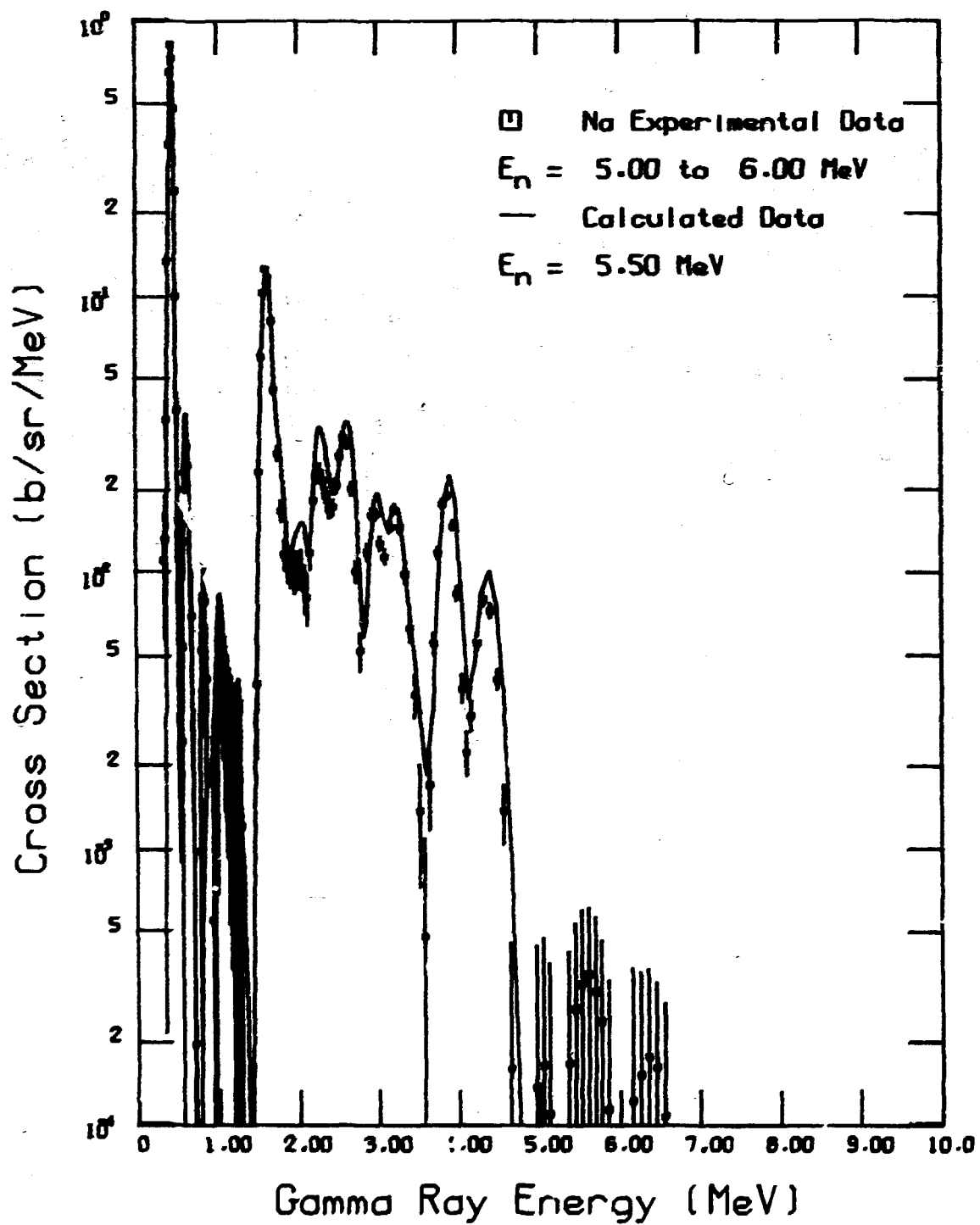


Fig. 122. Comparison of  $(n,xy)$  measurement of LA78 with calculated results.

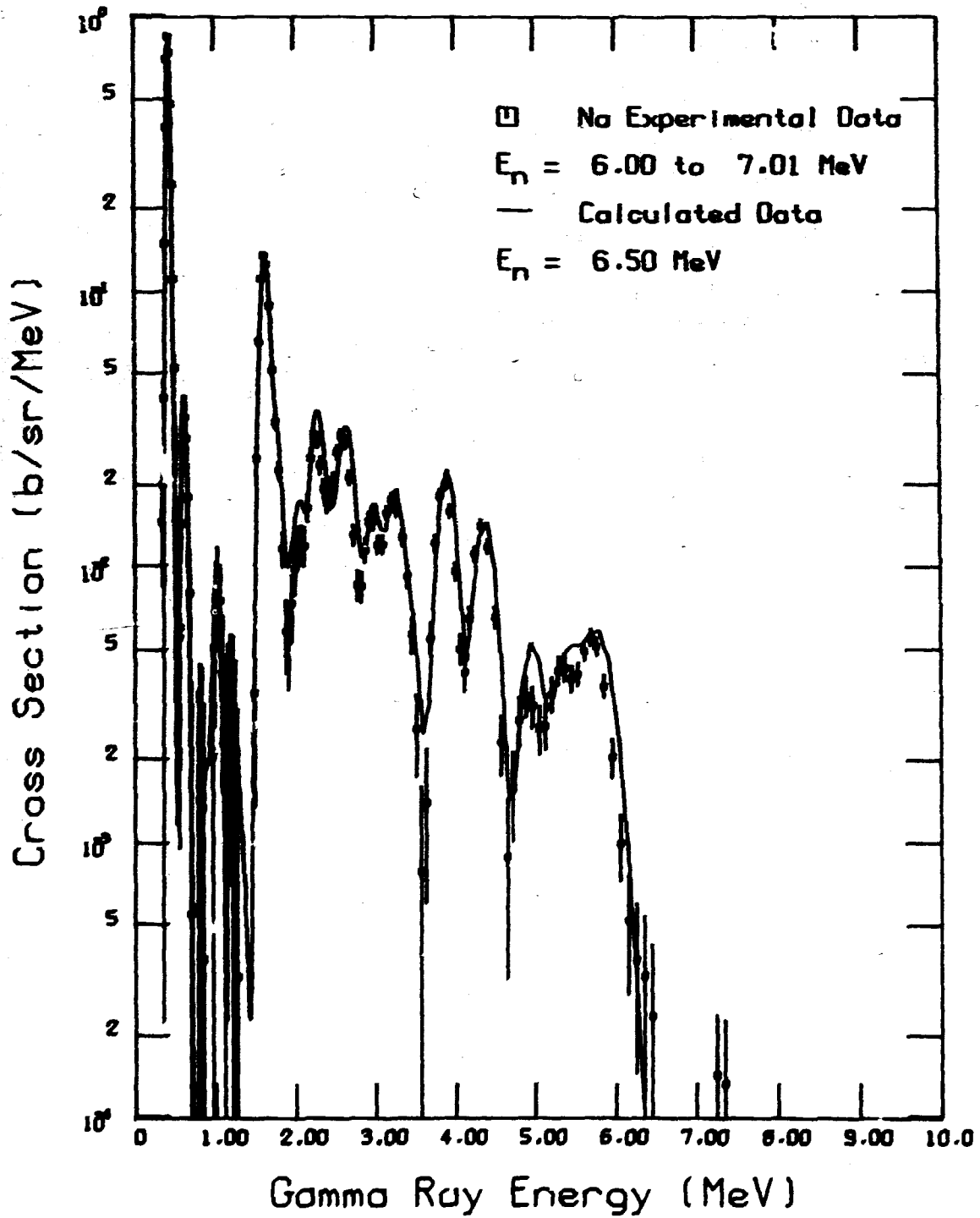


Fig. 123. Comparison of  $(n,\gamma)$  measurement of LA78 with calculated results.

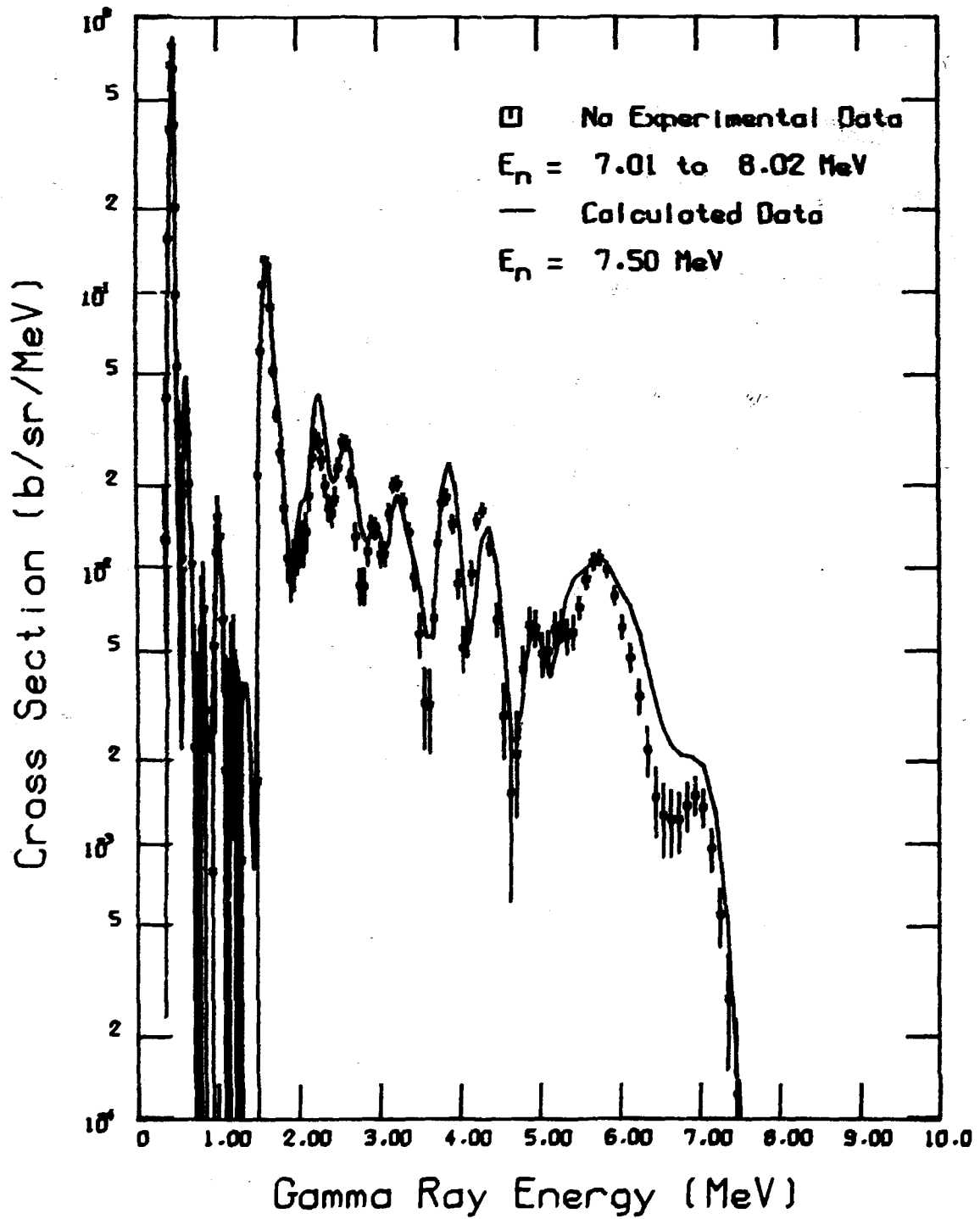


Fig. 124. Comparison of  $(n, x\gamma)$  measurement of LA78 with calculated results.

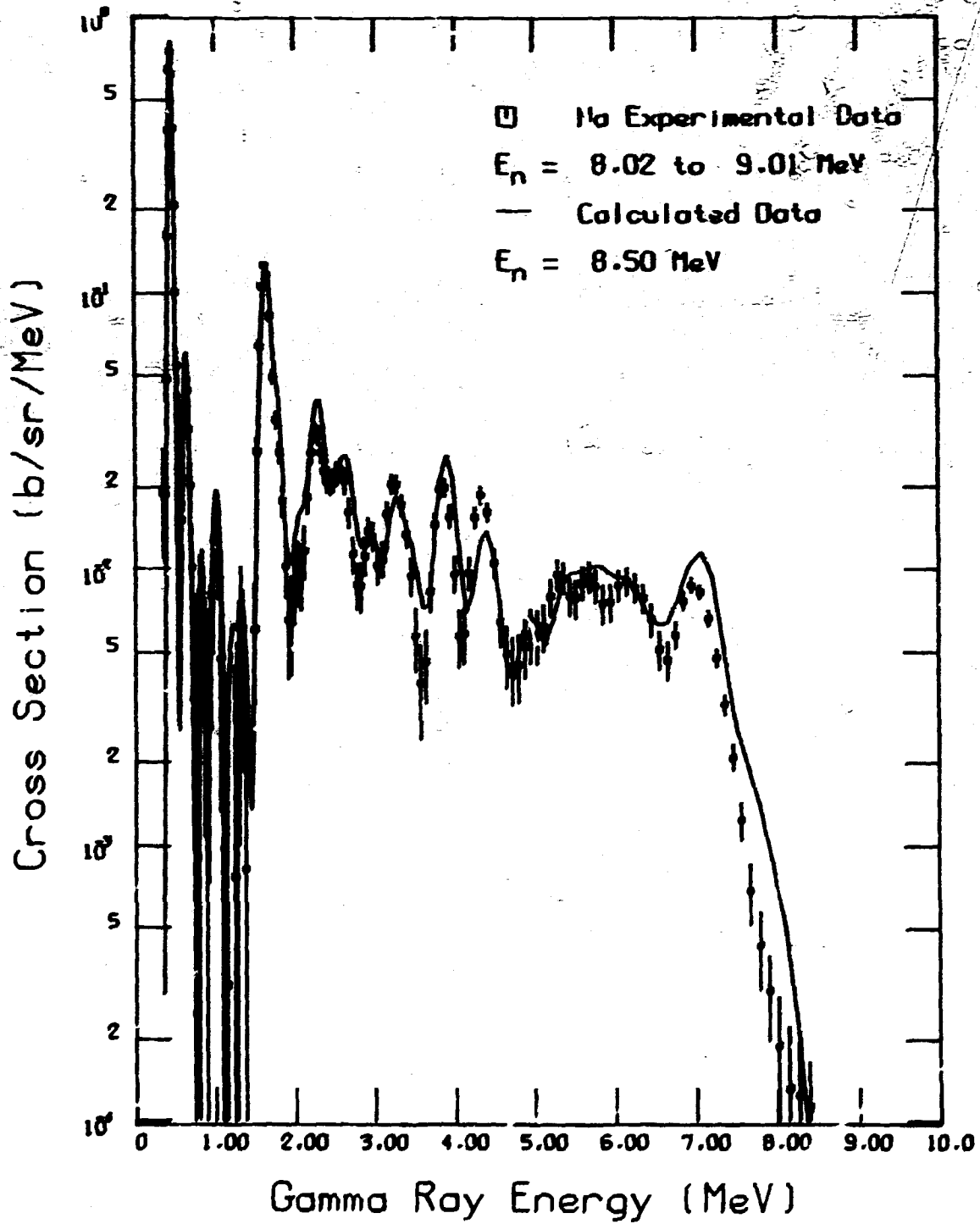


Fig. 125. Comparison of (n,xy) measurement of LA78 with calculated results.

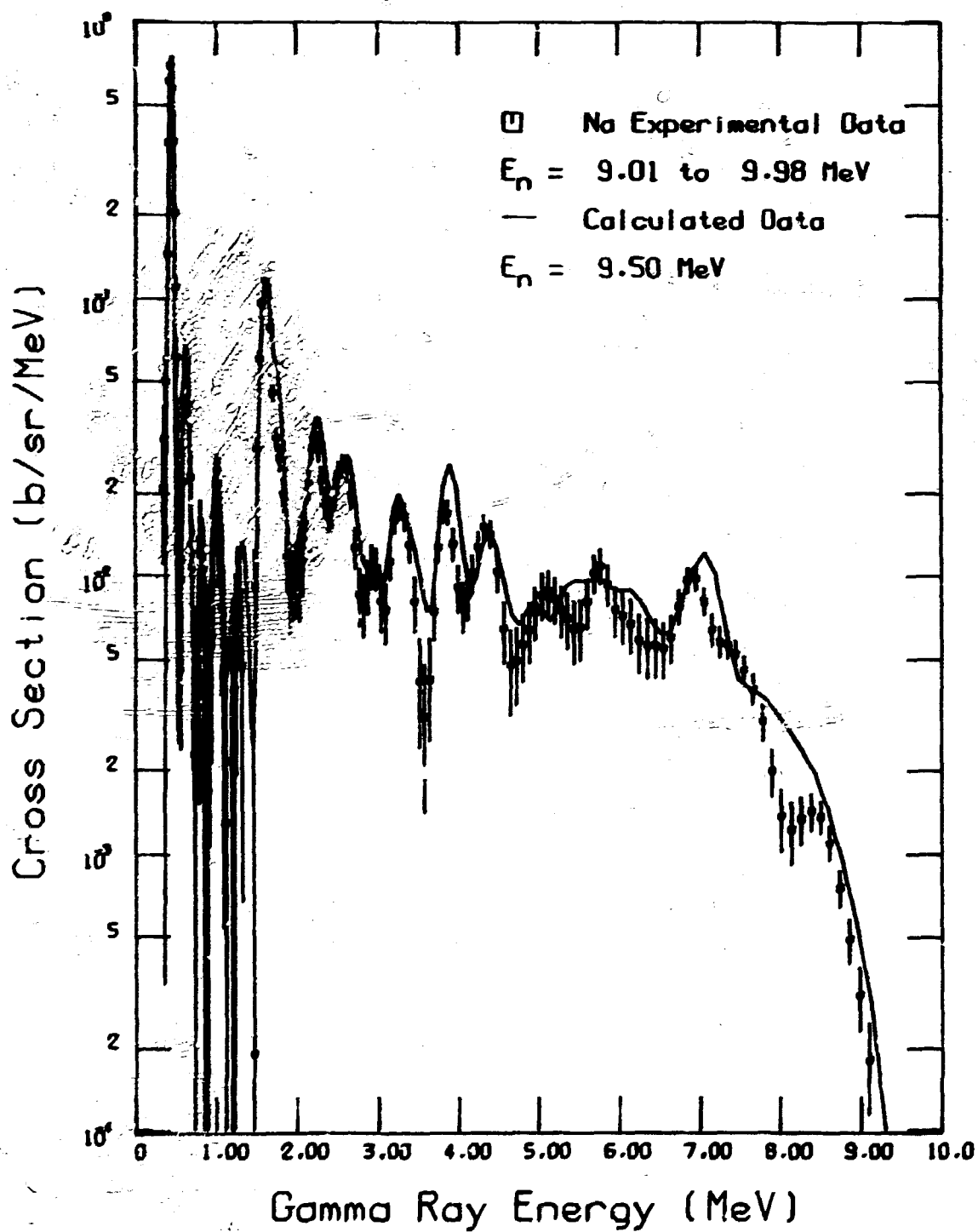


Fig. 126. Comparison of (n,xy) measurement of LA78 with calculated results.

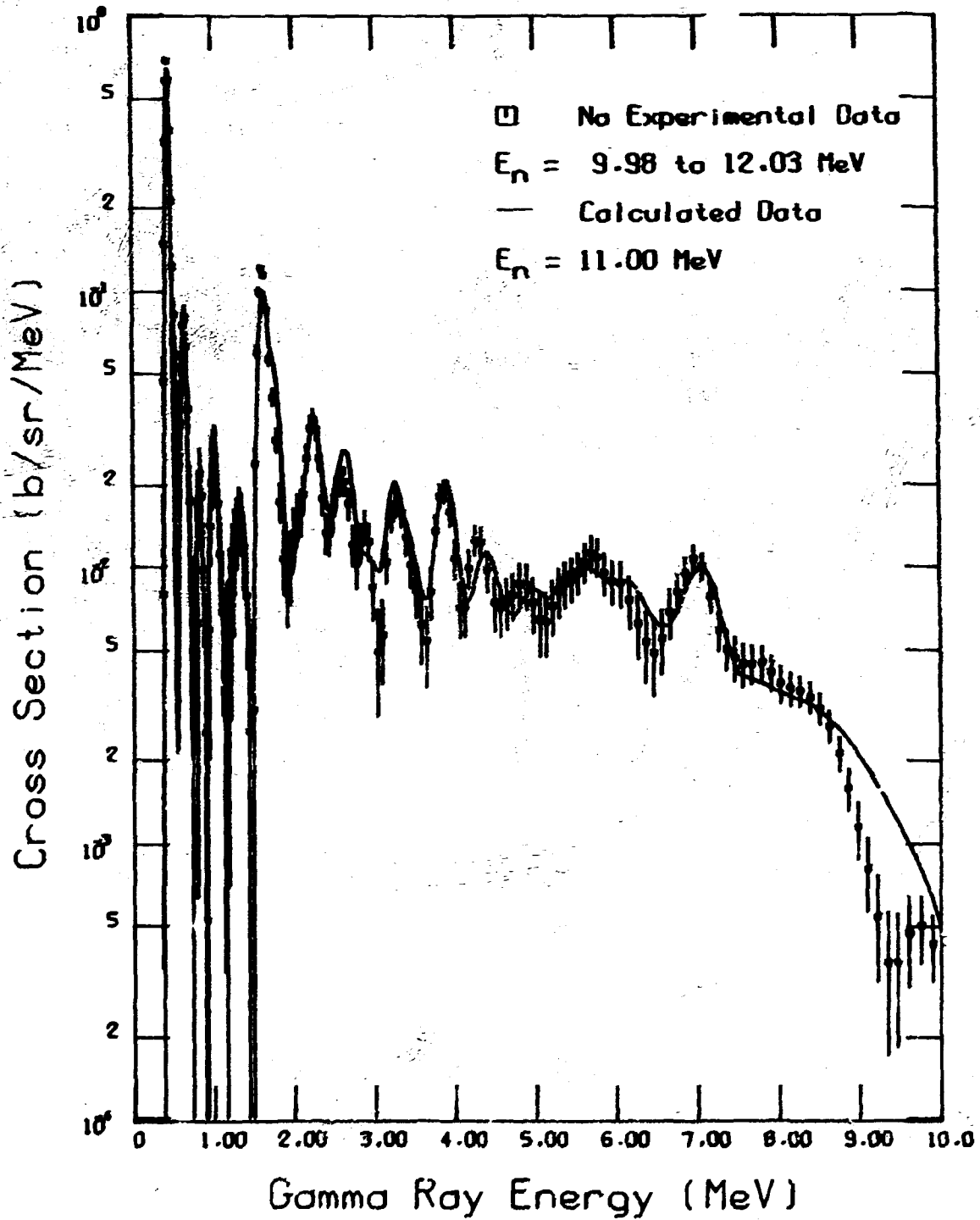


Fig. 127. Comparison of  $(n,xy)$  measurement of LA78 with calculated results.

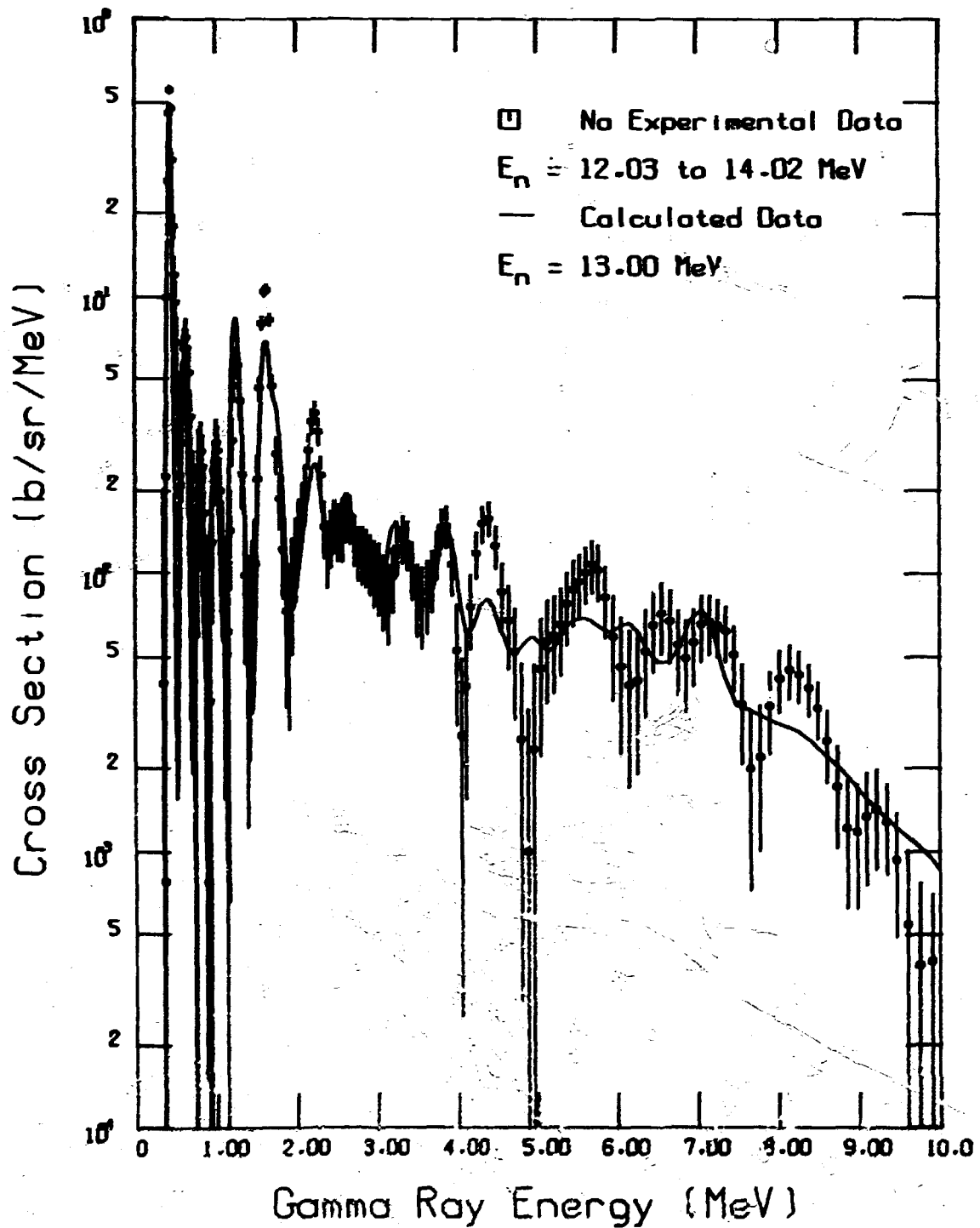


Fig. 128. Comparison of  $(n, \gamma)$  measurement of LA78 with calculated results.

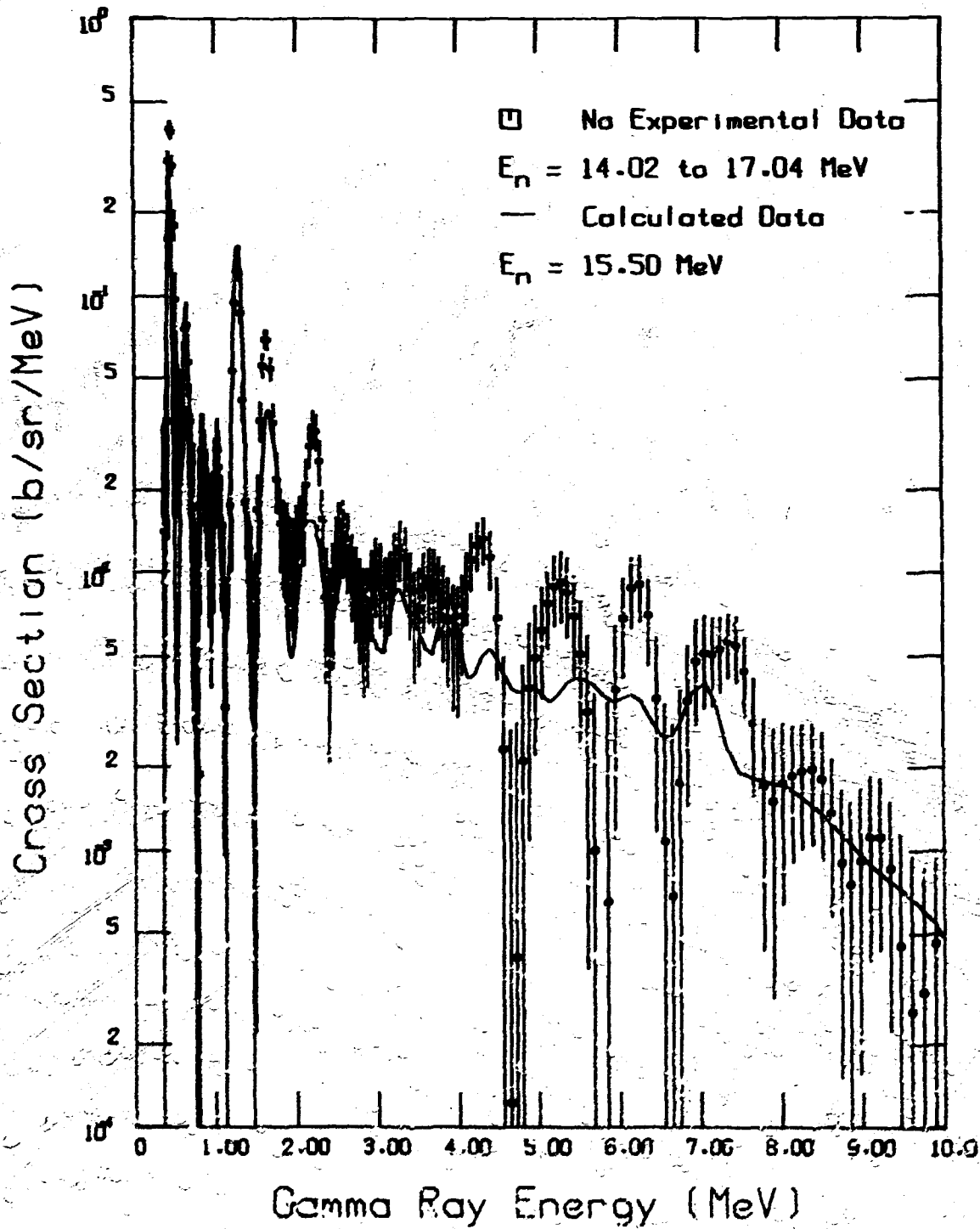


Fig. 129. Comparison of  $(n,xy)$  measurement of LA78 with calculated results.

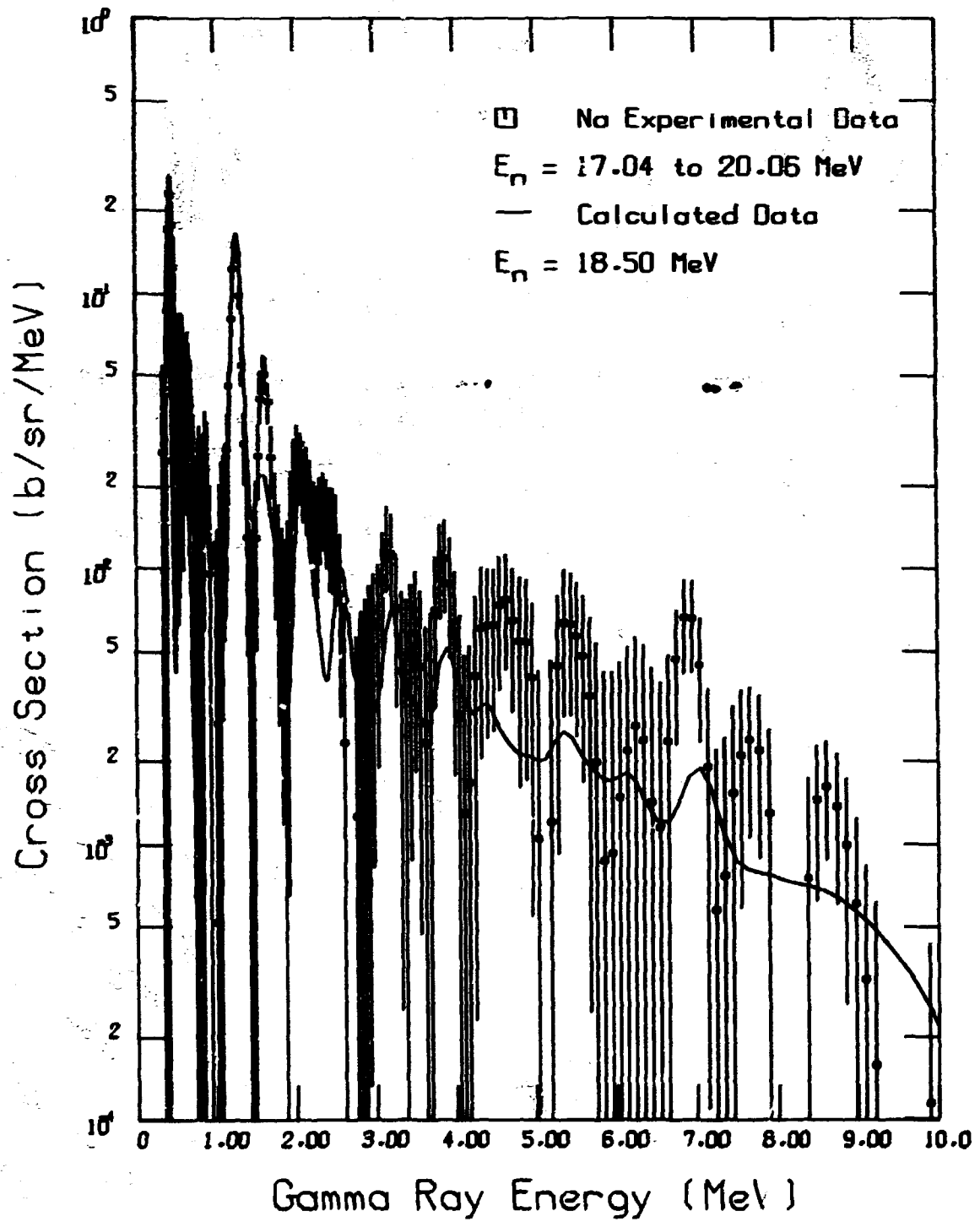


Fig. 130. Comparison of  $(n,\gamma)$  measurement of LA78 with calculated results.